UNIVERSITÀ
POLITECNICA
DELLE MARCHE

TECHNISCHE
UNIVERSITÄT
DARMSTADT

Università Politecnica delle Marche

FACOLTÀ DI INGEGNERIA
Corso di Dottorato di Ricerca in Ingegneria Industriale – Curriculum Ingegneria Energetica
XXXV Ciclo

Technische Universität Darmstadt

FACHBEREICH BAU- UND UMWELTINGENIEURWISSENSCHAFTEN

submitted in fulfilment of the requirements for the
degree of Doktor-Ingenieur (Dr.-Ing.)

Ph.D. Thesis

Experimental Characterization and Numerical Modelling of Solar Cooker Prototypes with Thermal Energy Storage

Advisor for UNIVPM:
Prof. Dr. Giovanni Di Nicola

Ph.D. Dissertation of:
M.Sc. Alessia Aquilanti

Advisor for TU Darmstadt:
Prof. Dr.ir. Eduardus A. B. Koenders

Ancona, Darmstadt 2023

Academic Year 2021 - 2022

To Giovanni

Contents

List of Figures

List of Tables

Abstract

Of all the different renewable energy sources, solar thermal energy, is one of the most promising alternatives to the consumption of highly polluting fossil fuels. Among its applications, solar cooking emerges as one of the most attractive ways to harness this type of energy. In the study presented, different types of solar cookers with and without a storage system were designed and tested: a high-efficiency solar box cooker (SBC), a concentrator cooker (CC), two prototype panel cookers (PSCs), and a medium-efficiency solar box cooker (SBC) equipped with thermal storage based on phase change materials (PCMs).

Regarding the latter, an extensive experimental campaign was carried out to characterize the selected PCMs both thermophysically and in terms of their thermal stability. From the analysis, sugar alcohols (SAs) were found to be suitable for use as PCMs in solar furnaces for applications in the low to medium temperature ranges (80-250 °C).

The high-efficiency SBC had a concentration ratio of 11.57. It consisted of a cooking chamber, a glazed top cover, and a double row of reflective mirrors. The prototype allowed both azimuthal and zenithal manual alignment. Tests without load were conducted to identify the maximum temperature that the cooker could reach, and load tests were conducted using water and peanut oil in various configurations: with one or two aluminum pots, painted black or unpainted. The cooker was able to bring 1 kg of water to the boiling point in about 11 minutes and get the peanut oil to a temperature of 220 °C in about 41 minutes.

The CC, called Heliac, had a concentration ratio of 40.97. It consisted mainly of a wooden lattice structure to which two wooden structures of different sizes were attached: one containing the larger Fresnel lens, and a smaller one containing the reflective surface. Tests with load were carried out using water and silicone oil as test fluids. The cooker was able to make 3 kg of water reach 90 °C in about half an hour and bring 3 kg of silicone oil to 170 °C in less than 1 hour.

The two PSCs made are the Newton and the Kimono panel solar cookers, respectively. The former consisted mainly of a prism-shaped glazed cooking chamber and two systems of reflective surfaces, a larger primary one and a smaller secondary one.Bby changing the inclination of the two reflective surfaces, the device, was able to vary its geometry. No-load tests and tests with load were carried out, using water and glycerin as test fluids. During the experimental campaign, two identical prototypes, one shielded from wind and the other not, were tested to assess how much this environmental parameter affects the final performance. Both devices were able to reach a stagnation temperature of 137 °C. The wind-shielded device was able to bring 2 kg of water to a temperature of 90 °C in about 2 hours and 2 kg of glycerin to a temperature of 110 °C in about 3 hours. These times were slightly longer in the case of the device tested without wind shielding. The Kimono panel solar cooker consisted of acrylic

panels connected together and covered with a reflective film. The prototype was tested in parallel with three other panel devices during three different times of the year by conducting no-load and water-load tests. The results showed that the Kimono panel solar cooker is among the best performing prototypes in all the three test periods, with a water heating time to boiling point of 1.74 hours.

The medium efficiency SBC had a concentration ratio of 4.08. It was mainly composed of a galvanized steel cooking chamber, a glass cover, and a system of 8 mirrors of two different shapes. Tests without load and tests with load were carried out using water and silicone oil as test fluids. In this case, the contribution to the overall system of the inclusion within the cooking chamber of a storage system based on phase change materials would make was also evaluated. The PCMs selected were erythritol and xylitol. The results showed that the cooling times of 1.5 kg of silicone oil in the chosen temperature range 125-100 °C increased by 350% when tested with the erythritol-based TES compared to when tested alone. In contrast, the cooling time of the same mass of silicone oil in the fluid temperature range 110-80 °C increased by 346% when tested with the xylitol-based TES equipped with a hand stirrer to stimulate nucleation of the material compared with when tested alone.

Experimental data from the latter device were used to validate the mathematical model developed specifically to simulate its thermodynamic performance. The model results show a very good fit with reality, managing to simulate the temperature of water and silicone oil in the heating phase of the selected tests with an average deviation from experimental data of 3% and 8%, respectively.

Sommario

L'energia solare termica, tra le fonti rinnovabili, rappresenta una tra le più promettenti alternative al consumo di fonti fossili altamente inquinanti. Tra le sue applicazioni, la cottura solare risulta uno dei modi più attrattivi per sfruttare questo tipo di energia. Nel presente studio sono state progettate e testate differenti tipologie di forni solari con e senza sistema di accumulo: un forno solare a scatola (SBC) ad alta efficienza, un forno a concentrazione (CC), due prototipi a pannelli (PSC) e un forno a scatola (SBC) a media efficienza dotato di accumulo termico a base di materiali a cambiamento di fase (PCM).

Per quanto riguarda questi ultimi, una estensiva campagna sperimentale è stata effettuata per caratterizzare i PCM selezionati dal punto di vista termofisico e della loro stabilità termica. Dall'analisi, i polialcoli sono risultati adatti all'impiego come PCM nei forni solari per applicazioni nei range di temperatura medio-bassa (80-250 °C).

Il SBC ad alta efficienza ha un rapporto di concentrazione di 11.57. È costituito da una camera di cottura, una copertura superiore vetrata e da una doppia fila di specchi riflettenti. Il prototipo consente un allineamento solare manuale sia azimutale che zenitale. Sono state svolte prove a vuoto per identificare la massima temperatura raggiungibile dal forno e prove a carico utilizzando acqua e olio di arachide in varie configurazioni: utilizzando una o due pentole di alluminio, verniciate o meno di nero.

Il forno è stato in grado di portare ad ebollizione 1 kg di acqua in circa 11 minuti e a far raggiungere all'olio di arachide la temperatura di 220 °C in circa 41 minuti.

Il CC, chiamato Heliac, ha un rapporto di concentrazione di 40.97. È costituito principalmente da una struttura reticolare lignea a cui sono fissate due strutture di legno di dimensioni differenti: una contenente la lente di Fresnel di dimensioni maggiori, e l'altra più piccola contenente la superficie riflettente. Sono state svolte prove a carico utilizzando acqua e olio siliconico come fluidi di prova. Il forno è stato in grado di far raggiungere i 90 °C a 3 kg di acqua in circa mezz'ora e a portare 3 kg di olio siliconico a 170 °C in meno di 1 ora.

I due PSC realizzati sono rispettivamente il Newton e il Kimono. Il primo è costituito principalmente da una camera di cottura vetrata a forma di prisma e da due sistemi di superfici riflettenti, quella primaria di dimensioni maggiori e quella secondaria di dimensioni ridotte. Il dispositivo, cambiando l'inclinazione delle due superfici riflettenti è in grado di variare la propria geometria. Sono state svolte prove a vuoto e a carico, utilizzando acqua e glicerina come fluidi di prova. Durante la campagna sperimentale sono stati testati due identici prototipi, uno schermato dal vento e l'altro no, per valutare quanto questo parametro ambientale va ad influenzare le performance finali. Entrambi i dispositivi sono stati in grado di raggiungere una temperatura di stagnazione di 137 °C. Il dispositivo schermato dal vento è riuscito a portare 2 kg di acqua ad una temperatura di 90 °C in circa 2 ore e 2 kg di glicerina ad una temperatura di 110 °C in circa 3 ore. Questi tempi sono risultati leggermente maggiori nel caso di dispositivo testato senza schermatura dal vento. Il Kimono è costituito da pannelli in acrilico collegati tra di loro e ricoperti da una pellicola riflettente. Il prototipo è stato testato in parallelo ad altri tre dispositivi a pannelli durante tre periodi differenti dell'anno, effettuando prove a vuoto e a carico con acqua. I risultati hanno mostrato che il Kimono è tra i prototipi con migliori prestazioni in tutti e tre i periodi di prova, con un tempo di riscaldamento dell'acqua fino al punto di ebollizione di 1.74 ore.

Il SBC a media efficienza ha un rapporto di concentrazione di 4.08. È principalmente composto da una camera di cottura in acciaio zincato, una copertura vetrata e un sistema di 8 specchi di due forme diverse. Sono state effettuate prove a vuoto e a carico utilizzando acqua e olio siliconico come fluidi di prova. In questo caso è stato anche valutato il contributo che l'inserimento all'interno della camera di cottura di un sistema di accumulo basato su materiali a cambiamento di fase andava ad apportare all'intero sistema. I PCM selezionati erano eritritolo e xilitolo. I risultati hanno mostrato che i tempi di raffreddamento di 1.5 kg di olio siliconico nel range di temperatura scelto 125-100 °C è aumentato del 350% quando testato con il TES a base di eritritolo rispetto a quando testato da solo. Il tempo di raffreddamento della stessa massa di olio siliconico nel range di temperatura del fluido 110-80 °C è invece aumentato del 346% quanto testato con il TES a base di xilitolo dotato di agitatore manuale per stimolare la nucleazione del materiale rispetto a quando testato da solo.

I dati sperimentali di quest'ultimo dispositivo sono stati utilizzati per validare il modello matematico sviluppato appositamente per simularne le performance termodinamiche. I risultati del modello mostrano un'ottima aderenza con la realtà, riuscendo a simulare la temperatura di acqua e olio siliconico nella fase di riscaldamento dei test selezionati con uno scostamento medio rispetto ai dati sperimentali del 3% e 8%,

rispettivamente.

Abstract

Die thermische Solarenergie ist unter den erneuerbaren Energiequellen eine der vielversprechendsten Alternativen zum Verbrauch stark umweltbelastender fossiler Brennstoffe. Unter den Anwendungen erweist sich das solare Kochen als eine der attraktivsten Möglichkeiten, diese Art von Energie zu nutzen. In der vorliegenden Studie wurden verschiedene Arten von Solarkochern mit und ohne Speichersystem entworfen und getestet: ein hocheffizienter Solarkasten-Kocher (SBC), ein Konzentratorkocher (CC), zwei Prototyp-Panelkocher (PSC) und ein Solarkasten-Kocher (SBC) mit mittlerem Wirkungsgrad, der mit einem thermischen Speicher auf der Basis von Phasenwechselmaterialien (PCM) ausgestattet ist.

Für letzteren wurde eine umfangreiche Versuchskampagne durchgeführt, um die ausgewählten PCMs thermophysikalisch und hinsichtlich ihrer thermischen Stabilität zu charakterisieren. Die Analyse ergab, dass die Zuckeralkohole (SA) für den Einsatz als PCM in Solaröfen für Anwendungen im niedrigen bis mittleren Temperaturbereich (80-250 °C) geeignet sind.

Der hocheffiziente SBC hat ein Konzentrationsverhältnis von 11.57. Er besteht aus einer Kochkammer, einer verglasten oberen Abdeckung und einer doppelten Reihe von reflektierenden Spiegeln. Der Prototyp ermöglicht sowohl eine azimutale als auch eine zenithale manuelle Ausrichtung. Es wurden Tests ohne Belastung durchgeführt, um die Höchsttemperatur zu ermitteln, die der Kocher erreichen kann, und es wurden Belastungstests mit Wasser und Erdnussöl in verschiedenen Konfigurationen durchgeführt: mit einem oder zwei Aluminiumtöpfen, schwarz lackiert oder unlackiert. Der Kocher war in der Lage, 1 kg Wasser in etwa 11 Minuten zum Sieden zu bringen und das Erdnussöl in etwa 41 Minuten auf eine Temperatur von 220 °C zu bringen.

Der CC, genannt Heliac, hat ein Konzentrationsverhältnis von 40.97. Er besteht im Wesentlichen aus einer Holzgitterstruktur, an der zwei unterschiedlich große Holzkonstruktionen befestigt sind: eine mit der größeren Fresnellinse und eine kleinere mit der reflektierenden Oberfläche. Die Belastungstests wurden mit Wasser und Silikonöl als Testflüssigkeit durchgeführt. Der Kocher war in der Lage, 3 kg Wasser in etwa einer halben Stunde auf 90 °C zu erhitzen und 3 kg Silikonöl in weniger als einer Stunde auf 170 °C zu bringen.

Bei den beiden hergestellten PSC handelt es sich um den Newton bzw. den Kimono. Ersterer besteht im Wesentlichen aus einer prismenförmigen, verglasten Kochkammer und zwei Systemen von Reflexionsflächen, einer größeren primären und einer kleineren sekundären. Durch Änderung der Neigung der beiden reflektierenden Flächen kann die Geometrie des Geräts variiert werden. Es wurden Tests ohne Last und mit Last durchgeführt, wobei Wasser und Glyzerin als Testflüssigkeiten verwendet wurden. Während der Versuchskampagne wurden zwei identische Prototypen getestet, von denen der eine windgeschützt und der andere nicht windgeschützt war, um festzustellen, wie stark dieser Umweltparameter die endgültige Leistung beeinflusst. Beide Geräte waren

in der Lage, eine Stagnationstemperatur von 137 °C zu erreichen. Das windgeschützte Gerät war in der Lage, 2 kg Wasser in etwa 2 Stunden auf eine Temperatur von 90 °C und 2 kg Glyzerin in etwa 3 Stunden auf eine Temperatur von 110 °C zu bringen. Diese Zeiten waren bei dem ohne Windschutz getesteten Gerät etwas länger. Der Kimono besteht aus Acrylplatten, die miteinander verbunden und mit einer reflektierenden Folie überzogen sind. Der Prototyp wurde parallel zu drei anderen Paneelgeräten zu drei verschiedenen Jahreszeiten in Leerlauf- und Wasserlasttests getestet. Die Ergebnisse zeigen, dass der Kimono in allen drei Testperioden zu den leistungsfähigsten Prototypen gehört, mit einer Wassererwärmungszeit bis zum Siedepunkt von 1.74 Stunden.

Der SBC mit mittlerem Wirkungsgrad hat ein Konzentrationsverhältnis von 4.08. Er besteht hauptsächlich aus einer Kochkammer aus verzinktem Stahl, einer Glasabdeckung und einem System aus 8 Spiegeln in zwei verschiedenen Formen. Es wurden Tests ohne Last und Tests mit Last mit Wasser und Silikonöl als Testflüssigkeiten durchgeführt. In diesem Fall wurde auch der Beitrag bewertet, den der Einbau eines auf Phasenwechselmaterialien basierenden Speichersystems in die Kochkammer zum Gesamtsystem leisten würde. Als PCMs wurden Erythritol und Xylitol ausgewählt. Die Ergebnisse zeigten, dass sich die Abkühlzeiten von 1.5 kg Silikonöl in dem gewählten Temperaturbereich von 125 bis 100 °C um 350% erhöhten, wenn sie mit dem TES auf Erythritol-Basis getestet wurden, als wenn sie allein getestet wurden. Im Gegensatz dazu verlängerte sich die Abkühlzeit der gleichen Masse Silikonöl im flüssigen Temperaturbereich von 110-80 °C um 346%, wenn sie mit dem TES auf Xylitol-Basis getestet wurde, das mit einem Handrührer ausgestattet war, um die Keimbildung des Materials zu stimulieren, als wenn sie allein getestet wurde.

Die experimentellen Daten des letztgenannten Geräts wurden zur Validierung des mathematischen Modells verwendet, das speziell zur Simulation der thermodynamischen Leistung des Geräts entwickelt wurde. Die Ergebnisse des Modells stimmen sehr gut mit der Realität überein, da es die Temperatur von Wasser und Silikonöl in der Erhitzungsphase der ausgewählten Tests mit einer durchschnittlichen Abweichung von den experimentellen Daten von 3% bzw. 8% simuliert.

Non chi comincia ma quel che persevera.

— Nave scuola Amerigo Vespucci, 1978

Acknowledgments

First of all, I would like to thank my mentors Prof. Dr. Giovanni Di Nicola and Prof. Dr.ir. Eddie Koenders for their advice, support and cooperation during my doctoral career between Italy and Germany. I would also like to thank Dr. Mariano Pierantozzi, Dr. Giovanni Ferrarini, Prof. Dipl.-Ing. Schäfer and Prof. Dr.-Ing. Eichhorn for reviewing this thesis.

Sincere thanks go to all those who worked with me during these three years, my colleagues at DIISM (Dipartimento di Ingegneria Industriale e Scienze Matematiche) and WiB (Institut für Werkstoffe im Bauwesen). In particular, thank you to Dr. Sebastiano Tomassetti, Dr. Gianluca Coccia, Dr. Francesco Pio Muciaccia, and Dr. Ignacio Peralta for the constant discussion and exchange of views, a necessary requirement to carry out research activities in the best possible way.

I would also like to thank the laboratory technicians at DIISM and WiB for their help in laboratory activities and during the various experimental campaigns, and all the students I tutored during the course of their internships and with whom I had the pleasure of sharing my experience.

I cannot mention the full list of people I would like to thank as it is too long, hoping for everyone's understanding.

My thanks also go to Eng. Matteo Muccioli, designer of some prototype solar panel cookers that I had the pleasure to build and test during my work, for his valuable advice during the design phase and during the outdoor experimental campaigns.

A very special thanks goes to my family, my parents and my brother for their continuous support and backing especially during times of discouragement and distance.

Finally, I would like to thank Giovanni for continuously motivating me not to give up, for his constant support and for being there on a daily basis; without him and my parents, I don't think I would have been able to complete this journey with these results.

Darmstadt, February 2023 Alessia Aquilanti

Introduction

The global demand for energy is constantly growing due to demographic and industrial development. To increasingly reduce the consumption of highly polluting fossil fuels, the use of renewable sources must be preferred and supported. Of the renewable sources found in nature, solar energy is the most abundant clean source on earth. However, applications using solar energy as a source have the problem that solar radiation is variable during the course of the day, with a consequent negative impact on the final efficiency of the system. A possible solution to this problem is to combine the system with storage devices capable of releasing energy when needed, i.e. when the radiation is intermittent (cloudy day) or completely absent (night hours).

The work presented studies a possible application of solar thermal energy, namely solar cooking. The thesis focuses on different types of solar cookers, i.e. systems capable of converting solar radiation into heat through the use of reflecting mirrors, the implementation of thermal storage systems (TES) and the characterization of phase change materials (PCM). It deals with the experimental thermal and optical characterization of prototypes implemented at the Dipartimento di Ingegneria Industriale e Scienze Matematiche (DIISM) of Università Politecnica delle Marche (UNIVPM) together with the mathematical model of one of them, which was validated with the tests carried out during an outdoor experimental campaign.

The thesis is divided into eight chapters. The state of the art is presented in Chapter 1, which is about solar thermal engineering fundamentals and the classification of solar cookers available on the market. The concept of energy savings associated with sustainable development is introduced with a focus on solar thermal and solar cooking. Several prototypes of solar cookers are presented.

One way to compensate for the variability of solar radiation is to use energy storage systems. The main forms of energy that can be stored include mechanical, electrical and thermal energy. As far as thermal energy storage is concerned, this can be stored in the form of latent heat through the phase transition of the material. The most exploited phase transition is that from solid to liquid and vice versa. Different types of PCM have been analysed in literature: paraffins, sugar alcohols, fatty acids, hydrated salts, metals, eutectic mixtures. In Chapter 2, the characteristics that a solid-liquid PCM should possess in order to be considered suitable for the design of a thermal storage system are described. In addition, the results of the thermophysical property measurements and thermal stability analysis obtained from the experimental campaign carried out in the micro-laboratory at the Institut für Werkstoffe im Bauwesen (WiB) of the Technische Universität Darmstadt (TU Darmstadt) are reported. In detail, using a differential scanning calorimeter (DSC), the temperatures and enthalpies of melting and crystallization were assessed, while a thermogravimetric analysis determined the maximum degradation temperatures of the six substances selected. The PCMs selected belong to the sugar alcohols family and are xylitol, sorbitol, erythritol, mannitol,

inositol and dulcitol. The measurements obtained from the experimental campaign were compared with those found in literature. Taking into account the melting temperature range and their thermophysical properties, the sugars above were considered suitable for use as PCMs in solar cookers for applications in the low to medium temperature range (80-250 °C).

The design, construction stages and experimental campaign of a prototype high-efficiency solar box cooker is presented in Chapter 3. The prototype, which is based on a design found in literature, has a concentration ratio of 11.57. During its construction, in order to increase its thermal insulation and optical efficiency, a number of components were modified, i.e. a black paint was used to increase the absorbance of the cooking chamber, a special aluminum film was used to increase the reflectivity of the reflective surfaces, double glazing was inserted and different insulation materials were selected. The cooker consists of a metal box that serves as a cooking chamber, which is closed at the top by double tempered glass. The cooking chamber is inserted inside a suitably insulated wooden structure. At the top, there is a double row of mirrors, each at a different angle to the horizontal plane. The oven is equipped with wooden handles and wheels to facilitate transport and its azimuthal orientation. The zenithal orientation is possible thanks to a rotation around the horizontal axis. The tilting plate, which is inserted inside the cooking chamber, holds the pot in position during testing while the zenith orientation changes.

The design and construction phases of a prototype concentrating solar cooker and the experimental campaign carried out using the prototype are presented in Chapter 4. The prototype was built following the construction specifications provided by the Danish company Heliac. It has a concentration ratio of 40.97 and consists mainly of a wooden lattice support structure equipped with wheels to facilitate transport and orientation with respect to the sun, and two wooden frames: a larger one to support the special lens and a smaller one to house the reflective surface. The Fresnel lens is able to concentrate the incident solar radiation at a small point on the reflective surface, which reflects the concentrated rays back to the cooking surface, i.e. the place where the pot is placed during testing.

The design and construction phases of two prototype panel solar cookers and the experimental campaign carried out using the two prototypes are presented in Chapter 5. Both prototypes were built according to the specifications of Engineer Matteo Muccioli. The first device, called the Newton solar cooker, is characterized by a prism-shaped glass cooking chamber and two reflective surfaces of different sizes. Its peculiarity with respect to other devices discussed so far is that it has a variable geometry. In fact, by changing the inclination of the primary and secondary mirrors (θ_1 and θ_2) with respect to the horizontal plane, the aperture area of the device changes. A simple 2D model was developed to find the optimal $\theta_1 - \theta_2$ pair as a function of sun elevation. The data obtained was entered into a table and used during the experimental campaign. Knowing the geographical coordinates of the terrace where the tests were carried out on the roof of the department, the exact angle of the sun's elevation at the beginning of the test could be calculated, and with this, the corresponding θ_1 and θ_2 were read in the table. With these two values, the inclinations of the primary and secondary mirrors were adjusted. The sun's elevation was calculated every 15 to 20 minutes and, in accordance, the inclinations of the two mirrors changed. The second panel device implemented, called the Kimono solar cooker, consists of several acrylic panels covered with a reflective material and joined together. Of all the prototypes made at DIISM, this one is the simplest and most economical tested in the laboratory to date. The cooking chamber consists of a glass container with a black cake tin inside covered by a

glass lid. During the experimental campaign, the Kimono solar cooker was tested in parallel with three other panel devices in order to compare its thermal performance with that of the other devices.

The design and construction phases of a medium-efficiency solar box cooker prototype and the experimental campaign carried out using the prototype are presented in Chapter 6. The prototype, which is based on a design found in literature, has a concentration ratio of 4.08. The device consists of a wooden outer box with a galvanized steel cooking chamber inside. The box has an easily removable tempered glass cover to allow the pot to be placed on the tilting plate inside the cooking chamber during the various tests. The upper part of the cooker consists of a system of 8 mirrors of two different shapes, i.e. square and wedge-shaped respectively. The special feature of the analysis carried out with this device is that, during the experimental campaign, in addition to vacuum and load tests, tests were also carried out by loading the thermal storage system based on phase change materials inside the cooking chamber. The realization of the TES is described in detail by providing the necessary steps to prepare the phase change material before the tests with the solar furnace can be carried out.

The development of the mathematical model describing the thermal behavior of the device introduced in Chapter 6 is presented in Chapter 7. The conductive, convective and radiative heat exchanges of seven elements of the solar furnace were considered: the pot lid, the pot, the fluid, the glass, the cooking chamber, the air inside the cooking chamber and the air inside the pot. The energy balance equations of the seven elements form the system of differential equations to be solved. To conclude, Chapter 8 provides some critical conclusions and future developments of the work presented.

With the aim of providing a complete overview of solar cookers, Appendix A, Appendix B and Appendix C describe the parameters derived from international procedures and standards with which solar ovens were characterized, the instrumentation used in the test rig to conduct the tests, and the geometric parameters, optical and thermophysical properties of the oven elements used in the development of the model, respectively.

Introduzione

La domanda globale di energia è costantemente in crescita a causa dello sviluppo demografico e industriale. Per ridurre sempre più il consumo di fonti fossili altamente inquinanti, l'utilizzo di fonti rinnovabili deve essere preferito e sostenuto. Tra le fonti rinnovabili presenti in natura, l'energia solare è la fonte pulita più abbondante sulla terra. Le applicazioni che utilizzano come fonte quella solare hanno il problema della variabilità che la radiazione solare presenta durante il corso della giornata, con un conseguente impatto negativo sull'efficienza finale del sistema. Una possibile soluzione a tale problema è quella di abbinare il sistema a dispositivi di accumulo in grado di rilasciare l'energia quando necessaria, ovvero quando la radiazione è intermittente (giornata nuvolosa) o del tutto assente (ore notturne).

Il presente lavoro studia una possibile applicazione dell'energia solare termica, ovvero la cottura solare. Questa tesi infatti è focalizzata su diverse tipologie di forni solari, sistemi abili a convertire la radiazione solare in calore attraverso l'utilizzo di specchi riflettenti, sulla realizzazione di sistemi di accumulo termico (TES) e sulla caratterizzazione di materiali a cambiamento di fase (PCM). Questo manoscritto tratta la caratterizzazione sperimentale termica e ottica di prototipi realizzati nel Dipartimento di Ingegneria Industriale e Scienze Matematiche (DIISM) dell'Università Politecnica delle Marche (UNIVPM) insieme al modello matematico di uno di questi, validato con i test effettuati durante la campagna sperimentale all'aperto.

Il manoscritto è diviso in otto capitoli. Lo stato dell'arte è presentato nel Capitolo 1, che presenta gli aspetti fondamentali del solare termico e la classificazione dei forni solari disponibili sul mercato. Il concetto di risparmio energetico associato allo sviluppo sostenibile viene introdotto, ponendo particolare attenzione al tema del solare termico e della cottura solare. Diversi prototipi di forni solari sono presentati.

Un modo per sopperire alla variabilità della radiazione solare consiste infatti nell'utilizzo di sistemi di accumulo dell'energia. Tra le forme principali di energia che si possono accumulare ci sono quella meccanica, quella elettrica e quella termica. Per quanto riguarda l'accumulo di energia termica, questa può essere accumulata sotto forma di calore latente attraverso la transizione di fase del materiale. La transizione di fase più sfruttata è quella da solido a liquido e viceversa. Tipi differenti di PCM sono stati analizzati in letteratura: paraffine, polialcoli, acidi grassi, sali idrati, metalli, miscele eutettiche. Nel Capitolo 2, dopo avere descritto le caratteristiche che un PCM solido-liquido dovrebbe possedere per essere considerato adatto al design di un sistema ad accumulo termico, vengono riportati i risultati delle misure delle proprietà termofisiche e dell'analisi della stabilità termica ottenute dalla campagna sperimentale effettuata nel microlaboratorio presso l' Institut für Werkstoffe im Bauwesen (WiB) della Technische Universität Darmstadt (TU Darmstadt). Nel dettaglio, attraverso un calorimetro differenziale a scansione (DSC) sono state valutate le temperature e le entalpie di fusione e cristallizzazione, mentre attraverso un'analisi termogravimetrica

sono state determinate le temperature massime di degradazione delle sei sostanze selezionate. I PCMs scelti appartengono alla famiglia dei polialcoli e sono: xilitolo, sorbitolo, eritritolo, mannitolo, inositolo e dulcitolo. Le misure ottenute dalla campagna sperimentale sono state confrontate con quelle presenti nella letteratura. Considerando l'intervallo di temperature di fusione e le loro proprietà termofisiche, gli zuccheri sono considerati adatti per l'utilizzo come PCM nei forni solari per applicazioni negli intervalli di temperatura medio-bassi (80-250 °C).

La progettazione, le fasi realizzative e la campagna sperimentale di un prototipo di forno solare a scatola ad alta efficienza è presentato nel Capitolo 3. Il prototipo, basato su un progetto presente in letteratura, ha un rapporto di concentrazione di 11.57. Durante la sua costruzione, con lo scopo di aumentarne l'isolamento termico e l'efficienza ottica, sono stati modificati alcuni componenti: è stata utilizzata una vernice nera per aumentare l'assorbanza della camera di cottura, è stato utilizzato un particolare film di alluminio per aumentare la riflettanza delle superfici riflettenti, è stato inserito un doppio vetro di chiusura e sono stati selezionati differenti materiali isolanti. Il forno è composto da una scatola di metallo che funge da camera di cottura chiusa superiormente dal doppio vetro temperato. La camera di cottura è inserita all'interno di una struttura lignea opportunatamente isolata. Nella parte alta del sistema c'è una doppia fila di specchi, ciascuna con un angolo di inclinazione differente rispetto al piano orizzontale. Il forno è dotato di maniglie di legno e ruote per agevolare il trasporto e la sua orientazione azimutale. L'orientamento zenitale è possibile grazie ad una rotazione intorno all'asse orizzontale. La piastra basculante, inserita all'interno della camera di cottura, mantiene in posizione la pentola durante le prove mentre l'orientamento zenitale cambia.

La progettazione, le fasi realizzative e la campagna sperimentale di un prototipo di forno solare a concentrazione è presentato nel Capitolo 4. Il prototipo è stato costruito seguendo le specifiche realizzative fornite dalla compagnia danese Heliac. Ha un rapporto di concentrazione pari a 40.97 ed è principalmente costituito da una struttura di supporto reticolare lignea dotata di ruote per agevolare il trasporto e l'orientamento rispetto al sole e da due cornici lignee: una di dimensioni maggiori per il supporto della lente speciale ed una più piccola per alloggiare la superficie riflettente. La lente di Fresnel è in grado di concentrare la radiazione solare incidente in un punto ridotto della superficie riflettente, la quale riflette i raggi concentrati verso la superficie di cottura, cioè il punto dove la pentola è posizionata durante i test.

La progettazione, le fasi realizzative e la campagna sperimentale di due prototipi di forni solari a pannelli sono presentati nel Capitolo 5. Entrambi i prototipi sono stati realizzati seguendo le specifiche dell'ingegnere Matteo Muccioli. Il primo dispositivo, chiamato Newton solar cooker, è caratterizzato da una camera di cottura in vetro a forma di prisma e da due superfici riflettenti di dimensioni diverse. La sua particolarità, rispetto agli altri dispositivi fino ad ora trattati, è che presenta una geometria variabile: infatti cambiando l'inclinazione degli specchi primario e secondario (θ_1 e θ_2) rispetto al piano orizzontale, l'area di apertura del dispositivo cambia. È stato sviluppato un semplice modello 2D per trovare la coppia $\theta_1 - \theta_2$ ottima in funzione dell'elevazione del sole. I dati ottenuti sono stati inseriti in una tabella e utilizzati durante la campagna sperimentale. Conoscendo le coordinate geografiche della terrazza dove si svolgevano le prove sul tetto del dipartimento, ad inizio prova veniva calcolato l'angolo di elevazione esatto del sole e con questo si leggevano i θ_1 e θ_2 corrispondenti. Con questi due valori, si regolavano le inclinazioni dello specchio primario e secondario. L'elevazione del sole veniva calcolata ogni 15/20 minuti e, in accordo, le inclinazioni dei due specchi modificate. Il secondo dispositivo a pannelli realizzato, chiamato Kimono solar cooker,

è costituito da diversi pannelli in acrilico ricoperti da un materiale riflettente uniti tra di loro. Questo, tra tutti i prototipi realizzati al DIISM, risulta il più semplice e più economico ad oggi testato in laboratorio. La camera di cottura è costituita da un contenitore di vetro con al suo interno una tortiera nera ricoperti da un coperchio in vetro. Durante la campagna sperimentale, il Kimono è stato testato in parallelo con altri 3 dispositivi a pannelli con il fine di confrontare le sue prestazioni termiche con quelle degli altri dispositivi.

La progettazione, le fasi realizzative e la campagna sperimentale di un prototipo di forno solare a scatola a media efficienza è presentato nel Capitolo 6. Il prototipo, basato su un progetto presente in letteratura, ha un rapporto di concentrazione di 4.08. Il dispositivo è costituito da una scatola esterna di legno con all'interno la camera di cottura in acciaio zincato. La scatola ha una copertura in vetro temperato facilmente rimuovibile per permettere il posizionamento della pentola sulla piastra basculante all'interno della camera di cottura durante i diversi test. La parte superiore del forno è composta dal sistema di 8 specchi di due forme diverse: quadrati e a cuneo, rispettivamente. La particolarità dell'analisi effettuata con questo dispositivo è che, durante la campagna sperimentale, oltre alle prove a vuoto e a carico sono state effettuate anche prove introducendo all'interno della camera di cottura il sistema di accumulo termico basato su materiali a cambiamento di fase. La realizzazione del TES viene descritta nel dettaglio fornendo gli step necessari per preparare il materiale a cambiamento di fase prima di poter effettuare i test con il forno solare.

Lo sviluppo del modello matematico che descrive il comportamento termico del dispositivo introdotto nel Capitolo 6 è presentato nel Capitolo 7. Sono stati considerati gli scambi termici conduttivi, convettivi e radiativi di sette elementi del forno solare: il coperchio della pentola, la pentola, il fluido, il vetro, la camera di cottura, l'aria all'interno della camera di cottura e l'aria all'interno della pentola. Le equazioni di bilancio energetico dei sette elementi vanno a costituire il sistema di equazioni differenziali da risolvere.

Per concludere, il Capitolo 8 riporta alcune conclusioni critiche e gli sviluppi futuri del lavoro presentato.

Con lo scopo di fornire una visione completa sui forni solari, l'Appendice A, l'Appendice B e l'Appendice C descrivono i parametri derivanti da procedure e standard internazionali con i quali sono stati caratterizzati i forni solari, la strumentazione utilizzata nel banco prova per condurre i test e i parametri geometrici, le proprietà ottiche e termofisiche degli elementi del forno utilizzati per lo sviluppo del modello, rispettivamente.

Einführung

Die weltweite Energienachfrage nimmt aufgrund der demografischen und industriellen Entwicklung ständig zu. Um den Verbrauch von stark umweltschädlichen fossilen Brennstoffen zunehmend zu verringern, muss die Nutzung erneuerbarer Energiequellen bevorzugt und gefördert werden. Von den in der Natur vorkommenden erneuerbaren Energiequellen, ist die Solarenergie die am häufigsten vorkommende saubere Energiequelle der Erde. Anwendungen, die Sonnenenergie als Energieträger nutzen, haben das Problem, dass die Sonneneinstrahlung selbst im Laufe des Tages schwankt, was sich negativ auf die endgültige Effizienz des Systems auswirkt. Eine mögliche Lösung dieses Problems besteht darin, das System mit Speichervorrichtungen zu kombinieren, die in der Lage sind, Energie dann freizusetzen, wenn sie benötigt wird, d. h. wenn die Strahlung intermittierend ist (bewölkter Tag) oder völlig fehlt (Nachtstunden).

Die vorliegende Arbeit untersucht eine mögliche Anwendung der thermischen Solarenergie, nämlich das solare Kochen. Im Mittelpunkt dieser Arbeit stehen verschiedene Arten von Solaröfen, Systeme zur Umwandlung von Sonnenstrahlung in Wärme durch den Einsatz von reflektierenden Spiegeln, die Realisierung von Wärmespeichern und die Charakterisierung von Phasenwechselmaterialien. Dieses Manuskript befasst sich mit der experimentellen thermischen und optischen Charakterisierung von Prototypen, die in der Dipartimento di Ingegneria Industriale e Scienze Matematiche (DIISM) der Università Politecnica delle Marche (UNIVPM) realisiert wurden, sowie mit dem mathematischen Modell eines dieser Prototypen, das mit den während der Versuchskampagne im Freien durchgeführten Tests validiert wurde.

Das Manuskript ist in acht Kapitel unterteilt. Der Stand der Technik wird in Kapitel 1 vorgestellt, das sich mit den Grundlagen der Solarthermie und der Klassifizierung der auf dem Markt erhältlichen Solarkocher befasst. Das Konzept der Energieeinsparung im Zusammenhang mit nachhaltiger Entwicklung wird mit Schwerpunkt auf Solarthermie und solares Kochen vorgestellt. Verschiedene Prototypen von Solarkochern werden vorgestellt.

Eine Möglichkeit, die Schwankungen der Sonneneinstrahlung auszugleichen, ist der Einsatz von Energiespeichersystemen. Zu den wichtigsten Formen von Energie, die gespeichert werden können, gehören mechanische, elektrische und thermische Energie. Was die Speicherung thermischer Energie betrifft, so kann diese in Form von latenter Wärme durch den Phasenübergang des Materials gespeichert werden. Der am meisten genutzte Phasenübergang ist der von fest zu flüssig und umgekehrt. In der Literatur wurden verschiedene Arten von PCM untersucht: Paraffine, Zuckeralkohole, Fettsäuren, Salzhydrate, Metalle und eutektische Gemische. In Kapitel 2 werden nach einer Beschreibung der Eigenschaften, die ein fest-flüssiges PCM besitzen sollte, um für die Auslegung eines Wärmespeichersystems als geeignet zu gelten, die Ergebnisse der Messungen der thermophysikalischen Eigenschaften und der Analyse

der thermischen Stabilität gezeigt, die im Rahmen der im Mikrolabor des Instituts für Werkstoffe im Bauwesen (WiB) der Technischen Universität Darmstadt (TU Darmstadt) durchgeführten Versuchskampagne gewonnen wurden. Im Einzelnen wurden mit Hilfe eines Differential-Scanning-Calorimeter (DSC) die Temperaturen und Enthalpien des Schmelzens und der Kristallisation ermittelt, während eine thermogravimetrische Analyse die maximalen Zersetzungstemperaturen der sechs ausgewählten Stoffe bestimmte. Die ausgewählten PCMs gehören zur Familie der Zuckeralkohole und sind: Xylitol, Sorbitol, Erythritol, Mannitol, Inositol und Dulcitol. Die bei der Versuchskampagne gewonnenen Messdaten wurden mit den in der Literatur gefundenen Werten verglichen. In Anbetracht des Schmelztemperaturbereichs und ihrer thermophysikalischen Eigenschaften werden die Zucker als geeignet für die Verwendung als PCM in Solaröfen für Anwendungen im niedrigen bis mittleren Temperaturbereich (80-250 °C) angesehen.

Der Entwurf, die Bauphasen und die Versuchskampagne eines Prototyps eines hocheffizienten solaren Kastenofens werden in Kapitel 3 vorgestellt. Der Prototyp, der auf einem in der Literatur gefundenen Entwurf basiert, hat ein Konzentrationsverhältnis von 11.57. Während des Baus wurden zur Erhöhung der Wärmedämmung und der optischen Effizienz des Prototyps eine Reihe von Komponenten verändert: Es wurde eine schwarze Farbe verwendet, um die Absorption der Kochkammer zu erhöhen, eine spezielle Aluminiumfolie wurde verwendet, um das Reflexionsvermögen der reflektierenden Oberflächen zu erhöhen, eine Doppelverglasung wurde eingesetzt und verschiedene Dämmstoffe wurden ausgewählt. Der Ofen besteht aus einem Metallkasten, der als Kochkammer dient und oben durch doppeltes gehärtetes Glas geschlossen ist. Die Kochkammer befindet sich in einer entsprechend isolierten Holzkonstruktion. An der Oberseite befindet sich eine doppelte Reihe von Spiegeln, die jeweils in einem anderen Winkel zur horizontalen Ebene stehen. Der Ofen ist mit Holzgriffen und Rädern ausgestattet, um den Transport und die azimutale Ausrichtung zu erleichtern. Die Ausrichtung im Zenit ist durch eine Drehung um die horizontale Achse möglich. Die Kippplatte, die sich im Inneren der Garkammer befindet, hält den Topf während der Versuche in Position, während sich die Zenitausrichtung ändert.

Der Entwurf, die Bauphasen und die Versuchskampagne eines Prototyps eines konzentrierenden Solarofens werden in Kapitel 4 vorgestellt. Der Prototyp wurde nach den von der dänischen Firma Heliac bereitgestellten Konstruktionsspezifikationen gebaut. Er hat ein Konzentrationsverhältnis von 40.97 und besteht im Wesentlichen aus einem Holzgitter, das mit Rädern ausgestattet ist, um den Transport und die Ausrichtung zur Sonne zu erleichtern, sowie aus zwei Holzrahmen: einem größeren, der die Speziallinse trägt, und einem kleineren, der die reflektierende Oberfläche aufnimmt. Die Fresnel-Linse ist in der Lage, die einfallende Sonnenstrahlung auf einen kleinen Punkt auf der Reflexionsfläche zu konzentrieren, die die konzentrierten Strahlen zurück auf die Kochfläche reflektiert, d. h. auf den Ort, an dem der Topf während des Versuchs platziert wird.

In Kapitel 5 werden der Entwurf, die Bauphasen und die Versuchskampagne von zwei Prototypen von Solarpanelöfen vorgestellt. Beide Prototypen wurden nach den Vorgaben des Ingenieurs Matteo Muccioli gebaut. Das erste Gerät, der Newton-Solarkocher, zeichnet sich durch eine prismenförmige Glaskochkammer und zwei unterschiedlich große reflektierende Flächen aus. Seine Besonderheit im Vergleich zu anderen bisher beschriebenen Geräten besteht darin, dass er eine variable Geometrie hat. Indem man die Neigung des Primär- und des Sekundärspiegels (θ_1 und θ_2) gegenüber der horizontalen Ebene verändert, ändert sich der Blendenbereich des Geräts. Es wurde ein einfaches 2D-Modell entwickelt, um das optimale Paar $\theta_1 - \theta_2$ in Abhängigkeit von der

Sonnenhöhe zu finden. Die gewonnenen Daten wurden in eine Tabelle eingetragen und während der Versuchskampagne verwendet. In Kenntnis der geografischen Koordinaten der Terrasse auf dem Dach des Departements, auf der die Versuche durchgeführt wurden, wurde der genaue Höhenwinkel der Sonne zu Beginn des Versuchs berechnet, und damit die entsprechenden θ_1 und θ_2 in die Tabelle eingelesen. Mit diesen beiden Werten wurden die Neigungen von Primär- und Sekundärspiegel eingestellt. Alle 15 bis 20 Minuten wurde die Sonnenhöhe berechnet und dementsprechend die Neigungen der beiden Spiegel verändert. Das zweite realisierte Panelgerät, der Kimono-Solarkocher, besteht aus mehreren Acrylglasplatten, die mit einem reflektierenden Material überzogen und miteinander verbunden sind. Von allen am DIISM hergestellten Prototypen ist dieser der einfachste und wirtschaftlichste, der bisher im Labor getestet wurde. Die Kochkammer besteht aus einem Glasbehälter, in dem sich eine schwarze Kuchenform befindet, die mit einer Glasscheibe abgedeckt ist. Während der Versuchskampagne wurde der Kimono parallel zu drei anderen Plattengeräten getestet, um seine thermische Leistung mit der der anderen Geräte zu vergleichen.

Der Entwurf, die Bauphasen und die Versuchskampagne eines Prototyps eines Solarkastenofens mit mittlerem Wirkungsgrad werden in Kapitel 6 vorgestellt. Der Prototyp, der auf einem in der Literatur gefundenen Entwurf basiert, hat ein Konzentrationsverhältnis von 4.08. Das Gerät besteht aus einem hölzernen Außenkasten mit einer Kochkammer aus verzinktem Stahl im Inneren. Der Kasten hat eine leicht abnehmbare Abdeckung aus gehärtetem Glas, damit der Topf während der verschiedenen Tests auf die Kippplatte im Inneren der Kochkammer gestellt werden kann. Der obere Teil des Ofens besteht aus einem System von 8 Spiegeln in zwei verschiedenen Formen: quadratisch bzw. keilförmig. Die Besonderheit der mit diesem Gerät durchgeführten Analyse besteht darin, dass während der Versuchskampagne neben Leerlauf- und Belastungstests auch Tests durch Beladung des Wärmespeichersystems auf der Basis von Phasenwechselmaterialien innerhalb der Kochkammer durchgeführt wurden. Die Realisierung des TES wird im Detail beschrieben, indem die notwendigen Schritte zur Vorbereitung des Phasenwechselmaterials angegeben werden, bevor die Tests mit dem Solarofen durchgeführt werden können.

Die Entwicklung des mathematischen Modells zur Beschreibung des thermischen Verhaltens der in Kapitel 6 vorgestellten Vorrichtung wird in Kapitel 7 vorgestellt. Der leitende, konvektive und strahlende Wärmeaustausch von sieben Elementen des Solarofens wurde berücksichtigt: der Topfdeckel, der Topf, die Flüssigkeit, das Glas, die Kochkammer, die Luft in der Kochkammer und die Luft im Topf. Die Energiebilanzgleichungen der sieben Elemente bilden das zu lösende System von Differentialgleichungen.

Abschließend werden in Kapitel 8 einige kritische Schlussfolgerungen und künftige Entwicklungen der vorgestellten Arbeit dargelegt.

Um einen vollständigen Überblick über Solaröfen zu geben, beschreiben Anhang A, Anhang B und Anhang C die aus internationalen Verfahren und Normen abgeleiteten Parameter, mit denen Solaröfen charakterisiert wurden, die im Prüfstand zur Durchführung der Tests verwendete Instrumentierung sowie die geometrischen Parameter, optischen und thermophysikalischen Eigenschaften der bei der Entwicklung des Modells verwendeten Ofenelemente.

Chapter 1

Overview on Solar Thermal Energy

In this chapter an overview on solar thermal energy and its applications will be given. Particular attention will be paid to the solar cooking sector. Different kinds of solar cooker devices will be presented, each with their own characteristics and peculiarities. The materials as well as the working principles will also be part of the treatment. Finally, the solar box cooker which is one of the main subjects of this thesis will be presented.

1.1 Solar Thermal Energy

Energy is a thermodynamic quantity that is often understood as the capacity of a physical system to perform work. In addition to this meaning, energy is fundamental to our relations with the environment. Research to solve energy-related problems is significant as life is directly influenced by it and its consumption. In the last forty years the world energy consumption has doubled and it is clear that, in the future, the problems related to the limited availability of fossil energy resources (oil and gas) and to the increase in emissions due to their use will take on ever greater importance.

Despite electricity demand being the priority, civil and industrial processes play an important role: in fact, heat production at the moment accounts for more than 50% of global final energy consumption [10]. An important aspect to highlight is that heat use per capita is very similar in the different regions of the world, but this cannot be said to the total energy use per capita, implying that thermal energy requirements have a profound impact on all countries.

In 2011 global energy use for heat production in industry, buildings and other sectors reached 172 EJ, about three-quarters of which (129 EJ) produced by means of fossil sources, causing around 10 Gt of CO_2 emissions per year. This represents a third of the global total emissions in the energy sector.

Two thirds of energy demand in Europe consists of heat, and half of this demand (it was about 300 TWh in 2000) is required at temperatures up to 250 °C. Low-temperature heat consumption is estimated to be globally about 10 EJ per year, and this only for hot water production [11].

To cope with these facts, it will be necessary to use energy in an increasingly more efficient way. This means that, in order to keep satisfying our needs, we will have to

make and use products and services using as little energy as possible. In this regard, the production of clean energy becomes more and more crucial from day to day due to the growing importance of environmental protection issues. Especially after the 1973 oil crisis, with the sudden rise in fuel prices, there was a strong increase in research on technologies that use renewable energy.

Currently, the supply of renewable energy resources is around 14% of the global total energy demand and a potential increase for the future is expected. It is important to note that energy saving, linked to sustainable development, has become in the recent years a central topic in scientific research in various technological fields. All this is closely related to the energy problem that plagues our planet.

The United Nations General Assembly (UNGA) in 2015 with the Sustainable Development Goals (SDGs) provided a powerful framework for international cooperation to achieve a sustainable future for the planet. A global energy transition is urgently needed to meet the objectives of limining average global surface temperature increase below 2 °C [12]. A transition away from fossil fuels to low-carbon solutions will play an essential role, as energy-related carbon dioxide (CO_2) emissions represent two-thirds of all greenhouse gases (GHG) [13]. This energy transition will be enabled by technological innovation, notably in the field of renewable energy.

Under the name of energy saving, various techniques are used to reduce the consumption of energy necessary to perform human activities and the energy-related CO_2 emission. It can be achieved either by modifying energy processes so that there is less waste, or by transforming energy from one form to another in a more efficient way. Among clean energy technologies, solar energy is recognized as one of the most promising choices as it is free, clean and environmentally friendly.

The sun, in fact, offers a wide variety of applications to exploit this energy source. Among the thermal applications of solar energy, solar cooking is considered as one of the simplest and most valid methods in terms of energy use [14], but even today the energy required for cooking is supplied by non-commercial fuels such as firewood, agricultural residues, animal dung and kerosene. In addition to the environmental and economic impact of using wood, there are some serious health issues such as eye problems and lung diseases that come precisely from the use of firewood. The World Health Organization (WHO) also pointed out that 1.6 million deaths a year are caused by air pollution [14], therefore there is a growing focus on the evaluation of various renewable energy options, so as to meet the cooking needs of people living in developing countries.

It is well known that most countries in the developing world benefit from abundant solar radiation, with average intensity of illumination every day in the range of 5-7 kWh/m^2 and have more than 275 days of sunshine in a year [15]. From this point of view, it can easily be said that solar cookers have great potential in these countries in order to satisfy energy needs, especially in the domestic sector. Furthermore, the use of solar cookers provides many advantages such as no recurring costs and high nutritional value of foods. Unfortunately, the large-scale dissemination of solar cookers still remains limited; such devices are diffused all over the world, but most of them are intended for research purposes only [16]. The main obstacles to the dissemination of the technology are the resistance to acceptance as it is a new technology, variable nature of solar radiation, limited space availability in urban areas, and higher initial costs [17].

1.2 Historical Overview of Solar Cooking

The history of solar cookers dates back to the 18th century. Halacy [18] reported that the first experiments on solar cookers were carried out by a German physicist named Tschirn Hausen (1651-1708). In 1767, the French-Swiss physicist Horace de Saussure attempted to cook food using solar energy, building a miniature greenhouse with 5 layers of overturned glass boxes on a black table and tried to bake fruit.

The English astronomer Sir John Herschel attempted to cook food in an isolated box and did so in an expedition to South Africa in 1830. A French mathematician, Augustin Mouchot, instead integrated the idea of trapping heat through a mirror and in 1860 built an efficient solar cooker. He also managed to create a solar steam engine, but it was too big to be practical.

In 1876, W. Adams developed an octagonal solar cooker with 8 mirrors and reported that it allowed rations to be cooked for 7 soldiers in 2 hours. A year later, Mouchot designed solar cookers for French soldiers in Algeria and also wrote the first book on solar energy and its industrial applications. In 1891, Clarence Kemp, an American thermo-hydraulic manufacturer, invented the first commercial solar water heater. In 1894 Xiao Duck Shop of Sichuan, China, managed to roast ducks through the principle of solar cooking. In 1930, France sent many solar cookers to its colonies in Africa. Meanwhile, India has begun to analyse solar energy as an option to avoid deforestation. In 1940 Dr. Maria Telkes, in the United States, analysed various types of materials and also published in 1968 a book called "The Solar Cookers".

The first type of solar box cooker was produced by an Indian pioneer named Sri MK Ghosh in 1945 and in 1950 Indian researchers designed and built commercial solar cookers and solar reflectors, but were not readily accepted due to low cost alternatives.

Furthermore, at the United Nations Food and Agriculture Association (FAO) they examined the heating capacities of a parabolic cooker and another type of cooker. In 1961, a United Nations Conference on new energy sources was held. In 1970, following the increase in fuel prices due to the oil crisis, an intense interest in renewable energy technologies was observed. Barbara Kerr in the United States built different types of solar box cookers using recycled materials and aluminum foil. In 1979 water sterilization was carried out by Dr. Metcalf and his student Marshall Longvin, using a solar box cooker. Heather Gurley Larson in 1983, wrote the first solar cookbook in the United States, entitled "Solar Cooking Naturally".

Regarding academic research, Mullick presented a method in 1987 to analyse the thermal performance of solar cookers [19].

In 2000, Funk proposed a standard to test the efficiency of such cookers. It has been observed that the curve obtained from this international standard is useful for assessing the heat capacity of the solar cooker. Particularly in recent years, the focus has been very much on trying to improve the cooking power of these cookers. Numerous analytical, numerical and experimental studies have been carried out on new solar cookers projects, in order to be able to find the best type that can guarantee the best performance. To date, solar cooking technology is very promising, with the fundamental aim of reducing the gap between conventional and renewable energy sources.

1.3 Solar Cookers

A solar cooker is a device capable of accumulating solar energy over time, concentrating it in a defined space, until reaching useful temperatures for cooking food.

It then converts the energy produced by solar radiation into thermal energy. In this regard, it will be fundamental to re-orient the cooker towards the sun, guaranteeing its tracking, to balance the effect of the Earth's rotation.

Thanks to such a clean, accessible and free resource, it is possible to cook in a healthy and ecological way using a solar cooker. Being able to capture and concentrate the sun's rays and convert them into energy, these cookers can be used for food purposes, such as cooking food or sterilizing water to make it drinkable. Even today, in many countries of the world, the energy required for cooking food is not readily available, both for technological and economic reasons, so these devices represent a possible solution to this problem, with an economic advantage since the sun is a form of energy available everywhere and with the added advantage of not using fossil fuels or producing emissions. It is therefore 100% eco-friendly and environmentally sustainable.

A criticality of solar cookers is the close dependence on the solar energy source, as in its absence, like during nights, it is not possible to use it. To overcome this problem, an energy storage system can be added to solar cookers to greatly increase their efficiency.

A storage system used for solar cookers is a thermal system and there are two different approaches: one external to the solar cooker, formed by solar collectors that release energy to the cooker, one internal when materials with a thermal accumulation function are inserted in a cavity of the pots used for solar cooking.

The external storage system is used to provide a surplus of heat to a solar cooker to increase the temperature and to provide heat in case of limited or total absence of solar radiation. Various prototypes have been made: some use electric resistances inserted in the absorber plate of the cooker, which receive energy from an integrated system of photovoltaic panels, others on the other hand use an integrated system with solar collectors which, by means of a recirculation pump, sets a heat transfer fluid in motion which varies according to the required temperature range, bringing heat to the cooker.

In the second method to provide heat, special materials are used, called PCM (Phase Change Materials): a PCM is positioned in a cavity of the pot formed by two concentric cylinders, it heats up passing from the solid phase to the liquid phase (the melting temperature depends on the type and mixture of PCM used), and stores thermal energy. When the solar radiation is absent and the cooker temperature goes down, the heat stored by the PCM is released to the pot in the form of latent heat as the material changes state again from the liquid to the solid phase. In this way it is possible to cook food hours after sunset thanks to the heat stored and then returned by the heat storage medium.

1.4 Types of Solar Cookers and Their Characteristics

It is known that there are countless solar cooker possible implementations and variations in the world and they are continuously developed and improved by researchers and producers. Therefore, a classification of solar cookers becomes necessary.

Regarding their classifications, it is possible to have different classifications depending on how they are studied [20]. A first possible classification is according to how the heat energy from the sun is transferred to the pot. In this case, there are two possible categories: direct and indirect [21].

Another possible classification is according to the configuration of the device. In this case, it is possible to have three distinct categories: box cooker, concentrating

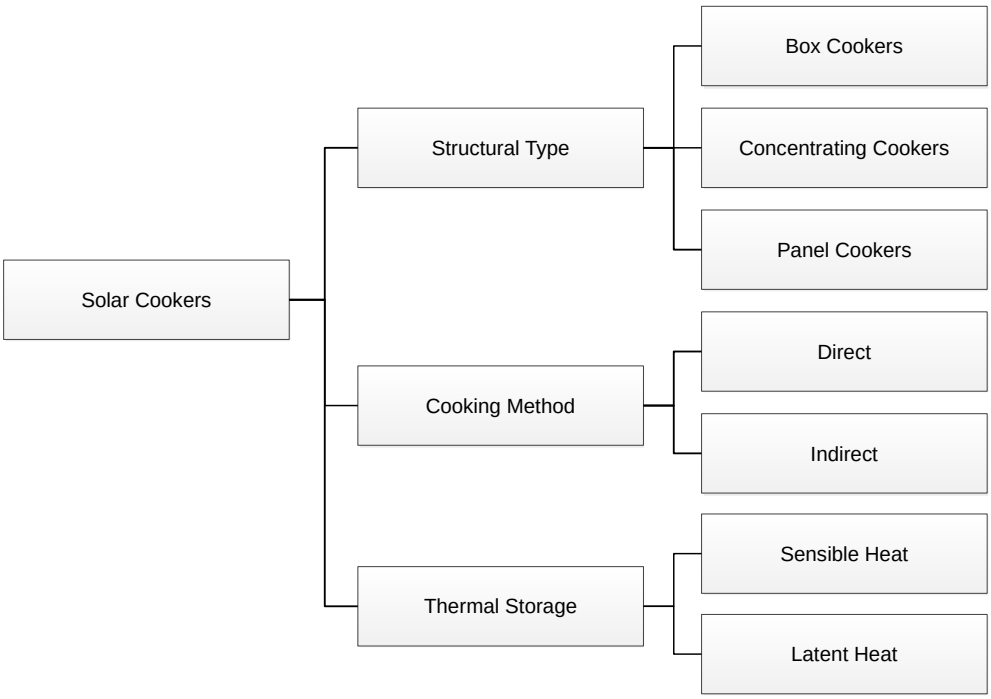

Figure 1.1: A general classification of solar cookers.

cooker and panel cooker [14].

As mentioned above, solar cookers can have a thermal storage system within their structure, resulting in the third possible classification. Solar cookers with thermal storage can be classified into two types: latent heat or sensible heat [22].

Figure 1.1 shows the three possible classifications graphically.

1.4.1 Solar Box Cookers

The history of solar cooking technology began with the invention of solar box cookers. They consist essentially of an insulated box with a transparent glass cover and surfaces reflecting direct sunlight. The inside of the box is painted black to maximize the absorption of sunlight. A maximum of four cooking containers are placed inside the box. A representation of a solar box cooker is shown in Figure 1.2

Each component of the solar box cooker has a significant influence on the cooking power. Therefore, the optimization of these parameters is vital to achieve maximum efficiency. Many researchers have been interested in analyzing this type of solar cooker [23], in fact it has been noticed that this type of cooker is slow to heat up, but works well even in the presence of diffuse radiation, loss of heat caused by the wind, intermittent cloudiness and low ambient temperature.

After the 1980s, research focused mainly on optimizing the geometric parameters of solar box cookers, given that these have a dominant effect on performance [24, 25]. In this context, the importance of aluminum mirrors has been explained, which increase the efficiency of the solar cooker by providing extra radiation [26]. The results indicated that the effectiveness of radiation concentration is highly dependent on the angle of the mirrors. Another fundamental element is the inner box, called absorber,

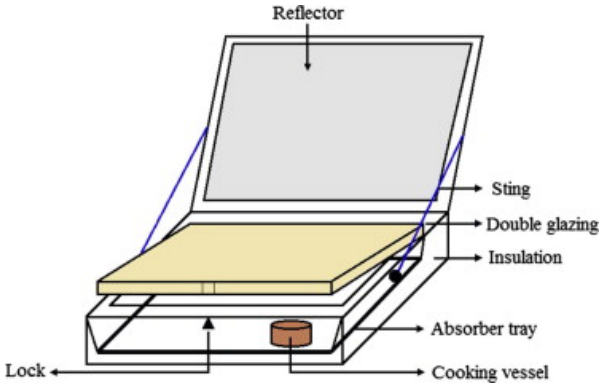

Figure 1.2: A solar box cooker [14].

which is one of the most significant components of a solar box cooker: solar radiation passes through the glass part and is absorbed by this surface, painted in black.

Simplicity of manufacture and operation is another advantage of box cookers, which provide also more stability and can keep the food warm for long periods of time. The payback period of a typical solar box cooker was evaluated around 12-14 months, even when used only 6-8 month a year [27].

Also when equipped with booster mirrors (and concentration ratios up to 10), solar box cookers rarely can go beyond 100 °C [17].

1.4.2 Solar Concentrating Cookers

Solar concentrating cookers are not as popular as the box prototypes. They are generally classified into two categories: parabolic and trough [16], although other special designs have been introduced [28].

The first parabolic solar cooker was developed in the early 1950s at the National Physical Laboratory, in India by Ghai and Bansal [29]. Subsequently, Lof et al. [30] analyzed different geometries and configurations regarding the assembly of this type of solar cooker. Parabolic solar cookers can reach high temperatures in a very short time. Unlike solar panel cookers or solar box cookers, they do not need a special cooking container. However, a parabolic cooker could run the risk of burning the food, if left unattended for a certain period of time, due to the concentrated heat. This cooker consists of a parabolic reflector with a cooking pot located on the focal point of the cooker itself and a support to carry the cooking system, as shown in Figure 1.3

1.4.3 Solar Panel Cookers

Solar panel cookers can be considered the most common type available due to their ease of construction and low-cost materials [31]. They are usually simple setups that can be easily produced [32]. In solar panel cookers, sunlight is concentrated from above. This method of solar cooking is not widely used as it provides limited cooking power.

On the other hand, this type of solar cooker is highly appreciated by those people who live alone or travel, as it is easily transportable. Such solar cookers use reflective equipment for the direct sunlight for a cooking vessel that is enclosed in a transparent plastic bag. Due to the flexibility of the structure, many different configurations have been designed [33, 34].

Figure 1.3: Parabolic solar cooker.

Figure 1.4: Panel solar cooker.

The solar panel cooker shown in Figure 1.4 is one of the most popular designs in this category. Only cardboard and film were used to produce this cooker, with the advantage of preserving food without burning it.

1.4.4 Solar Cookers with Thermal Storage

The main objective of thermal storage in solar cookers is to allow the device to cook while the sun is not available [35]. Usually, indirect cookers are equipped with thermal storage system [36], but also direct cookers can have thermal storage components [37].

In some cookers, the thermal storage and cooking units are the same [38, 39], while in other cases, separate units are considered [15, 40]. It is possible to have two types of solar cookers considering the thermal storage mode: latent heat thermal energy storage (LHTES) and sensible heat thermal energy storage (SHTES) [41].

In sensible heat storage, thermal energy is stored by raising the temperature of a solid or a liquid. For the purpose, researchers used engine oil [15], sand [42], and vegetable oil [43]. Limitations of sensible heat storage materials include low specific heat capacity and the decrease in effectiveness of cooking since the temperature of the

storage material decreases rapidly during discharging [17].

Latent heat storage uses the energy stored when a substance changes from one phase to another, as said before. The use of PCMs (Phase Change Materials) for storing latent heat has been recognized to be a compact and efficient way because of their high storage density and constant operating temperature. For this reason, many researchers have investigated the effects of applying PCMs in solar cookers.

Chapter 2

Phase Change Materials: Testing and Characterization

In order to bridge the growing gap between energy supply and demand due to accelerating urbanisation, increasing productivity and depletion of fossil fuel resources, there is a growing need to develop new technologies that foreground the development of renewable energies [44]. This need to make more effective use of various renewable energy sources is also driven by the ever-increasing greenhouse gas emissions and the rising cost of fuels [45]. Phase change materials are the most appropriate materials for the effective utilization of thermal energy from renewable energy resources.

2.1 Thermal Energy Storage

In many parts of the world, solar radiation is considered one of the most promising sources of energy. In fact, many developing countries benefit from abundant solar radiation, with an average intensity of illumination in the range of 5-7 kW/m^2, and more than 275 sunny days in a year [14, 46]. However, solar radiation is variable by nature and depends on the day-night cycle, seasons and meteorological conditions, thus it is not able to cover alone the energy demand. One way to compensate for this intermittence would be to make use of energy storage systems to accumulate the excess of solar energy and use it when solar radiation is absent.

It is therefore evident that the storage of energy in suitable forms, which can conventionally be converted into the required form, is a present day challenge to the technologists. Energy storage not only reduces the imbalance between supply and demand, but also improves the performance and reliability of energy systems and also plays an important role in energy conservation [45].

The main forms of energy that can be stored are mechanical, electrical and thermal. Considering thermal energy storage, this can be stored as a change in the internal energy of a material in the form of sensible heat, latent heat and thermochemical, or as a combination of these:

- Sensible heat storage (SHS). In this case, thermal energy is stored by raising the temperature of a solid or a liquid. The thermal capacity and temperature difference of the material during the charge and discharge cycle play an important role. The accumulated heat depends in fact on the quantity of the material, the specific heat of the medium and the temperature difference:

$$Q = \int_{T_\mathrm{i}}^{T_\mathrm{f}} mc_\mathrm{p}\Delta T = mc_\mathrm{p}(T_\mathrm{f} - T_\mathrm{i}) \tag{2.1}$$

- Latent heat storage (LHS). This is based on the heat absorption or release when a material undergoes a phase change from solid to liquid or liquid to gas or vice versa. In this case, the stored heat can be calculated with the following formula:

$$Q = \int_{T_\mathrm{i}}^{T_\mathrm{m}} mc_\mathrm{p,s}\Delta T + ma_\mathrm{m}\Delta h_\mathrm{m} + \int_{T_\mathrm{m}}^{T_\mathrm{f}} mc_\mathrm{p,l}\Delta T \tag{2.2}$$

  where:

  - T_i is the initial temperature of the material;
  - T_m is the melting temperature of the material;
  - T_f is the final temperature of the material;
  - m is the mass of the material;
  - $c_\mathrm{p,s}$ is the specific heat of the material (solid state);
  - $c_\mathrm{p,l}$ is the specific heat of the material (liquid state);
  - a_m is the melted material fraction;
  - Δh_m is the melting latent heat of the material per unit of mass.

- Thermochemical energy storage. Thermochemical systems rely on the energy absorbed and released in breaking and reforming molecular bonds in a completely reversible chemical reaction. In this case, the heat stored depends on the amount of storage material, the endothermic heat of reaction and the extent of conversion:

$$Q = a_\mathrm{r} m \Delta h_\mathrm{r} \tag{2.3}$$

Among the thermal heat storage techniques described above, latent heat energy storage is particularly attractive due to its ability to provide high-energy storage density and its characteristics to store heat at constant temperature corresponding to the phase transition temperature of the phase change material (PCM). There are three possible phase changes:

- Solid - Solid: swap from one crystal structure to another, typically with moderate latent heat and small volume variation;
- Solid - Gas/ Liquid - Gas: high latent heat and substantial volume variation;
- Solid - Liquid: moderate latent heat and volume variation.

Generally, the most commonly used PCM phase transition for thermal storage systems is that from solid to liquid and vice versa. Everything that will be reported in this chapter therefore refers to this category of phase change.

It is important to emphasize that any latent heat energy storage system has at least the following components:

- a suitable PCM with its melting point in the desired temperature range;

- a suitable heat exchange surface;
- a suitable container compatible with the PCM.

Thus, the development of a latent heat thermal energy storage system involves the understanding of three essential subjects: phase change materials, containers materials and heat exchangers.

2.2 PCMs Characteristics

The solid-liquid PCMs to be used in the design of a thermal energy storage systems (TESs) should meet desirable thermophysical, kinetics, chemical and economic requirements [47–49]:

- phase change temperatures, i.e. the melting (T_{m}) and crystallization (T_{c}) temperatures, within the operating temperature range of the specific application;
- high latent heats of melting (ΔH_{m}) and crystallization (ΔH_{c}), to achieve high storage density and to build compact LHTES systems;
- high specific heat (c_{p}), to effectively exploit also the sensible heat;
- high thermal conductivity (λ) in both phases, to have good LHTES charge/discharge rates;
- small volume changes in the phase transition and low vapor pressure at the operating temperatures, to reduce containment issues;
- high density (ρ), to minimize the physical size of the LHTES system;
- limited supercooling degree, high rate of nucleation, and high rate of crystal growth, to achieve effective heat release in a narrow temperature range around the required value;
- high thermal stability at temperatures higher than their T_{m}, to use PCMs in a wide operating temperature range;
- reproducible phase change properties (i.e. cyclic stability without degradation), to not affect the performance of the LHTES system over time;
- long-therm chemical stability, to increase the lifetime of the LHTES system;
- congruent melting, to avoid phase segregation and to have a constant heat storage capacity in each freezing/melting cycle;
- non-corrosiveness, non-toxicity, non-flammability, and non-explosiveness;
- cost-effectiveness and availability in large quantities.

Even if not explicitly mentioned, a good quality for a PCM should be the absence of environmental impacts in the production, operation and disposal phases. At this point in time, however, no PCM possesses all the listed characteristics, therefore the choice must be driven by the field of application and the need of the user.

2.2.1 PCM Characterization

As mentioned above, for the selection of PCMs and the design of latent heat thermal energy storage (LHTES) systems, a reliable and accurate knowledge of their thermophysical properties is fundamental. This is also essential to develop reliable mathematical models to analyze their thermal performance in specific LHTES applications [50, 51].

For this purpose, different thermophysical properties for numerous materials must be experimentally determined using specific measurement methods [52, 53]. The values of melting (T_m) and crystallization temperature (T_c), latent heat of melting (ΔH_m) and crystallization (ΔH_c), as well as specific heat (c_p) can be determined through thermal analysis techniques as a function of temperature or time.

The differential scanning calorimetry (DSC) and the T-history method are two well-known techniques for the measurements of these properties. The DSC is a widely used and standardized non-isothermal method allowing to accurately measure T_m, T_c, ΔH_m, ΔH_c, and c_p by subjecting the materials to controlled heating/cooling rates [53–55].

However, this analysis technique has various limitations [53, 54]:

- a small amount of material is measured (masses of about few milligrams);
- the thermal response is influenced by the sample mass and the used heating/-cooling rate;
- lack of repeatability may occur for heterogeneous samples;
- in composite materials, the main component can interfere in the measurement signal.

In addition, the DSC is an expensive device and the analysis of a material can be time-consuming as the DSC allows to analyze only one sample at a time [53, 56].

The T-history method is a simple isothermal method that allows to measure T_m, T_c, ΔH_m, ΔH_c, and c_p of samples of a few grams. The material is subjected to constant charge/discharge temperatures [53, 57, 58]. Since the samples tested with the T-history method are larger than those measured with the DSC and are exposed to constant charge/discharge temperatures, the results of the T-history method are considered to be closer to the real macro properties of the studied materials [58–61].

Moreover, the T-history method is less expensive and less time-consuming than the DSC, enabling simultaneous measurements of more samples. However, one of the main drawbacks of this analysis technique is the lack of standardization, which does not allow an accurate comparison between the values provided by different apparatus. Also, different mathematical models are used to derive the values of the properties from the measurements [56, 59].

In addition, to assess if a PCM is suitable for practical LHTES applications, an accurate knowledge of its thermal stability is fundamental [62, 63]. At this point it becomes necessary to distinguish between: thermal endurance, degradation temperature, and long-term thermal stability or cycling stability.

- Thermal endurance tests allow to evaluate the variations of the physical and chemical characteristics and the thermal performance of PCMs as function of time by keeping them at different constant working temperatures, higher than their melting points [64].

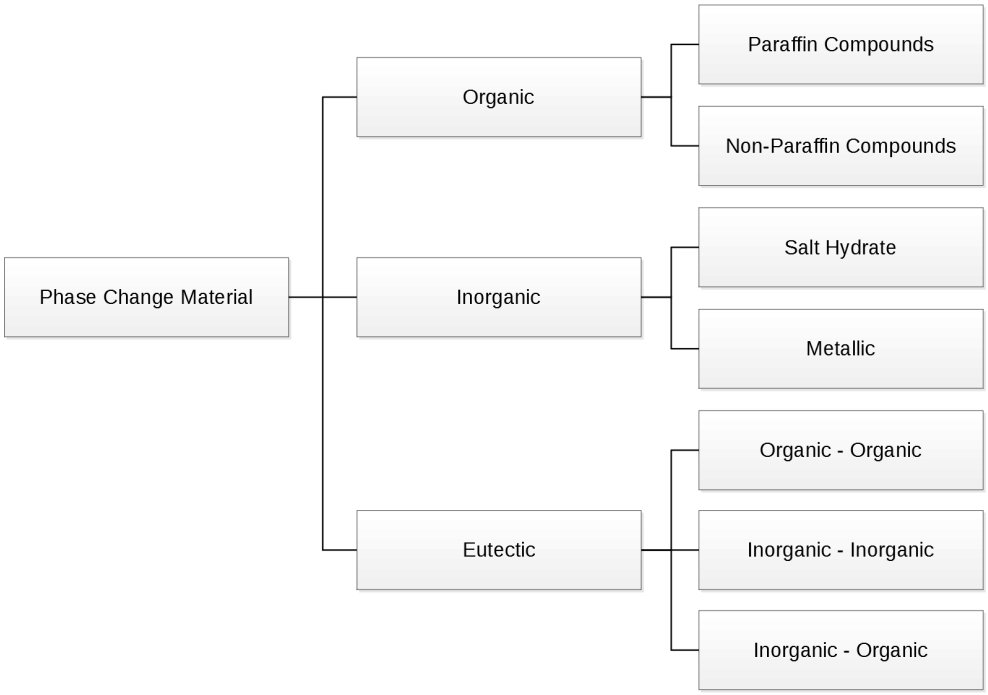

Figure 2.1: PCMs classification.

- Chemical stability of PCMs is generally evaluated by the Fourier transform infrared spectroscopy (FTIR) [62]. The degradation temperature analysis determines the maximum temperature of a PCM below which the material does not show thermal decomposition. It is usually carried out by means of the thermogravimetric analysis (TGA) technique [65].
- The long-term stability of PCMs is analyzed by performing several consecutive thermal cycles of heating and cooling with the aim to evaluate if the materials show deterioration of thermal performance and/or degradation [62, 66].

Since no standard procedures for long-term stability analysis have been developed, different techniques taking into account various application conditions (e.g., temperature interval, heating and cooling rates, contact to atmosphere, contact to container, container material, sample size) have been employed [52, 62, 66].

2.3 PCM Classifications

It is possible to classify PCM materials following two different approaches, the first based on the material nature (organic, inorganic and eutectic), the second on the melting temperature.

2.3.1 Classification Based on the Material Nature

The scheme reported in Figure 2.1 describes this classification approach. PCMs can be divided into:

- Organic PCMs: they are not subject to degradation and can be used for many phase transition cycles, they are not corrosive and their melting temperature is mostly constant throughout the process. They are further divided into paraffins and non-paraffins;

- Inorganic PCMs: compared with organic PCMs, inorganic PCMs have a higher latent heat of fusion but degrade over time. Among the inorganic phase change materials there are hydrated salts and metallic materials;

- Eutectic PCMs: they are a mixture of substances with a resulting melting point lower than the one of each single substance that compose them. In an eutectic blend, all the elements melt and solidify simultaneously and congruently, without segregation. Furthermore, these particular PCMs can be obtained from the mix of both organic and inorganic compounds, and have characteristics similar to metallic materials.

Table 2.1 provides the advantages and disadvantages of some of the main classes of PCMs.

2.3.2 Classification Based on Melting Temperature

Table 2.2 reported hereafter, illustrates the possible applications based on the melting temperature range [9].

2.4 PCMs Most Commonly Used in Solar Cooker Applications

Recently [67–70] a large number of PCMs of the solid-liquid category with melting temperatures and physical properties suited to develop LHTES systems has been investigated for different applications: solar energy [71, 72], building sector [49, 73–75], cold storage [67, 70], industrial sector [74, 76, 77].

Referring to applications using solar energy, numerous studies demonstrated that solar cookers equipped with a PCM-based TES constitute a sound alternative to more traditional cooking solutions involving in particular environmentally harmful fuels (e.g., firewood, manure and agricultural waste, coal) [15, 43].

A pratical summary of some of these studies is reported in Table 2.3, which focuses on the main properties of the substances used as PCM (i.e., melting temperature, T_{m}, and latent heat of fusion, ΔH_{m}), on the cooking medium used during the tests and on the main results obtained from the experimental campaign. The studies reported are subdivided according to the PCM chemical family: hydroxides, amides, plastic materials, acids, salts, paraffins, sugar alcohols.

2.5 Sugar Alcohols, Measurement Methods and Thermophysical Properties

Among the various families of PCMs, the one of sugar alcohols was chosen for further study. This choice was made for several reasons, including the fact that they belong to the category of natural organic substances and are therefore suitable for

Table 2.1: Advantages and disadvantages of organic, inorganic, end eutectic PCMs.

	Organic materials			**Inorganic materials**		**Eutectics**
	Paraffins	*Fatty acids*	*Sugar alcohols*	*Salt hydrates*	*Metallic with low* T_m	
Advantages	• Good melting latent heat • Absence of supercooling • No phase segregation • Congruent melting • Chemical stability • Compatible with all metal containers • Available in high quantity • Safe • Non-corrosive • Recyclable	• High melting latent heat • Sharp phase transformation • Absence of supercooling • Reproducible melting and freezing behavior • Recyclable	• High melting latent heat • No phase segregation • Compatibility with conventional materials of construction • Non-flammability • Safe and non-reactive • Non-toxic • Low environmental impact • Available in high quantity • Recyclable	• High melting latent heat per volume unit • High thermal conductivity • High density • Sharp melting point • Compatible with plastics containers • Non-flammability • Low environmental impact • Available in high quantity • Inexpensive	• High melting latent heat per volume unit • High thermal conductivity • Low vapor pressure	• High thermal storage density • Good thermal conductivity • Sharp melting point • No phase segregation and congruent phase change
Disadvantages	• Not well-defined sharp melting point • Low thermal conductivity • Low density • Incompatible with plastic container • High volume change • Volatile • Moderately flammable • Expensive	• Low thermal conductivity • Instable at high temperature • Highly inflammable • Low flash point • Toxic • Mild corrosive • Expensive	• Low thermal conductivity • High degree of supercooling • Lack of thermal stability • Prone to degradation	• Supercooling • Phase segregation • Chemically instable when heated • High vapor pressure • Incongruent melting • Corrosion on metal containers • No thermal stability • Slightly toxic • Irritant	• Low latent heat of melting per unit of weight • Low specific heat capacity • Non-flammable • Expensive	• Low latent heat of melting per unit of weight • Some eutectics suffer from supercooling • Expensive • Limited data on thermophysical properties

Table 2.2: Temperature ranges and PCMs applications [9].

Temperature range	Thermal classification	Possible application
$< 120\,^{\circ}C$	Low temperature	Solar thermal without concentrating or low concentration (flat panels)
120-200 °C	Low-medium temperature	Supply of process heat, power generation with organic cycles, high efficiency air conditioning, desalination. At these temperature low pressure water can also be used as the heat transfer fluid
200-300 °C	Medium temperature	Multi-generation application but, of course, the temperature levels require the use of diathermic oils and allow for power generation with quite high efficiency
300-400 °C	Medium-high temperature	Power generation with linear parabolic solar plants with diathermic oil. Thermo-electric conversion efficiencies are high
400-600 °C	High temperature	Power generation with linear parabolic or tower solar plants but diathermic oil can no longer be used. The heat transfer fluid will be a molten salt. In this case the thermo-electric conversion efficiencies are very high
$> 600\,^{\circ}C$	Very high temperature	Very concentrated solar energy applications such as dish or solar furnaces. The heat transfer fluid is often air/gas. The use of PCMs, in this case, is still possible but in extreme conditions

Table 2.3: Literature summary of phase change materials (PCMs) used in direct and indirect solar cookers.

PCM	Type of study	T_m (°C)	ΔH_m (kJ/kg)	Solar cooker design	Cooking medium	Main results	Reference
Magnesium nitrate hexahydrate	Experimental	89	134	Indirect (FPC)	Water	• The solar cooker can be used successfully for cooking different kinds of meals during all the day, while it can be used for heating or keeping meals hot at night and early morning.	[78]
Magnesium chloride hexahydrate	Experimental	116.7	165-169	-	-	• $MgCl_2 \cdot 6H_2O$ was not stable during its thermal cycling due to the phase segregation problem; therefore, it is not recommended for cooking indoors.	[79]
Acetanilide		116	142	-	-	• Acetanilide was a hopeful PCM for cooking application even withlow solar irradiance.	
Acetanilide	Experimental	118.9	222	Parabolic dish collector	Water	• PCM in SC with outer surface painted black and with surface painted black along with glazing stored 26.8% and 32.3% more heat respectively as compared to PCM in ordinary SC.	[39]
Acetamide	Numerical and experimental	82	263	Solar stove	Rice	• Results established that acetamide is a promising PCM in solar cooker applications.	[80]
Stearic acid	Experimental	55-70	-	Collapsible parabolic	Rice, lentils, barley	• The PCM kept the food warm for subsequent meals. The SC payback period was less than 52 weeks for a family of 4 members.	[81]
Solar salt binary mixture	Experimental	220	-	Parabolic concentrating dish	Rice and potatoes	• In less than two hours, the system was able to store heat. The oil frying temperature of 170-180 °C was easily achieved during indoor cooking.	[82]
Solar salt ternary mixture	Experimental	145.14	101.50	Box	Water and silicone oil	• The cooling time of silicone oil from 170 °C to 130 °C was calculated to be from 65.12% to 107.98% higher than thatwithout the TES based on solar-salt.	[83]
Paraffin wax	Experimental	60	-	Box	Water, rice	• The food cooked in SC equipped with the PCM can be kept hot for 3-4 h.	[84]
Erythritol	Experimental	118.0	340	Concentrating parabolic	Water	• Three meals for a family were possible simultaneously with the heat heat storage both in summer and in wintertime. The storage utensil, left inside an insulating box, allowed to cook dinner and breakfast of the next day with the retained heat.	[85]
Erythritol	Experimental	117.7	339.8	Box	Water and silicone oil	• The use of TES resulted in an extension of the average load cooling time by approximately 351% with respect to the system without PCM.	[5]
Xylitol	Experimental	92.2	227.1	Box	Water and silicone oil	• The average load cooling time, in the temperature range of the silicone oil from 110 °C to 80 °C, increased by about 346% when the solar cooker was equipped with the xylitol-triggered TES.	[6]
D-Mannitol	Experimental	167-169	326.8	Indirect SC with parabolic trough collector	Olive oil	• The cooking unit had an efficiency of 73.5% while the overall system efficiency was equal to 10.2%. • The main heat losses were identified to be concentrated in the pipes (54.3%), the TES tank (25.3%) and the cooking unit (4.1%).	[86]

solar cooking, and have melting temperatures suitable for the solar cooker prototypes that have been characterized.

In this section, the six polyalcohols selected for this study are presented: xylitol, sorbitol, erythritol, mannitol, inositol and dulcitol.

The measurement methods for determining the temperatures and latent heats of melting and crystallization as well as the maximum degradation temperature of substances will be presented, together with the measured thermophysical quantities.

2.5.1 Sugar Alcohols

Sugar alcohols (SAs), also known as polyalcohols, polyols, hydrogenated carbohydrates or polyhydric alcohols, are hydrogenated forms of carbohydrates and belong to the low molecular weight carbohydrate family. Their general formula is $C_nH_{2n+2}O_n$. They can be either of natural origin, some of them can be found in various fruits and vegetables, or derived with chemical processes from carbohydrates reduction. Many of them are commonly used as sweeteners to replace sugar in the pharmaceutical and food industries to develop products suitable for diabetics and non-cariogenic food [87, 88].

As reported in Table 2.1, apart from being non-flammable, non-toxic, and usually available in large quantities, these substances have a high latent heat storage capacity with respect to their melting points, higher than that of other organic PCMs such as paraffins. Moreover, as by-products of the food industry, their environmental impact is low [89]. The promising SAs for LHTES systems can be further selected on the basis of their prices.

Considering their melting temperatures and thermophysical properties, some SAs are considered suitable to be used as PCMs in solar cookers for applications in the low-medium temperature range (80-250 °C). However, it is important to note that, despite their promising properties, most of the selected SAs exhibits severe issues that could hinder their use as PCMs (Table 2.1).

One of their main drawbacks lies in the fact that SAs may undergo supercooling, which makes it difficult to control the constant temperature heat recovery [61, 90, 91]. Some SAs may also have a slow growth rate of crystallization and a poor nucleation triggering, leading to a low discharging power and a difficult energy discharge triggering, respectively, in LHTES systems [89, 92]. Furthermore, different SAs present the following issues [93–95]:

- low thermal conductivity, resulting in too slow charge and discharge rates for use in TESs;
- various polymorphic forms, which give changes on melting properties;
- and poor stability (thermal, chemical, and cycling), which implies unsuitable long-term performance of the LHTES systems based on SAs.

Table 2.4 shows the health hazard of the studied SAs provided in the National Fire Protection Association (NFPA) 704 [96] diamond standard.

2.5.2 Measurement Methods

Differential Scanning Calorimeter

To measure T_m, T_c, ΔH_m, and ΔH_c of the studied SAs a differential scanning calorimeter (DSC), the NETZSCH DSC 214 POLYMA, was used.

Table 2.4: Health hazard of the studied SAs reported in the National Fire Protection Association (NFPA) 704 [96] diamond standard.

Sugar alcohol	Health hazard	Fire hazard	Instability - reactivity
Xylitol	1[a]	1[b]	0[c]
Sorbitol	1[a]	1[b]	0[c]
Erythritol	1[a]	1[b]	0[c]
Mannitol	1[a]	1[b]	0[c]
Inositol	1[a]	0[d]	0[c]
Dulcitol	0[e]	0[d]	0[c]

[a] Significant irritation. [b] It requires preheating for ignition.
[c] It is normally stable, even under fire exposure conditions, and is not reactive with water. [d] It will not burn under normal fire conditions.
[e] No health hazard.

Three different samples of approximately 10 mg each were prepared for each substance, weighed with a WAAGEN-Kissling Sartorius microbalance and placed into aluminum crucibles with perforated lids. The characterization of each sample was carried out by performing three continuous heating/cooling cycles at a heating/cooling rate of 1 °C/min over specific temperature ranges.

In detail, according to the melting temperature of each SA, the instrument was set as follows:

- (25 to 30) °C – (30 to 120) °C – (120 to 30) °C for xylitol;
- (25 to 30) °C – (30 to 130) °C – (130 to 30) °C for sorbitol;
- (25 to 30) °C – (30 to 140) °C – (140 to 30) °C for erythritol;
- (25 to 100) °C – (100 to 200) °C – (200 to 100) °C for mannitol;
- (25 to 160) °C – (160 to 250) °C – (250 to 160) °C for inositol;
- (25 to 100) °C – (100 to 210) °C – (210 to 100) °C for dulcitol.

Thermogravimetric Analysis

To measure the mass variation of the six selected sugar alcohols as a function of temperature, a thermogravimetric analysis (TGA) was performed. The NETZSCH STA 449 F5 JUPITER system was used to perform the analyses. The purging gas was nitrogen. Aluminum crucibles, one for each selected SAs, were filled with about 34 mg of substance and preheated at 40 °C for 30 minutes. Subsequently, each substance was further heated at a constant heating rate of 20 °C/min.

In detail, the instrument was set to reach a temperature of:

- 350 °C for erythritol;
- 400 °C for mannitol;
- 450 °C for dulcitol;
- 500 °C for xylitol;
- 500 °C for sorbitol;
- 500 °C for inositol.

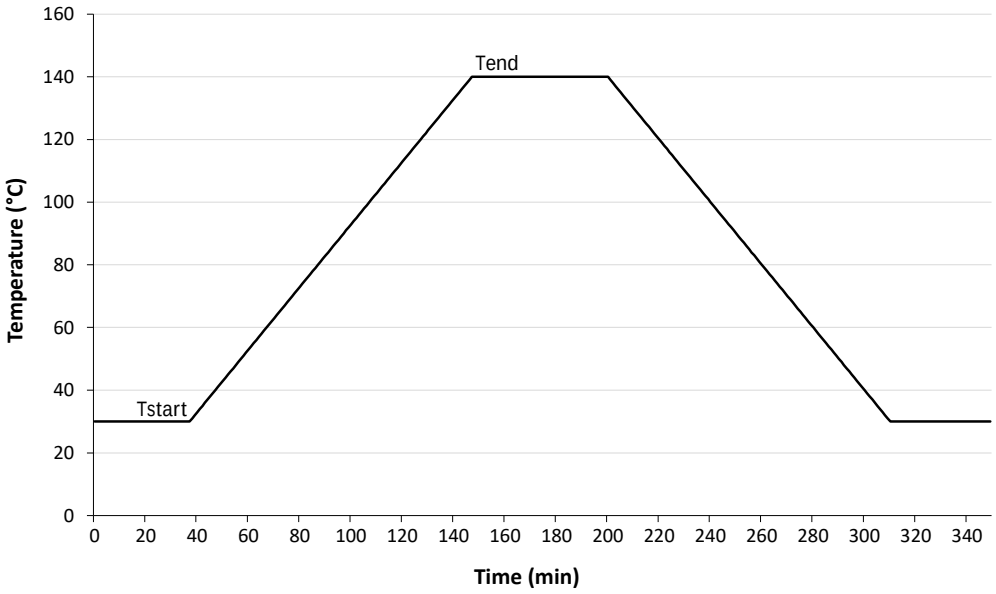

Figure 2.2: Dynamic DSC method.

Further information on the instruments used to conduct the experimental campaign is given in the Appendix B.

2.5.3 Thermophysical Properties

In this section, the results obtained from the experimental campaign carried out in the microlaboratory at the WiB institute are reported. The results of the measured thermophysical properties (i.e. temperatures and latent heats of the melting and crystallisation points) will be compared with those found in the scientific literature. For a complete characterization of the selected sugar alcohols, information on specific heat, thermal conductivity, viscosity and density please refer to [97].

Melting And Crystallization Properties

As explained in section 2.5.2, three samples of approximately 10 mg of substance were prepared for each of the six selected sugar alcohols for a total of 18 specimens. The accurately weighed samples were sealed in aluminium containers and one at a time were tested by setting the instrument with the various temperature ranges according to the melting temperature of the substance under test.

For each heating-cooling cycle, three different temperature ranges were set according to the state of the substance: first step for the solid state, intermediate step for the solid-liquid transition and finally third step for the liquid phase. Once the final temperature of the step under test was reached, the instrument maintained that temperature for 10 minutes to allow the entire mass of substance in the specimen to reach that temperature and then move on to the temperature of the next step. Figure 2.2 shows as an example the instrument setting for the temperature trend as a function of time for one heating-cooling cycle.

The melting and crystallization behaviors of the six sugar alcohols analyzed with the DSC for two consecutive tests, are reported in Figure 2.3. The results obtained

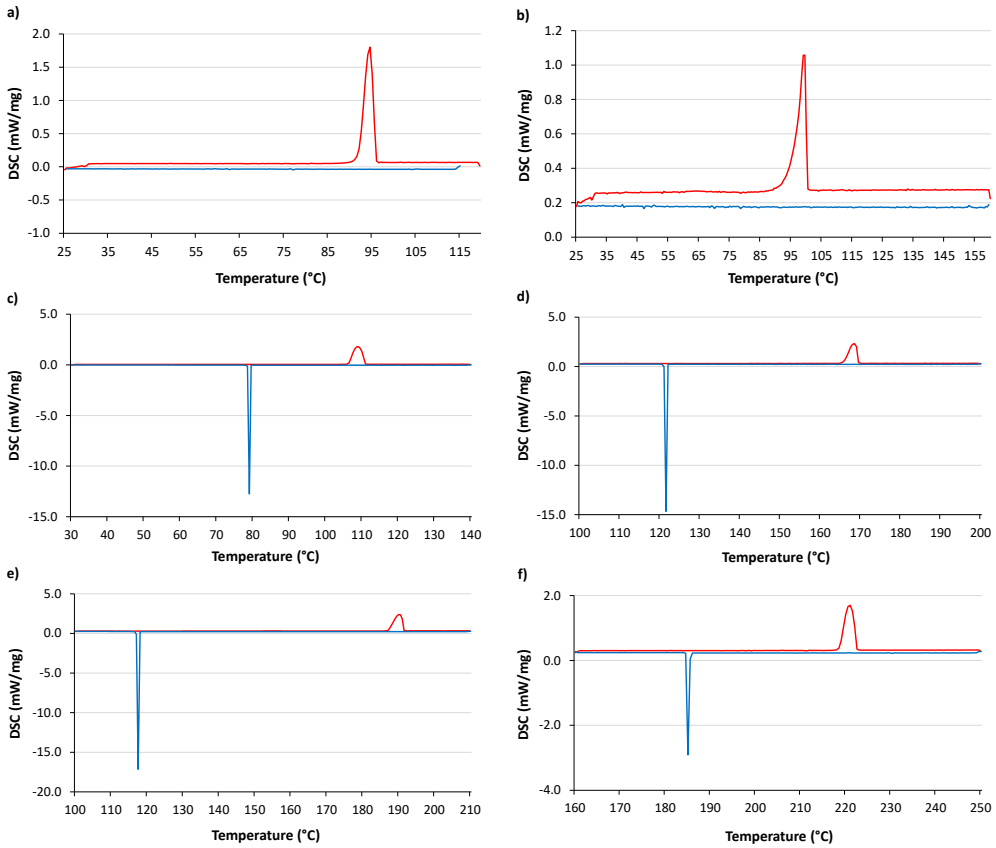

Figure 2.3: DSC thermograms of the selected sugar alcohols: (a) xylitol, (b) d-sorbitol, (c) erythritol, (d) d-mannitol, (e) d-dulcitol and (f) inositol with a heating/cooling rate of 1 °C/min.

from the experimental campaign of the 18 samples together with the heating and cooling rate and the mass tested for each sample are given in Table 2.5.

Below a comparison between the data (T_m, T_c, ΔH_m and ΔH_c) obtained from the experimental campaign and those collected from the literature is reported. The values collected from the literature were selected by following these criteria:

- The measurements performed using a differential scanning calorimeter (DSC) or a T-history method were collected.
- Among the studies reporting measurements performed using a DSC, only the ones providing experimental data of all the aforementioned properties were selected.

The selected data of T_m, T_c, ΔH_m, and ΔH_c measured with a DSC are reported in Table 2.6 for xylitol, Table 2.7 for sorbitol, Table 2.8 for erythritol, Table 2.9 for mannitol, Table 2.10 for inositol, and Table 2.11 for dulcitol.

If not otherwise stated, T_m and T_c correspond to onset temperatures. In addition, these tables show the available measurement uncertainties, heating/cooling rates, and sample purities reported in the selected works.

From the comparison presented, the following considerations can be made:

Table 2.5: Measurements of melting and crystallization temperature (onset) (T_m and T_c) and latent heat of melting and crystallization (ΔH_m and ΔH_c) for the six sugar alcohols purchased from Sigma Aldrich carried out with DSC.

Sugar alcohol	Mass (mg)	HR/CR (°C/min)	T_m (°C)	ΔH_m (J/g)	T_c (°C)	ΔH_c (J/g)	N. of specimens -
Xyliyol	11.2	1	94.8	244.3	-	-	First sample
	11.6	1	94.8	235.1	-	-	Second sample
	10.9	1	95.0	222.4	-	-	Third sample
Sorbitol	13.7	1	94.9	170.5	-	-	First sample
	11.1	1	95.5	164.1	-	-	Second sample
	10.5	1	96.2	172.8	-	-	Third sample
Erythritol	10.6	1	121.4	339.4	46.6	242.4	First sample
	10.1	1	121.2	326.8	81.7	280.0	Second sample
	12.2	1	121.2	331.0	81.2	280.3	Third sample
Mannitol	10.6	1	168.3	281.3	120.5	231.7	First sample
	11.1	1	168.3	280.4	121.4	244.1	Second sample
	11.2	1	168.1	288.1	120.2	245.4	Third sample
Dulcitol	12.1	1	190.1	335.1	121.4	238.6	First sample
	11.1	1	190.2	330.4	119.8	237.9	Second sample
	10.3	1	190.0	329.5	121.3	239.8	Third sample
Inositol	12.4	1	226.5	239.1	184.8	186.8	First sample
	11.3	1	226.1	241.0	184.3	186.7	Second sample
	11.1	1	220.8	258.1	185.4	196.0	Third sample

- Not all six of the selected sugars are widely studied in the scientific community. With regard to inositol, for example, there is only a limited number of works in the literature compared to studies on the other sugars.

- It is evident that the thermophysical properties measured on the six sugars are in line with those found in the literature. Their absolute relative deviations respect to the mean values are always less than 2% for T_m and 6% for ΔH_m.

- The collected values of T_m for all the studied sugars are generally consistent with each other as can be noted observing the standard deviations reported in the tables, while the discrepancy for ΔH_m measurements is slightly higher. These differences can be due to the purity of the samples or the accuracy of the measurement.

- The values of T_c and ΔH_c for xylitol and sorbitol are not reported in Table 2.6 and Table 2.7, respectively, because no liquid-solid transition (exothermic peak) was recorded during the cooling phase of the DSC measurements presented in different works [91, 92, 109, 113], even at low temperatures. The same behavior was also found for the samples of xylitol and sorbitol measured by me. In particular, no endothermic peaks were recorded by repeating the DSC measurements in the following heating phase on the same samples, given that no liquid-solid phase transitions occurred during the cooling period of the previous cycle.

  As explained by different authors [91, 94, 102], these two SAs have a very stable supercooling due to high resistance to crystallization, remaining supercooled liquids until amorphous metastable solid states appear at low temperatures. It was shown that the resistance to crystallization of xylitol is linked to its high

Table 2.6: Measurements of melting temperature (onset) (T_m) and latent heat of melting (ΔH_m) for **xylitol** carried out with DSC at various heating rates (HR).

Reference	T_m (°C)	ΔH_m (J/g)	HR (°C/min)	Purity %
[92]	92.0	249.0	0.5	i.q.[a]
[98]	92.8	241.2	0.5	99
[99]	93.0 ± 1.0	236.0 ± 4.0	0.5	f.g.[b]
[100]	92.5 ± 0.1	246 ± 2	1	-
[94]	92.7	240.1	1	99
[95]	95.1[c]	251.0	1	99
this work	92.0 ± 0.5	232.7 ± 9.2	1	≥ 99
[101]	93.0	245.0 ± 5.0	2	≥99
[102]	93.1	226.2	5	≥99
[91]	93.4 ± 0.3	237.5 ± 3.5	5	99
[91]	93.3 ± 0.2	231.4 ± 2.5	5	98
[99]	93.0 ± 1.0	241.0 ± 2.0	5	f.g.[b]
[103]	92.7 ± 0.1	232.0 ± 1.0	5	>99
[104]	95.0[c]	248.0	5	-
[105]	93.0	280.0	5	>99
[106]	92.0	243.3	5	99
[107]	95.0	267.0	10	>98
[108]	93.0	259.7	10	99
[89]	93.0 ± 0.5	263.0 ± 13.0	10	>98
[109]	90.0 ± 1.0	237.6 ± 1.3	10	t.g.[d]
[110]	91.1	286.6	10	-
[111]	94.4[e]	221.4 ± 2.2	10	>99
[112]	92.7	273.0	10	>98
[113]	95.7[e]	246.0 ± 1.0	-	>99
-	**93.0 ± 1.2[f]**	**247.3 ± 16.3[f]**	**-**	**-**

[a] industrial quality [b] food grade
[c] unspecified type of temperature [d] technical grade
[e] peak temperature [f] mean value ± standard deviation

Table 2.7: Measurements of melting temperature (onset) (T_m) and latent heat of melting (ΔH_m) for **sorbitol** carried out with DSC at various heating rates (HR).

Reference	T_m (°C)	ΔH_m (J/g)	HR (°C/min)	Purity %
[94]	93.2	153.0	1	99.5
[95]	100.0	185.0	1	98
[100]	93.4 ± 0.3	166.0 ± 2.0	1	-
this work	95.6 ± 0.3	167.3 ± 6.2	1	≥99.5
[114]	95.3 ± 0.5	172.2 ± 4.3	2–5	-
[115]	96.8	217.0	3.5	-
[102]	95.1	132.5	5	≥98
[91]	97.4 ± 0.2	164.0 ± 3.2	5	98
[91]	99.4 ± 0.2	184.4 ± 2.6	5	98
[103]	95.0 ± 1.2	165.0 ± 1.0	5	>97
[105]	97.0	110.0	5	>99
[116]	101.1 ± 0.1[a]	173 ± 5	10	>97
[117]	99.2[b]	168.3 ± 1.7	10	>99
[118]	98.0 ± 0.3	174.0 ± 2.0	10	98.9
[119]	98.8	196.8	10	-
[120]	94.2	135.3	-	-
-	**96.8 ± 2.3[c]**	**166.5 ± 24.7[c]**	**-**	**-**

[a] unspecified type of temperature [b] peak temperature
[c] mean value ± standard deviation

Table 2.8: Measurements of melting temperature (onset) (T_m), latent heat of melting (ΔH_m), crystallization temperature (onset) (T_c), and latent heat of crystallization (ΔH_c) for **erythritol** carried out with DSC at various heating/cooling rates (HR/CR).

Reference	T_m (°C)	ΔH_m (J/g)	T_c (°C)	ΔH_c (J/g)	HR/CR (°C/min)	Purity %
[91]	118.8 ± 0.1	325.4 ± 0.6	31.1 ± 0.7	200.5 ± 5.5	0.5	99
[99]	119.0 ± 1.0	329.0 ± 14.0	25.0 ± 28.0	204.0 ± 26.0	0.5[a]	f.g.[b]
[99]	119.0 ± 1.0	329.0 ± 14.0	52.0 ± 30.0	204.0 ± 25.0	0.5[c]	f.g.[b]
[91]	118.3 ± 0.7	327.3 ± 1.3	28.4 ± 1.5	208.5 ± 6.6	1	99
this work	118.7 ± 0.1	333.1 ± 6.3	56.5 ± 17.7	250.4 ± 19.7	1	≥99
[121]	118.1	340.6	38.8	252.3	2	-
[122]	118.8[d]	374.3	55.3[d]	194.1	3	-
[123]	127.5	311.0	53.1	308.2	5	-
[91]	118.9 ± 0.1	332.3 ± 0.8	22.4 ± 5.8	186.3 ± 5.7	5	99
[91]	118.8 ± 0.1	333.7 ± 1.2	16.9 ± 1.8	171.3 ± 5.6	5	99
[99]	116.0 ± 1.0	319.0 ± 20.0	22.0 ± 31.0	101.0 ± 65.0	5[a]	f.g.[b]
[99]	116.0 ± 1.0	319.0 ± 20.0	24.0 ± 20.0	203.0 ± 20.0	5[c]	f.g.[b]
[124]	119.5	328.0	33.5	224.2	5	99
[91]	119.7 ± 0.3	337.8 ± 2.6	18.7 ± 1.1	191.8 ± 6.5	10	99
[125]	118.7	357.3	19.8	141.8	10	-
[126]	118.6	349.9	33.9	224.2	10	c.g.[e]
[127]	118.9	342.2	38.5[f]	213.9	10	99
[128]	118.7	345.3	15.6	127.4	10	a.g.[g]
[129]	119.2 ± 0.1	334.4 ± 3.6	46.5 ± 1.1	224.8 ± 2.3	10	99
[130]	117.2	308.8	20.4	246.6	10	>95
[131]	118.4	310.6	33.0	213.1	10	99
[132]	118.4[d]	379.6	36.2[d]	256.0	10	≥99
[133]	119.0	349.9	33.5	224.2	-	-
-	**118.9 ± 2.0[h]**	**335.5 ± 17.8[h]**	**32.8 ± 12.5[h]**	**207.5 ± 43.5[h]**	**-**	**-**

[a] in smooth crucible [b] food grade [c] in rough crucible [d] unspecified type of temperature
[e] commercial grade [f] peak temperature [g] analytical grade [h] mean value ± standard deviation

Table 2.9: Measurements of melting temperature (onset) (T_m), latent heat of melting (ΔH_m), crystallization temperature (onset) (T_c), and latent heat of crystallization (ΔH_c) for **mannitol** carried out with DSC at various heating/cooling rates (HR/CR).

Reference	T_m (°C)	ΔH_m (J/g)	T_c (°C)	ΔH_c (J/g)	HR/CR (°C/min)	Purity %
[91]	166.2 ± 0.2	278.6 ± 0.9	118.5 ± 0.1	243.0 ± 0.6	0.5	98
[134]	151.0	234.4	114.1	224.6	1	-
[91]	166.3 ± 0.2	278.7 ± 0.1	119.1 ± 0.1	242.8 ± 0.7	1	98
[135]	165.7	334.5	122.9	234.8	1	≥98
this work	165.6 ± 0.1	284.3 ± 3.9	120.0 ± 0.2	238.6 ± 6.9	1	≥98
[91]	166.1 ± 0.0	281.1 ± 1.3	111.1 ± 1.7	238.3 ± 5.9	5	98
[91]	166.0 ± 0.1	277.4 ± 1.1	114.1 ± 0.6	227.9 ± 0.9	5	99
[91]	166.6 ± 0.1	299.5 ± 0.4	110.9 ± 1.0	234.5 ± 0.7	10	98
[136]	166.4	281.9	120.2	219.5	10	99
[137]	165.3	282.0	123.0	241.3	10	98
[138]	166.2	288.1	115.0	228.0	10	-
[139]	165.0	295.2	109.4	213.0	10	98
[140]	168.8[a]	284.9	107.7[a]	214.4	10	99
[141]	170.2	293.1	118.0	238.2	-	99.5
-	**165.4 ± 4.2[b]**	**285.3 ± 19.9[b]**	**116.0 ± 4.8[b]**	**231.4± 9.9[b]**	**-**	**-**

[a] peak temperature [b] mean value ± standard deviation

Table 2.10: Measurements of melting temperature (onset) (T_m), latent heat of melting (ΔH_m), crystallization temperature (onset) (T_c), and latent heat of crystallization (ΔH_c) for **inositol** carried out with DSC at various heating/cooling rates (HR/CR).

Reference	T_m (°C)	ΔH_m (J/g)	T_c (°C)	ΔH_c (J/g)	HR/CR (°C/min)	Purity %
[91]	224.0 ± 0.2	257.1 ± 0.4	186.3 ± 1.7	196.5 ± 0.6	0.5	99
[134]	216.3	185.3	182.3	206.6	1	-
[91]	224.2 ± 0.1	257.6 ± 0.4	185.5 ± 1.9	198.6 ± 0.5	1	99
this work	224.0 ± 0.2	249.6 ± 8.6	184.4 ± 0.6	191.4 ± 4.6	1	≥99
[91]	224.3 ± 0.2	256.3 ± 1.5	180.9 ± 0.2	196.9 ± 1.8	5	99
[91]	224.5 ± 0.2	261.8 ± 0.1	181.4 ± 0.5	198.6 ± 0.2	5	99
[142]	225.5[a]	351.6	185.7[a]	325.8	6	99
[91]	224.8 ± 0.4	256.9 ± 1.0	178.1 ± 0.4	190.4 ± 1.3	10	99
[143]	227.9[a]	260.7	183.8[a]	190.9	10	≥99
[144]	224.9[b]	260.9	191.4[b]	198.0	10	98
-	**224.0 ± 2.8[c]**	**259.8 ± 37.6[c]**	**184.0 ± 3.5[c]**	**209.4 ± 39.1[c]**	**-**	**-**

[a] peak temperature [b] unspecified type of temperature [c] mean value ± standard deviation

Table 2.11: Measurements of melting temperature (onset) (T_m), latent heat of melting (ΔH_m), crystallization temperature (onset) (T_c), and latent heat of crystallization (ΔH_c) for **dulcitol** carried out with DSC at various heating/cooling rates (HR/CR).

Reference	T_m (°C)	ΔH_m (J/g)	T_c (°C)	ΔH_c (J/g)	HR/CR (°C/min)	Purity %
[91]	186.4 ± 0.1	322.6 ± 0.7	120.5 ± 1.3	239.5 ± 6.1	0.5	99
[134]	180.1	257.2	102.1	245.7	1	-
[91]	186.0 ± 0.1	323.2 ± 2.1	120.2 ± 1.1	216.8 ± 3.5	1	99
this work	187.2 ± 0.1	330.0 ± 0.5	120.1 ± 0.8	235.8 ± 2.1	1	≥99
[91]	185.9 ± 0.2	334.1 ± 0.6	116.9 ± 2.4	232.4 ± 5.1	5	99
[91]	187.3 ± 0.1	350.8 ± 2.1	116.9 ± 1.3	232.4 ± 0.9	5	98
[145]	187.4	401.8	115.8	285.2	10	≥99
[91]	187.8 ± 0.8	333.5 ± 0.8	113.9 ± 0.9	254.9 ± 0.6	10	99
-	**186.0 ± 2.3[a]**	**331.7 ± 37.1[a]**	**115.8 ± 5.6[a]**	**242.8 ± 19.1[a]**	**-**	**-**

[a] mean value ± standard deviation

degree of cooperation in molecular motion and slow molecular mobility [113]. Therefore, the difficulties in crystallization of xylitol and sorbitol should be appropriately taken into account to assess their possible use as PCMs for different LHTES applications.

In general, this behavior is considered a significant drawback that could hinder their use as PCMs for short-term LHTESs [90]. In fact, these issues result in a complicated energy discharge triggering and a low discharge power, respectively. For this reason, among the studied active nucleation triggering techniques that allow to release the stored heat on demand [146], methods suitable for these two SAs should be used to appropriately allow energy discharge at the temperatures required for the specific applications.

Figure 2.4 shows the latent heat of melting and crystallization as a function of the melting and crystallization temperatures of the sugars analyzed. It can be seen that the temperature range covered by the melting temperature of the six sugars is between 90 °C and 220 °C. This confirms the fact that this family of substances can be considered as potential PCMs for low to medium temperatures LHTES as mentioned in Table 2.2.

For more information on the comparison of temperatures and latent heats of melting and crystallization, please refer to the review on thermophysical properties and thermal stability of sugar alcohols as PCMs already published and available in the literature [97].

2.5.4 Thermal Stability

As specified before, to understand whether a PCM is suitable for LHTES applications, it is necessary to know not only the thermophysical properties of the material but also its thermal stability under certain conditions of use. Three different aspects can be analyzed: thermal endurance, degradation temperature, and long-term thermal stability or cycling stability.

In this section, the results obtained from the experimental campaign regarding the maximum thermal stable temperature and the final degradation temperature will be reported. These results will also be compared with those found in the literature.

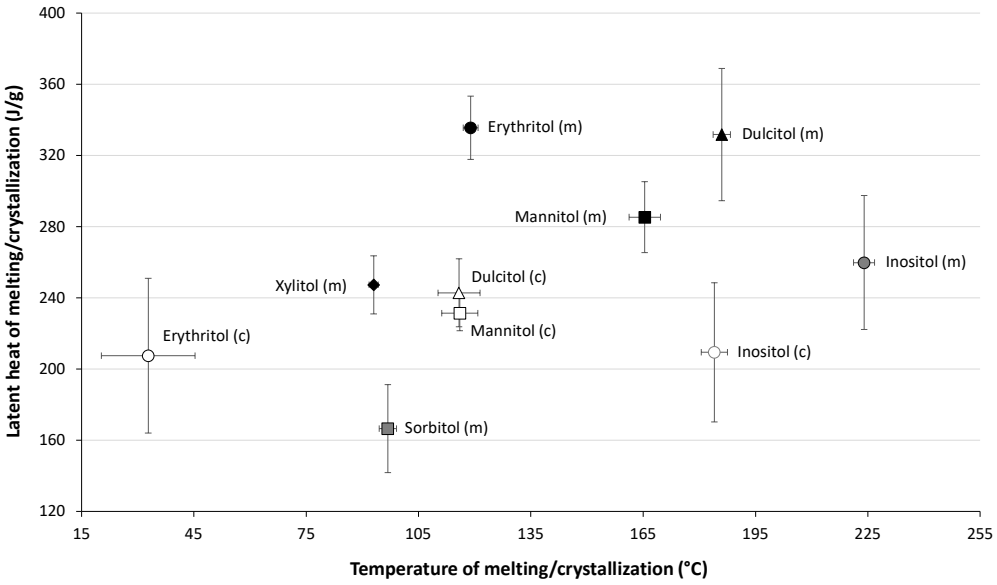

Figure 2.4: Average melting and crystallization properties of the studied SAs taken from the literature and reported in the previous Tables. The bars in the figure indicate the standard deviations of the properties. The letters (m) and (c) indicate the melting and crystallizazion points, respectively.

Degradation temperature

The literature degradation temperature measurements for the studied SAs carried out with the TGA technique are shown in Table 2.12, together with the values measured from my experimental campaign in the microlaboratory at the WiB institute. The maximum thermal stable temperature, $T_{\max}$ (i.e. the maximum temperature at which the substance can be heated with negligible loss of mass), and the final degradation temperature, $T_{\deg}$ (i.e. the temperature at which the substance is completely evaporated), are provided. In my measurements, the values of $T_{\max}$ and $T_{\deg}$ refer to the achievement of a mass loss of 1% and 95%, respectively. The purge gas and the heating rate used during the TGA are also provided.

Figure 2.5 represents the measured sugar alcohols percentage mass as a function of temperature. It can be seen that in all the analyzed SAs, the loss of mass occurs in a single step. From this figure, the initial onset temperature values, $T_{\text{onset,i}}$ (i.e. the temperature obtained from the intersection of the tangents to the point of deviation from the initial weight and to the inflection point of the TG curve of each sugars), were also calculated according to the standards [147]. This temperature is equal to 314.0 °C for xylitol, 352.4 °C for sorbitol, 303.2 °C for erythritol, 363.9 °C for mannitol, 377.1 °C for inositol, and 365.9 °C for dulcitol.

Here again, it is evident from the amount of data collected from the literature that, as with the thermophysical properties described in the section 2.5.3, some SAs have been analyzed more than others. From Table 2.12, in fact, it is evident that there are several studies where the authors performed thermogravimetric analysis for erythritol, mannitol, xylitol, and dulcitol, while a very limited number of results were collected for sorbitol and inositol. As a general comment, the $T_{\max}$ for the six SAs are on average equal to about 200 °C for xylitol, about 250 °C for sorbitol, slightly lower than 200 °C

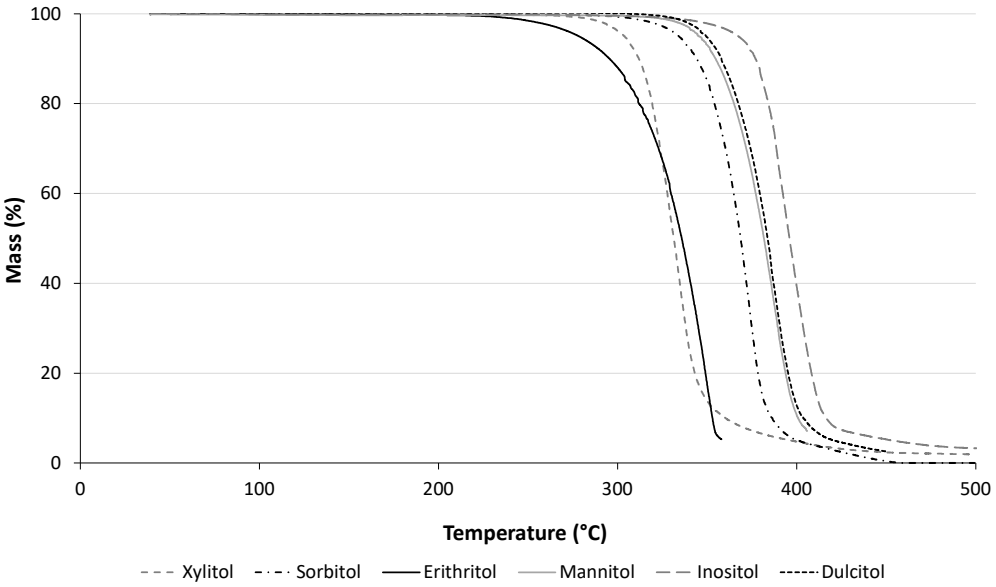

Figure 2.5: TG curves of xylitol, sorbitol, erythritol, mannitol, inositol and dulcitol.

for erythritol, about 250 °C for mannitol, lower than 300 °C for inositol, and about 250 °C for dulcitol.

It can be noted that the difference between $T_{\max}$ and T_{m} is about 60 °C for dulcitol, about 89 °C for erythritol, mannitol, and inositol, and more than 100 °C for xylitol and sorbitol. From this it follows that the maximum temperatures that these SAs can be heaten up to with respect to their T_{m} must be considered in order to properly use them in LHTES applications.

However, it should be noted that the measured values for the same SA are in certain cases very different among the various sources. Reason for that might be the instrumentation type, the used purging gas, material purity grade, heating/cooling rates, and the choice of mass loss percentage associated with $T_{\max}$ and $T_{\deg}$.

Regarding the value of mass loss chosen to define $T_{\max}$ and $T_{\deg}$, it should be noted that not much information and justification is available in the literature, nor there is agreement between the various works.

In this regard, Salyan and Suresh [148] and Salyan et al. [136] explained that the reported $T_{\max}$ for mannitol (equal to 300 °C) corresponds to a mass loss of less than 2%. Instead, John et al. [149] reported a $T_{\max}$ of 190 °C for dulcitol, corresponding to a mass loss lower than 1%.

Salyan and Suresh [150], Salyan and Suresh [151], and Pethurajan et al. [137] reported a $T_{\deg}$ of 500 °C for mannitol, corresponding to a residual mass of 2.84%. The $T_{\deg}$ of 557 °C for mannitol measured by Mojiri et al. [152] corresponds to a residual mass of 0.172%.

Table 2.12: Measurements of maximum thermal stable temperature (T_{max}) and final degradation temperature (T_{deg}) for the studied SAs carried out with TGA at various heating rates (HR). The values of the temperatures are slightly different depending on the various heating rates from 5 to 25 °C/min.

	T_{max} (°C)	T_{deg} (°C)	HR (°C/min)	Purge gas	Reference
Xylitol	200.0	330.0	10	air	[98]
	178.1	402.2	10	nitrogen	[111]
	-	359.5	10	nitrogen	[112]
	200.0	-	10	argon	[105]
	200.0	328.2	10	nitrogen	[106]
	278.6	395.3	20	nitrogen	this work
Sorbitol	256.4	491.4	10	nitrogen	[117]
	240.0	-	10	argon	[105]
	307.1	399.6	20	nitrogen	this work
Erythritol	183.7	250.0	3	nitrogen	[153]
	180.0	255.0	5	argon	[124]
	160.0	-	5	argon	[105]
	240.0	335.0	10	nitrogen	[154]
	203.6	309.2	10	-	[155]
	180.0	300.0	10	nitrogen	[127]
	240.0	335.0	10	nitrogen	[128]
	200.0	318.0	10	nitrogen	[156]
	-	326.2	10	nitrogen	[112]
	238.2	358.0	20	nitrogen	this work
	215.0	316.0	-	-	[133]
Mannitol	267.0	427.0	5–25 [a]	nitrogen	[157]
	259.0	424.0	10	air	[68]
	294.0	410.0	10	nitrogen	[154]
	235.6	312.5	10	nitrogen	[158]
	207.0	557.0	10	nitrogen	[152]
	300.2	397.0	10	nitrogen	[159]
	252.0	386.0	10	nitrogen	[139]
	280.0	360.0	10	nitrogen	[141]
	50.0	340.0	10	nitrogen	[138]
	300.0	-	10	nitrogen	[160]
	280.0	-	10	argon	[105]
	270.0	-	10	air or argon	[161]
	300.0	500.0	20	-	[150]
	300.0	380.0	20	nitrogen	[148]
	323.0	405.8	20	nitrogen	this work
	208.9	500.0	-	nitrogen	[137]
	310.0	500.0	-	-	[151]
	300.0	-	-	-	[136]
Inositol	271.6	526.7	10	dry air	[143]
	323.1	456.5	20	nitrogen	this work
Dulcitol	190.0	-	2	nitrogen	[149]
	293.0	481.0	10	air	[68]
	263.5	349.5	10	nitrogen	[158]
	202.0	312.0	10	air	[145]
	295.0	-	10	nitrogen	[160]
	332.1	420.3	20	nitrogen	this work

[a] mean value ± standard deviation

Chapter 3

High Concentration Ratio Solar Box Cooker: Design, Manufacture, and Test

The first prototype presented in this manuscript falls into the category of solar box cookers. The device was built and tested at the DIISM laboratories. The materials used and the steps followed for the construction are reported together with the experimental setup developed to characterize the device. During the outdoor experimental campaign, two different types of tests were carried out: no-load tests and tests with load. The fluids used for the load tests were water and peanut oil. Different load configurations were tested, and the impact on the final performance of the device when a black-painted pot was used in the cooking chamber compared to a normal aluminum pot was also studied. The results obtained from the experimental campaign are reported in detail.

3.1 Solar Box Cookers in Literature

Hereafter some of the most significant works present in the literature regarding solar box cookers are reported.

Mahavar et al. [162] tested a novel solar cooker called the Single Family Solar Cooker. The authors performed different tests on different days under different conditions using water as test fluid. Under no-load condition, the maximum temperature reached by the plate was 144 °C. The two figure of merits were 0.116 °Cm^2/W and 0.466, respectively and the initial cooking power was 103.5 W.

Kahsay et al. [163] constructed two solar box cookers with a wooden outer box, a metal inner box and a double glazing as upper cover equipped with internal reflector. The only difference lies in the geometry of the metal box: one is painted in black and the other is covered with reflecting film. The authors compared the performance to an identical cooker without the reflectors, in two modes: dry and boiling. The maximum temperature and efficiency achieved for the cooker with reflectors were about 22 °C and 5%, respectively.

Kumar et al. [164] designed and constructed a truncated pyramid solar box cooker with the aim of meeting farming household demands in India. The maximum temperatures reached were 140 °C during no-load test and 98.6 °C at full-load of water modes, respectively.

In another study by Kumar et al. [165], the maximum efficiency of the device was reported to be 54%. They also compared economic aspects of their device to common cooking methods. Their results showed that, in India, the design was more costeffective than the methods using electricity or LPG. However, systems using wood or kerosene were found to be more affordable.

A novel, modified box type cooker was presented by Singh and Sethi [166]. Characterized by an inclined configuration with three shelves for the placement of cooking vessels, the authors claimed that their cooker can absorb 16%-54% more solar thermal energy compared to normal box cookers. During testing, they also reported that it can reach up to 100 °C and 80 °C with and without booster mirrors, respectively.

Saxena and Agarwal [167] presented a novel hybrid design of solar box cooker. A trapezoidal duct was attached to the cooker with the aim of improving hot air circulation inside the cooker. A halogen lamp was placed inside the duct, and some copper balls were put into the cooker itself. The authors claimed that these modifications enabled the cooker to operate even under low solar irradiance circumstances. The overall efficiency of the cooker was reported to be 38.10%, with an overall efficiency increase of 45.11%.

Sagade et al. [168] evaluated the performance of a solar box cooker using a modified cooking pot. The pot was equipped with a glazed lid. The authors used glycerin as an intermediate temperature test load. The results shown that the presence of a glass lid reduced the heat loss and improved the final performances of the device.

3.2 Design and Optical Analysis

The presented solar box cooker is an high efficiency prototype based on a design developed by Eng. Gianni Crovatto [169]. Starting from the construction diagrams and schemes available on its website, some modifications were made in terms of selected materials to improve the final thermal and optical performance of the device.

The final proposed cooker is shown in Figure 3.1, Figure 3.2 and 3.3. The device is composed of a large box with the function of cooking chamber covered on the top by a double glass cover with diameter 46 cm. The aim of this transparent cover is to allow solar radiation to be transmitted to the absorber.

In the higher part of the box there is a double row of booster mirrors. These mirrors allow an additional amount of solar radiation to be reflected and, then, concentrated towards the cover and the cooking chamber. Each row includes 12 mirrors and has a different inclination angle with respect to the horizontal plane. In the upper row, each mirror has a length of 63 cm, a rounded top and can be reclined to reduce the space occupied by the cooker when it is not used and to facilitate transportation. The lower row mirrors, instead, have a trapezoidal shape and are 61.6 cm long; one of the lower mirrors includes a fissure which allows solar radiation to be projected on an indicator. This indicator is used to evaluate the correct cooker alignment with the sun. Figure 3.4 shows some booster mirror details and how solar radiation is concentrated.

The cooker aperture area A_{a} is represented by the maximum section area of the upper mirrors. From Figure 3.4, it is possible to find that the aperture area is equal to:

$$\begin{aligned} A_{\mathrm{a}} &= A_{\mathrm{dod}} + 12\, A_{\mathrm{cs}} \cos\theta_2 \\ &= 1.80 + 0.09 \\ &= 1.89\,\mathrm{m}^2 \end{aligned} \tag{3.1}$$

Figure 3.1: A picture of the solar box cooker prototype.

where A_{dod} is the dodecagon area having a side of 40.1 cm, A_{cs} is the circular segment area of one upper mirror, and θ_2 is the upper row inclination angle. The cooker geometrical concentration ratio is:

$$C = \frac{A_{\mathrm{a}}}{A_{\mathrm{g}}} = \frac{1.89}{0.17} = 11.12 \tag{3.2}$$

where A_{g} is the glass cover surface area.

The obtained concentration ratio value is very high for a solar box cooker and allows to classify this prototype between box and concentrating cookers.

The specific booster mirror geometry, inspired to a funnel/cone shape cooker, makes the prototype almost completely dependent on direct solar radiation. In other words, the cooker is not able to exploit diffuse solar radiation, thus it requires good clear-sky conditions in order to work properly and reach high temperatures.

The cooker has two border wooden hands and two wheels that allow both its movement and its azimuthal orientation. A zenithal orientation is also possible as the main structure (cooking chamber, glass cover and booster mirrors) is able to rotate around the horizontal axis. A removable hand brake keeps the cooker fixed when the zenithal tracking is not necessary. A small door allows food to be inserted in the cooking chamber, which is realized with zinc metal sheets painted with a special black coating. In the chamber, there is a vessel support able to rotate of 360°, so that it can maintain in balance the pots put on it when the zenithal orientation changes.

The prototype has a mass of about 84 kg and its volume is about 2.6 m^3.

3.3 Manufacture and Materials

The cooker manufacturing process consisted of 4 consecutive phases:

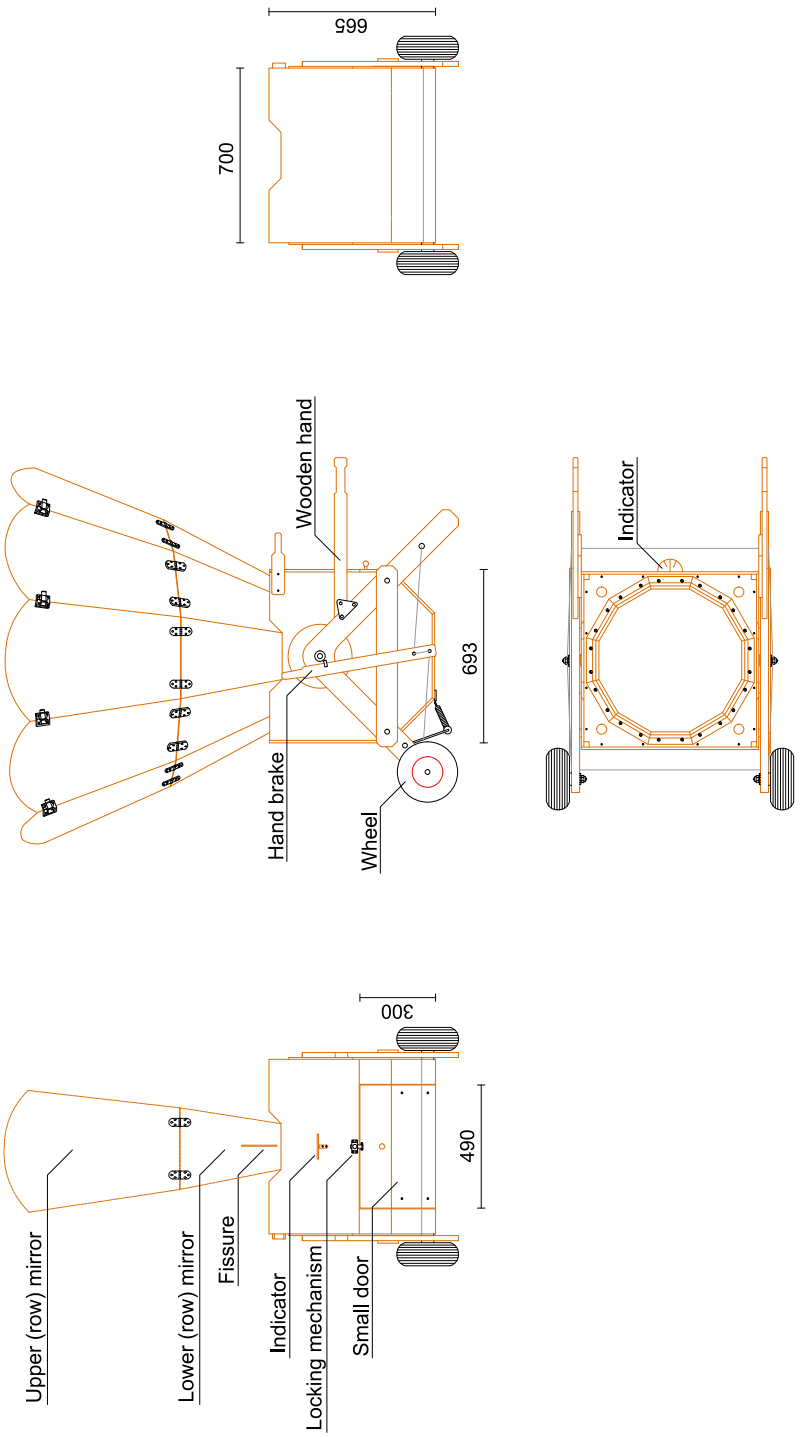

Figure 3.2: Solar box cooker prototype views [1].

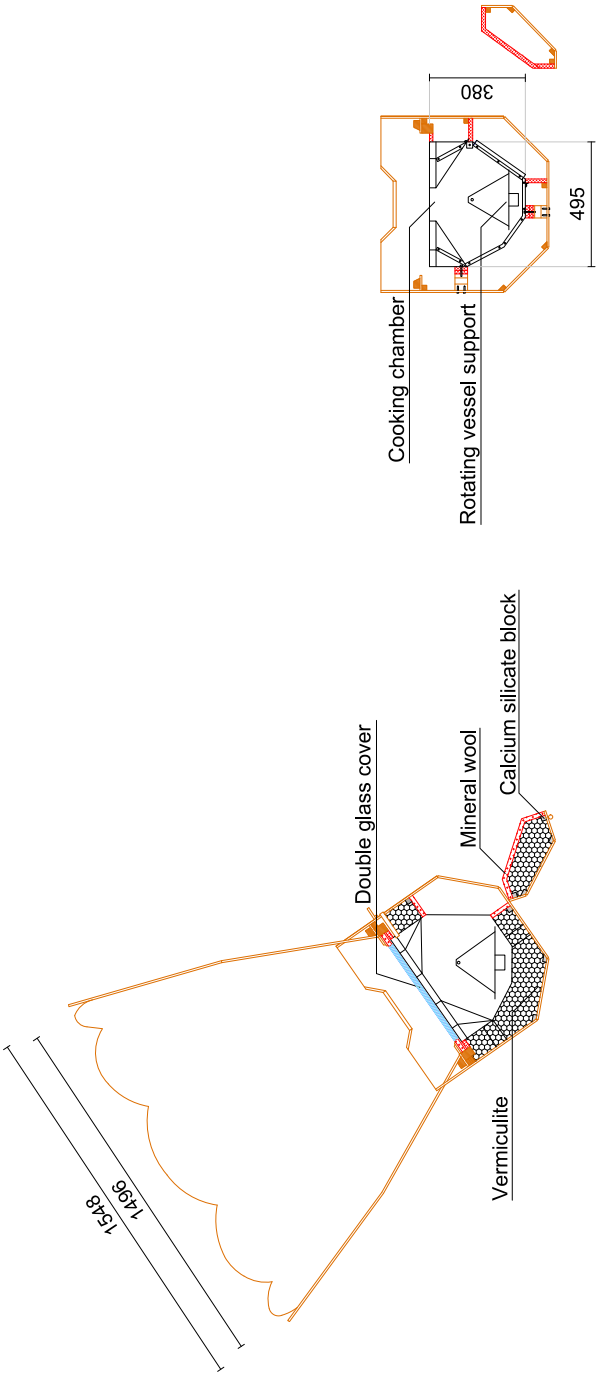

Figure 3.3: Solar box cooker prototype sections [1].

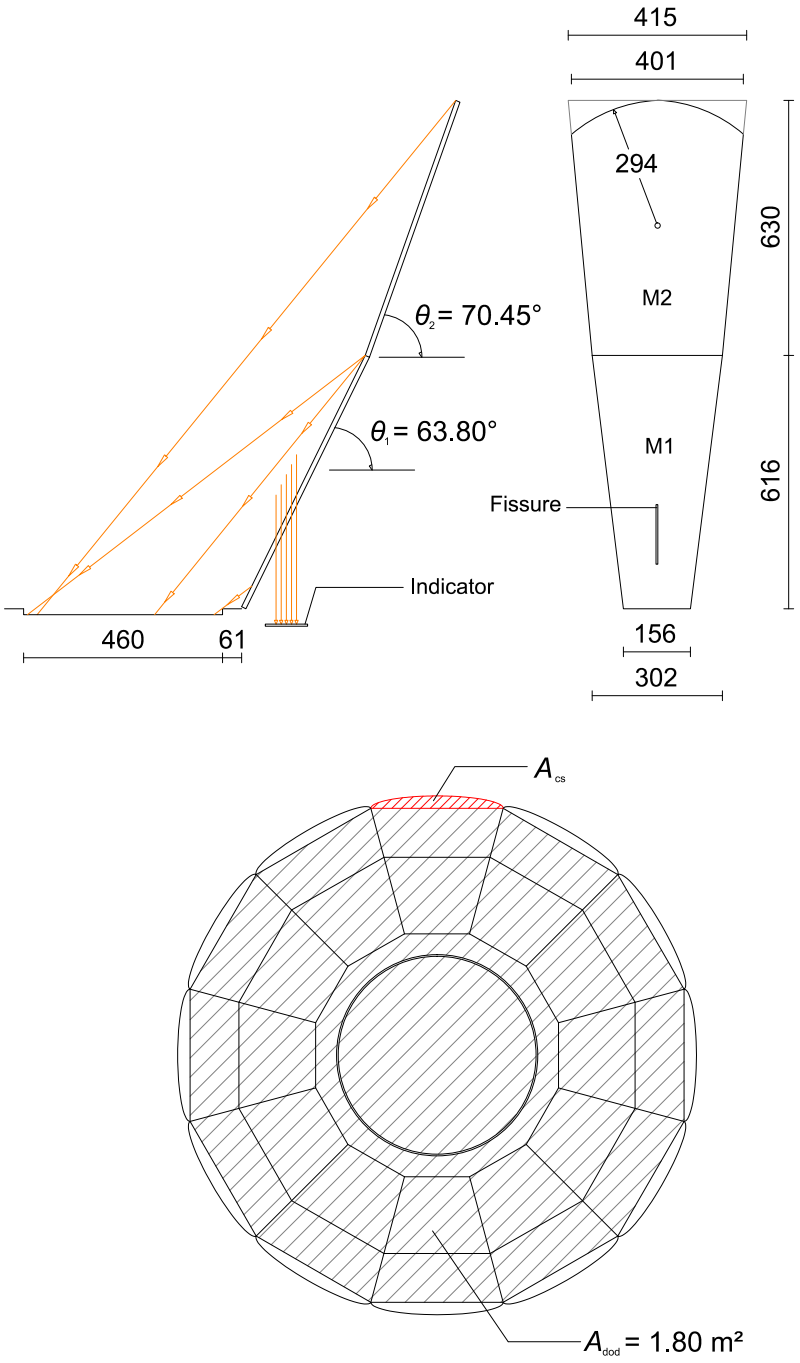

Figure 3.4: Solar box cooker optical scheme [1].

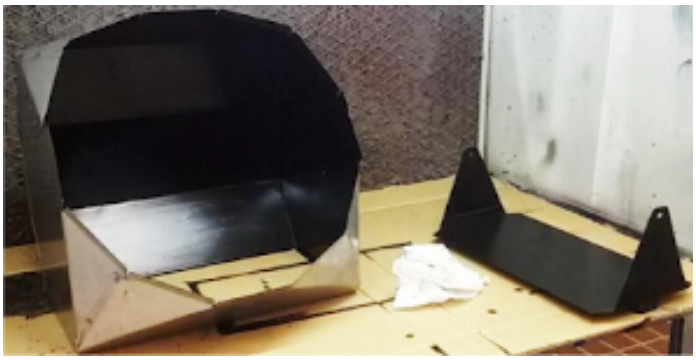

Figure 3.5: Painted cooking chamber and vessel support.

1. cooking chamber realization and painting;
2. external structure realization;
3. insulating material installation;
4. booster mirror assembly.

3.3.1 Cooking Chamber Realization and Painting

Starting from a stainless steel frame 6/10 mm thick, which was bended and drilled where required, the cooking chamber walls were obtained. Once all the components were finished, they were welded to assume the cooking chamber final shape. The box structure is open on two sides: one is used to introduce food, while the second to let solar radiation reaching the absorber.

The small door was the second element to be realized. Using a stainless steel frame 10/10 mm thick, the vessel support was manufactured. The support was bended by 90° along the shortest sides and includes two holes and two pivots for its oscillation. A steel ballast of 2 kg was attached to the support for balance improvement.

A special selective coating (SOLKOTE HI/SORB-II) usually adopted in solar thermal applications was used to paint the cooking chamber. This selective coating is resistant to high temperature, moisture, and UV degradation, its absorptance in the solar spectrum ranges from 0.88 to 0.94 and its emissivity from 0.20 to 0.49, depending on dry film thickness and substrate. The cooking chamber and the painted vessel support are shown in Figure 3.5.

3.3.2 External Structure Realization

Starting from the side walls, which were obtained by wooden foils 0.7 mm thick, the external structure of the device was realized. The two booster mirror rows are supported by the upper frame, which has a dodecagonal shape. Several sticks were cut and embedded in each other to form the dodecagon (Figure 3.6).

Two 4 mm-thick tempered glasses were inserted in the upper frame as insulating glazing. The tempered glass has a high resistance (about four times greater than a traditional glass) and is suitable for solar thermal applications. The transmittance is about 90% in the solar spectrum, while its reflection coefficient is 8%. The lower glass

Figure 3.6: Dodecagonal upper frame.

was glued to the cooker insulating material, while the upper one was located on the insulating material and blocked in place with metal clips.

The cooker truck consists of two border hands and four legs made of phenolic compound, two of which provided with wheels to allow the cooker movement and azimuthal tracking. Two pivots connect the truck to the cooker.

To fix its zenithal orientation, a simple mechanism based on a spring, stretcher, lever and nylon wire was deployed to allow for manual blocking of the rotation.

Finally, the cooking chamber was placed inside the external structure. Its correct alignment with respect to the external structure was guaranteed by spacers made of mineral wool and phenolic compound.

3.3.3 Insulating Material Installation

In order to reduce heat losses and obtain higher cooking temperatures, the cooking chamber metal walls were thermally insulated. The first insulation material chosen was glass wool. During an experimental test, due to the high temperatures reached by the walls of the cooking chamber, the glass wool started to produce smoke, as evident from Figure 3.7. For this reason, the insulation material was changed: instead of glass wool, silicate blocks and vermiculite were inserted between the metal frame and the external wooden structure. Some cooker parts were also insulated using mineral wool.

Calcium silicate sheets with hydrate mineral matrix are usually obtained with special productive systems and they can be also used for structural purposes. Their main properties are: lightness, fire stability, A1 class incombustibility, environmental resistance, and thermal conductivity in the range of 0.1 to 0.2 $\mathrm{W/(m\,K)}$. The silicate blocks adopted in the solar box cooker also include special additives to further enhance fire protection and lightness. This kind of blocks is generally used in slabs and false ceilings.

Vermiculite is a natural product, very widespread thanks to its mechanical and physical properties: it is used stand alone or mixed with cementive substances in the building sector, as thermal and acoustic insulating material, and in finishings, in agriculture as draining material and fertilizing/pesticide carrier, and in other industries as fireproof material and lubricant. Standard vermiculite used in the building industry looks like unrefined gravel and is very light, presenting irregular fragments of 1–2 cm diameter. Each fragment has a shining grey-yellow color and consists of a large number

Figure 3.7: Smoke from the solar box cooker during an experimental test.

of stacked layers, which can be squashed with a reduced force. Vermiculite has a density and a thermal conductivity of about 90 kg/m^3 and 0.049 W/(m K), respectively. Figure 3.8 shown the Vermiculite inserted in the small door cavity between the two silicate blocks.

3.3.4 Booster Mirror Assembly

The booster mirrors were realized using phenolic compound elements covered by aluminum mirrors. To increment the amount of solar radiation collected by the absorber, special aluminum-based reflective foils (MIRO-SUN Weatherproof Reflective 90) were used. When compared to standard aluminum foils, these mirrors can better withstand atmospheric agents and guarantee an overall reflection of about 94% in the solar spectrum with a negligible dependence on the incident angle.

3.4 Experimental Tests And Setup

In this section, the tests performed, the test bench used and the parameters calculated for the final characterization of the prototype are described.

3.4.1 Experimental Tests

Experimental tests were carried out in the months from May to July 2016 and March 2017 on the DIISM roof (latitude 43.5867 N, longitude 13.5150 E). The cooker orientation was adjusted by the operator about every 5 minutes taking the solar ray indicator as a reference, in order to guarantee a correct alignment towards the sun. Two kinds of experimental tests were conducted: with and without load. Tests without load allowed to evaluate the maximum temperature reachable by the solar box cooker.

Tests with load, instead, were accomplished inserting in the cooking chamber of the device a certain amount of fluid contained in cylindrical aluminum vessels having 18 cm diameter and 16 cm height. Each vessel can contain up to 4 liters of fluid. The

Figure 3.8: Vermiculite inserted in the small door cavity.

lids were provided with a small hole: this was used to let a thermocouple inside the vessels. Different load test combinations were carried out:

1. with standard and black vessels;
2. with one and two vessels;
3. with water and peanut oil.

It is evident that the two test fluids selected for the tests with load were water and peanut oil. Water was selected because of its availability and representativity of a cooking scenario, moreover it is the best choice to be able to compare the experimental results with the literature. The main drawback of water is that at atmospheric pressure its boiling temperature is equal to 100 °C, thus the useful testing range before boiling is rather limited. This hinders a complete solar cooker characterization, especially if the cooker is intended to work at high temperatures.

For this reason, it was decided to use an additional substance to better characterize the solar box cooker. Peanut oil was finally chosen as it has a boiling temperature higher than 200 °C and is a diffused cooking oil. Its specific heat ranges from 2045 to 2342 J/(kg °C) in the interval 35–165 °C [170].

3.4.2 Test Bench

Figure 3.9 shown the test bench used to characterize the solar box cooker.

The quantities recorded during the tests were ambient temperature T_{amb}, outer and inner glass cover temperatures T_{go} and T_{gi}, absorber temperature T_{a}, air inside the cooking chamber temperature T_{air}, testing fluid temperature T_{f} and direct normal solar

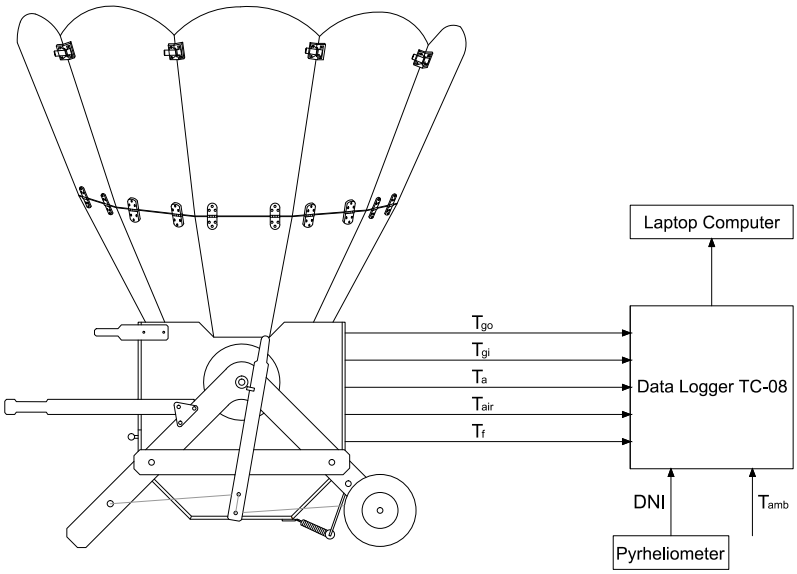

Figure 3.9: Solar box cooker test bench.

irradiance *DNI*. The sensors used to detect all temperatures were K-type thermocouples, while a first-class Eppley NIP (Normal Incidence Pyrheliometer) mounted on a solar tracker was used to measure the solar irradiance. For additional information regarding the instrument and their uncertainties please refer to the Appendix B.

Global (and diffuse) solar radiation was not measured as this solar box cooker has a high concentration ratio and its optical behavior is more similar to a concentrating cooker than a box one [171].

The signals from the thermocouples and the pyrheliometer were acquired and elaborated by a Pico Technology TC-08 data logger. The temperature and solar radiation evolution was visualized in real-time during tests on a laptop computer through the PicoLog data acquisition program, and data was exported to be further analyzed after testing.

3.4.3 Experimental Parameters

The main parameters used to characterize the optical and thermal performances of the solar box cooker are provided in Table 3.1.

In addition to the parameters in Table 3.1, also the solar cooker cooking power proposed by Funk [7] was calculated as:

$$P = \frac{m\, c\, \Delta T}{\Delta t} \tag{3.3}$$

where, for each 10-minute time interval, ΔT is the fluid temperature difference and Δt is equal to 600 s. Funk [7] presented an additional term called standard (or adjusted) cooking power which is given as follows:

$$P_{\mathrm{s}} = P\, \frac{G_{\mathrm{ref}}}{G_{\mathrm{av}}} \tag{3.4}$$

Table 3.1: Parameters calculated for the experimental characterization of the solar box cooker.

Experimental parameter	Equation	Equation parameters
First figure of merit [19]	$F_1 = \frac{T_{\mathrm{a,max}} - T_{\mathrm{amb}}}{G_{\mathrm{n}}}$	A_{a} = aperture area of the solar cooker c_{f} = specific heat of the test fluid
Heating time interval	$\Delta t_{\mathrm{h}} = t(T_2) - t(T_1)$	C = geometrical concentration ratio G_{n} = global normal solar irradiance
Second figure of merit [19]	$F_2 = \frac{F_1 m_{\mathrm{f}}\, c_{\mathrm{f}}}{A_{\mathrm{a}} \Delta t_{\mathrm{h}}} \ln \left[\frac{1 - \frac{1}{F_1}(T_1 - T_{\mathrm{amb,av}})/G_{\mathrm{n,av}}}{1 - \frac{1}{F_1}(T_2 - T_{\mathrm{amb,av}})/G_{\mathrm{n,av}}} \right]$	$G_{\mathrm{n,av}}$ = mean G_{n} measured at Δt_{h} $G_{\mathrm{n,ref}} = 900\,\mathrm{W/m^2}$ (for t_{s} calculation)
Specific boiling time [172]	$t_{\mathrm{s}} = \frac{\Delta t_{\mathrm{h}} A_{\mathrm{a}}}{m_{\mathrm{f}}}$	η_0 = optical efficiency F' = heat exchange efficiency factor
Characteristic boiling time [172]	$t_{\mathrm{ch}} = t_{\mathrm{s}} \frac{G_{\mathrm{n,av}}}{G_{\mathrm{n,ref}}}$	m_{f} = mass of the test fluid T_{amb} = ambient temperature
Overall efficiency [172]	$\eta_{\mathrm{av}} = \frac{m_{\mathrm{f}}\, c_{\mathrm{f}} (T_2 - T_1)}{G_{\mathrm{n,av}} A_{\mathrm{a}} \Delta t_{\mathrm{h}}}$	$T_{\mathrm{a,max}}$ = absorber stagnation temperature $T_{\mathrm{amb,av}}$ = mean T_{amb} measured at Δt_{h}
Cooker opto-thermal ratio [173]	$COR = \frac{\eta_0 C}{U_{\mathrm{l}}}$	$T_{\mathrm{f,av}}$ = mean T_{f} measured at Δt_{h} $t(T_1)$ = starting time of the heating phase $t(T_2)$ = ending time of the heating phase
Maximum achievable fluid temperature [173]	$T_{\mathrm{fx}} = T_{\mathrm{amb,av}} + \frac{F' \eta_0 G_{\mathrm{n,av}}}{F' U_{\mathrm{l}} / C}$	U_{l} = heat loss factor

Table 3.2: Summary of tests without load.

Quantity	Test 1	Test 2	Test 3
Date	23/06/2016	15/03/2017	17/03/2017
T_{amb} (°C)	29.10	15.53	20.71
$T_{amb,av}$ (°C)	27.74	14.49	20.10
DNI (W/m^2)	630.36	709.18	865.19
DNI_{av} (W/m^2)	683.59	771.63	865.22
$T_{a,max}$ (°C)	283.73	283.35	298.67
F_1 (°C/(W/m^2))	0.40	0.38	0.32
$F_{1,av}$ (°C/(W/m^2))	0.37	0.35	0.32

where G_{av} is the average solar irradiance for each time interval and G_{ref} is a reference illumination intensity level equal to 700 W/m^2.

All the parameters reported in Table 3.1 were calculated over a time interval Δt_h required to raise the temperature of the fluid from 40 °C to 90 °C for the tests with water (as suggested by Funk [7]) and in the range 40–220 °C for the tests with peanut oil.

For the determination of the cooker opto-thermal ratio (COR) proposed by Lahkar et al. [173], the total time interval chosen for water (40–90 °C) and peanut oil (40–220 °C) is divided into sub-intervals of 5 minutes each. For each sub-interval, the average global normal solar irradiance, the average ambient temperature, the average test fluid temperature, the efficiency and the parameter χ are determined, where $\chi = (T_f - T_{amb})/DNI$. By plotting the thermal efficiency η against the parameter χ for each identified sub-interval, it is possible to identify the regression line of the efficiency curve and its coefficient of determination R^2. The regression line's intercept and opposite value of the slope correspond to the parameters $F'\eta_0$ and $F'U_l/C$, which are necessary for the determination of the COR parameter.

3.5 Experimental Results

All the results obtained from the no-load and load tests are described in detail.

3.5.1 Tests without Load

Three tests without load were conducted under different environmental conditions. From Table 3.2 it can be seen that the most representative is test 3, since ambient temperature and direct normal irradiance corresponding to the maximum absorber temperature were very similar to their daily averages. In addition, this test was characterized by the highest DNI_{av}.

Figure 3.10 reports temperatures and solar radiation measured during test 3. The maximum absorber temperature was about 300 °C and the first figure of merit, F_1, resulted equal to 0.32 °C/(W/m^2). This value was then adopted for the cooker under study.

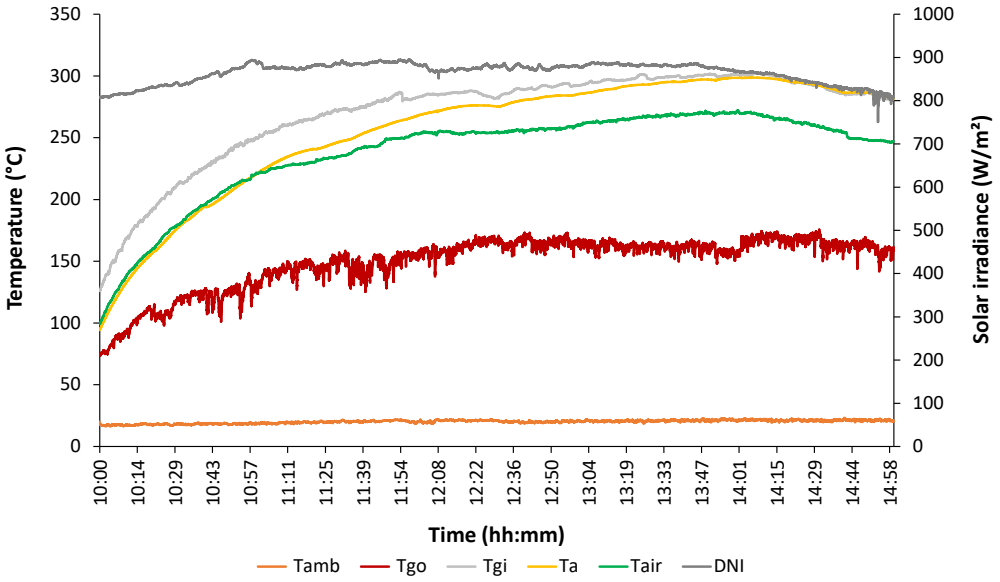

Figure 3.10: Test without load (17/03/2017).

3.5.2 Water Load Tests

Six tests were carried out using water as test fluid. As example, Figure 3.11 shows the temperatures and the solar irradiace trends of the test on May 18$^{\text{th}}$, 2016. The average direct normal irradiance was 970.29 W/m^2 and the average ambient temperature was 20.78 °C. An aluminum vessel was filled with a water mass of 3.82 kg which took about 2 hours to reach boiling.

Since the qualitative trend shown in Figure 3.11 resulted the same for the other tests, the remaining graphs were not reported. Instead, the overall water temperature trends detected during the load tests is depicted in Figure 3.12, while a summary of all measurements is reported in Table 3.3.

From Figure 3.12 and Table 3.3, it can be clearly seen that using a black vessel strongly improves the overall system performance, allowing the device to bring water to boiling in considerably less time when similar ambient conditions are registered. Moreover, tests 4, 6, and 9 in Figure 3.12 show that even with a lower average solar radiation a black vessel is able to perform better than a standard one. Furthermore, when using two vessels, either standard or black-painted, more time is always required to boil water than one vessel. Making use of two black vessels to heat water, though, demonstrated to be as fast as when one standard vessel is used (compare test 4 and 5 in Figure 3.12).

Another consideration that can be made is that two vessels (standard or black) generally exhibit better average thermal efficiency and F_2 with respect to only one vessel. This was observed also in other works [174–176].

Finally, it can be concluded that solar radiation is a critical parameter for the cooker performance, while ambient temperature plays a less important role.

Looking at Figure 3.11 or Figure 3.12, it is possible to note that the fluid temperature is described by a convex function.

Figure 3.13 reports the relation between P_{s} vs. $(T_{\text{f}} - T_{\text{amb}})$, where P_{s} is the standard cooking power defined by Funk [7], while T_{f} and T_{amb} are the average fluid and ambient

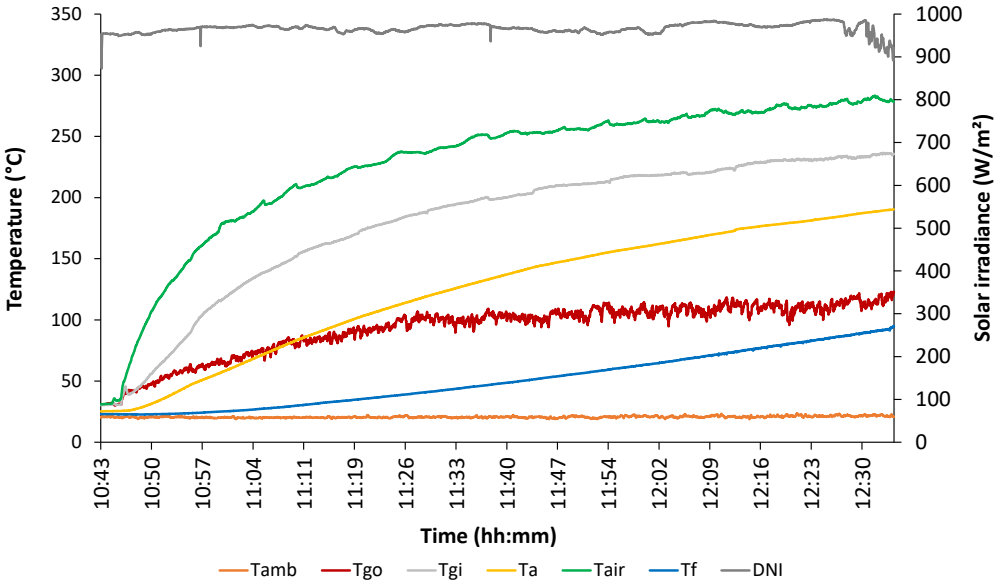

Figure 3.11: Water load test (18/05/2016, standard vessel).

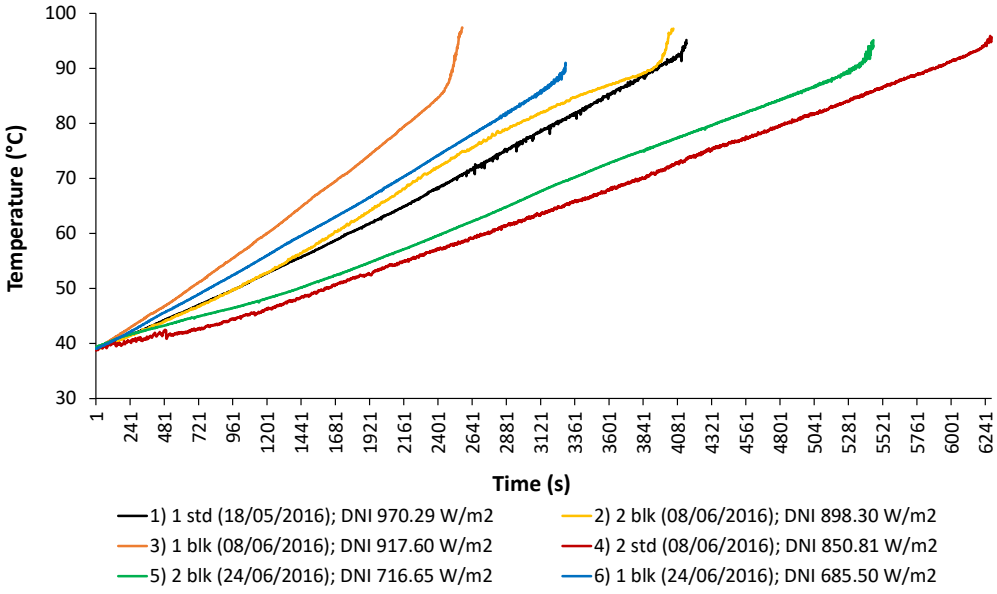

Figure 3.12: Water temperature trend.

Table 3.3: Water load test summary. Testing parameters are referred to a time interval during which water temperature rose from 40 to 90 °C.

Quantity	Test 4	Test5	Test 6	Test 7	Test 8	Test 9
Date	18/05/2016	08/06/2016	08/06/2016	08/06/2016	24/06/2016	24/06/2016
Vessel type	Standard	Black	Black	Standard	Black	Black
Vessel number	1	2	1	2	2	1
$T_{\mathrm{amb,av}}$ (°C)	20.78	24.71	27.00	28.96	30.63	31.54
DNI_{av} (W/m^2)	970.29	898.30	917.60	850.81	716.65	685.50
m_1 (kg)	3.82	3.64	3.77	3.76	3.87	3.84
m_2 (kg)	-	3.67	-	3.76	3.86	-
Δt (h)	1.07	1.06	0.68	1.58	1.46	0.89
t_{s} (min m^2/kg)	31.77	16.42	20.40	23.87	21.48	26.33
t_{c} (min m^2/kg)	34.25	16.39	20.79	22.56	17.10	20.05
η_{av}	0.11	0.24	0.19	0.17	0.23	0.20
F_2	0.13	0.28	0.21	0.20	0.27	0.24

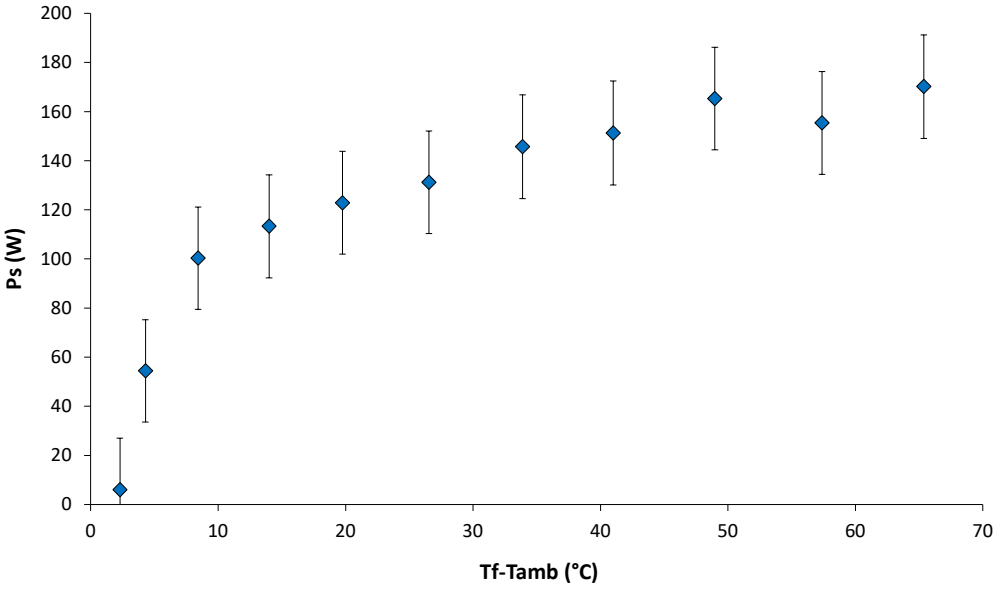

Figure 3.13: Standard cooking power as a function of temperature difference for water (18/05/2016, standard vessel).

temperature, respectively, in each time interval.

The trend shown in Figure 3.13 goes against the forecasts, as the expected trend would have been linearly decreasing with the temperature difference. The bigger thermal losses to the environment as the temperature difference increases, in fact, should cause the cooker power to decrease, but also other tests with water performed with this cooker showed a similar trend. Further, also Sethi et al. [177] in their work reported a similar trend.

A possible explanation is that, at the tested temperatures, the cooker thermal losses are too low to influence the useful fluid gain: the cooker during tests is not able to reach a quasi-steady state, as its thermal load is too low to be able to bring an appreciable contribution. The standard cooking power trend in Figure 3.13 could be further explained by looking at the fluid temperature trend in Figure 3.11. In fact, the fluid convex trend implies that, in successive equal time intervals, the delta temperature increases continuously, and so behaves the cooking power.

Since water load tests did not allow to completely characterize the solar box cooker, peanut oil load tests were carried out to verify how the cooker works at high temperatures.

3.5.3 Peanut Oil Load Tests

Two tests with peanut oil were carried out. As an example, Figure 3.14 shows temperatures and solar radiation trends detected during the test performed on July 1st, 2016. A black vessel was filled with 3 kg of oil. The average ambient temperature and direct solar irradiance were, respectively, 30.80 °C and 807.78 W/m^2. The test was interrupted when the oil reached its smoke point, around 220 °C, in order to avoid degradation.

Comparing Figure 3.14 with Figure 3.11, it is possible to see that oil and water

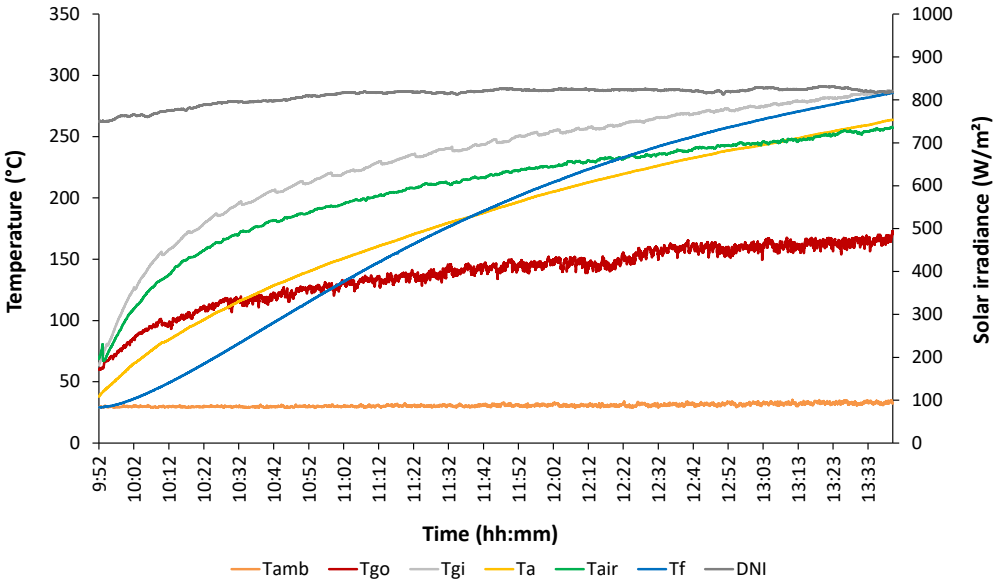

Figure 3.14: Peanut oil load test (01/07/2016, black vessel).

temperature trends are different: in fact, the oil curve is initially convex, then, starting from about 90 °C, concave. Thus, the standard cooking power procedure [7] was repeated for the peanut oil and a linear regression was fitted for the points having a decreasing linear trend. The results of the procedure are visible in Figure 3.15, which shows the curve fitting equation and the coefficient of determination R^2.

By plotting the thermal efficiency defined by Lahkar et al. [173] against the term $(T_\mathrm{f} - T_\mathrm{amb})/DNI$, where T_f, T_amb and DNI are, respectively, the average fluid temperature, ambient temperature, and direct normal irradiance, Figure 3.16 is obtained. In addition to the experimental points, also the thermal efficiency curve fitting equation and the coefficient of determination R^2 are shown.

The slope and the intercept coefficients of the thermal efficiency curve fitting correspond to the $F^{'}\eta_\mathrm{o}$ and $F^{'}U_\mathrm{L}/C$ parameters, where $F^{'}$ is the heat exchange efficiency factor, η_o the optical efficiency, and U_L the heat loss factor. The coefficients can also be used to determine the cooker opto-thermal ratio, COR, and the maximum achievable fluid temperature, T_fx.

A summary of the load tests carried out with peanut oil is reported in Table 3.4. From the analysis of this table, the following considerations can be outlined.

- As for the case of water, two vessels exhibit better parameters with respect to only one vessel when the solar radiation levels are comparable. This is due to the fact that the cooking chamber is better employed, resulting in a higher heat exchange efficiency factor.

- With respect to water tests, η_av is lower, as the delta temperature under consideration is higher and, hence, also the thermal losses. F_2, instead, seems to be less temperature range-dependent, especially when two vessels are considered.

- Parameters COR and T_fx are very similar in both cases, resulting almost independent of cooking load.

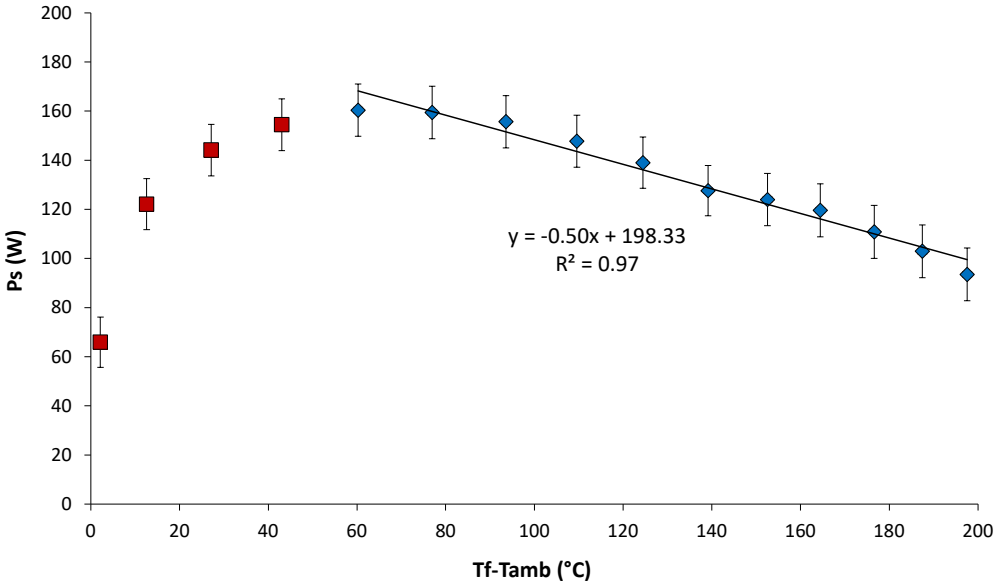

Figure 3.15: Standard cooking power as a function of temperature difference for peanut oil (01/07/2016, black vessel).

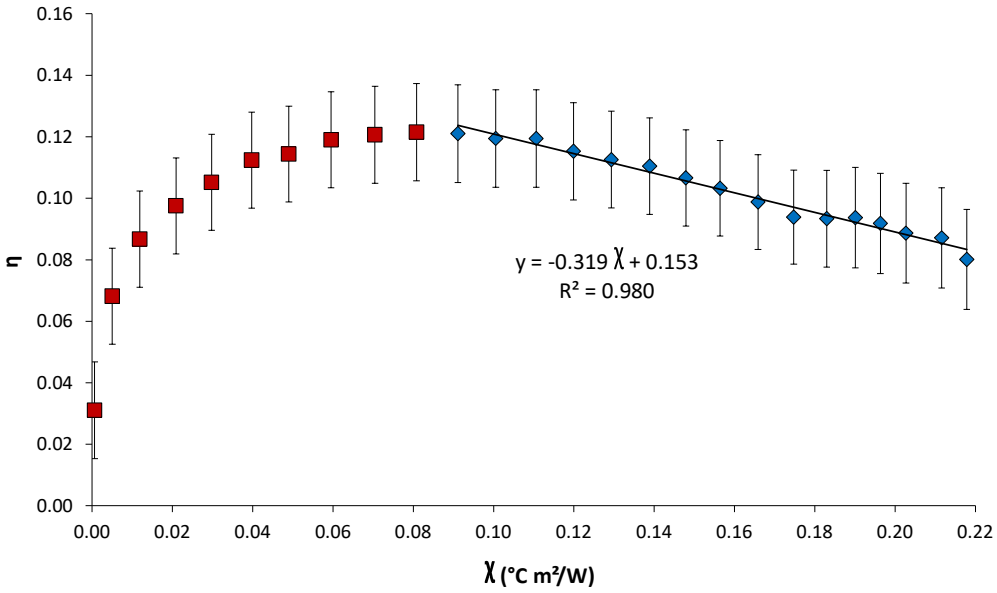

Figure 3.16: Thermal efficiency for peanut oil (01/07/2016, black vessel).

Table 3.4: Peanut oil load test summary. Testing parameters are referred to a time interval during which the oil temperature rose from 40 to 220 °C.

Quantity	Test 10	Test 11
Date	01/07/2016	12/07/2016
Vessel type	Black	Black
Vessel number	1	2
$T_{\mathrm{amb,av}}$ (°C)	30.80	33.02
DNI_{av} (W/m^2)	807.78	794.80
m_1 (kg)	3.00	3.00
m_2 (kg)	-	3.00
Δt (h)	2.06	2.76
t_{s} (min m^2/kg)	77.72	52.11
t_{c} (min m^2/kg)	69.76	46.02
η_{av}	0.10	0.17
F_2	0.19	0.30
P_{s} intercept (W)	198.33	316.15
P_{s} slope (W/°C)	0.500	0.850
$F^{'}\eta_{\mathrm{o}}$	0.153	0.245
$F^{'}U_{\mathrm{L}}/C$ (W/(m^2 °C))	0.319	0.567
COR (°C/(W/m^2))	0.480	0.432
T_{fx}	418.23	376.45

- Comparing the standard cooking power coefficients obtained during the tests, a higher intercept characterizes the case with two vessels. As the aperture area is the same, the only reason for this difference is represented by a better usage of the cooking chamber: two vessels are able to collect more solar radiation than one. Instead, the cooking power slope is higher for two vessels, and this is because heat losses are more prominent. These considerations are also valid for the thermal efficiency coefficients.

Chapter 4

Solar Cooker Prototype Equipped with High Performance Concentrating Lens Experimental Characterization

The prototype presented in this chapter falls into the category of concentrating solar cookers. The device was constructed and tested at the DIISM laboratories. The materials used and the steps followed in its construction are reported together with the experimental setup developed to characterize the device. Being an open device, the solar cooker under study does not have an enclosed cooking chamber, hence tests without load to reach the stagnation condition were not performed. The results of the experimental campaign considering as test fluids water and silicone oil will be discussed.

4.1 Concentrating Solar Cookers in Literature

Hereafter a presentation of the most recent publications regarding concentrating solar cookers.

Mbodji and Hajji [178] designed and built a parabolic solar concentrating cooker and tested it in Rabat, Morocco. The main components were a parabolic concentrator and a cylindrical absorber. The maximum temperatures achieved by water and synthetic oil during tests were 97 °C in 2.5 hours and 153 °C in 5 hours, respectively.

A curved Fresnel lens-equipped portable solar cooker was presented by Zhao et al. [179]. The high concentration ratio (40.6) provided by the lens is used to heat food via an evacuated tube collector where the sunlight is focused. The no-load experimental test carried out by the authors revealed that the maximum temperature reachable by the system with a direct normal irradiance of 712 W/m^2 is 361 °C. The maximum energy efficiency of the system is equal to 22.6%.

A simple mathematical model to evaluate a parabolic trough solar cooker's performance was developed by Noman et al. [180]. The prototype features a 9.867

concentration ratio and is made of polished stainless steel. The sunrays are focused towards the pot, where water was able to reach the maximum temperature of 53.6 °C. The conclusion of the authors was the a larger aperture area, up to six to seven time larger than the one used, was needed to be able to reach a temperature of 300 °C, making the prototype suitable for cooking in cold winter conditions.

Ahmed et al. [181] built and tested a parabolic solar cooker prototype suited for developing countries and for refugee camps in disastrous situations. Different reflective materials were used for the prototype: stainless steel, aluminum foil and Mylar tape. The first solution allowed to achieve a maximum water temperature of 58.2 °C in about 1 hour and half; in the second setup, maximum water temperature in the same time was 75.4 °C; the latter delivered the best results, as water boiling achieved in about 1 hour.

Sagade et al. [182] tested in parallel in two locations (Faro and Malaga) at intermediate temperature two concentrating solar cookers: the first with an aperture area of 1.41 m^2, the second of 0.34 m^2. During the seven days of testing glycerin was used as test fluid. The results showed that the maximum fluid temperature reached by the first cooker was 192.9 °C, whereas that reached by the second cooker was 113.9 °C.

4.2 Design and Optical Analysis

The high thermal efficiency prototype presented in this work, shown in Figure 4.1 and Figure 4.2, was manufactured following the technical specifications provided by Heliac [183]. The main features of the proposed solar cooker are its structure and materials. Some parts of the cooker, such as the lens and the mirror, are movable; thus, it is possible both to track the sun and to fold the system, allowing to reduce its size and to transport it easily. The prototype consists mainly of a wooden reticular support equipped with wheels to facilitate transport and two wooden frames: one for the special lens support and the other, smaller than the previous one, for the reflecting surface. The Fresnel lens is able to capture solar radiation and concentrate it towards the focal area of the reflective surface. The latter, suitably oriented, is able to concentrate all the rays at a specific point of the cooking surface that corresponds to the spot where the pot is positioned. The working scheme of the system is shown in Figure 4.3.

The Danish company Heliac has developed a process to create a transparent film from a thin sheet of polymer material. The result is, in terms of performance and shape, the same as conventional Fresnel lenses but at a much lower cost. The dimensions of the main components of the concentrating solar cooker are given in Figure 4.2. Specifically, the lens has a size of 1120×1390 mm and its area represents the aperture area, A_a, of the solar cooker. The concentration ratio of the prototype is equal to:

$$C = \frac{A_a}{A_p} = \frac{1.557}{0.038} = 40.97 \tag{4.1}$$

where A_p is the area of the pot lower surface, i.e. the surface where the radiation is concentrated by the lens-mirror system.

The mirror, with dimensions 730×900 mm, is made of a special film which, in order to obtain the maximum reflectivity, needs to be kept always clean and tensioned. The film surface is capable of reflecting a large portion of the solar spectrum.

Two wooden arms, each 1408 mm long, were used to attach the lens to the wooden reticular structure. The two arms allowed the rotation of the lens from 0 to 90° in order to have a correct and continuous alignment to the sun's rays. The combined

Figure 4.1: A photo of the Heliac solar cooker during the experimental campaign.

inclination of the mirror and the lens allows the operator to continuously track the sun with good accuracy and to obtain high performance.

4.3 Manufacture and Assembly

The final prototype was obtained by following four consecutive production phases:

- realization of the wooden structural frame;
- realization of the cooking surface;
- realization of the lens and the mirror;
- final assembly.

4.3.1 Realization of The Wooden Structural Frame

Starting with recycled materials, the structure that supports the entire system was created. The wooden boards were cut, planed and sanded in order to obtain laths of various sizes and shapes. The laths were connected to each other using screws and bolts to create the final reticular structure. To facilitate transportation and constant tracking of the sun by the operator, the base of the wooden structure was equipped with wheels. For a greater user comfort during the operation of the device, a sunrays protection cover was added in the upper part of the main structure.

A fire-retardant paint based on acrylic/silicone resins capable of withstanding temperatures up to 450 °C was used to coat all the wooden components and protect them from continuous exposure to sunlight and external seasonal cycles (Figure 4.4).

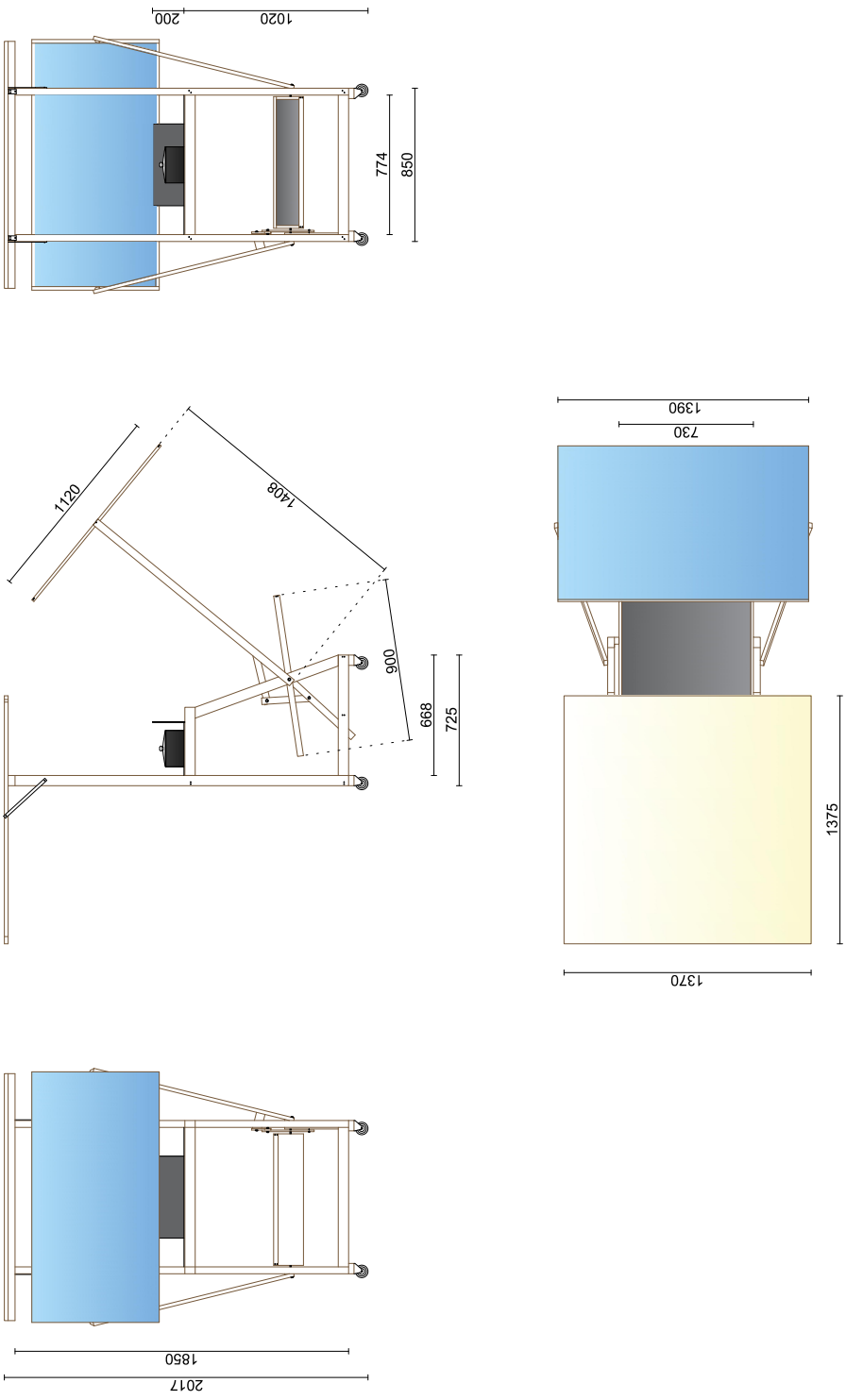

Figure 4.2: Concentrating solar cooker views [2].

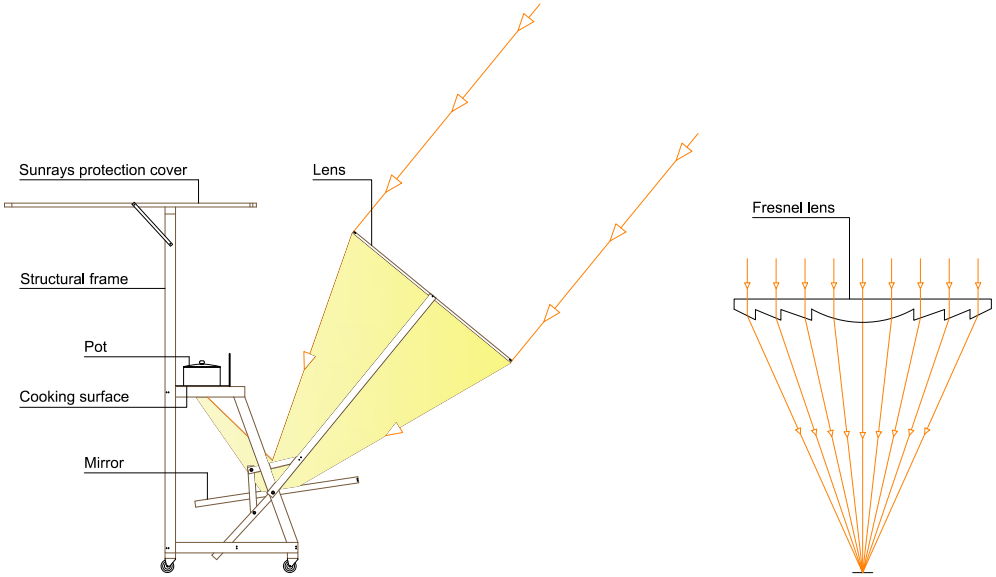

Figure 4.3: Working scheme of the concentrating solar cooker [2].

4.3.2 Realization of the Cooking Surface

A 2 mm thick aluminium foil was used to obtain the rectangular cooking surface. The latter, measuring 850 × 537 mm, had in the center a hole with a diameter of 220 mm at a distance of 140 mm from one of the long sides (Figure 4.5). Furthermore, the sheet was bent 90° downwards along a parallel line to the other rectangle long side, at 57 mm from it, to create the support points to be anchored to the wooden structure.

An aluminium plate measuring 600 × 200 mm was finally fixed vertically to the long side of the primary surface as a support for the pot. In order to reduce the risk of fire and to protect the eyes of those using the device, a second, smaller alliminium plate was placed under the hole. Once the lens-mirror system is correctly oriented in the direction of the sun and the pot is positioned on the cooking surface to cover the hole, thanks to a lever it is possible to slide the protective plate and safely let the concentrated sunlight reach the bottom of the cooker.

4.3.3 Realization of The Lens and The Mirror

The frames housing the mirror and lens were made from 4 wooden laths fixed with screws. The lens was placed over its own frame (1120 × 1390 mm) and anchored to it with a stapler.

A 3 mm thick plywood panel was glued on top of the aluminum film, previously spread over a worktop with the reflective surface facing downwards, and was attached to its frame (730 × 900 mm) with the aid of glue suitable for wood.

4.3.4 Final Assembly

Two wooden arms of 1408 mm length each were fixed to the structure. The lens frame was mounted at the top of the two arms. In the lower part of the arms, two

Figure 4.4: Application of the fire-retardant paint on wooden structures.

Figure 4.5: Detail of the cooking surface.

bolts were positioned and inserted as pivots for the frame containing the mirror. As last operation, the cooking surface was positioned and fixed.

4.4 Experimental Tests and Setup

The prototype was characterized through the determination of parameters derived from experimental procedures and international standards described in the literature. The calculated parameters, the test bench developed and the description of the fluids used during the experimental campaign are described.

4.4.1 Experimental Parameters

As explained above, the Heliac concentrating solar cooker is an open device. For this reason, no tests without load were carried out during the experimental campaign due to the lack of an enclosed and thermally insulated cooking chamber, and consequently the first figure of merit (F_1 by Mullick et al. [19]) was not determined. Tests with load were carried out using water and silicone oil. In detail, the parameters calculated for the thermal and optical characterization of the device are the specific and characteristic boiling times defined by Khalifa et al. [172], t_s and t_{ch} respectively, the overall thermal efficiency η_{av} ([172]) and the utilizable efficiency η_u given by El-Sebaii and Ibrahim [176], the cooker opto-thermal ratio, COR and the maximum temperature reachable by the test fluid (T_{fx}) proposed by Lahkar et al. [173].

Details on the formula for calculating the parameters listed above are given in the Appendix A.

One aspect to be emphasized is that, although these parameters are generally referred to water, they were adapted for the case of silicone oil as test fluid and were calculated to evaluate the behavior and performance of the concentrating solar cooker. In particular, all parameters were computed considering a time interval Δt_h required for the fluid to pass from an initial temperature T_1 to a final temperature T_2. The chosen temperatures are 40 °C and 90 °C for water (as suggested by Funk [7]), while they are respectively 40 °C and 170 °C for silicone oil.

4.4.2 Experimental Methodology

The Heliac solar cooker was tested through an outdoor experimental campaign on the roof of DIISM (latitude 43.5867 N, longitude 13.5150 E) in the period June-July 2020 and March-April 2021.

Figure 4.6 shows a schema of the experimental test bench used during the experimental campaign. The quantities recorded during each test were the direct normal solar irradiance DNI, the ambient temperature T_{amb}, and the fluid temperature T_f. Details of the instruments and sensors used in the test bench together with their uncertainties and range of use can be found in Appendix B. A 22 cm diameter stainless steel pot, with the external bottom painted with a special black heat-resistant coating suitable for solar thermal applications, served as a vessel for the test fluid during the tests. The paint had a silicone resin binder base and was able to withstand temperatures up to 600 °C.

The test fluids were water and silicone oil. The first was chosen for an easy comparison of the results with the literature; the silicone oil (Rhodorsil Oil 47 V 100) was used to overcome the 100 °C limit of water and to study the behavior of the solar cooker at higher temperatures.

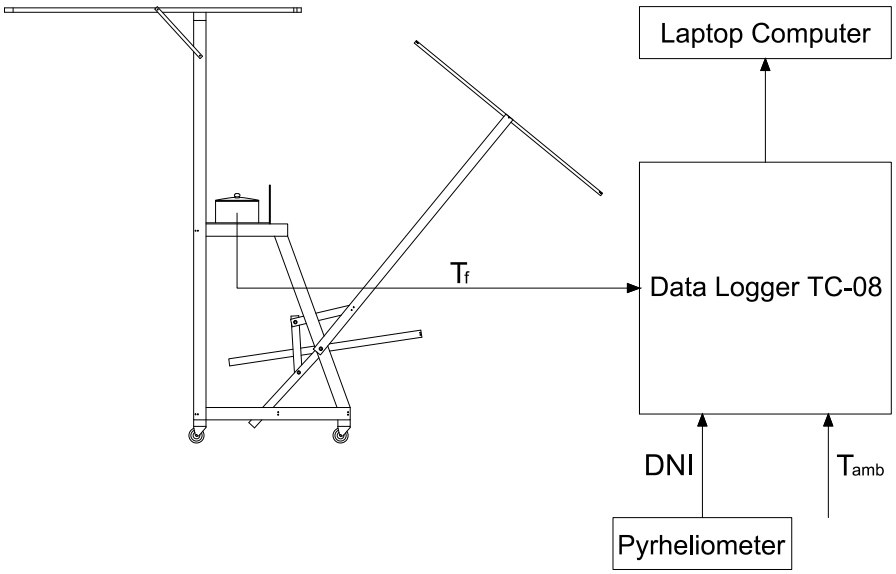

Figure 4.6: Test bench. T_{f}: testing fluid temperature; T_{amb}: ambient temperature; *DNI*: direct normal solar irradiance.

4.5 Experimental Results

In this section, the results obtained through the experimental tests with water and silicone oil are provided.

4.5.1 Tests with Water

A total of eight water tests were carried out in June 2020 and March-April 2021. All tests were carried out using the same pot with the external bottom painted in black and the same mass of water of 3 kg. Figure 4.7 shows the *DNI* and temperatures recorded during the test on 23$^{\mathrm{rd}}$ of June 2020 (test 3). In detail, the average direct normal irradiance was 879.41 W/m^2 and the average ambient temperature was 26.09 °C. Water took about 30 minutes to change its temperature from 40 to 90 °C.

The remaining seven tests showed fluid temperature trends very similar qualitatively to that shown in Figure 4.7, so they are not reported.

Instead, the overall water temperature trend detected during the load tests is shown in Figure 4.8, while a summary of all the measurements and the calculated parameters in the range interval of the tested fluid between 40 and 90 °C is reported in Table 4.1.

Table 4.1 highlights some differences in the cooking time and in other parameters of the various tests. These differences do not have a clear link with environmental conditions (average solar radiation and ambient temperature). Test 7, for example, registered the lowest average ambient temperature, but the performance parameters of the solar cooker are better than those calculated in test 5 which, despite presenting a comparable average solar radiation, was characterized by a higher average ambient temperature.

Other aspects can play an important role in determining the thermal performance of a concentrating solar cooker, for instance:

- sudden variations of direct solar radiation (due to e.g. clouds or mist);

Table 4.1: Water load test summary.

Quantity	Test 1	Test 2	Test 3	Test 4	Test 5	Test 6	Test 7	Test 8
Date	19/06/2020	23/06/2020	23/06/2020	23/06/2020	26/06/2020	26/06/2020	30/03/2021	01/04/2021
m_{f} (kg)	3.0	3.0	3.0	3.0	3.0	3.0	3.0	3.0
T_1 (°C)	40	40	40	40	40	40	40	40
T_2 (°C)	90	90	90	90	90	90	90	90
DNI_{av} (W/m^2)	868.41	854.06	879.41	883.43	850.00	833.61	850.86	825.47
$T_{\mathrm{amb,av}}$ (°C)	26.34	25.56	26.09	26.78	30.20	30.77	17.72	24.53
Δt_{h} (h)	0.50	0.51	0.52	0.54	0.61	0.53	0.56	0.65
t_{s} (h m^2/kg)	0.26	0.27	0.27	0.28	0.32	0.27	0.29	0.34
t_{ch} (h m^2/kg)	0.25	0.25	0.26	0.28	0.30	0.25	0.28	0.31
η_{av}	0.26	0.26	0.24	0.23	0.22	0.26	0.23	0.21
η_{u}	0.33	0.33	0.31	0.29	0.26	0.30	0.34	0.28
$F'\eta_0$	0.373	0.377	0.377	0.360	0.363	0.370	0.391	0.340
$F'U_{\mathrm{l}}/C$ (W/m^2 °C)	2.368	2.462	2.804	2.738	3.396	2.832	2.432	2.355
COR	0.158	0.153	0.134	0.132	0.107	0.131	0.161	0.144
T_{fx} (°C)	163.20	156.37	144.22	143.05	121.15	139.78	154.52	143.71

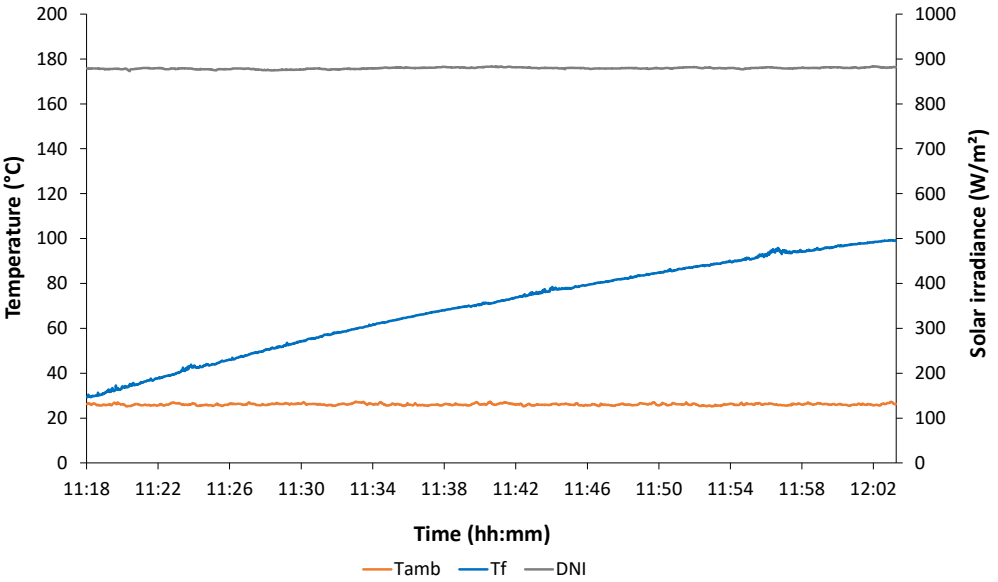

Figure 4.7: Test with water (23/06/2020, test 3).

- wind gusts;
- delay in adjusting the solar cooker azimuthal and/or zenithal orientation by the operator.

In addition to the parameters t_s, t_c and η_{av}, the COR parameter and T_{fx} (the maximum temperature reachable by the fluid) were also calculated. In order to evaluate these additional two parameters, it was necessary to sub-divide the time required by water to cover the temperature range 40–90 °C into 5 minutes intervals where the average solar irradiance (DNI_{av}), the average ambient temperature ($T_{amb,av}$), the average fluid temperature ($T_{f,av}$), the efficiency (η), and the parameter ($(T_f - T_{amb})/DNI$) were determined.

Figure 4.9 reports the thermal efficiency η against the term χ for each sub-interval. In the figure, in addition to the experimental points, the linear regression equation of the thermal efficiency curve is reported: the intercept and the slope coefficients correspond to the parameters $F'\eta_0$ and $F'U_l/C$ respectively. The coefficient of determination R^2 is also reported.

Based on that, it is possible to determine the COR parameter and T_{fx}. According to the values registered for the different tests (Table 6.4), it is possible to note that the optical efficiency factor $F'\eta_0$ is almost constant, while the heat loss factor $F'U_l/C$ shows greater variations that depend on the average ambient temperature and wind speed.

4.5.2 Tests with Silicone Oil

Five outdoor tests were carried out in June–July 2020 and March 2021 loading the solar cooker with 3 kg of silicone oil. Table 4.2 summarize the parameters calculated using silicone oil as test fluid in the temperature range between 40 and 170 °C for the first three tests (from test 9 to test 11) and between 40–155 °C for the latter tests (tests 12 and 13).

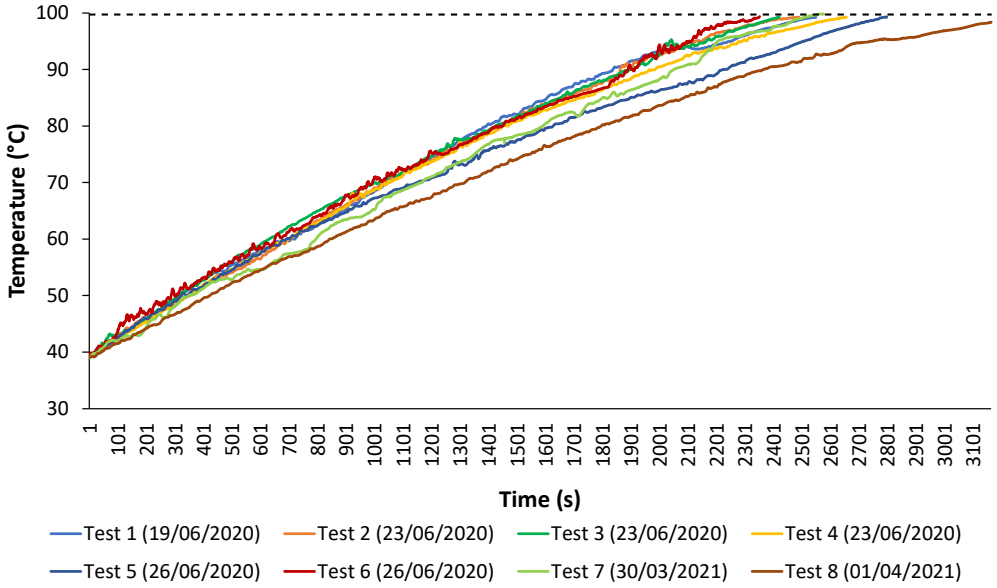

Figure 4.8: Water temperature trends.

Figure 4.10 shows as example the test conducted on 24/06/2020 (test 9). During the test period, the average *DNI* was 810.59 W/m^2 and the average ambient temperature was 26.73 °C. It took less than one hour for the fluid to raise its temperature from 40 to 170 °C. Considering the same test, the thermal efficiency experimental points, the linear regression equation and the R^2 coefficient are shown in Figure 4.11.

The temperature trends of silicone oil during the five tests are reported in Figure 4.12. It can be seen that the thermal performance of the solar cooker is strongly affected by the average ambient temperature, especially at high fluid temperatures. Based on the data reported in Table 4.2, in fact, it can be seen that the average T_{amb} of test 12 and 13 conducted at the end of March (around 19 °C) is by far lower than that detected in the other tests (range 26–28 °C), which were carried out in June–July. Differently from the tests conducted with water, ambient temperature did not only influence the

Table 4.2: Silicone oil load test summary. Note that the parameters for test 12 and 13 are referred to the range 40–155 °C, not 40–170 °C

Quantity	Test 9	Test 10	Test 11	Test 12	Test 13
Date	24/06/2020	09/07/2020	09/07/2020	31/03/2021	31/03/2021
m_f (kg)	3.0	3.0	3.0	3.0	3.0
T_1 (°C)	40	40	40	40	40
T_2 (°C)	170	170	170	155	155
DNI_{av} (W/m^2)	810.59	901.26	924.17	878.70	889.37
$T_{amb,av}$ (°C)	26.73	25.96	28.10	19.19	18.97
Δt_h (h)	0.91	1.05	0.91	1.14	1.49
t_s (h m^2/kg)	0.47	0.54	0.47	0.59	0.77
t_{ch} (h m^2/kg)	0.43	0.54	0.49	0.58	0.77
η_{av}	0.16	0.12	0.14	0.10	0.08
η_u	0.17	0.14	0.15	0.12	0.09
$F'\eta_0$	0.334	0.314	0.271	0.222	0.196
$F'U_l/C$ (W/m^2 °C)	1.522	1.751	1.346	1.148	1.109
COR	0.219	0.179	0.201	0.193	0.177
T_{fx} (°C)	204.42	187.65	214.21	189.11	176.15

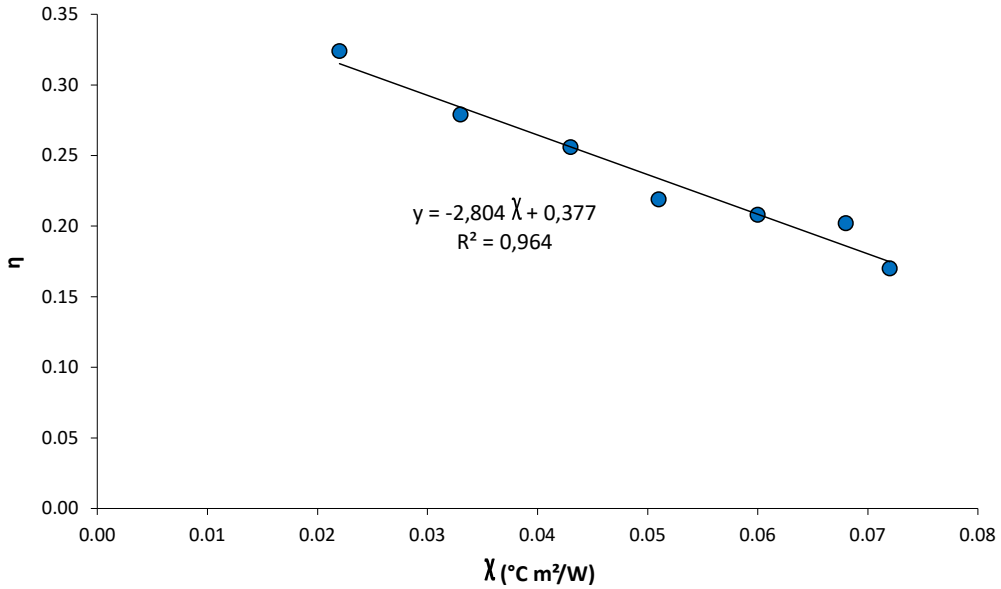

Figure 4.9: Thermal efficiency for water (23/06/2020, test 3).

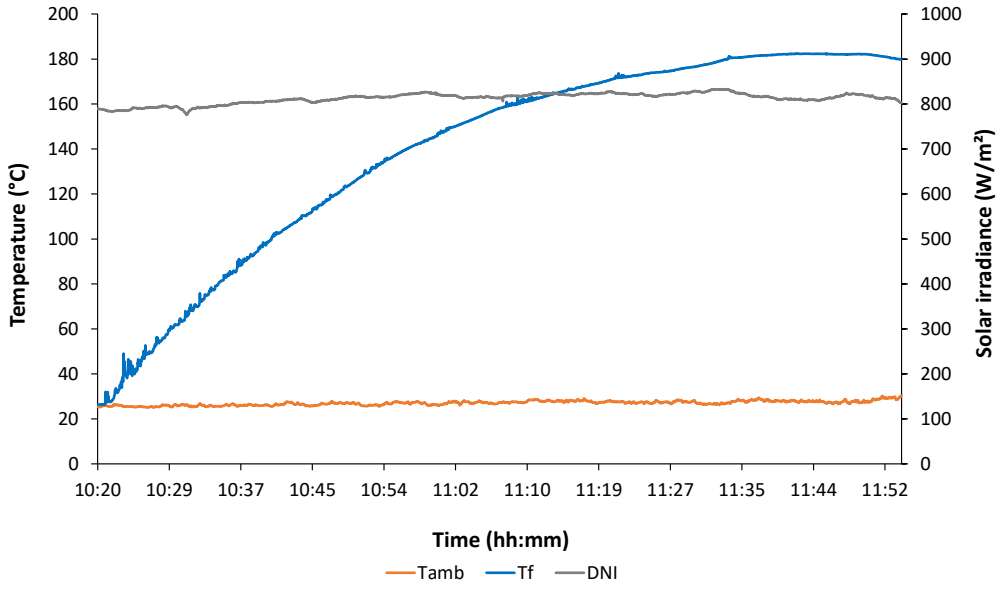

Figure 4.10: Test with silicone oil (24/06/2020, test 9).

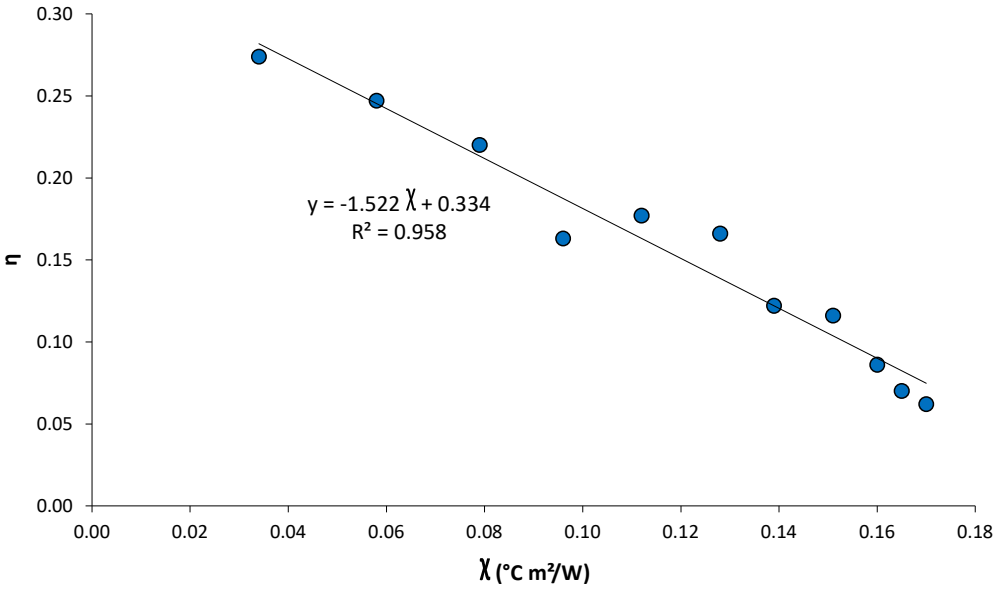

Figure 4.11: Thermal efficiency for silicone oil (24/06/2020, test 9).

thermal performance of the cooker, but also prevented the test fluid to reach high temperatures: while the tests carried out in summertime (test 9, 10, 11) allowed to reach an actual fluid stagnation temperature of about 180 °C, the tests carried out in springtime (test 12 and 13) did not allow to go beyond 160 °C (Figure 4.12).

Performing a comparison between tests with water and silicone oil, one can note that, for the same mass of fluid, the average thermal efficiency η_{av} is lower in tests with silicone oil. This can be explained by the higher temperatures reached by the test fluid and the consequent higher thermal losses to the environment.

From Table 4.2 it can be noted that the optical efficiency factor $F'\eta_0$ stays almost constant in the first three tests with silicone oil, with an average value not too lower than that determined for water. This is in line with the fact that $F'\eta_0$ does not depend much on the thermo-physical properties of the test fluid. On the other hand, the heat loss factor $F'U_l/C$ values determined for silicone oil are lower in absolute value with respect to those of water. This is a consequence of the different specific heat of the two substances, that of water being greater than that of silicone oil: in the same amount of time its temperature increases more slowly, resulting in a thermal efficiency that decreases more rapidly during heating.

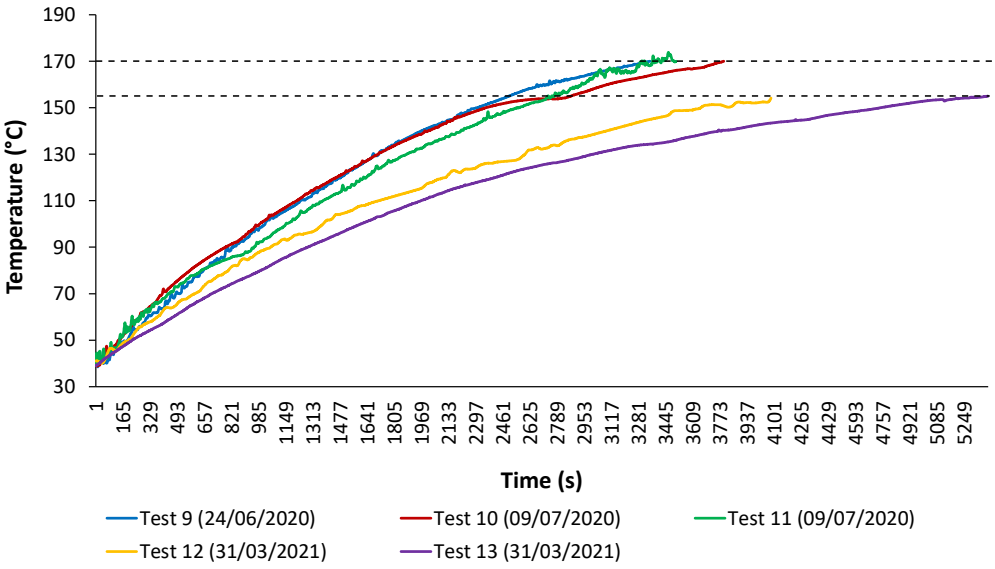

Figure 4.12: Silicone oil temperature trends.

Chapter 5

Experimental Characterization of Two Panel Solar Cooker Prototypes: Newton and Kimono

This chapter will present two prototypes that fall into the category of solar panel cooker: the Newton and the Kimono solar cookers, respectively. Again, the devices were manufactured and tested within the DIISM laboratories. Both prototypes follow the construction schemes of engineer Matteo Muccioli, the creator of the cookers. Modifications were made to the Newton in terms of the materials used in its construction in order to increase its final efficiency.

Two identical Newton devices were built and tested in parallel, with the only difference being that one was shielded from the wind. The aim of the experimental campaign in this case was to understand how much the the wind affected the final performance of a device with that geometry, which does not have a thermally insulated cooking chamber as in box devices.

Instead, the Kimono was tested in parallel with three other panel devices: the Funnel, the Dual Setting and the Cookit, respectively. Tests were carried out during three different periods of the solar year using the four devices in two different configurations depending on the elevation of the sun during the studied period. The results obtained from both experimental campaigns will be reported.

5.1 Panel Solar Cookers in Literature

Hereafter are reported some of the most representative works on panel solar cookers.

Ozturk [184] built a solar box cooker from a plastic sheet box and a plastic plate which is simple and economic. The authors tested the prototype using an aluminum pot filled with water and calculated the energy and exergy efficiencies. The results showed that the device was able to heat water only up to 73.2 °C, while the average energy and exergy efficiencies were respectively 18.3% and 2.2%.

A low-cost small-sized solar box cooker manufactured with inexpensive materials, known as Single Family Solar Cooker, was designed by Mahavar et al. [162]. Two

aluminum cylindrical pots were used to test the device, and the experimental results demonstrated that it was able to cook also in winter two meals of soft load for two persons. The calculated performance parameters were similar to those of other box solar cookers in the literature.

Ebersviller and Jetter [185] compared the performances of a panel cooker, called Hot Pot, with those of a parabolic cooker (Sun Chef Cooker) and a box cooker (Global Sun Oven) following the ASAE S580.1 Standard [186]. The prototypes were tested using the load ratio of 7 kg of water per square meter of intercept area, as recommended by the Standard. 25 W was obtained as standardized cooking power for the panel cooker, a lower value than those obtained for the box cooker (65 W) and the parabolic cooker (198 W). The smaller aperture area of the panel cooker device is the most likely cause of the lower performance, which was further confirmed also by other experimental parameters.

The performance of a small solar box cooker with a booster reflector was experimentally investigated by Sagade et al. [187]. The authors defined the effective concentration ratio, a new parameter to evaluate the effectiveness of the reflector booster. From the experimental tests it was found that this new parameter helped in the evaluation of the thermal performance of the device when it was or was not equipped with the booster system. Additionally, different test fluids [188] and a modified cooking pot [168] were used to evaluate the thermal performance of the device.

Weldu et al. [189] experimentally evaluated the thermal performance of a simple solar box cooker with different reflector configurations. The tests without load showed that the cooker with optimal reflector tracking reached the highest stagnation temperature of 145.4 °C and the first figure of merit $F_1 = 0.154\,°C/(W/m^2)$. The results of the tests with water inside an aluminum pot showed that the cooker with optimal reflector tracking allowed for better thermal performance than that obtained with a stainless steel pot and a fixed angle reflector configuration.

Two identical funnel cookers were tested in parallel ollowing the ASAE S580.1 Standard [186] by Ruivo et al. [190] to investigate the influence of the type of lid for the pot. The selected configurations were a glass lid and a black metal lid, one pot per cooker. The pots were further wrapped in a transparent cover. Different tests were carried out by the authors using as test fluid water and water mixed with ice during a period with low sun elevations. The results showed that the pot with the glass lid produced an average standardized cooker power of 73.9 W, higher than that of the pot with the black metal lid (50.6 W).

Apaolaza-Pagoaga et al. [191] tested simultaneously four configurations of the Copenhagen Solar Cooker. It was found that solar altitude has a greater effect on the device performance only when one configuration is used, as it was shown from the tests without load. The experimental tests with water, carried out following in part the ASAE S580.1 Standard [186], showed that the linear trend of the standardized power is not universal, proving that the procedure for evaluating this parameter should be improved. This was also discussed by by Ruivo et al. in [192, 193].

Two prototypes of Haines 2 Solar Cooker were tested in parallel by [194]. The focus of the investigation was the influence of the solar altitude on the performance of the devices. Tests without load and with water were conducted, and the results brought the authors to formulate the suggestion that in future versions of the ASAE S580.1 Standard [186] the influence of both solar altitude angle and partial loads should be considered.

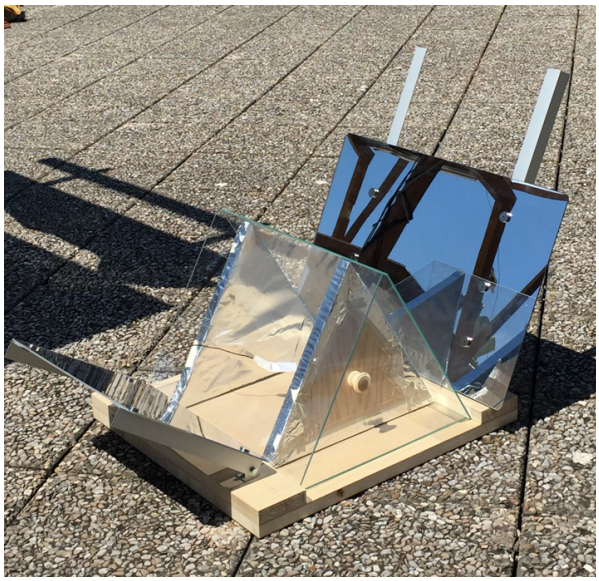

Figure 5.1: A photo of the Newton solar cooker first version.

5.2 Newton Solar Cooker

The first panel solar cooker presented in this chapter, named Newton solar cooker, was designed to be easy to build and use: its main strengths are the ease of construction, ease of movement and transportation, and the use of common and inexpensive materials at quasi-zero cost, given their extensive use. The device can be constructed quickly since only common tools are required. In addition, the prototype can be easily transported since it can be easily disassembled and resealed. Finally, the choice of the materials is a crucial aspect since it affects the efficiency and performance of the prototype.

Two identical prototypes were built using the same materials. The purpose of this study, in fact, was to simultaneously test the two identical prototypes, one wind-shielded and the other not, to determine their thermal performance considering the influence of wind.

5.2.1 Design and Optical Analysis

The Newton solar cooker (NSC), developed by Eng. Matteo Muccioli, was born with its basic version ([195]) consisting of a glass prism cooking chamber, base and side supports in fire wood and two reflective surfaces, one on each side (Figure 5.1). The basic version was tested outdoors by carrying out some preliminary tests in order to thermally characterize the prototype. Analyzing the obtained results, the prototype was modified in order to improve its thermal and optical performance.

First, an insulating layer of wood was added between the steel plate and the wooden plate at the base; a second insulating layer of sintered expanded polystyrene with a thickness of 60 mm was added under the wooden base; additional mirrors were added increasing the overall reflecting surface of the prototype; different reflecting materials were evaluated including Mylar for the mirrors; the possibility of having an additional glass plate in contact with the base panel was evaluated. The various preliminary tests carried out served to make choices in the design and materials used until the current

Figure 5.2: A picture of the Newton solar cooker.

prototype version was obtained.

The new version of the solar cooker used to carry out the outdoor experimental campaign is shown in Figure 5.2 and Figure 5.3. From Figure 5.3 are visible the dimensions of all the cooker components together with the reflective panel systems adopted. Figure 5.4 shows the working scheme of the new device: it consists of a glass prism cooking chamber made of two tempered glass panes, a wooden panel placed at the base and two side doors. The glass panes are supported by the two side panels and the two side doors. An insulating layer and a steel plate are placed at the base of the chamber. Moreover, the device comprises two rotating reflector support structures placed at the sides of the chamber: a longer support for the primary reflective surface and a shorter one for the secondary reflective surface.

From Figure 5.4, it can be seen that the device has variable geometry: by changing θ_1 and θ_2, i.e. the inclination angles of the primary and secondary reflective panel, depending on the elevation of the sun, it is possible to obtain different aperture areas (A_a) of the device. A_a is calculated as the projection of the area bounded by the outer edges of the prototype on a plane perpendicular to the direction of the sun's rays. By optimizing the values of θ_1 and θ_2 according to the elevation of the sun (H_sun), it is possible to maximize the amount of solar radiation concentrated on the steel plate where the pot is placed.

In order to calculate pairs of optimal θ_1 and θ_2 values associated with different sun

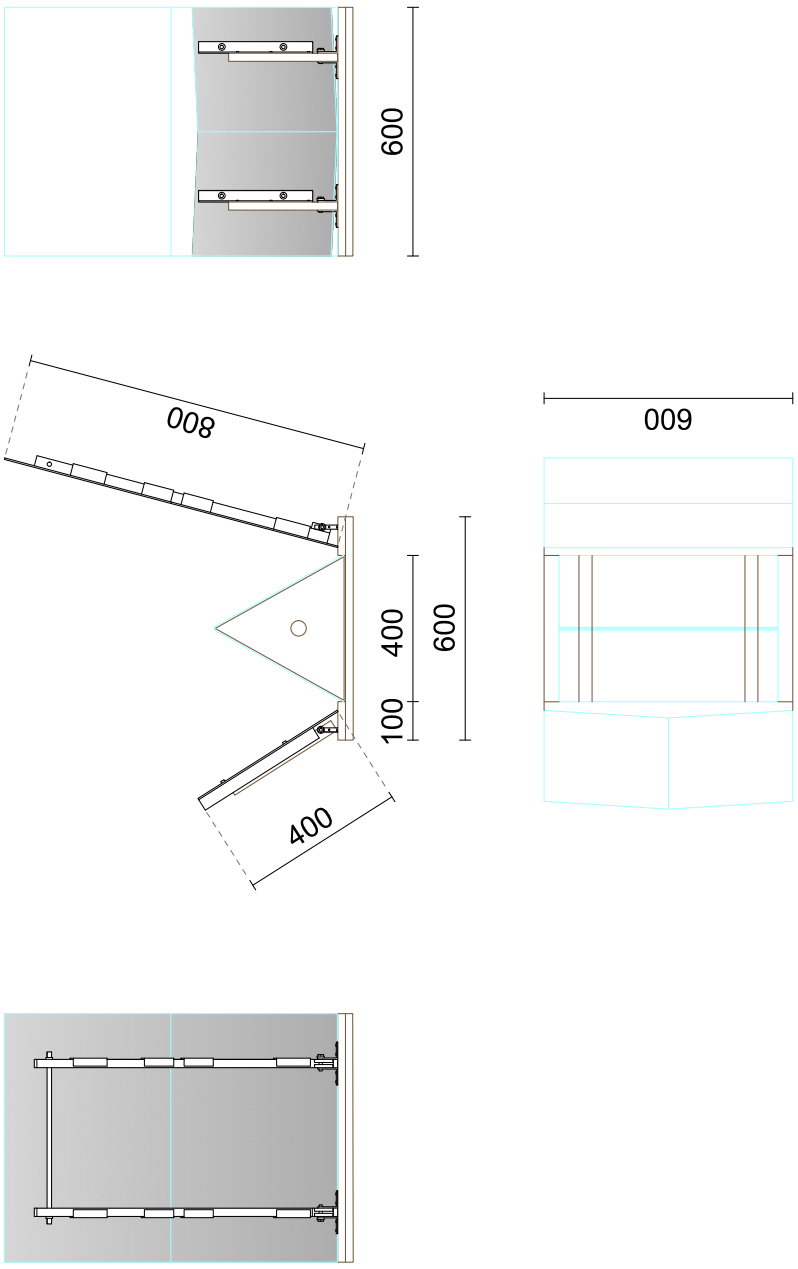

Figure 5.3: Newton solar cooker views (dimensions in mm) [3].

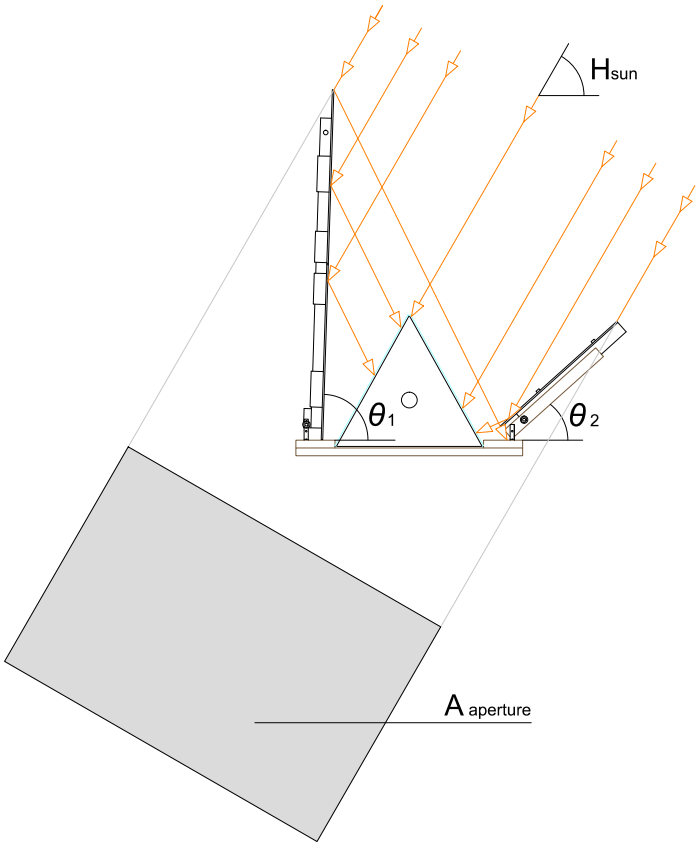

Figure 5.4: Working scheme of the Newton solar cooker [3].

elevations, a simplified 2D model of the solar cooker was developed using MATLAB software [196]. The solar rays are represented by vectors from the direction of the sun and initially have unit modulus. The solar cooker surfaces are modeled as obstacles to the propagation of sun rays, dividing them between reflective surfaces (the 2 reflectors) and glazed surfaces (the 2 glasses), according to the prototype design.

The sun's rays are propagated along their direction and impact the various surfaces of the solar cooker, which cause either reflection or transmission. The transmittance and reflectance values of the materials were used to correct the modulus of the solar ray vectors at each transmission or reflection in order to more realistically compute the final amount of concentrated energy. The model accounts for multiple reflections between mirrors, should they occur.

A ray is no longer propagated if it does not impact the cooker at all or if it hits the cooker surface where the pot will be placed. The moduli of the rays that meet the latter condition are summed. This sum, when there are no more rays to propagate, is the score assigned to a certain configuration of θ_1 and θ_2 for a given solar elevation. The configuration that gets the highest score is considered the optimal one for that elevation of the sun.

For the possible sun elevations at the latitude of Ancona (latitude of 43.5871° N), discretized with 1°-steps, the optimal configuration of θ_1 and θ_2 values was determined using the Particle Swarm Optimization algorithm [197]. As an example, below are reported the optimal values of θ_1 and θ_2 at 12:00 noon solar time on the days of the equinox, summer solstice and winter solstice:

- Spring Equinox, 20/03/2022: $H_{\text{sun}} = 46.24°$, $\theta_1 = 76.40°$, $\theta_2 = 22.99°$;
- Summer Solstice, 21/06/2022: $H_{\text{sun}} = 69.79°$, $\theta_1 = 96.09°$, $\theta_2 = 47.62°$;
- Winter Solstice, 21/12/2022: $H_{\text{sun}} = 22.97°$, $\theta_1 = 56.49°$, $\theta_2 = 2.33°$.

Figure 5.5 shows the score (on the z-axis) for each pair of θ_1 (x-axis) and θ_2 (y-axis), again for 12:00 solar time on the equinox, summer solstice, and winter solstice days.

The optimal θ_1 and θ_2 pairs associated with each sun elevation were collected in a table that will be used during the experimental campaign by the operator to adjust the solar cooker geometry according to the sun elevation during each test. Table 5.1 shows the optimal values of θ_1 and θ_2 for H_{sun} between 40° and 74°, with the corresponding aperture area of the NSC.

5.2.2 Manufacture and Assembly

The Newton solar cooker manufacturing process consisted of 5 consecutive steps:

1. realization of the base panel;
2. cutting and assembly of supports;
3. realization of the side doors;
4. construction of the cooking chamber;
5. arrangement of the reflectors and final assembly.

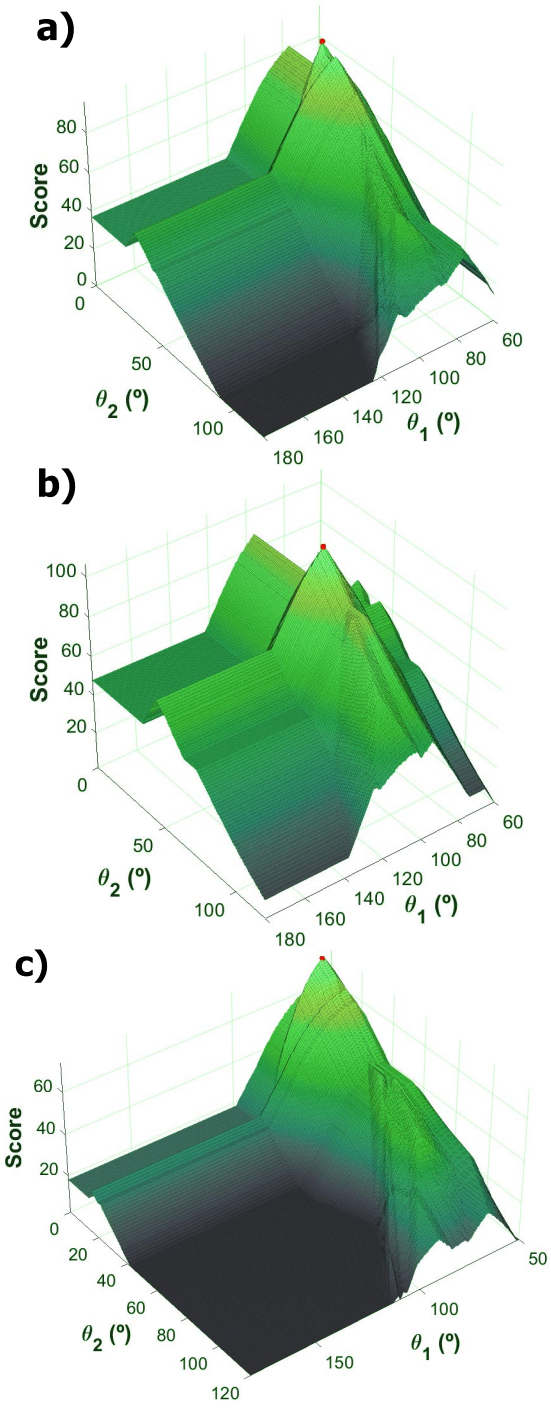

Figure 5.5: Score (z-axis) obtained by a 2D model for the distribution of the solar radiation on the NSC for each pair of θ_1 (x-axis) and θ_2 (y-axis) at 12:00 solar time: a) Spring Equinox, 20/03/2022; b) Summer Solstice, 21/06/2022; c) Winter Solstice, 21/12/2022.

Table 5.1: Newton solar cooker optimal configurations in Ancona for different sun elevations and corresponding aperture areas.

H_{sun} (°)	θ_1 (°)	θ_2 (°)	A_{a} (m^2)
40	71.52	17.59	0.396
42	72.82	19.55	0.398
44	74.33	20.94	0.402
46	76.31	23.04	0.407
48	77.77	24.38	0.411
50	80.29	34.72	0.394
52	81.21	35.92	0.396
54	83.16	37.44	0.401
56	84.28	39.48	0.401
58	86.43	39.93	0.410
60	88.10	41.79	0.413
62	90.28	42.67	0.421
64	91.19	43.82	0.421
66	93.18	44.99	0.426
68	94.06	46.83	0.423
70	96.85	47.76	0.434
72	97.57	49.40	0.430
74	98.92	50.39	0.431

Realization of The Base Panel

A $600 \times 600 \times 20$ mm multilayer poplar wood panel was used as the base on which the other elements of the cooker rest. Two poplar wood panels measuring $600 \times 100 \times 20$ mm were fixed with screws at the top of the base panel along two opposite edges. Their task is to keep two tempered glass panes that form the glass prism cooking chamber in position, preventing them from sliding outwards and guaranteeing the closure of the cooking chamber. To facilitate the prototype's usage and ensure its manual alignment to solar radiation, the base panel was fitted with 3 wheels.

Cutting and Assembly of Supports

Starting from a square steel hollow profile with a 20×20 mm cross-section, two bars with a length of 650 mm were cut using a metal saw to form the support arms for the primary panel reflectors. Figure 5.6a, shows how the square metal bars were fixed and anchored to the base of the solar cooker using angle brackets. A self-locking system was used to fix the angle brackets to the bars to allow the entire support system to change the angle for proper sun tracking.

The primary reflectors were fastened to the support arms through eight 100 mm-long pieces that were first cut from an aluminum C-profile and then attached vertically to the reflectors using double-sided adhesive tape.

In addition, the two square bars were fixed together with a metal rod at the top to make the entire system more stable.

Starting from a 1000 mm long aluminum L-profile with a 30×30 mm cross-section, two profiles of 300 mm in length were cut using an aluminum saw to form the support arms for the secondary reflectors. To make the reflector supports more stable during use, the aluminum profiles were reinforced by joining them to 350 mm long wooden strips with a 20×20 mm square section. The same fixing method used for the square metal bars was also used to fix and anchor the wooden supports to the base of the

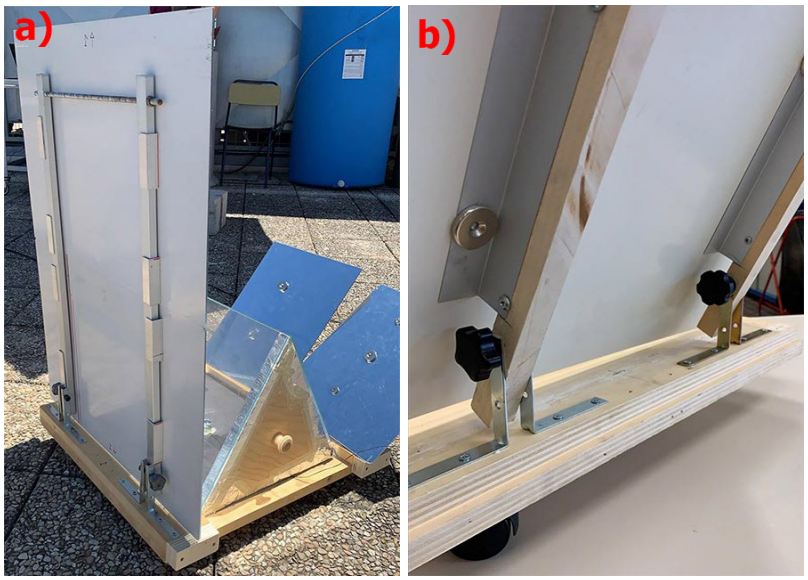

Figure 5.6: Detail of the connection of the reflector supports to the wooden base: a) primary reflectors and b) secondary reflectors.

solar cooker as shown in Figure 5.6b.

The secondary reflectors were fixed to the aluminum supports and held in position by magnets.

Realization of The Side Doors

To complete the cooking chamber structure, two side doors to support the glass surfaces are required. These components are made of solid fir wood in the shape of isosceles triangles and are equipped with a side handle to ease the solar cooker movement. The dimensions are $400 \times 332 \times 30$ mm. Additionally, the side doors are movable, thus allowing a rearrangement of the internal volume to fit different types of pots and loads.

The internal doors' sides were coated with an aluminum film to reflect direct sunrays inside the cooking chamber (reducing radiation dispersions) and to avoid that any steam generated inside the cooking chamber penetrates the wood and affects the thermal insulation provided by the material.

Construction of The Cooking Chamber

A $430 \times 375 \times 8$ mm cork panel inserted over the poplar wood base was used to thermally insulate the base of the cooking chamber. The cork panel was shaped to fit perfectly into the section created between the poplar base and the two side panels anchored to it. A steel plate measuring $420 \times 365 \times 1$ mm was placed on top of the cork layer. The plate was painted with a high-performance black paint to increase its ability to absorb heat from solar radiation.

Two panes of tempered extra-clear glass measuring 380×480 mm and 4 mm thick make up the actual cooking chamber. The two panes of glass were placed on the triangular side doors and held in place by the two poplar wood panels.

A gap was left on the top to prevent condensation inside the cooking chamber by spacing the two glass panes about 2 mm. This allows for improving the cooking performance of the device.

Arrangement of The Reflectors and Final Assembly

The reflective system is composed of sheets of Polymethylmethacrylate (PMMA): this was chosed for the low cost of the material and for operations safety. Four sheets arranged on three planes are needed to build the mirrors:

- the primary mirror is made of two 600×400 mm reflectors placed one alond the other's long side, thus forming a single plane reflector of 600×800 mm;
- the secondary mirror is made up of two 300×400 mm reflectors in a V configuration.

The reflectors are fixed to the supports as described in Section 5.2.2.

5.2.3 Experimental Tests and Methodology

In this section, the types of tests carried out, the test fluids and the instrumentation used in the outdoor experimental campaign together with the methodology adopted are described. Then, the main parameters used to characterize the NSC are presented.

Experimental Methodology

Experimental tests were carried out in June 2021 on the roof of the DIISM (latitude 43.5871° N, longitude 13.5149° E). The test bench used during the experimental campaign is shown in Figure 5.7. The two devices were placed on the ground and tested in parallel under the same outdoor conditions and avoiding shaded areas at the test site. To understand the effect of wind on this type of solar device, one of the two devices was shielded from the wind during all tests with a wind shielding system specifically constructed for the experimental campaign.

With reference to wind intensity, Figure 5.8 shows the average wind speed recorded in a location near the testing area (latitude 43.6098° N, longitude 13.5105° E) during the time slot when the measures were conducted. The data were collected from the website of the Marche Region - Civil Protection Service [198]. From the Figure 5.8 it is possible to note that, in all performed tests, the average wind speed values exceed the limit of 1 m/s imposed by the ASAE standard [186, 199]. For this reason, as suggested by the Standard itself ([186, 199]) and following the same strategy adopted by other authors [185], the prototypes were tested by placing them near the parapets and walls of buildings, shielding them from direct wind exposure.

The experimental campaign was divided into two phases: the first phase consisted of testing the two devices without any load in order to reach the stagnation condition of the devices, while in the second phase the remaining tests were carried out by loading the cooking chamber with a test fluid.

In detail, tests with load were conducted using a black stainless-steel pot as a vessel for the fluid. The pot has a diameter of 200 mm, a height of 130 mm, a thickness of 2 mm and a mass of 476 g. The selected fluids were water and glycerin. Water was selected because the obtained results could be easily compared with those obtained by other researchers; glycerin was selected because it is widely used to test the performance of solar cookers [168, 188, 200].

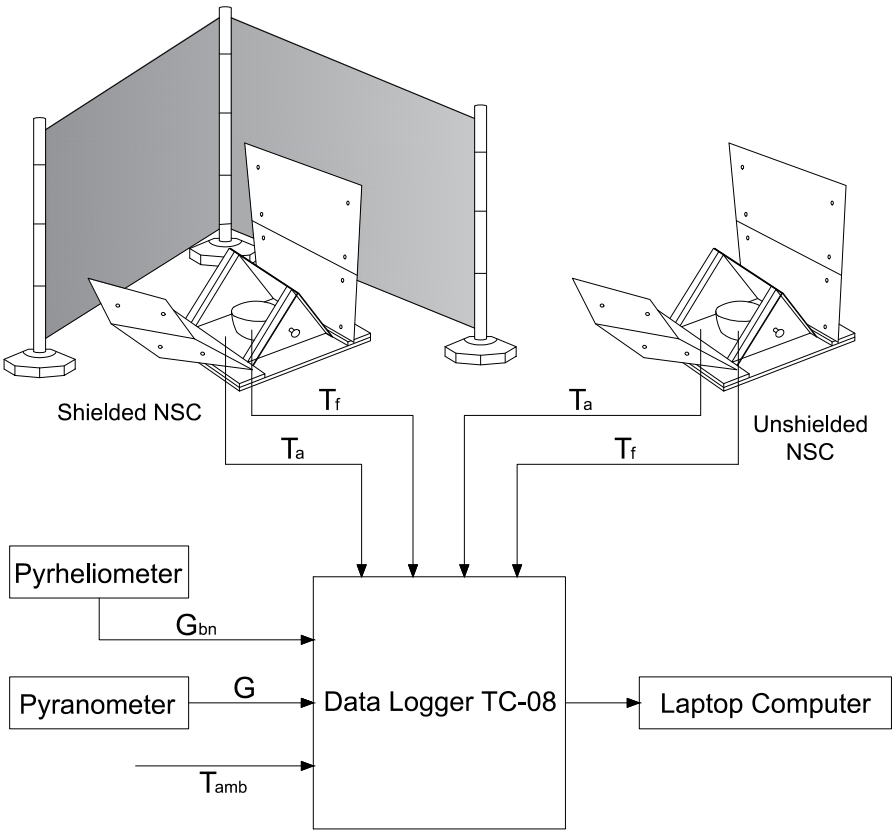

Figure 5.7: Experimental setup. T_{a}: absorber temperature; T_{f}: testing fluid temperature; T_{amb}: ambient temperature; G_{bn}: direct normal solar irradiance; G: global horizontal solar irradiance.

The recorded quantities during the tests were the absorber plate temperatures of the two devices (T_{a}), the fluid temperatures inside the pots (T_{f}), the ambient temperature (T_{amb}), the direct normal solar irradiance (G_{bn}), and the global horizontal solar irradiance (G), as shown in Figure 5.7.

The sensors used to record the temperatures were T-type thermocouples: the one used to record the fluid temperature was immersed in the considered fluid and held in place throughout the test; the one used to record the absorber plate temperature was fixed to the plate using high-temperature adhesive tape, shielding it from direct sun exposure, while the one used to record the ambient temperature was placed in a shady place to avoid influencing the measurement.

An Epply NIP pyrheliometer was used to record the direct normal solar irradiance while a pyranometer SR30-M2-D1 was used to measure the global horizontal solar irradiance. By following the same procedure described by other authors [190, 191, 194, 200], the global normal solar irradiance was calculated using the Liu Jordan isotropic sky model [201] considering an albedo of 0.2.

All the information regarding the instrumentation used during the tests with the respective uncertainties can be found in Appendix B.

During the tests, the operator maintained solar pointing for the cooking chamber

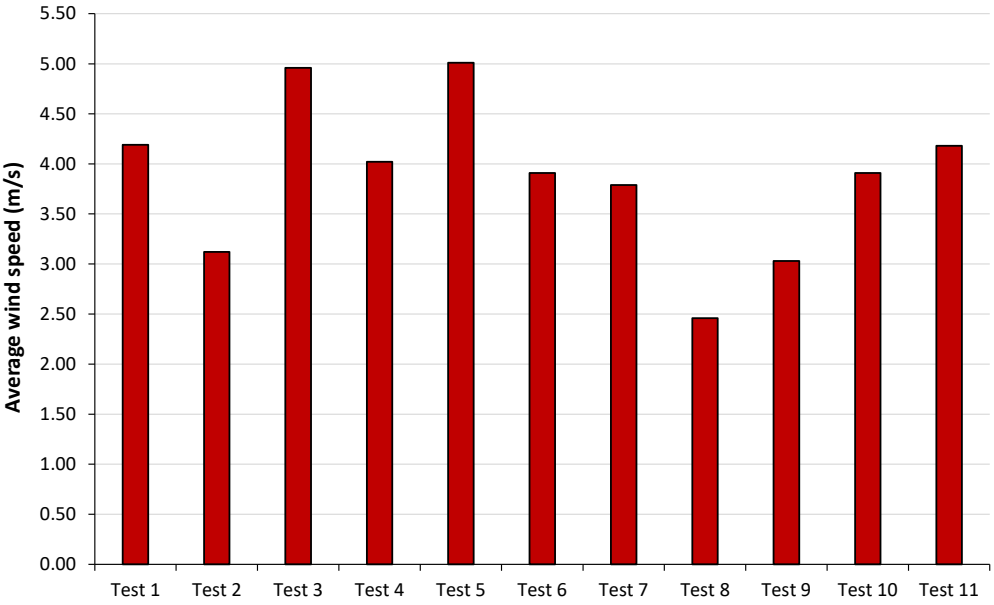

Figure 5.8: Average wind speed recorded in Ancona, Italy (latitude 43.6098° N, longitude 13.5105° E) during the testing period.

and reflector system of the two devices. Additionally, to best use the reflective surfaces and concentrate as much solar radiation as possible into the cooking chamber, the sun elevation (H_{sun}) was checked every 20 minutes and the θ_1 and θ_2 angles of the primary and secondary mirrors were adjusted according to Table 5.1. Every time that a configuration change was applied to the cooker, the operator logged the corresponding time, H_{sun}, θ_1 and θ_2 angles. These values were later weighted according to the time interval they remained in effect and averaged across the test duration to obtain $H_{\text{sun,av}}$, $\theta_{1,\text{av}}$ and $\theta_{2,\text{av}}$ for each test. The average aperture area, $A_{\text{a,av}}$, was calculated in a similar fashion. These quantities were used for the parameters calculation.

The main parameters used to characterize the optical and thermal performances of the panel solar cookers are provided in Table 3.1.

All the parameters reported in Table 3.1 were calculated over a time interval Δt_{h} required to raise the temperature of the fluid from 40 °C to 90 °C for the tests with water (as suggested by Funk [7]). Regarding the glycerin temperature range within which all parameters were calculated was 40–110 °C.

For the determination of the cooker opto-thermal ratio (COR) proposed by Lahkar et al. [173], it is necessary to start from the Hottel-Whillier-Bliss equation for solar cookers:

$$\eta = F'\eta_0 - \left(\frac{F'U_{\text{l}}}{C}\right)\chi \tag{5.1}$$

where $\chi = (T_{\text{f}} - T_{\text{amb}})/G_{\text{n}}$. The parameters $F'\eta_0$ and $F'U_{\text{l}}/C$ of the equation can be identified from the data obtained from the experimental tests. These are the intercept and the opposite value of the slope of the efficiency line regression.

The total time interval to cover the chosen temperature range for water (40–90 °C) and glycerin (40–110 °C) is divided into sub-intervals of 5 minutes each. For each sub-interval, the average global normal solar irradiance, the average ambient temperature,

Table 5.2: Summary of tests without load carried out with the shielded and unshielded NSC.

Quantity	Test 1		Test 2		Test 3	
Date	31/05/2021		03/06/2021		30/06/2021	
Type of cooker	Unshielded	Shielded	Unshielded	Shielded	Unshielded	Shielded
$H_{\text{sun,av}}$ (°)	65.64	65.64	56.22	56.22	62.34	62.34
$\theta_{1,\text{av}}$ (°)	92.48	92.48	84.90	84.90	89.98	89.98
$\theta_{2,\text{av}}$ (°)	45.14	45.14	38.83	38.83	42.93	42.93
$A_{\text{a,av}}$ (m^2)	0.425	0.425	0.401	0.401	0.421	0.421
T_{amb} (°C)	21.07	20.99	30.05	29.70	32.60	33.40
G_{n} (W/m^2)	981.19	977.35	908.86	907.25	936.19	932.46
G_{bn} (W/m^2)	925.74	923.02	866.71	865.17	859.29	858.67
$T_{\text{a,max}}$ (°C)	125.66	120.81	137.47	137.36	133.95	129.07
F_1 (°C/(W/m^2))	0.107	0.102	0.118	0.119	0.108	0.103

the average test fluid temperature, the efficiency and the parameter χ are determined. Plotting the thermal efficiency η against the parameter χ for each identified sub-interval, it is possible to identify the regression line of the efficiency curve and its coefficient of determination R^2.

The regression line's intercept and opposite value of the slope correspond to the parameters $F'\eta_0$ and $F'U_l/C$, which are necessary for the determination of the COR parameter.

5.2.4 Experimental Results

The results obtained from the experimental campaign through tests without load and tests with water and glycerine are presented.

Test without Load

Different environmental conditions characterize the three tests without load that were carried out. In Table 5.2 are reported the ambient temperature associated with the maximum temperature reached by the absorber plate ($T_{\text{a,max}}$) and the F_1 parameter calculated for each device in each test. The average sun elevation ($H_{\text{sun,av}}$), the average angles θ_1 and θ_2 and the average aperture area ($A_{\text{a,av}}$) are also reported. As a preliminary observation, it can be noted that similar values of $T_{\text{a,max}}$ and F_1 were obtained for the two devices in each test.

Figure 5.9 shows the temperature trends of the absorber plate of the unshielded and shielded NSC prototypes for the test of 03/06/2021 (test 2). It can be seen that the maximum temperature was about 137 °C for both NSC prototypes. This $T_{\text{a,max}}$ was associated with a global normal solar irradiance and an ambient temperature of 908.86 W/m^2 and 30.05 °C for the unshielded NSC, and 907.25 W/m^2 and 29.70 °C for the shielded NSC, respectively.

For the three tests without load, the following average values of the F_1 were obtained:

- $F_{1,\text{av}} = 0.111\,°\text{C}/(\text{W/m}^2)$ for the unshielded device;
- $F_{1,\text{av}} = 0.108\,°\text{C}/(\text{W/m}^2)$ for the shielded prototype.

These last values of $F_{1,\text{av}}$ were used for calculating the second figure of merit (F_2) for the tests with load.

Table 5.3: Summary of tests with water carried out with the shielded and unshielded NSC.

	Test 4		Test 5		Test 6		Test 7	
Date	01/06/2021		01/06/2021		09/06/2021		17/06/2021	
Type of cooker	Unshielded	Shielded	Unshielded	Shielded	Unshielded	Shielded	Unshielded	Shielded
$H_{\mathrm{sun,av}}$ (°)	58.60	58.60	61.26	61.26	63.13	63.13	62.96	62.96
$\theta_{1,\mathrm{av}}$ (°)	87.04	87.04	88.81	88.81	90.46	90.46	90.41	90.41
$\theta_{2,\mathrm{av}}$ (°)	39.59	39.59	41.98	41.98	43.45	43.45	43.26	43.26
$A_{\mathrm{a,av}}$ (m^2)	0.411	0.411	0.416	0.416	0.417	0.417	0.419	0.419
m_{f} (kg)	2.0	2.0	2.0	2.0	2.0	2.0	2.0	2.0
T_1 (°C)	40	40	40	40	40	40	40	40
T_2 (°C)	90	90	90	90	90	90	90	90
$G_{\mathrm{n,av}}$ ($\mathrm{W/m}^2$)	1051.95	1049.64	951.90	954.14	824.15	830.93	918.31	918.31
$G_{\mathrm{bn,av}}$ ($\mathrm{W/m}^2$)	908.40	906.41	908.93	911.07	696.92	702.65	738.05	738.12
$T_{\mathrm{amb,av}}$ (°C)	22.03	21.99	23.69	23.59	23.76	23.54	30.22	30.21
Δt_{h} (min)	127	128	122	118	170	134	112	113
t_{s} ($\mathrm{h\,m}^2/\mathrm{kg}$)	0.44	0.44	0.42	0.41	0.59	0.47	0.39	0.40
t_{ch} ($\mathrm{h\,m}^2/\mathrm{kg}$)	0.51	0.51	0.45	0.43	0.54	0.43	0.40	0.40
η_{av}	0.13	0.13	0.15	0.15	0.12	0.15	0.16	0.16
η_{u}	0.17	0.17	0.19	0.20	0.16	0.20	0.19	0.19
F_2	0.21	0.21	0.25	0.27	0.24	0.31	0.26	0.26
$F'\eta_0$	0.247	0.255	0.271	0.329	0.285	0.345	0.279	0.268
$F'U_{\mathrm{l}}/C$ ($\mathrm{W/m}^2\,°\mathrm{C}$)	2.722	2.866	2.683	3.750	2.879	3.424	2.804	2.552
COR ($\mathrm{W/m}^2\,°\mathrm{C}$)	0.091	0.089	0.101	0.088	0.099	0.101	0.100	0.105
T_{fx} (°C)	117.56	115.37	119.93	107.24	105.19	107.26	121.68	126.49
R^2	0.974	0.941	0.867	0.886	0.910	0.909	0.929	0.948

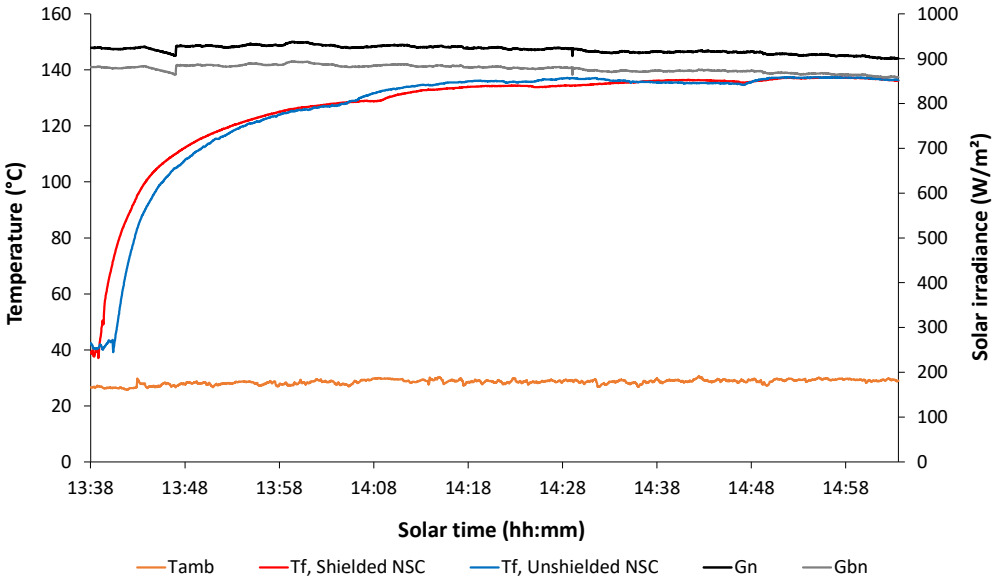

Figure 5.9: Test without load (03/06/2021, test 2).

5.2.5 Tests with Water

The two NSC devices were loaded with 2 kg of water in four outdoor tests. Table 5.3 reports the main parameters for each test calculated in the fluid temperature range 40–90 °C.

Trends of water temperatures, ambient temperature and global and direct normal solar irradiances for test 4 (01/06/2021) are shown in Figure 5.10. The average global normal solar irradiance and ambient temperature were 1050.80 W/m^2 and 21.65 °C, respectively. It took 127 minutes for water to cover the temperature range from 40 °C to 90 °C with the unshielded NSC, 128 minutes when tested with the shielded device.

The water temperature trends obtained with the two prototypes during all tests are reported in Figure 5.11: it is possible to note that the trends are very similar despite the tests were conducted in different days characterized by different solar irradiances and ambient temperatures. It can also be seen that the time taken by water to reach 90 °C was about the same for the two devices in all tests. In particular, it was slightly longer in the case of the unshielded device (on average 133 minutes) with respect to the shielded one (on average 123 minutes).

A marked decrease in the time is evident in test 6 (09/06/2021) for the shielded prototype: in fact, it was able to warm up water in 134 minutes, whereas it took 170 minutes for the unshielded NSC to cover the same water temperature range. In general, the shortest time was recorded in the test of 17/06/2021 (test 7): 112 minutes for the unshielded NSC and 113 minutes for the shielded NSC. During the test, an average global normal solar irradiance of 918.31 W/m^2 and an average ambient temperature of 30.22 °C were recorded.

Comparing tests 4 and 5 with test 7, it is possible to notice that the first two were characterized by higher values of $G_{\mathrm{n,av}}$ and $G_{\mathrm{bn,av}}$ than the latter. Their Δt_{h} are nonetheless higher than that of test 7, hinting to the fact that T_{amb} might affect the device performance more than solar irradiance. In fact, this temperature was much higher in test 7 than in tests 4 and 5 (30.22 °C vs. 21.6 °C and 23.6 °C).

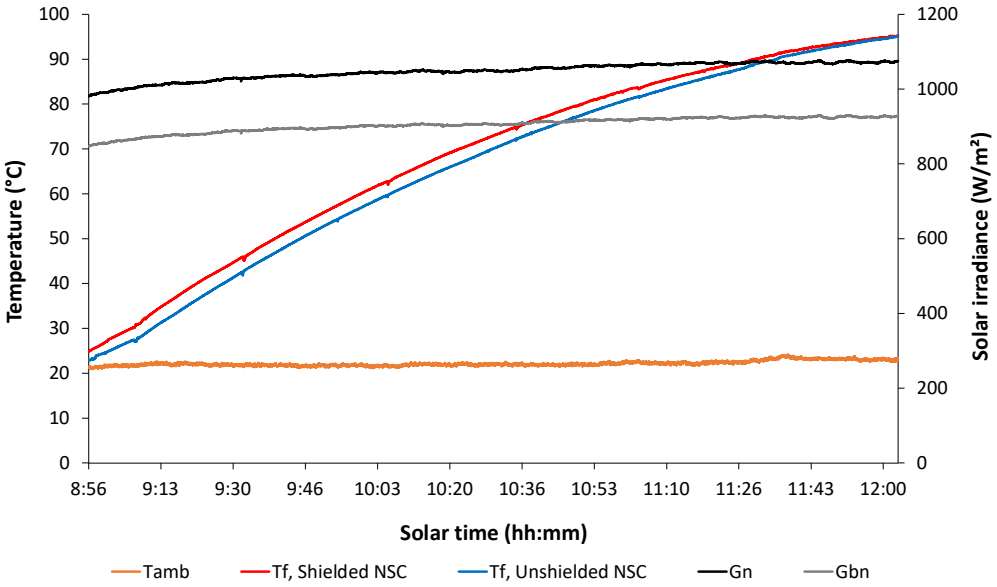

Figure 5.10: Test with water (01/06/2021, test 4).

However, the effects of a lower solar irradiance are evident in tests 5 and 6: in fact, test 6 (average Δt_h of 152 min and G_n of 827.54 W/m^2) registered a longer time for water to reach the boiling point with respect to test 5 (average Δt_h of 120 min and G_n of 953.02 W/m^2), despite both being characterized by a similar ambient temperature.

In addition to the average efficiency (η_{av}) and the specific and characteristic boiling times (t_s and t_c), the COR parameter and the maximum temperature reachable by the fluid (T_{fx}) were also calculated.

Figure 5.12 shows the thermal efficiency η plotted against χ for each identified 5-minutes sub-interval. From the points, the regression line of the efficiency curve was determined and together with its coefficients, which correspond to the parameters $F'\eta_0$ (intercept) and $F'U_l/C$ (opposite of the slope). The COR parameter and T_{fx} were calculated through these two coefficients.

From the performance parameters derived from the different tests (Table 5.3), it can be pointed out that their values for the unshielded device are usually similar to those of the shielded NSC in all the tests. However, it is also possible to note that, while the optical efficiency factor $F'\eta_0$ of the two prototypes is almost constant, the heat loss factor $F'U_l/C$ shows wider variations that depend on the average ambient temperature and wind speed.

5.2.6 Tests with Glycerin

Four outdoor tests were performed by loading each pot with 2 kg of glycerin. Table 5.4 shows the results obtained for two NSC prototypes. The parameters reported in this table were calculated for glycerin in the temperature range 40–110 °C.

Figure 5.13 depicts glycerin and ambient temperature trends, and global and direct normal solar irradiances recorded on 04/06/2021 (test 9). The average global normal solar irradiances was 963.96 W/m^2, while the average ambient temperature was 26.88 °C. It took 199 minutes for the fluid when tested with the unshielded NSC

Table 5.4: Summary of tests with glycerin carried out with the shielded and unshielded NSC.

	Test 8		Test 9		Test 10		Test 11	
Date	03/06/2021		04/06/2021		22/06/2021		29/06/2021	
Type of cooker	Unshielded	Shielded	Unshielded	Shielded	Unshielded	Shielded	Unshielded	Shielded
$H_{\mathrm{sun,av}}$ (°)	60.93	60.93	60.48	60.48	63.77	63.77	61.39	61.39
$\theta_{1,\mathrm{av}}$ (°)	88.69	88.69	88.53	88.53	90.98	90.98	89.19	89.19
$\theta_{2,\mathrm{av}}$ (°)	40.75	40.75	40.73	40.73	43.75	43.75	41.64	41.64
$A_{\mathrm{a,av}}$ (m^2)	0.414	0.414	0.413	0.413	0.419	0.419	0.416	0.416
m_{f} (kg)	2.0	2.0	2.0	2.0	2.0	2.0	2.0	2.0
T_1 (°C)	40	40	40	40	40	40	40	40
T_2 (°C)	110	110	110	110	110	110	110	110
$G_{\mathrm{n,av}}$ ($\mathrm{W/m}^2$)	1058.05	1048.19	962.39	965.53	934.34	934.96	910.08	910.85
$G_{\mathrm{bn,av}}$ ($\mathrm{W/m}^2$)	879.44	871.25	837.81	846.06	766.25	766.75	744.91	745.54
$T_{\mathrm{amb,av}}$ (°C)	24.06	23.43	26.78	26.94	31.05	30.92	32.10	32.12
Δt_{h} (min)	236	174	199	187	214	175	140	146
t_{s} ($\mathrm{h\,m}^2/\mathrm{kg}$)	0.81	0.60	0.60	0.64	0.75	0.61	0.49	0.51
t_{ch} ($\mathrm{h\,m}^2/\mathrm{kg}$)	0.96	0.70	0.64	0.69	0.78	0.63	0.49	0.51
η_{av}	0.06	0.08	0.09	0.08	0.08	0.09	0.12	0.11
η_{u}	0.08	0.10	0.11	0.10	0.09	0.10	0.13	0.13
F_2	0.12	0.17	0.19	0.18	0.15	0.19	0.24	0.24
$F'\eta_0$	0.156	0.204	0.216	0.206	0.177	0.230	0.265	0.295
$F'U_{\mathrm{l}}/C$ ($\mathrm{W/m}^2\,°\mathrm{C}$)	1.682	2.124	2.240	2.046	1.776	2.347	2.810	3.206
COR ($°\mathrm{C}/(\mathrm{W/m}^2)$)	0.093	0.096	0.096	0.100	0.100	0.098	0.094	0.092
T_{fx} (°C)	122.14	124.27	119.65	123.99	124.17	122.54	117.93	116.03
R^2	0.932	0.957	0.883	0.968	0.922	0.883	0.856	0.910

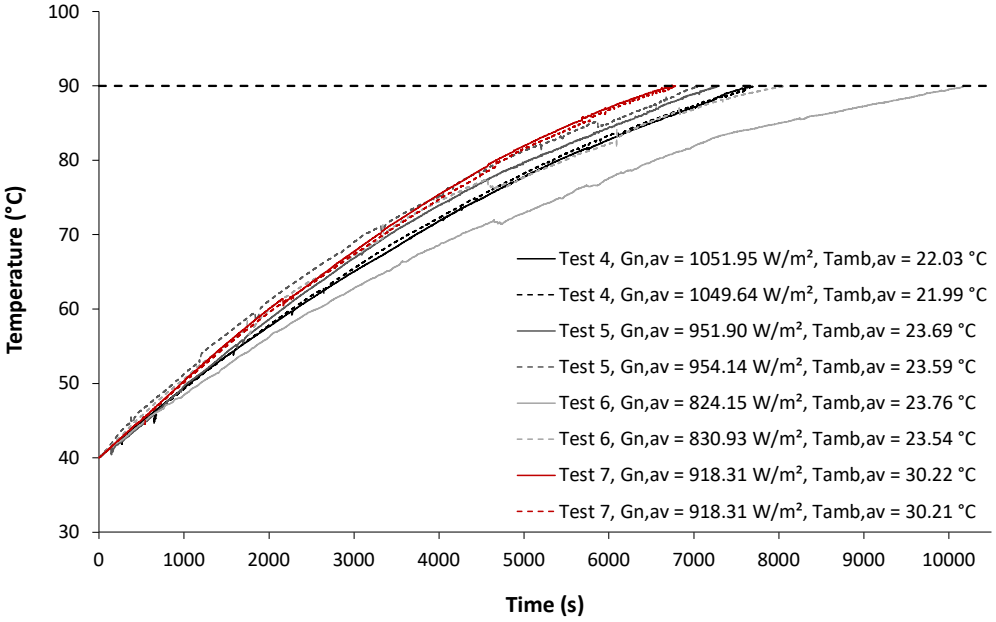

Figure 5.11: Water temperature trends. The continuous line refers to the unshielded NSC, the dotted one to the shielded NSC.

and 187 minutes when tested with the shielded device to cover the temperature range 40–110 °C.

Figure 5.14 shows the glycerin temperature trends obtained with the unshielded and shielded NSC devices during all tests. From Figure 5.14 it is possible to note that, as in the case of water tests, the curves follow a very similar trend even though the external conditions were different.

Anyway, it is important noticing that the benefits of shielding are more evident in the tests with glycerin: in fact, the times required for the fluid to go from 40 to 110 °C were generally longer in the case of the unshielded solar cooker. This is especially evident in tests 8 (03/06/2021) and 10 (22/06/2021): Δt_{h} were 236 and 214 minutes for the unshielded NSC, and 174 and 175 minutes, respectively, for the shielded one.

As for the tests with water, the COR parameter and T_{fx} were calculated in addition to η_{av}, t_{s} and t_{ch}. The same procedure described for the water tests was used, with the only difference being the temperature range (40–110 °C).

Figure 5.15 shows the efficiency (η) referred to test 10 (04/06/2021). Also in this case, the values of the calculated parameters are very similar for all tests (Table 5.4). As for the tests with water, the optical efficiency factor ($F'\eta_0$) of the two prototypes is almost constant, while wider variations are present for the heat loss factor ($F'U_{\mathrm{l}}/C$).

Finally, from Tables 5.3 and 5.4 it can be pointed out that, for the same mass of fluid, the average thermal efficiency (η_{av}) for the tests with glycerin is lower than that for the tests with water. This outcome can be due to the higher temperatures used to test glycerin.

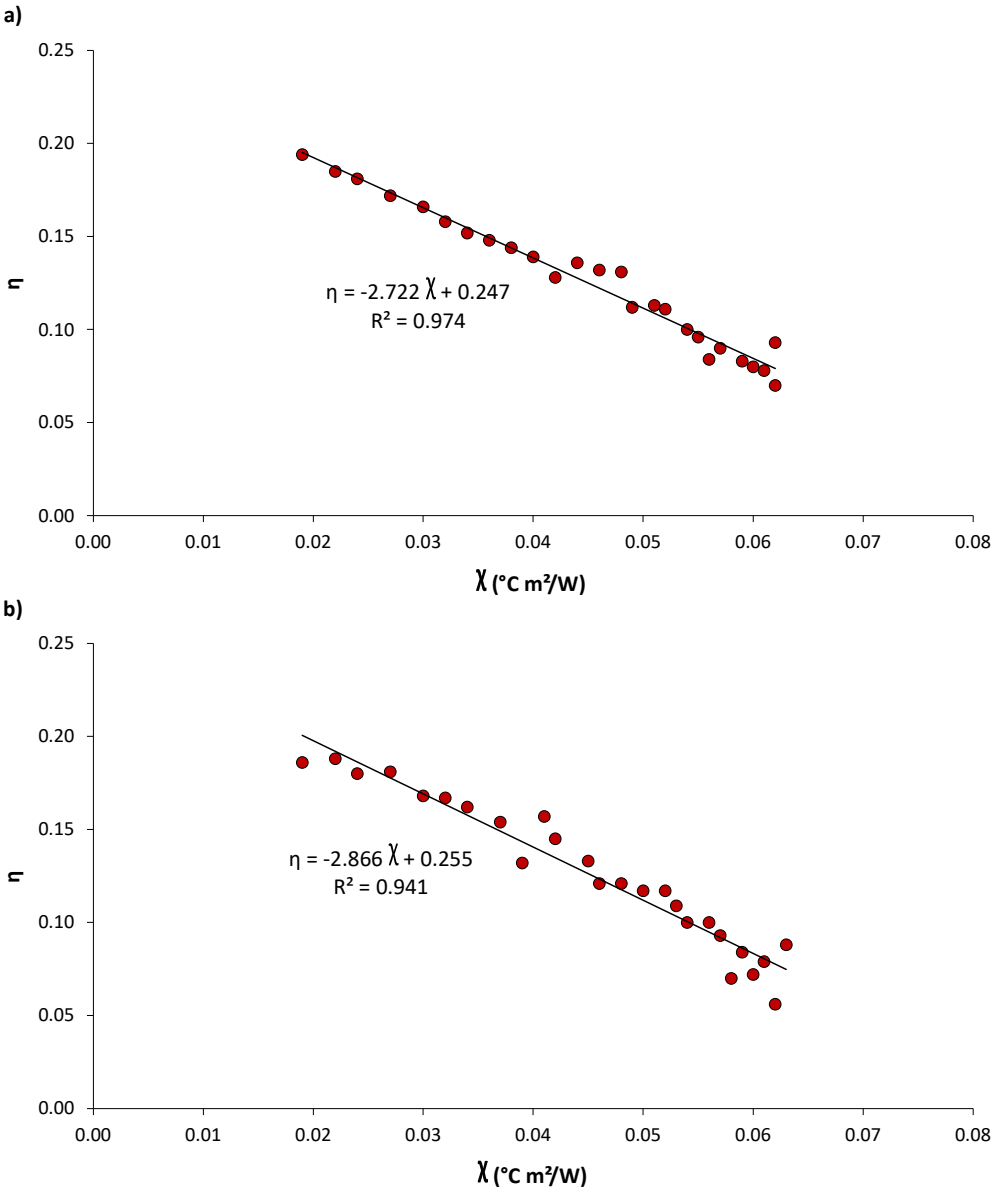

Figure 5.12: Efficiency of the cookers tested with water (01/06/2021, test 4): a) unshielded Newton solar cooker and b) shielded Newton solar cooker.

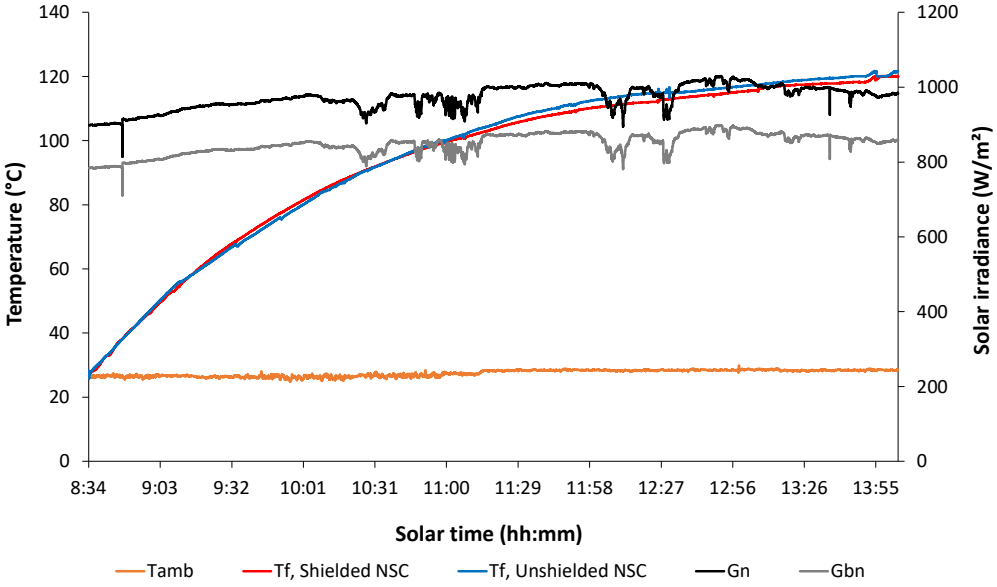

Figure 5.13: Test with glycerin (04/06/2021, test 9).

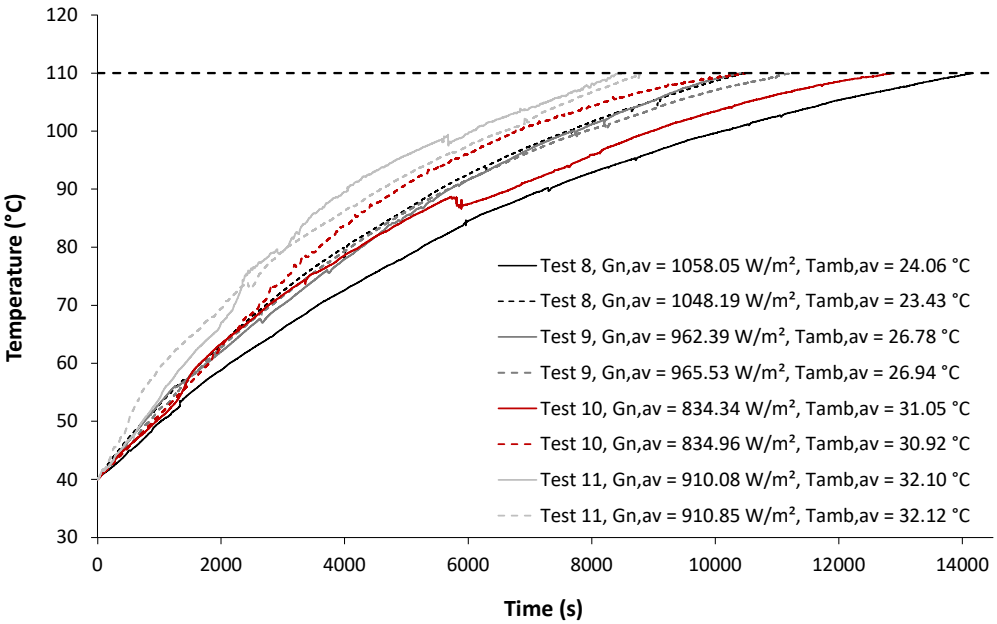

Figure 5.14: Glycerin temperature trends. The continuous line refers to the unshielded NSC, the dotted one to the shielded NSC.

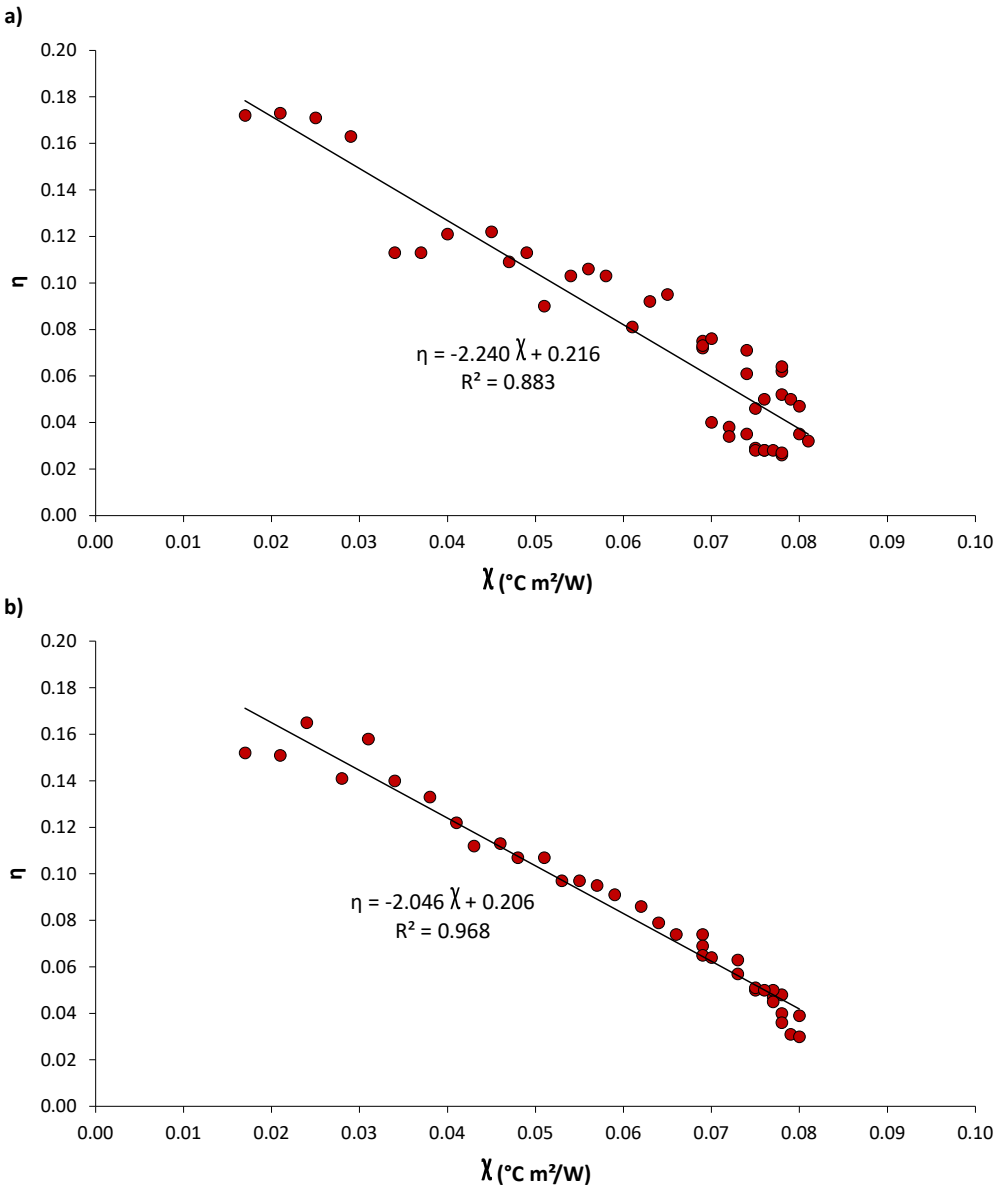

Figure 5.15: Efficiency of the cookers tested with glycerin (04/06/2021, test 9): a) unshielded Newton solar cooker and b) shielded Newton solar cooker.

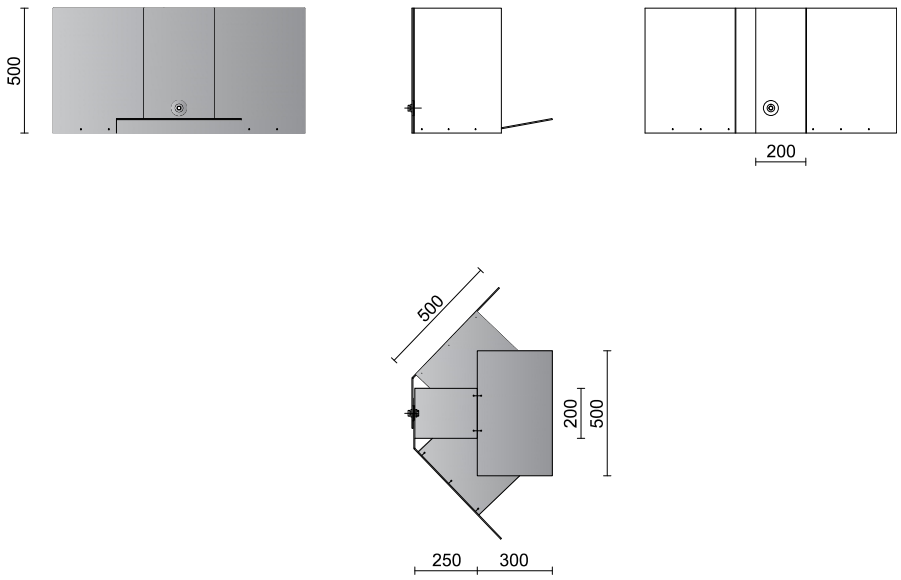

Figure 5.16: Kimono solar cooker views (dimensions in mm) [4].

5.3 Kimono Solar Cooker

The second panel solar cooker presented in this chapter is the Kimono solar cooker. This device has an original design and is the most economical and the simplest made and tested within the DIISM laboratories. Three other panel cookers were selected for this analysis: the Funnel, the Dual Setting and the Cookit. The aim of the study was to evaluate the thermal and optical performance of these devices, which, due to the materials used and the steps required to manufacture them, are the simplest and cheapest solar devices. The performance of the cookers at different sun elevation angles were investigated, using suitable configurations.

5.3.1 Design, Manufacture and Materials

The Kimono solar cooker, shown in Figure 5.16 and Figure 5.17a,b, was realized by following the design specification provided by Eng. Matteo Muccioli [202]. Starting from a Plexiglas sheet with a thickness of 3 mm, two side panels (500 × 500 mm each), two bottom panels (300 × 350 mm each), a front panel (250 × 200 mm) and two rear panels (500 × 200 mm each) were cut and drilled.

A Mylar film, chosen as reflective material, was fixed to the seven panels using double-sided adhesive tape, obtaining a smooth and uniform surface. Then, one side panel, one bottom panel and one rear panel were joined together with a wire, creating one part. A symmetrical part was obtained by assembling together the three remaining panels. The two parts were joined together by two holes, one in each rear panel, specifically designed for this purpose.

A knob was inserted to adjust the tightening torque and to be able to change the panels alignment in order to adjust the solar collecting area during usage.

Finally, the front panel was placed in front of the two parts and its tilt angle was adjusted according to the position of the sun.

Figures 5.17a and 5.17b shown the two main configurations that the Kimono

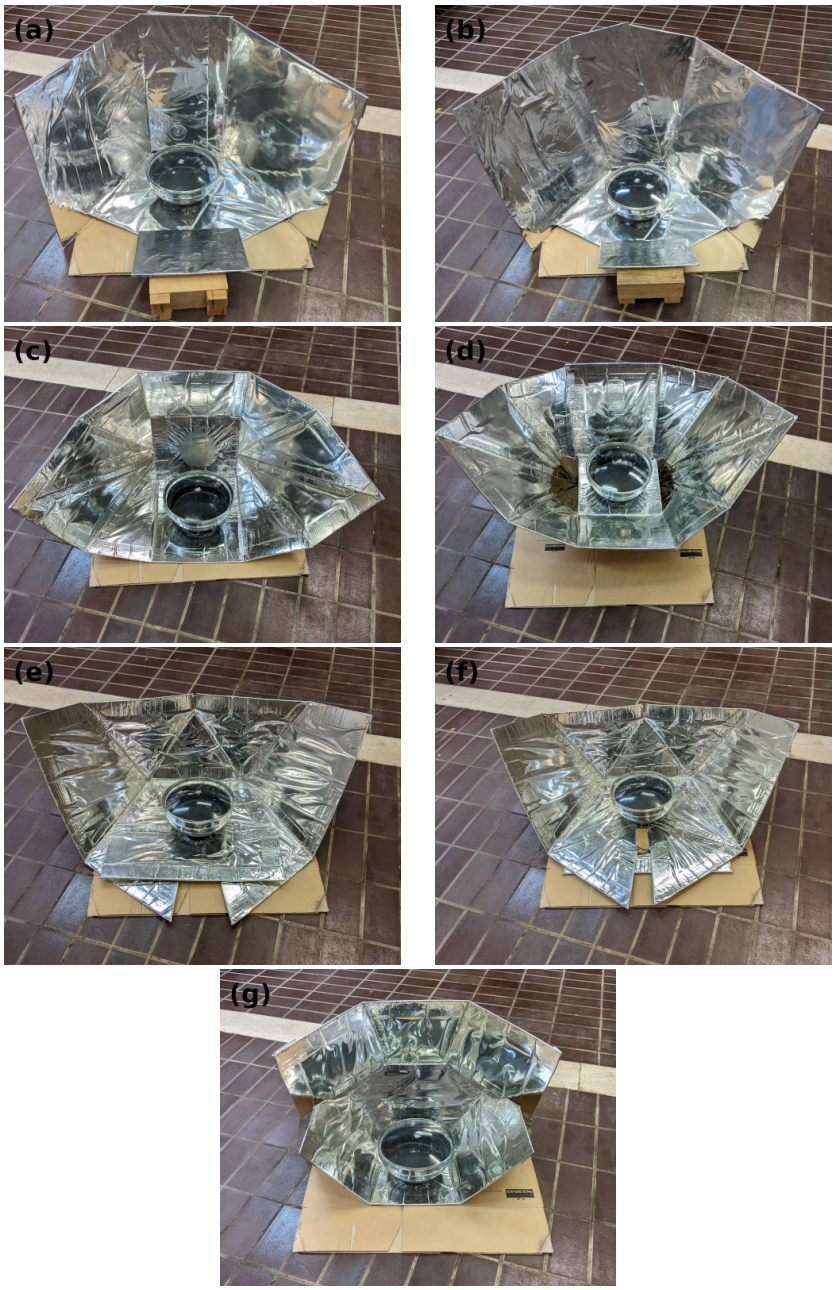

Figure 5.17: Pictures of the four analyzed prototypes: (a) Kimono solar cooker for low-medium sun elevations; (b) Kimono solar cooker for medium-high sun elevations; (c) Funnel solar cooker for low-medium sun elevations; (d) Funnel solar cooker for medium-high sun elevations; (e) Dual Setting Panel Cooker for low-medium sun elevations; (f) Dual Setting Panel Cooker for medium-high sun elevations; (g) Cookit solar cooker for low-medium sun elevations.

solar cooker can assume to better concentrate the solar radiation toward the receiver according to the sun elevation: the first one for low-medium sun elevation, the latter for medium-high sun elevation. In the former, the two rear panels are perfectly overlapped and perpendicular to the bottom panels. Instead, the rear panels of the latter configuration are tilted back to increase the solar collecting area when the solar elevation is medium-high. In this latter configuration, the tilt angle of the rear panels is not fixed but can be adjusted according to the elevation of the sun.

The remaining three prototypes were all made from cardboard sheets. After folding and cutting the cardboard according to the specifications in the manuals, the various components were attached to each other with double-sided adhesive tape and glue. Mylar film was also used as a reflective material for these prototypes, following the same procedure as for the Kimono.

The Funnel solar cooker realized for this experimental analysis was derived from the portable version design by [203] and has a maximum aperture area 16 % smaller than that of the prototype tested by Ruivo et al. [190]. As explained by Müller [204] (the author that defined the dimensions of this panel device), the Funnel can be arranged in a configuration for low-medium sun elevations (Figure 5.17c) and one for medium-high sun elevations (Figure 5.17d), according to sun elevation during tests.

The Dual-setting panel cooker realized for this analysis follows the design conceived by [205] and is shown in Figure 5.17e,f. This device can change the geometry of its basis in accordance with the sun elevation. Figure 5.17e shows its configuration for low-medium sun elevations while igure 5.17f for medium-high sun elevations.

The Cookit design chosen for this study was proposed by [206, 207]. Unlike other prototype designs, only the configuration for low-medium sun elevations, shown in Figure 5.17g, was analyzed.

5.3.2 Working Configuration of The Four Prototypes

The four prototypes during the tests were positioned directly on the the ground, limiting therefore their ability to track the sun only to the azimuth. Depending on the period of the year when the tests were carried out (and hence on the sun elevation), the Kimono, the Funnel and the DSPC solar cookers were placed in the proper configuration between the two described above. The Cookit solar cooker, instead, required for all tests only one configuration, the one for low-medium sun elevations, as this was found to be suitable in all the test periods.

Regarding the medium-high sun elevations of the Kimono solar cooker (Figure 5.17b), it is important to point out that a single fixed tilt angle of the rear panels was used in all the tests.

Details regarding the configurations used in each measurement are reported in Section 5.3.4.

The aperture area of these panel solar cookers depends on the sun elevation during the tests and the chosen configuration of the reflective system. To simplify the analysis of the results, the performance parameters were calculated considering the average aperture areas (A_a) of the devices during the tests. In particular, the A_a values of the cookers' configuration used for low-medium sun elevations were calculated considering the average sun elevation of $\alpha_{sun,av} \sim 41°$, while for the medium-high sun elevations configuration $\alpha_{sun,av} \sim 62°$ was selected. These average sun elevations were estimated by means of the algorithms described by Meeus [208], taking into account that the tests were carried out in Ancona in the periods September-October, March-April and July-August between 10:00 and 16:00 local solar time.

Table 5.5: Aperture areas of the four solar cookers.

Type of cooker	Aperture area, A_a (m^2)			
	Kimono	Funnel	DSPC	Cookit
Configuration A (low-medium sun elevation)	0.526	0.417	0.419	0.323
Configuration B (medium-high sun elevation)	0.540	0.420	0.440	-

Table 5.6: Components of the receiver.

Quantity	Black steinless-steel cake pan	Glass bowl	Glass lid
Diameter (cm)	20	23	22
Height (cm)	6	10	-
Volume (dm^3)	1.8	2.9	-
Mass (kg)	0.12	0.85	0.43

Table 5.5 reports the A_a for each solar cooker for the low-medium sun elevations configuration (configuration A) and the one for medium-high sun elevations (configuration B). From the table it can be seen that the A_a values of the Funnel cooker considered in this work are smaller than those of the Funnel cookers tested by Ruivo et al. [190, 200] and Apaolaza-Pagoaga et al. [209, 210].

5.3.3 Experimental Tests and Setup

In this section, the test bench designed to carry out the experimental campaign is presented, together with the parameters used to characterize the performance of the prototypes.

Test Bench

Figure 5.18 shows the test bench used to perform the tests during the experimental campaign. The four prototypes, arranged side by side, were tested simultaneously under the same external conditions and using identical receivers. Figure 5.19 shows the system used as receiver with the aim of creating a kind of closed cooking chamber. Each receiver consisted of a black stainless-steel cake pan placed inside a glass bowl and covered by a glass lid. The lid knob was removed in order to place the fluid temperature sensor in the center of the cake pan (Figure 5.19). All the information regarding the diameters, heights, volumes and masses of the components of the receivers are collected in Table 5.6.

Water was used as test fluid in the sets of tests with load.

The quantities detected during the test were the absorber temperature, T_a, the fluid temperature, T_f, the ambient temperature, T_{amb}, the direct normal solar irradiance, G_{bn} and the global horizontal solar irradiance G_h. In the tests with load, the thermocouples used to measure the fluid temperature were placed at the center of each receiver through the hole in the knob and immersed 2 cm into the fluid (Figure 5.19).

The thermocouple used for the ambient temperature was positioned in a shaded spot, so as not to be exposed to direct solar radiation. The sensors used to record all the temperatures were T-type thermocouples, while an Eppley NIP (normal incidence

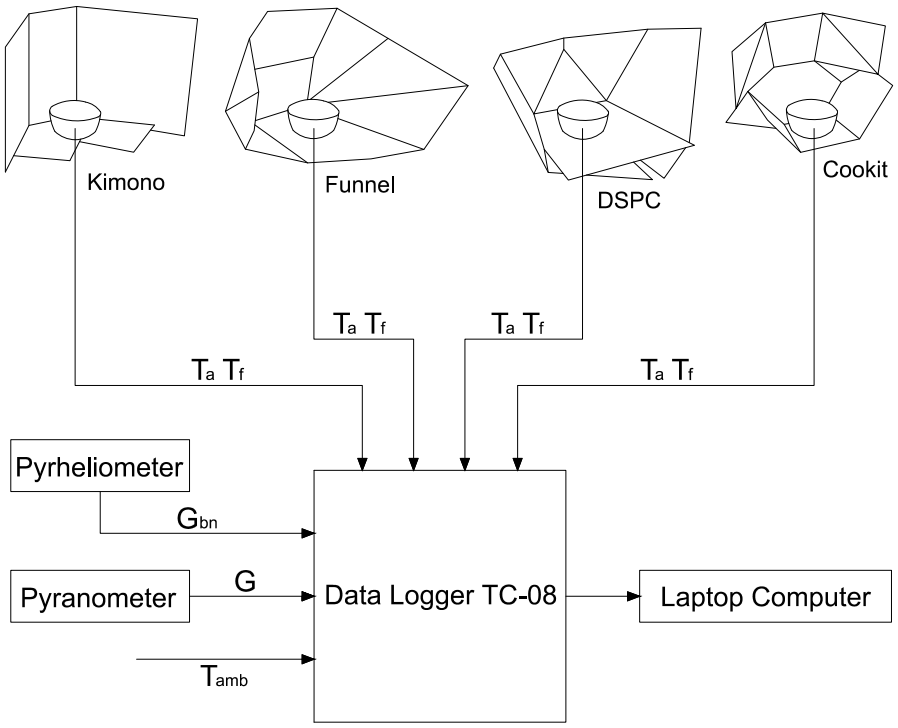

Figure 5.18: Test bench: absorber temperature, T_{a}, test fluid temperature, T_{f}, ambient temperature, T_{amb}, direct normal solar irradiance, G_{bn}, and global horizontal solar irradiance, G.

pyrheliometer) was used to measure the direct normal solar irradiance. The thermocouples and pyrheliometer signals were collected via a Pico Technology TC-08 data logger connected to a laptop. By using a pyranometer SR30-M2-D1 placed horizontally near the solar cookers was recorded the global horizontal solar irradiance.

By following the same procedure described by other authors ([3, 190, 191, 194, 200]), the global normal solar irradiance, G_{n}, was obtained using the Liu-Jordan isotropic sky model [201] considering an albedo value of 0.2.

Performance Parameters

Given the same uncontrollable external variables such as wind, solar irradiance and ambient temperature, the aim of testing the four prototypes in parallel was to assess how the different devices with different geometries behaved in terms of thermal and optical performances.

Table 5.7 collected the main parameters used to characterize the performance of the four panel solar cookers under no-load and load conditions.

Panel solar cookers fall into the category of open device, i.e. they do not have an enclosed cooking chamber where the pot can be inserted. However, as also reported in recent works on panel solar cookers [191, 194], the stagnation condition (i.e. the equilibrium between the incoming heat due to the incident solar radiation and the outgoing heat due to thermal losses) can be investigated.

The no-load tests were made possible by the choice of the receiver: in fact, as

Figure 5.19: Receiver components (on the left); detail of immersed temperature sensor (on the right).

described above, the cake pan was placed inside a glass container and closed with a glass lid, making the system closed.

For the calculation of the first figure of merit, F_1, it is important to emphasize that the considered values of ambient temperature, T_{amb}, and global normal solar irradiance, G_{n}, are those corresponding to when the absorber reaches its stagnation temperature, $T_{\mathrm{a,max}}$.

It is evident from the Table 5.7 that not all parameters derived from the international standards have been calculated. A qualitative analysis was chosen for the characterization of the four devices under consideration, given the initial choice of wanting to produce prototypes at almost zero cost. This made it possible to understand whether, however, following the methodology established in conducting the tests, it was possible to achieve remarkable results in terms of thermal and optical performance with cardboard prototypes.

Most of the parameters described in Table 5.7 were calculated in a time interval Δt_{h} necessary for the test fluid to evolve from the initial temperature T_1 to the final temperature T_2. As suggested by Funk [7], $T_1 = 40\,^{\circ}\mathrm{C}$ and $T_2 = 90\,^{\circ}\mathrm{C}$ were chosen for the tests with water.

The procedure proposed by Lahkar et al. [173] was used to determine the *COR* parameter, starting from the Hottel-Whillier-Bliss equation expressed for solar cookers 5.1. Here again the parameters $F'\eta_0$ and $F'U_{\mathrm{l}}/C$, i.e. the intercept and the opposite value of the slope of the efficiency linear regression were determined starting from the data obtained from the experimental tests.

The same methodology for the characterization of the two Newton prototypes was also followed here: the total time interval Δt_{h} necessary for water to evolve from 40 to 90 °C was divided into sub-intervals of 5 minutes each. For each sub-interval, the average global normal solar irradiance, $G_{\mathrm{n,av}}$, the average ambient temperature, $T_{\mathrm{amb,av}}$, the average temperature of the tested fluid, $T_{\mathrm{f,av}}$, the efficiency, η, and the specific temperature difference, χ, were determined. By plotting the efficiency η against the associated parameter χ for each identified sub-interval, it is possible to determine the linear regression equation of the efficiency curve and the coefficient of determination R^2. From the regression, the value of the intercept and the opposite value of the slope that correspond to the parameters $F'\eta_0$ and $F'U_{\mathrm{l}}/C$, necessary for the determination of the *COR* parameter, are obtained.

5.3.4 Experimental Results

All the tests were carried out in Ancona, Italy, on the roof of the DIISM (latitude 43.5871° N, longitude 13.5149° E) using the four prototypes in parallel and four identical

Table 5.7: Parameters for the characterization of the solar cookers.

Parameter	Equation	Equation parameters
Test without load		
First figure of merit [19]	$F_1 = \frac{T_{\mathrm{a,max}} - T_{\mathrm{amb}}}{G_{\mathrm{n}}}$	G_{n}: global normal solar irradiance T_{amb}: ambient temperature $T_{\mathrm{a,max}}$: absorber stagnation temperature
Test with load		
Heating time interval	$\Delta t_{\mathrm{h}} = t(T_2) - t(T_1)$	A_{a}: aperture area of the solar cooker C: geometrical concentration ratio η_0: optical efficiency
Second figure of merit [19]	$F_2 = \frac{F_1 m_{\mathrm{f}} c_{\mathrm{f}}}{A_{\mathrm{a}} \Delta t_{\mathrm{h}}} \ln \left[\frac{1 - \frac{1}{F_1}(T_1 - T_{\mathrm{amb,av}})/G_{\mathrm{n,av}}}{1 - \frac{1}{F_1}(T_2 - T_{\mathrm{amb,av}})/G_{\mathrm{n,av}}} \right]$	$G_{\mathrm{n,av}}$: mean G_{n} measured at Δt_{h}
Overall efficiency [172]	$\eta_{\mathrm{av}} = \frac{m_{\mathrm{f}} c_{\mathrm{f}} (T_2 - T_1)}{G_{\mathrm{n,av}} A_{\mathrm{a}} \Delta t_{\mathrm{h}}}$	m_{f}: mass of the test fluid c_{f}: specific heat of the test fluid
Cooker opto-thermal ratio [173]	$COR = \frac{\eta_0 C}{U_{\mathrm{l}}}$	$T_{\mathrm{amb,av}}$: mean T_{amb} measured at Δt_{h} $t(T_1)$: starting time of the heating period $t(T_2)$: ending time of the heating period U_{l}: heat loss factor

receivers, as already described in section 5.3.2. In order to have all the prototypes properly exposed to solar radiation, a manual azimuthal tracking was carried out at regular intervals of about 15 minutes.

Three sets of measurements were carried out at different times of the calendar year to obtain an overall picture of the operation and performance of each of the four devices. They were tested under no-load and in load conditions. Water was selected as test fluid to perform the load tests. The three sets of tests were divided as follows:

- first set: September and October 2020;
- second set: between March and April 2021, and April 2022;
- third set: July and August 2021.

In planning the experimental campaign, it was decided not to consider the coldest months of the year, i.e. winter months: given that for the geographic position of Ancona the ambient temperature and the solar irradiance are on average below 20 °C and 450 W/m^2 (which are the minimum acceptable values indicated by the ASAE Standards [186, 199]), tests with the studied panel cookers would not have led to suitable results.

As regards the effect of wind, Figure 5.21 shows the average wind speed recorded in a location near the testing site (latitude 43.6098° N, longitude 13.5105° E) considering the time slot when the measures were conducted. As for the wind investigation for the Newton experimental campaign, also here the data referring to the wind intensity were collected from [198]. Is is evident from Figure 5.21 that in all carried out tests, the average wind speed values exceed the limit of 1 m/s imposed by the ASAE standard [186, 199]. For this reason, also in this experimental campaign, following the Standard itself ([186, 199]) and the strategy adopted by other authors [185], all solar cookers were shielded testing them near parapet walls and buildings with no overhead obstruction and clear line of sight to the sun. Figure 5.20 shows as an example the configuration adopted during a water test of the 4 devices arranged in pairs, close to the terrace parapet and with the wind shielding systems adopted.

For the sake of simplicity, the results obtained from the tests without load and tests with water will be reported for the Kimono only. All results obtained from the experimental campaign together with the respective comparisons between the 4 prototypes are available in [4].

First Set of Tests: No-load Tests and Tests with Water

The experimental tests of the first set of measure were carried out in September and October 2020. In detail, 3 no-load tests and 2 load tests with water were performed. Since this is a period of low-medium sun elevation in Ancona, the configuration of the solar cookers for low-medium sun elevations was used in the tests. For this reason, the A_a values of configuration A have been employed for the calculation of the performance parameters of all prototypes.

The three test without load were carried out under different environmental conditions. Table 5.8 shows a summary of the tests with the quantities measured during the tests for the Kimono solar cooker.

As an example, Figure 5.22 shows the temperatures and the solar irradiances detected during the test of 18/09/2020 (test 1). In test 1 (Table 5.8) the Kimono reached the highest recorded absorber temperatures: 138.78 °C.

From Table 5.8 and Figure 5.22, the following considerations can be made:

Figure 5.20: A picture of the four panels solar cookers placed side by side during a test with water with the wind shielding systems adopted.

Table 5.8: Summary of the tests without load of the first set of tests for the Kimono solar cooker.

Quantity	Test 1	Test 2	Test 3
Date	18/09/2020	05/10/2020	13/10/2020
Type of cooker	Kimono	Kimono	Kimono
Configuration	A	A	A
T_{amb} (°C)	24.91	22.26	13.76
G_n (W/m^2)	883.56	975.86	926.73
G_{bn} (W/m^2)	715.09	890.17	825.55
$T_{a,max}$ (°C)	138.78	135.32	113.40
F_1 (°C/(W/m^2))	0.129	0.116	0.108

- Tests 1 and 2 are the ones that best describe the thermal performance of the panel cooker given the good environmental conditions detected (G_n and T_{amb}) and the repeatability of the values found for $T_{a,max}$.
- Test 3 shows that ambient temperature plays a primary role in the performance of the devices. In fact, the ambient temperature of the kimono recorded in this test, 13.76 °C, is significantly lower than that recorded in the two previous tests: (24.91 °C for test 1 and 22.26 °C for test 2). Despite G_n is comparable with those of the other tests, the significantly lower T_{amb} led to lower maximum absorber temperatures than those recorded in the other two tests.
- In general, the Kimono was able to reach a very high maximum absorber temperature when the environmental conditions were optimal, exceeding 135 °C in test 1 and test 2.

Table 5.9 shows a summary of the two tests conducted with water. These tests were carried out using the same experimental setup and a mass of 1 kg of water in the receiver.

Figure 5.23 shows the solar irradiances and the fluid temperature recorded during the test on 24/09/2020 (test 4). The global normal solar irradiance was about 862 W/m^2

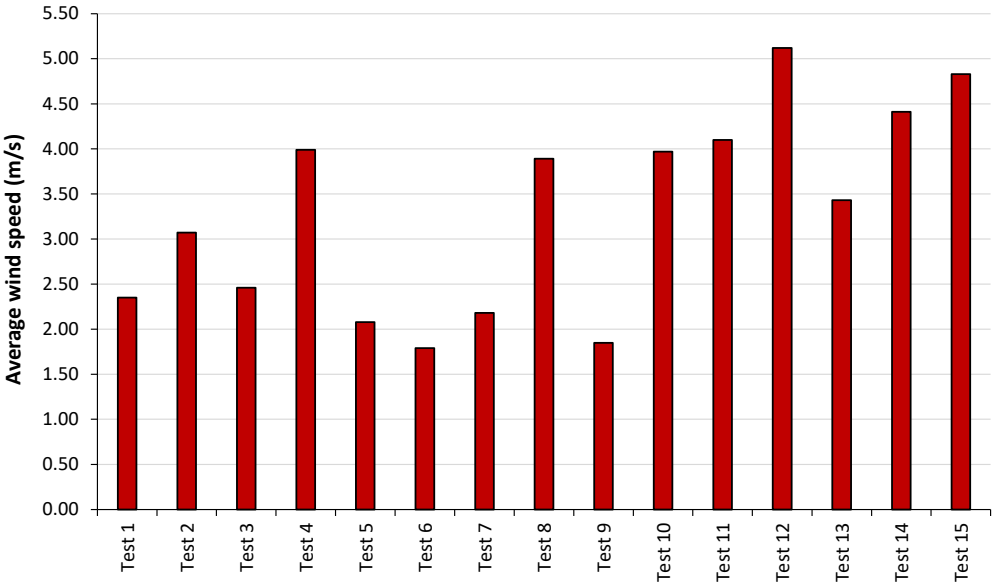

Figure 5.21: Average wind speed recorded in Ancona, Italy (latitude 43.6098° N, longitude 13.5105° E) during the testing period.

and the average ambient temperature was 27.24 °C during the test. Water took about 1 hour to go from 40 to 90 °C in the Kimono solar cooker.

Second Set of Tests: No-load tests and Tests with Water

The experimental tests of the second set of measurements were carried out in March, April 2021 and in April 2022. In detail, 3 no-load tests and 2 load tests with water were performed. Although these months are a period of medium sun elevation in Ancona, the configuration of the Kimono for low-medium sun elevations was used in all tests.

Three tests without load were carried out under different environmental conditions. Table 5.10 shows a summary of the tests with the measured quantities for the Kimono

Table 5.9: Summary of the water load tests of the first set of tests for the Kimono solar cooker.

Quantity	Test 4	Test 5
Date	24/09/2020	09/10/2020
Type of cooker	Kimono	Kimono
Configuration	A	A
m_f (kg)	1.0	1.0
T_1 (°C)	40	40
T_2 (°C)	90	90
$G_{n,av}$ (W/m^2)	862.37	779.02
$G_{bn,av}$ (W/m^2)	814.75	638.66
$T_{amb,av}$ (°C)	27.24	19.81
Δt_h (h)	1.09	2.26
η_{av}	0.12	0.06
F_2	0.20	0.13
COR (°C/(W/m^2))	0.092	0.101

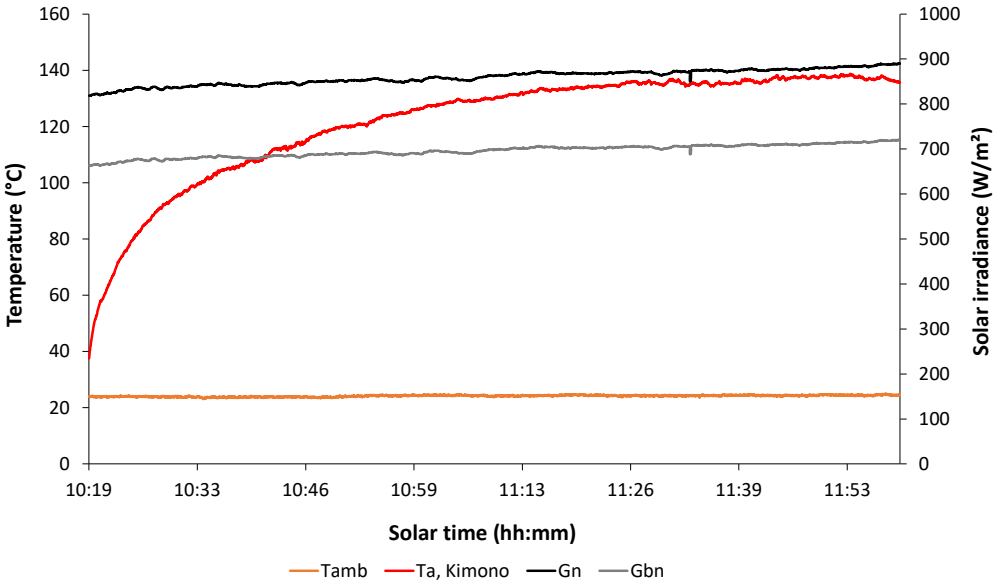

Figure 5.22: Tests without load (18/09/2020, test 1).

Table 5.10: Summary of the tests without load of the second set of tests for the Kimono solar cooker.

Quantity	Test 6	Test 7	Test 8
Date	29/03/2021	01/04/2021	28/04/2022
Type of cooker	Kimono	Kimono	Kimono
Configuration	A	A	A
T_{amb} (°C)	18.23	23.21	15.98
G_n (W/m^2)	926.52	996.92	983.79
G_{bn} (W/m^2)	805.47	902.17	920.30
$T_{a,max}$ (°C)	122.59	133.77	131.00
F_1 (°C/(W/m^2))	0.113	0.111	0.117

solar cooker.

As an example, Figure 5.24 shows the ambient and the absorber temperatures and the variation of the solar irradiances detected during the test of 01/04/2021 (test 7). The Kimono, also in this second set of measure was able to reach a very high absorber temperature equal to 133.77 °C.

Table 5.11 shows a summary of the two tests carried out by loading the receiver with 1 kg of water. Figure 5.25 shows the trend of the fluid temperature inside the Kimono and the solar irradiances recorded during the test on 24/03/2021 (test 9). The average $G_{n,av}$ and $T_{amb,av}$ recorded during the test were 1008.68 W/m^2 and 11.88 °C, respectively.

In this second set of measure, water took more than 2 hours to go from 40 to 90 °C: the time required for the fluid to reach 90 °C was 2.21 h and 2.12 h for test 9 and test 10, respectively.

From Table 5.11 and Figure 5.25, the following considerations can be made:

- Unlike the first set of measures, in this second set it was more difficult to carry out satisfactory tests due to the variable weather conditions recorded during the

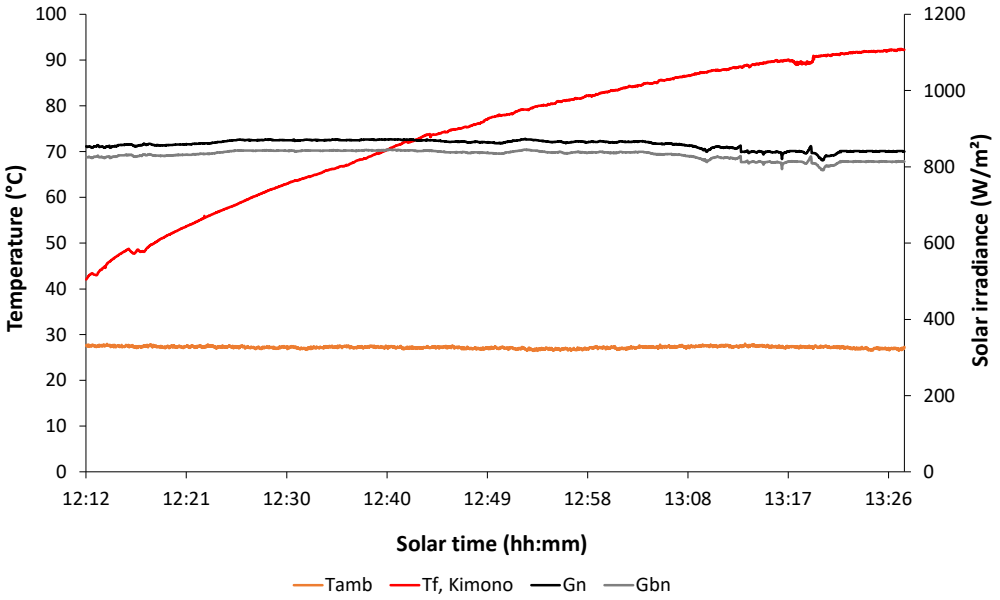

Figure 5.23: Tests with water (24/09/2020, test 4).

months of March and April in Ancona. In fact, some days were very cold and windy.

- Test 9 was characterized by a very low average ambient temperature equal to 11.88 °C, but also by a very high global normal solar irradiance of about 1008.68 W/m^2, which remained almost unchanged throughout the test (Figure 5.25). These external environmental conditions during the test allowed the Kimono to bring water to its boiling point in a relatively short time.

- The time required by water to reach 90 °C for the Kimono was similar in the two tests, although test 10 registered a higher ambient temperature.

Table 5.11: Summary of the water load tests of the second set of tests for the Kimono solar cooker.

Quantity	Test 9	Test 10
Date	24/03/2021	26/04/2022
Type of cooker	Kimono	Kimono
Configuration	A	A
m_f (kg)	1.0	1.0
T_1 (°C)	40	40
T_2 (°C)	90	90
$G_{n,av}$ (W/m^2)	1008.68	1005.76
$G_{bn,av}$ (W/m^2)	911.11	889.38
$T_{amb,av}$ (°C)	11.88	19.26
Δt_h (h)	2.21	2.12
η_{av}	0.05	0.05
F_2	0.10	0.09
COR (°C/(W/m^2))	0.081	0.071

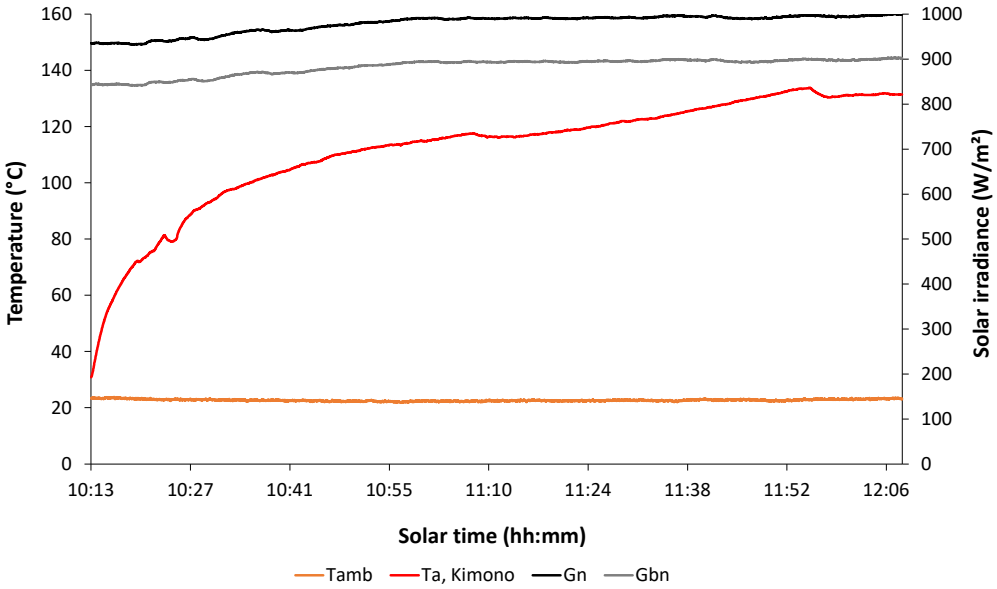

Figure 5.24: Tests without load (01/04/2021, test 7).

Table 5.12: Summary of the tests without load of the third set of tests for the Kimono solar cooker.

Quantity	Test 11	Test 12	Test 13
Date	21/07/2021	22/07/2021	02/08/2021
Type of cooker	Kimono	Kimono	Kimono
Configuration	B	B	B
T_{amb} (°C)	33.06	28.21	27.90
G_n (W/m^2)	947.62	916.51	926.98
G_{bn} (W/m^2)	764.02	748.01	797.58
$T_{a,max}$ (°C)	132.23	141.81	134.93
F_1 (°C/(W/m^2))	0.105	0.124	0.115

Third Set of Tests: No-load Tests and Tests with Water

The experimental tests of the third set of measurements were carried out in July and August 2021. In detail, 3 no-load tests and 2 tests with water were performed. Since this is a period of medium-high sun elevation in Ancona, the configuration of the Kimono for medium-high sun elevations was used during all tests. Consequently, the A_a values of configuration B (reported in Table 5.5) have been employed for the calculation of the performance parameters of the prototype.

Three no-load tests were carried out under different environmental conditions. Table 5.12 shows a summary of the measured quantities.

As an example, Figure 5.26 shows the ambient and the absorber temperatures, and the variation of solar irradiances recorded during the test on 02/08/2021 (test 13). Also in this third set of measures the Kimono device was able to reach high temperatures as evident in Table 5.12: in all three tests the fluid temperature exceeded 130 °C.

The results obtained from the tests using water as test fluid are summarized in Table 5.13. Figure 5.27 shows the trend of water temperature recorded in the Kimono solar cooker, ambient temperature and solar irradiances during the test on 03/08/2021

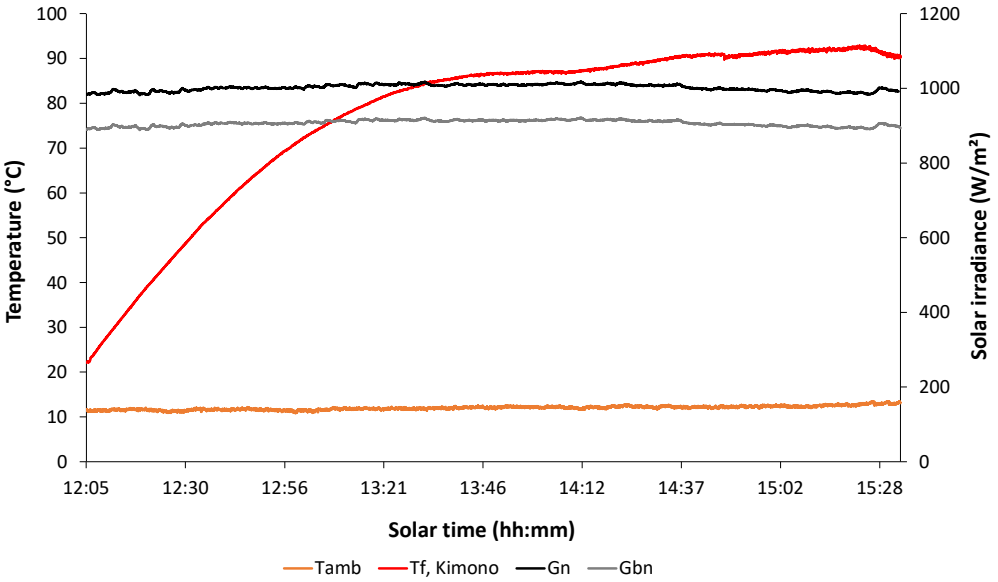

Figure 5.25: Tests with water (24/03/2021, test 9).

(test 14). The average values of $G_{n,av}$ and $T_{amb,av}$ recorded during the test were 945.49 W/m^2 and 28.35 °C, respectively. Water took 1.29 hour to cover the 50 °C temperature range.

In this third set of measurements, it can clearly be seen that the high global normal solar irradiance and the high ambient temperature recorded during the testing period had a positive influence on the success of the tests. In general, in fact, the device, thanks also to the change in its geometry making it suitable for high sun elevations, was able to guarantee water boiling at sea level.

Table 5.13: Summary of the water load tests of the third set of tests for the Kimono solar cooker.

Quantity	Test 14	Test 15
Date	03/08/2021	03/08/2021
Type of cooker	Kimono	Kimono
Configuration	B	B
m_f (kg)	1.0	1.0
T_1 (°C)	40	40
T_2 (°C)	90	90
$G_{n,av}$ (W/m^2)	945.49	917.12
$G_{bn,av}$ (W/m^2)	844.78	829.05
$T_{amb,av}$ (°C)	28.35	29.10
Δt_h (h)	1.29	1.84
η_{av}	0.09	0.06
F_2	0.14	0.10
COR (°C/(W/m^2))	0.080	0.080

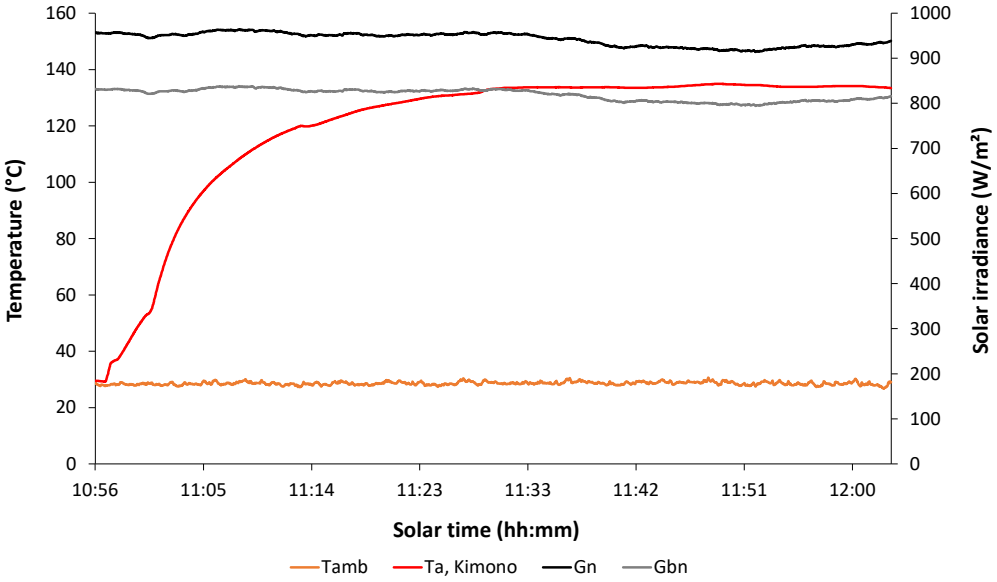

Figure 5.26: Tests without load (02/08/2021, test 13).

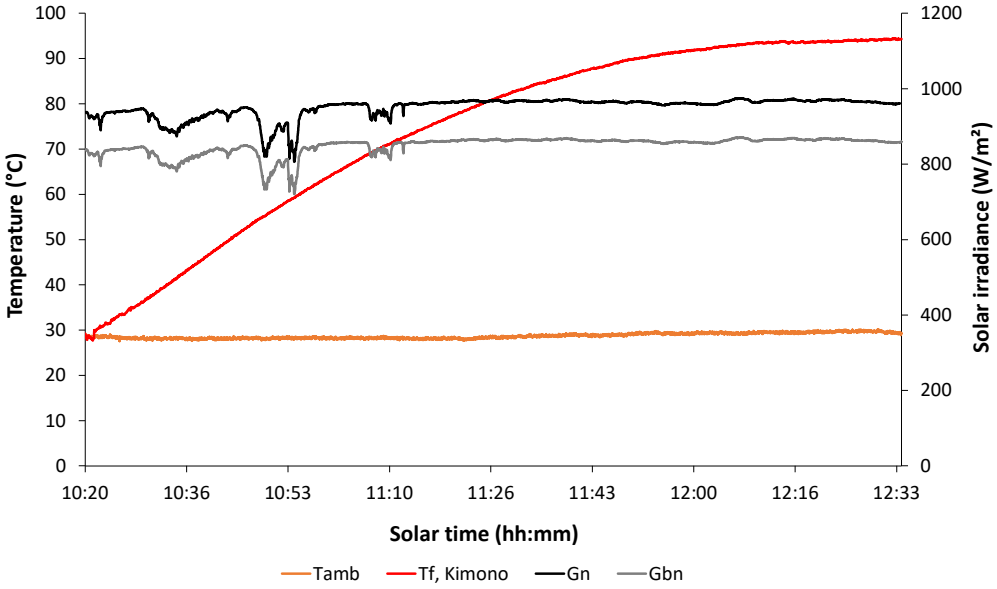

Figure 5.27: Tests with water (03/08/2021, test 14).

Chapter 6

Portable Solar Box Cooker Prototype: Realisation, Manufacture and Test

The prototype to be presented in this chapter falls into the category of solar box cookers. As with its predecessors, this device was built and tested in the DIISM laboratories. The prototype, based on a design found in the literature, was modified to improve the elements that have the greatest impact on its final optical and thermal efficiency: the mirror system, the absorbing paint and the insulating layer.

The characteristics as well as all the construction phases of the device are reported in detail along with the test bench used to carry out the experimental campaign necessary to characterize the cooker.

No-load and load tests were carried out using two different test fluids: water and silicone oil respectively. The device was also tested by inserting a thermal energy storage system based on phase change materials in the cooking chamber. All the results obtained from the experimental campaign will be reported, bringing to the reader's attention especially those obtained in terms of extending the fluid cooling time due to the latent contribution of PCMs.

6.1 Solar Box Cookers with TESs in Literature

In this section a brief review of the literature on solar box cookers equipped with TES systems will be given.

In the work by Ramadan et al. [42], a cheap flat-plate solar cooker was tested with sand and barium hydroxide octahydrate (respectively, a sensible and a PCM thermal storage). The two materials were used as external envelope of the cooking pot. The authors reported a PCM melting point of 78 °C, suitable to cook meat, but also issues like chemical decomposition and supercooling.

Hussein et al. [78] designed and manufactured a thermal storage with magnesium-nitrate-hexahydrate. The storage was coupled with an elliptical indirect solar cooker, and the researchers showed that food could be kept hot even in absence of solar radiation.

El-Sebaii et al. [79] analyzed how two substances, magnesium chloride hexahydrate and acetanilide, behaved under several thermal cycles. The two PCMs were also

inserted in different materials (aluminum and stainless steel), in order to verify their compatibility. Acetanilide proved to have adequate thermal stability and compatibility with aluminum, while magnesium chloride hexahydrate resulted to be not stable and compatible with the two materials.

Buddhi et al. [211] designed and developed a PCM storage unit to be used with a solar cooker to store energy during daytime. The authors used 4 kg of commercial grade acetanilide with a melting point of 118.9 °C and latent heat of fusion of 222 kJ/kg. Evening cooking experiments were conducted with different loads and loading times during the winter months of December and February. The stored energy was utilized to cook food (water and rice) and the experimental results showed that late evening cooking is feasible.

Acetanilide was also used by Chaudhary et al. [39]. The authors investigated the performance of a solar cooker based on a parabolic dish collector with a PCM storage unit. In the experimental campaign, three cases were considered: an ordinary solar cooker, a solar cooker with the external surface painted black, and a setup with glazing. It was observed that the last configuration performs better than the first two. In addition, the PCM stored 26.8% more thermal energy when the solar cooker was equipped with the outer surface painted black, while the configuration with the surfaces painted black and glazing stored 32.3% more thermal energy when compared to the PCM performance with the ordinary solar cooker.

Sharma et al. [212] built a thermal energy storage made of two concentric aluminum cylinders with the annulus filled with acetamide. This system was introduced in a solar cooker and experimental tests carried out under different conditions showed that this device can enable cooking during evening hours.

Abu-Hamdeh and Alnefaie [80] constructed small cylindrical aluminum capsules used as PCM storage units in a solar stove. The capsules, placed in the receiver of a parabolic reflector, were tested during sunny days. The absorbed heat was stored as latent heat in the PCM, which was commercial-grade acetamide. The authors analyzed the thermal performance of the system at three air flow rates. The results provided significant information for the design of a solar stove prototype equipped with a PCM, and established that acetamide is a promising substance in this kind of solar applications.

Nandwani et al. [213] designed and tested a solar box cooker composed of a wooden box insulated with glass wool and surmounted by a double glass at the top. The authors compared the behavior of a metal plate filled with PCM, used as a tray, with a normal plate. The selected PCM was a high-density polyethylene, Vestolen A6016. The maximum recorded temperature variation of the plate was 25 °C in the case of the normal tray and 10 °C in the case of the storage plate, during the same period and without cooking load.

Domanski et al. [214] investigated the performance of two concentric pots mounted to form a double-wall aluminum cooking vessel filled with stearic acid and magnesium nitrate hexahydrate. The experimental tests, carried out under different outdoor conditions, proved the solar cooker efficiency to be three to four times higher than that of solar cookers not equipped with the PCM.

Stearic acid was also used by Buddhi and Sahoo [215] as PCM to be inserted in a solar box cooker. In this preliminary study, the substance was confined between two trays made of aluminum, with one of the trays supporting the cooking vessel. Results showed that it was possible to cook food in the evening, and at a nearly constant temperature.

Keith et al. [81] proposed an alternative solution to the use of firewood for cooking

food by refugees through a solar energy-based cooking. The proposed solar cooker was a collapsible parabolic system with 12 panels and a thermal energy storage composed by a double pot filled with stearic acid. The authors conducted several tests and three types of grains mixed with some vegetables were used as representative cooking ingredients: rice, lentils and pearled barley. In addition, a cost-benefit analysis of the solution was presented and the results showed that the payback period is 52 weeks or less if the device is used by a family unit of four members.

Foong et al. [216] tested a small-scale double-reflector solar concentrating system with heat storage. The objective of the work was to develop a system with a high temperature storage which can charge a PCM thermal storage unit during the day and use it in the night for cooking purposes. The authors demonstrated that, with that arrangement, the insulated storage was heated directly and no heat transport fluid was needed in the final system. The chosen PCM was a binary mixture composed by $NaNO_3$ and KNO_3 in 60:40 percent ratio, with a melting temperature of about 220 °C. The authors carried out several outdoor tests and the experimental results demonstrated that the melting temperature of PCM occurred within 2–2.5 hours and reached the temperature range of 230–260 °C.

Bhave and Kale [82] designed and tested a device able to store latent heat in a solar salt mixture, which enables its storage in an insulated container, and cooking in the shade of a kitchen when needed. The PCM was an eutectic mixture composed by $NaNO_3$ and KNO_3 in 60:40 percent ratio, with a melting point of 220 °C. The authors easily obtained a temperature of 170–180 °C for the oil during the indoor cooking, and the frying of chips and the cooking of rice was possible in 17 and 20 minutes, respectively.

Coccia et al. [83] designed and characterized a TES composed of two pots, with different diameter, inserted one inside the other. The annulus created by the two pots was filled with 4 kg of a solar salt ternary mixture constituted by 53 wt% KNO_3, 40 wt% $NaNO_2$, and 7 wt% $NaNO_3$. The TES was then introduced into a 10.78 concentration ratio solar box cooker [1], in order to study the system performance. Thanks to numerous outdoor tests and using different test fluids, the authors discovered that when the cooker was loaded with the solar-salt-based TES, the thermal load stabilization in absence of solar radiation was greatly improved. In fact, the load cooling time in the temperature range between 170–130 °C was, on average, 88.58% higher than that registered in the tests without TES.

The performance of an evacuated tube solar collector (ETC) equipped with an erythritol-based TES used for cooking was studied by Sharma et al. [38]. The authors found that, thanks to the thermal energy storage, evening cooking was faster than noon cooking.

An innovative layout for a portable solar cooker that incorporates a daily thermal storage utensil was studied by Lecuona et al. [85]. The storage utensil was composed by two conventional coaxial cylindrical pots with different diameters, and the space between the pots was filled with a phase change material. The authors tested the system with two different PCMs: technical grade paraffin and erythritol. A numerical model with convective heat transfer correlations was used to study the transient behavior of the storage utensil for the climatic conditions of Madrid, and validated with experimental data. The obtained results indicate that cooking three meals for a family is possible simultaneously with the heat storage both in summertime as well as in wintertime. The utensil, left inside an insulating box, allows to cook dinner and breakfast of the next day with the retained heat.

Table 6.1: Geometrical dimensions and thermo-optical properties of the solar box cooker.

Quantity	Value
Mass (kg)	20.1
Aperture area, A_a (m^2)	0.681
Glass cover area, A_g (m^2)	0.167
Concentration ratio, C	4.08
Maximum height (m)	0.75
Number of mirrors	8
Inclination angles of square mirrors (°)	63.43
Inclination angles of wedge-shape mirrors (°)	56.98
Mirror solar reflectance	0.94
Glass cover solar transmittance	0.90
Black coating solar absorptance	0.90

6.2 Design and Optical Analysis

The solar box cooker presented in this work is a prototype based on a design developed by Eng. Gianni Crovatto [217]. On his website, it is possible to find numerous solar cooker prototypes, as mentioned in Chapter 3, classified according to their efficiency. In this case, it was decided to realize and test a medium-efficiency solar cooker, and the construction diagrams and tables of Eng. Crovatto's medium-efficiency prototype were therefore followed.

The resulting solar box cooker, called portable both because of its small size and the lightweight material used in its construction is shown in Figure 6.1 and Figure 6.2. The prototype is composed by a wooden box containing a zinc-coated steel frame with the function of cooking chamber. The box has a glass cover on the top, which allows solar radiation to be transmitted to the cooking chamber. The glass cover can be easily removed to allow loading of vessels. The higher part of the box is surrounded by 8 booster mirrors that allow an additional amount of solar radiation to be reflected and concentrated towards the cover and the cooking chamber. Thanks to the Figure 6.2, it is possible to see the dimensions of the various cooker elements and the inclinations of the mirror systems.

The cooker aperture area, A_a, is equal to $0.681\,m^2$, while the glass cover area, A_g, is $0.167\,m^2$. Thus, the cooker concentration ratio is:

$$C = \frac{A_a}{A_g} = 4.08 \tag{6.1}$$

Additionally, the prototype has two border wooden hands that allow both its handling and its azimuthal orientation. A zenithal orientation is also possible as the cooker is able to rotate around the horizontal axis via a bolt moving into a runner. This rotation can be blocked with an external butterfly screw.

The cooker prototype has a maximum height of 75 cm and a mass of about 20 kg. Table 6.1 summarizes the main geometrical dimensions and thermo-optical properties of the portable solar box cooker.

6.3 Manufacture and Materials

The cooker manufacturing process consisted of 4 consecutive phases:

Figure 6.1: A photo of the portable solar box cooker prototype.

1. cooking chamber realization and painting;

2. external structure realization;

3. insulation with glass wool;

4. realization of the booster mirror system.

6.3.1 Cooking Chamber Realization and Painting

The first manufacturing process involved the cooking chamber. Its walls were obtained starting from a stainless steel sheet 6/10 mm thick. Following the instructions reported in Eng. Crovatto schema [217], the required pieces were cut, folded and finally riveted to form the assembly. All joints have been secured with a high temperature and non-toxic sealant such as that used in commercial ovens (Figure 6.3).

A tilting support is placed inside the cooking chamber: the purpose of this element is to keep the vessels steady when the solar box cooker is being rotated, and is made from a stainless-steel sheet. The cooking chamber was painted with a selective black coating (SOLKOTE HI/SORB-II) typically involved in more advanced solar thermal systems such as parabolic trough collectors. This paint, apart from increasing the amount of absorbed solar radiation, protects the metal parts from oxidation. With respect to a common black paint, this selective coating shows a solar absorptance factor of about 90%, while its emissivity ranges from 0.20 to 0.49 depending on the thickness. Figure 6.4 shows the painted cooking chamber and the tilting support.

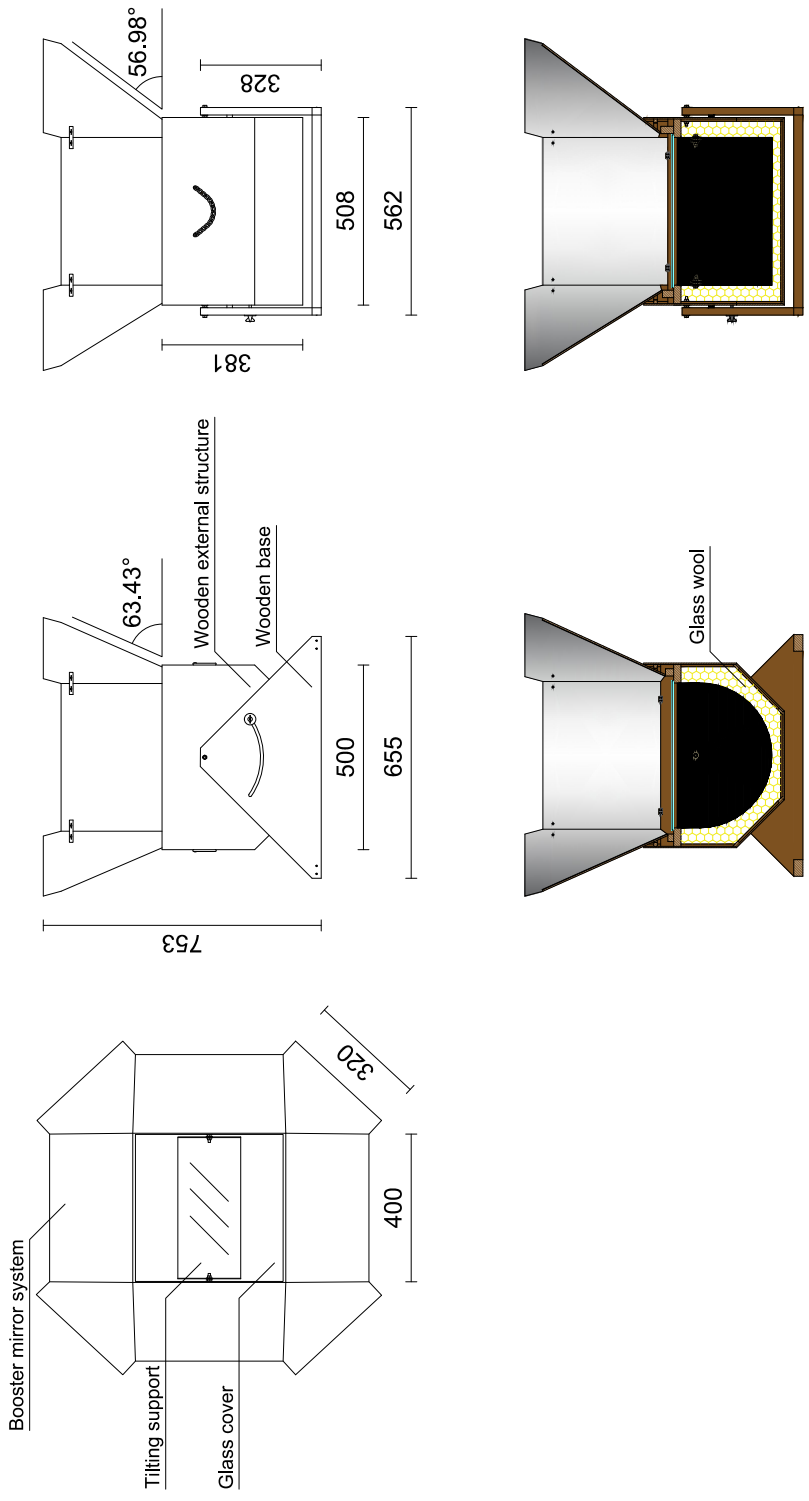

Figure 6.2: Views and cross-sections of the portable solar box cooker [5, 6].

Figure 6.3: Cooking chamber of the prototype.

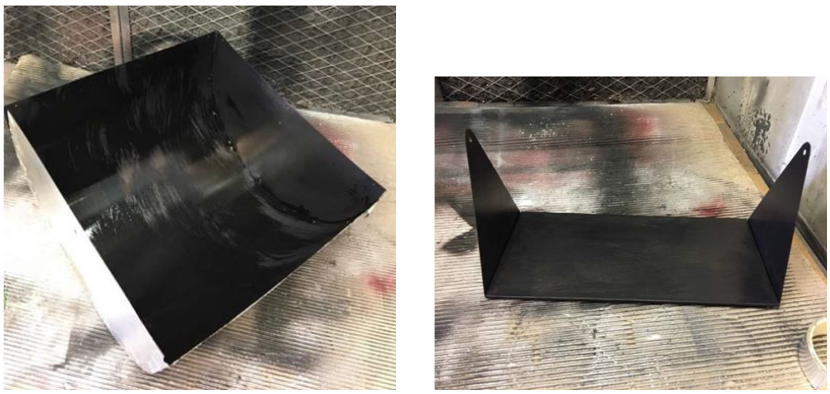

Figure 6.4: Painted cooking chamber and tilting support.

6.3.2 External Structure Realization

The external structure was realized with medium-density fiberboards (MDFs) 0.7 mm thick. In order to make the external MDF structure more stable and resistant, reinforcement fir laths were applied inside the inner cavity (Figure 6.5). The prototype was also equipped with handles for ease of movement. More robust wooden panels were used to build the base of the cooker and the locking system for its zenithal rotation. Finally, the cooking chamber was placed inside the external structure (Figure 6.6). Correct alignment was guaranteed by fir spacers. A cover made of tempered glass (transmittance factor of about 90%) was placed on the upper part of the box to allow both solar radiation transmittance and the loading/unloading of the vessels.

6.3.3 Insulation with Glass Wool

To obtain higher operating temperatures it was necessary to thermally insulate the cooking chamber. It was insulated by means of layers and flakes of glass wool inserted in the cavity between the cooking chamber and the external MDF structure (Figure 6.7). To prevent moisture from damaging the wood panels, a protective coating

Figure 6.5: External structure with base.

was applied on all the MDF elements.

6.3.4 Realization of the Booster Mirror System

The booster mirror system was composed of 8 reflective panels. Each panel consisted of a wooden support on which an aluminum foil was glued. 4 panels are square-shaped and attached to the box with hinges, while the remaining 4 are wedge-shaped and inserted between the square-shaped ones (Figure 6.8). In this way, the booster mirror system assumes a funnel-type shape (Figure 6.9). The reflective foils used for the mirrors (MIRO-SUN Weatherproof Reflective 90) are able to withstand atmospheric agents and guarantee an overall solar reflectance of about 94%.

6.4 Phase Change Materials

The PCMs selected in this study were erythritol and xylitol, both sugar polyalcohols that belong to the organic material family. The two materials were chosen not only for the fact that they are natural substances extracted mainly from fruit and vegetables and therefore suitable for solar cooking applications because they are edible and non-toxic, but also for their melting temperature. In detail, the latter temperature is in the range 100–120 °C for erythritol and 90–95 °C for xylitol, guaranteeing an optimal coupling with the solar cooker studied, which is capable of reaching temperatures in the order of 200 °C.

Both phase change materials considered in this experimental campaign are commercial-grade. In order to evaluate the sample quality of erythritol, the sugar was analyzed using a Fourier Transform Infrared (FTIR) spectrometer (Spectrum GX I, Perkin Elmer). Spectra were acquired in reflection, using an attenuated total reflectance (ATR) crystal (DuraSampl IR II, SensIR Technologies) with a spectral resolution of $4\,\mathrm{cm}^{-1}$ from 4000 to $650\,\mathrm{cm}^{-1}$. Each spectrum is the result of 16 consecutive scans. The results of the analysis shown that despite being a commercial-grade substance, the erythritol sample considered in the experiment does not contain relevant amounts of other components.

The two commercial-grade PCMs were also tested in the microlaboratory at the WiB institute with a differential scanning calorimeter (DSC) to evaluate their melting

Figure 6.6: Cooking chamber built into the external wooden structure.

Figure 6.7: Glass wool layers and flakes inserted in the cavity of the prototype.

temperatures and latent heats of fusion. Three different samples of erythritol and xylitol were analyzed with a NETZSCH DSC 214 Polyma at a rate of 1 K/min. Figure 6.10 shows the heating/cooling behaviors obtained with the software NETZSCH Proteus 7.0 for one of the samples. It was noted that the melting phase is very repeatable among the three samples. The average melting temperature and latent heat of fusion were calculated to be 108.7 °C and 312.8 kJ/kg for erythritol and 92.2 °C and 227.1 kJ/kg for xylitol, respectively.

For the preparation of the TES the following steps were followed. A mass of about 2.5 kg of erythritol was heated in an electric furnace at a temperature higher than 100 °C for about 2 hours. This operation was repeated a second time and only after these two steps, erythritol was inserted inside the thermal storage system. In this way, the possible presence of moisture in the sample was avoided. Later, the sample was inserted in the TES gap and the whole system was heated in the electric furnace at about 200 °C for 2 hours. With the completion of this process, erythritol was finally ready to be used for experimental testing.

The same methodology was also followed for the preparation of the second PCM.

Figure 6.8: Square and wedge-shaped aluminum mirrors.

A mass of about 2.5 kg of commercial-grade xylitol was heated in a static oven for two hours at over 80 °C. Here again, in order to remove any possible moisture from the substance, the same operation was repeated a second time. Later, the PCM was inserted in the TES cavity and the static oven was used to heat the entire system for two hours at a temperature of 150 °C. After adding the manual device to the xylitol-based TES, additional tests were carried out to check the efficiency of the nucleation triggering device. Results proved that the mechanical agitation allowed the initiation of sample crystallization in a short time and at temperatures close to the xylitol melting temperature.

6.5 Thermal energy storage systems

Two different thermal energy storage (TESs) systems were developed to carry out the tests. Figure 6.11 shows the first TES used with the first chosen PCM. The system consists of two connected cylindrical stainless steel pots. The outer pot has a diameter of 23 cm and was painted with a black coating to increase its solar energy absorption. The inner pot, instead, has a diameter of 19 cm and was filled with the testing fluid (silicone oil). The pots were connected by means of four bolts and the resulting gap was filled with the PCM.

Two K-type thermocouples (T_{PCM1} and T_{PCM2} in Figure 6.11) were located in two opposite stainless steel tubes, to measure the PCM temperature. In this way, the thermocouples were always embedded in the PCM during phase transitions of the material. The testing fluid temperature, instead, was measured through a T-type thermocouple (T_{f} in Figure 6.11) installed in the center of the TES.

Figure 6.12 shows the thermal energy storage (TES) chosen to perform the tests with commercial-grade xylitol: starting from the one used for erythritol, the TES was additionally equipped with a manual device for the mechanical agitation of the sample, with the aim of triggering xylitol nucleation. The device, highlighted in red in Figure 6.12, consists of a C-shaped rod able to rotate on the axis of the T-type

Figure 6.9: Final booster mirror system with a funnel-type shape.

thermocouple support used to measure the temperature of the testing fluid (T_f). Two thin iron wires (with one end connected to the rod and the other end free, outside the cooking chamber) were used to rotate the rod without opening the cooking chamber. Thanks to its simplicity and ease of use, the device can be considered a cost-effective solution that can be easily implemented in TESs used for solar cookers.

6.6 Experimental Tests and Setup

In this section, the types of tests performed, the test fluids chosen and the experimental setup used during the experimental campaign, together with the experimental parameters calculated to characterize the device, are described.

6.6.1 Experimental Tests

Outdoor tests were conducted from May to October during the years 2017, 2018, and 2019 and on May 2021 on the DIISM roof (latitude 43.5867 N, longitude 13.5150 E). To guarantee a proper tracking of the sun, the cooker alignment with the sun was adjusted about every 5–10 minutes.

Three different kinds of test were carried out.

- Tests without load. They allowed to reach the stagnation condition of the system an so determine the maximum temperature reachable by the solar cooker.

- Tests with load. These tests were carried out by loading the solar cooker with a testing fluid, water or silicone oil. The former fluid was used due to ease of comparison with the results obtained by other authors. The latter fluid (Rhodorsil Oil 47 V 100), instead, was used to exceed the limit of 100 °C that water present. This allowed to study the behavior of the cooker at higher temperatures.

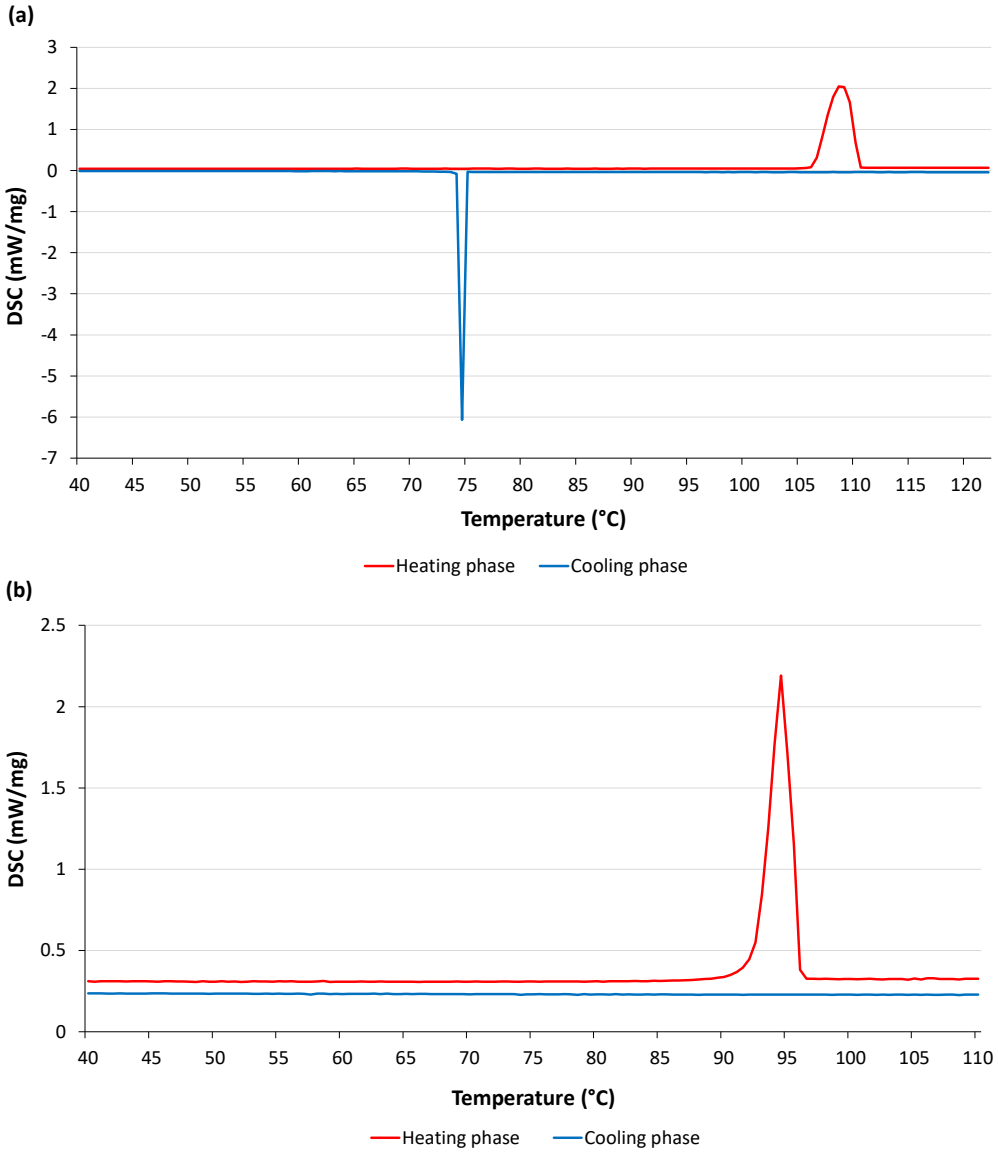

Figure 6.10: DSC analysis of the samples: (a) erythritol and (b) xylitol.

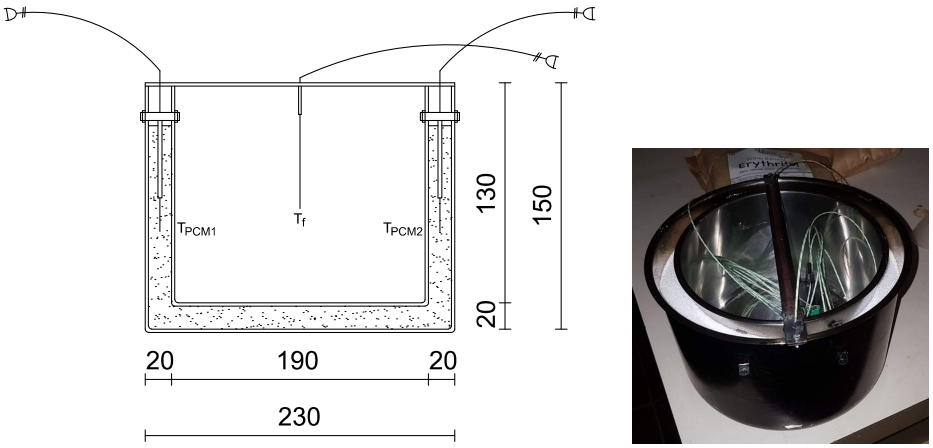

Figure 6.11: Thermal energy storage based on erythritol. T_{PCM1} and T_{PCM2} are two K-type thermocouples used to detect the PCM temperature, while T_{f} is a T-type thermocouple used to detect the testing fluid temperature. On the right a picture of the TES.

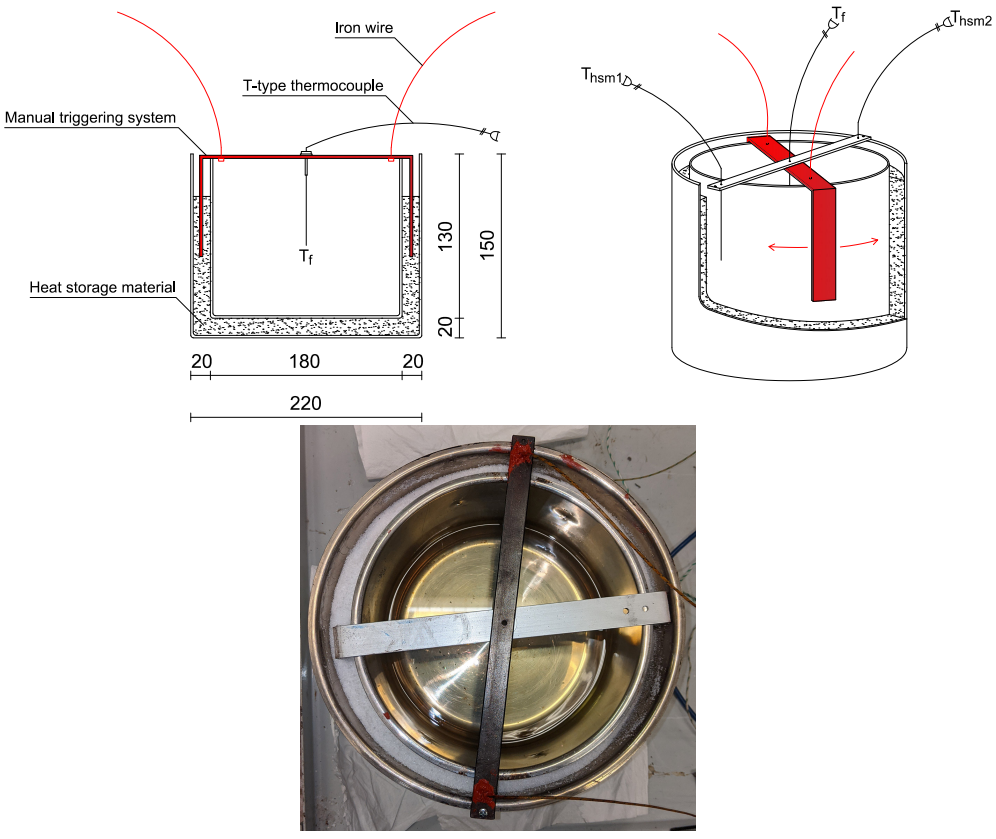

Figure 6.12: Thermal energy storage based on xylitol. The device used for the mechanical agitation of xylitol is drawn in red. Below a picture of the TES.

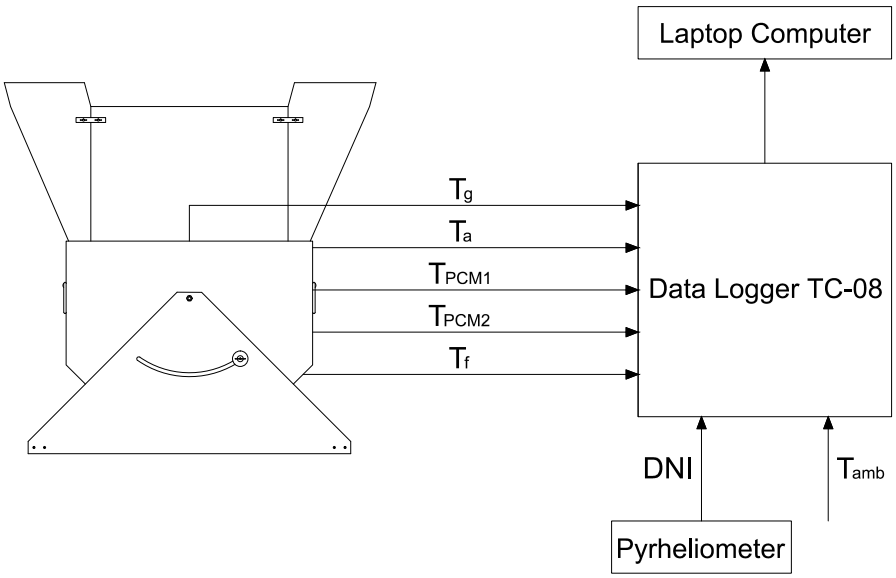

Figure 6.13: Experimental setup. T_{g}: glass temperature; T_{a}: absorber temperature; T_{PCM}: phase change material temperature; T_{f}: testing fluid temperature; T_{amb}: ambient temperature; *DNI*: direct normal irradiance.

- Test with load and thermal storage materials. These tests were carried out by loading the previously described thermal energy storage system containing silicone oil as the test fluid and erythritol or xylitol as the phase change material into the cooking chamber. These tests made it possible to assess the latent contribution that the different PCMs made to the overall system.

6.6.2 Experimental Setup

Figure 6.13 shows the experimental setup used to experimentally characterize the portable solar box cooker. The cooking chamber of the prototype was loaded or with a normal black stainless-steel pot with a diameter of 19 cm containing the fluid to be tested (water or silicone oil) or with the TES systems described in section 6.5 containing the silicone oil and the phase change materials (erythritol or xylitol). The recorded quantities during the tests were the absorber plate temperature T_{a}, the fluid temperature T_{f}, the ambient temperature T_{amb}, the glass temperature T_{g}, the PCM temperature T_{PCM}, and the direct normal solar irradiance *DNI*. The sensors used to detect the first three temperature were T-type thermocouples while for the remaining temperatures were used K-type thermocouples.

An Eppley NIP (Normal Incidence Pyrheliometer) was used to measure direct normal irradiance (*DNI*). Diffuse solar radiation was not taken into account in the present experiment as the considered solar box cooker has a concentration ratio of 4.08, thus it can basically work with direct solar radiation only.

The signals generated by the thermocouples and the pyrheliometer were acquired and processed by a Pico Technology TC-08 data logger, connected to a laptop computer.

For more information on instrument uncertainties please refer to the Appendix B.

6.6.3 Experimental Parameters

Table 6.2 reports the parameters that were used for the characterization of the solar box cooker oupled with the PCM-based TES. Although these parameters consider water as testing fluid, in the present work they were adapted to allow their use also in the case of silicone oil.

Additional information regarding the international procedures followed in these experimental campaigns are reported in the Appendix A.

As mentioned in section 6.6.1, the first tests carried out during the experimental campaign were no-load tests in order to determine the maximum temperature ($T_{\mathrm{a,max}}$) attainable by the device under investigation and its first figure of merit, F_1.

Tests with load, instead, were divided into two phases: an initial heating phase and a following cooling phase. The heating phase simulated the system behavior in presence of solar radiation. In this case, the parameters t_{s}, t_{ch}, η_{av} and F_1 were calculated in a time range Δt_{h}, the time required by the solar cooker to take water and silicone oil from $T_1 = 40$ to $T_2 = 90\,^{\circ}\mathrm{C}$, and from $T_1 = 55$ to $T_2 = 125\,^{\circ}\mathrm{C}$, respectively. The temperature range chosen for the silicone oil allowed to include the phase change of erythritol, that for the sample under consideration occurred at about $109\,^{\circ}\mathrm{C}$.

The cooling phase, instead, was introduced to simulate absence of solar radiation. During this phase, the solar cooker was shaded and the time Δt_{c} required by the silicone oil to reduce its temperature from $T_2 = 125\,^{\circ}\mathrm{C}$ to $T_3 = 100\,^{\circ}\mathrm{C}$ was recorded.

The tests with silicone oil were subsequently re-elaborated by calculating the various parameters for the heating phase in a fluid temperature range from $T_1 = 55$ to $T_2 = 110\,^{\circ}\mathrm{C}$. The temperature range chosen for the silicone oil in this second case considered the phase transition of xylitol (T_{melting} equal to $92.2\,^{\circ}\mathrm{C}$).

The cooling phase for this second elaboration of the silicone oil tests was calculated in a fluid temperature range from $T_2 = 110$ to $T_3 = 80\,^{\circ}\mathrm{C}$.

6.7 Experimental Results

All results obtained from the no-load and load tests will be described in detail. The results of the load tests will be divided into those with water, silicone oil and silicone oil with the TESs based on phase change materials.

6.7.1 Tests Without Load

Three tests without load were carried out under different environmental conditions. Table 6.3 shown a summary of the data collected for each test.

As an example, Figure 6.14 shows the temperatures and the solar radiation detected during the test carried out on 13/06/2017 (Test 3). The maximum absorber temperature was about $189\,^{\circ}\mathrm{C}$ and the corresponding solar radiation and ambient temperature were $841\,\mathrm{W/m^2}$ and $31.27\,^{\circ}\mathrm{C}$, respectively.

The three F_1 values (Table 6.3) were then averaged, resulting in an average $F_1 = 0.19\,^{\circ}\mathrm{C}/(\mathrm{W/m^2})$. This value represents the first figure of merit of the solar box cooker under study.

6.7.2 Tests with Water

Table 6.4 shown a summary of the 5 outdoor tests carried out with water. As explained in the section 6.6.3 all the experimental parameters contained in the Table 6.4

Table 6.2: Experimental parameters for the assessment of the solar cooker performance.

Experimental parameter	Equation/Formulation	Equation parameters
First figure of merit [19]	$F_1 = \frac{T_{\mathrm{a,max}} - T_{\mathrm{amb}}}{DNI}$ (°C/(W/m^2))	A_{a} = aperture area of the solar cooker (m^2) c_{f} = specific heat of the test fluid (J/(kg K)) DNI = direct normal irradiance (W/m^2) DNI_{av} = mean DNI measured at Δt_{h} (W/m^2) $DNI_{\mathrm{ref}} = 900\,\mathrm{W/m^2}$ m_{f} = mass of the test fluid (kg) T_{amb} = ambient temperature (°C) $T_{\mathrm{a,max}}$ = absorber stagnation temperature (°C) $T_{\mathrm{amb,av}}$ = mean T_{amb} measured at Δt_{h} (°C) $t(T_1)$ = starting time of the heating phase (h) $t(T_2)$ = ending/starting time of the heating/cooling phase (h) $t(T_3)$ = ending time of the cooling phase (h)
Heating time interval	$\Delta t_{\mathrm{h}} = t(T_2) - t(T_1)$ (h)	
Second figure of merit [19]	$F_2 = \frac{F_1 m_{\mathrm{f}}\, c_{\mathrm{f}}}{A_{\mathrm{a}} \Delta t_{\mathrm{h}}} \ln \left[\frac{1 - \frac{1}{F_1}(T_1 - T_{\mathrm{amb,av}})/DNI_{\mathrm{av}}}{1 - \frac{1}{F_1}(T_2 - T_{\mathrm{amb,av}})/DNI_{\mathrm{av}}} \right]$	
Specific boiling time [172]	$t_{\mathrm{s}} = \frac{\Delta t_{\mathrm{h}} A_{\mathrm{a}}}{m_{\mathrm{f}}}$ (h m^2/kg)	
Characteristic boiling time [172]	$t_{\mathrm{ch}} = t_{\mathrm{s}} \frac{DNI_{\mathrm{av}}}{DNI_{\mathrm{ref}}}$ (h m^2/kg)	
Overall thermal efficiency [172]	$\eta_{\mathrm{av}} = \frac{m_{\mathrm{f}}\, c_{\mathrm{f}} (T_2 - T_1)}{DNI_{\mathrm{av}} A_{\mathrm{a}} \Delta t_{\mathrm{h}}}$	
Cooling time interval	$\Delta t_{\mathrm{c}} = t(T_2) - t(T_3)$ (h)	

Table 6.3: Summary of tests without load.

Quantity	Test 1	Test 2	Test 3
Date	23/05/2017	09/06/2017	13/06/2017
T_{amb} (°C)	29.39	23.39	31.27
DNI (W/m^2)	839.71	971.75	841.24
$T_{\text{a,max}}$ (°C)	197.30	187.42	189.10
F_1 (°C/(W/m^2))	0.20	0.17	0.19

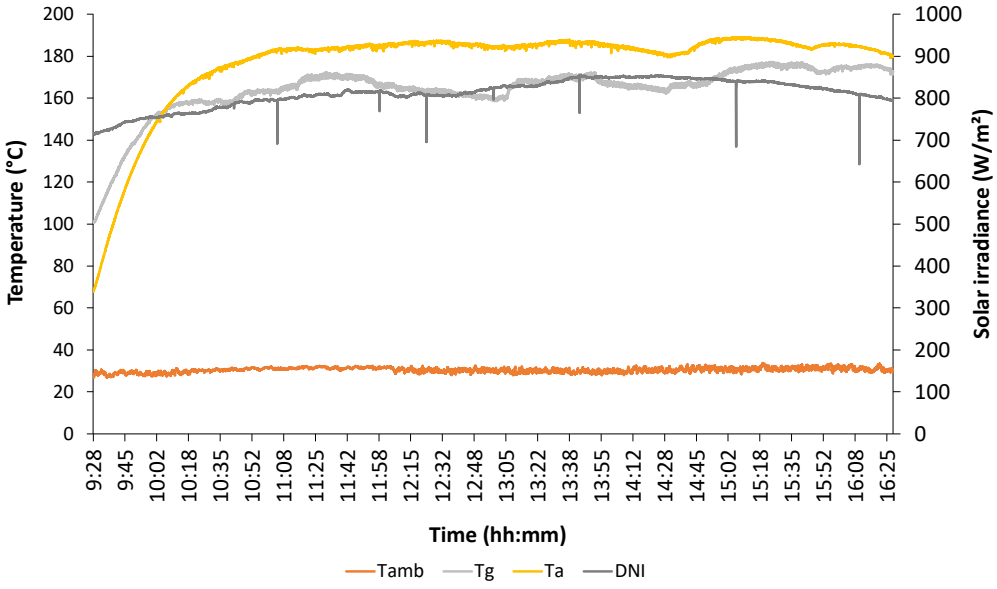

Figure 6.14: Test without load (13/06/2017, Test 3).

Table 6.4: Summary of tests with water.

Quantity	Test 4	Test 5	Test 6	Test 7	Test 8
Date	02/08/2017	14/09/2017	01/06/2018	20/06/2018	04/07/2018
m_f (kg)	2.0	2.0	3.0	3.0	3.0
T_1 (°C)	40	40	40	40	40
T_2 (°C)	90	90	90	90	90
DNI_{av} (W/m^2)	736.84	867.18	869.28	825.54	597.10
$T_{amb,av}$ (°C)	36.59	25.00	27.23	28.29	27.88
Δt_h (h)	1.45	1.68	1.20	1.44	1.77
t_s (h m^2/kg)	0.49	0.57	0.27	0.33	0.40
t_{ch} (h m^2/kg)	0.40	0.55	0.26	0.30	0.27
η_{av}	0.16	0.12	0.25	0.22	0.24
F_2	0.09	0.07	0.14	0.12	0.16

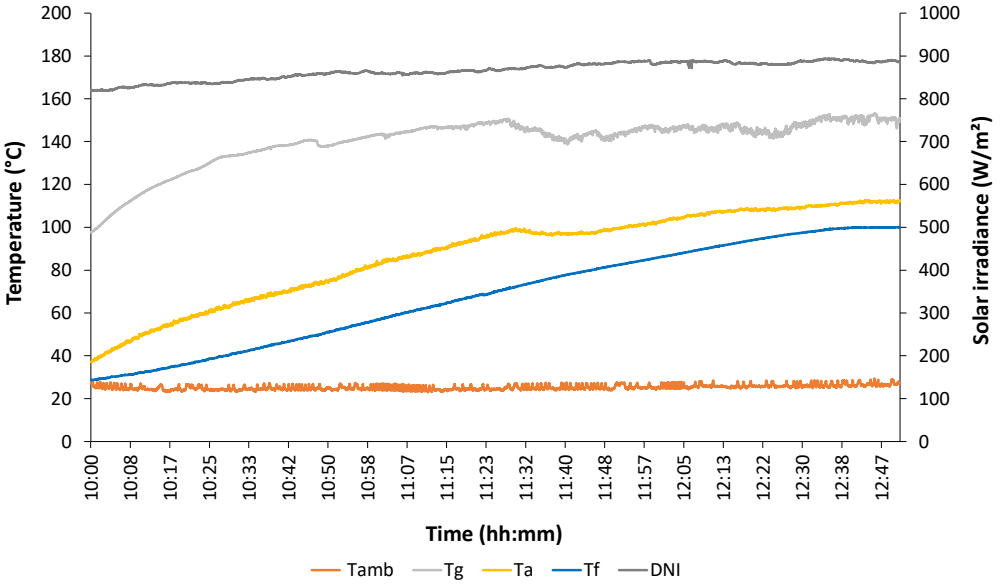

Figure 6.15: Tests with water (14/09/2017, Test 5).

are referred to a time interval Δt_h during which water temperature rose from 40 to 90 °C. Tests were conducted with two different masses of water, 2 and 3 kg.

Figure 6.15 depicts the load test carried out on September 14th, 2017 (Test 5 in Table 6.4) loading the solar cooker with 2 kg of water. The average direct normal irradiance was 867.18 W/m^2 and the average ambient temperature was 25 °C during the Δt_h interval. Water took about 1.68 hours to heat up in the range 40–90 °C. Tests conducted on different days showed similar trends. Referring again to Table 6.4, it is possible to note that a larger mass of testing fluid positively influenced the second figure of merit and the average thermal efficiency of the solar box cooker. This effect is well-known in literature [174] and can be explained by considering that larger masses and volumes of vessels allow to use the cooking chamber in a more efficient way.

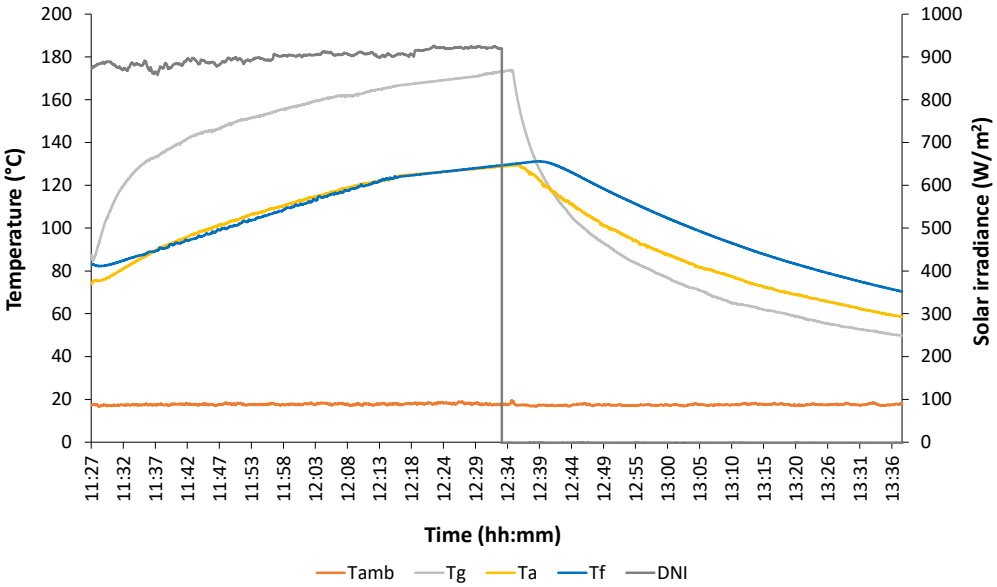

Figure 6.16: Test with silicone oil (27/09/2018, Test 10).

6.7.3 Tests with Silicone Oil

Five tests (tests 9 to 13) were performed using the cooker loaded with 1.5 kg of silicone oil. As explained in section 6.6.3, the tests with silicone oil were divided into two phases and the results are presented in Table 6.5 and 6.6. The first two tests were conducted in June and September 2018, while the remaining three were conducted in June 2019.

Figure 6.16 shows, for instance, the temperatures and the direct normal irradiance detected on September 27$^{\text{th}}$, 2018. During the period considered, DNI_{av} was 882.77 W/m^2 and $T_{\text{amb,av}}$ was 17.35 °C. It is possible to note that the test is divided into an initial heating phase and a following cooling phase. The former phase took about 1.58 hours to take the silicone oil temperature from 55 °C to 125 °C. The cooker average efficiency and its second figure of merit were lower than those determined with water, as silicone oil was tested at higher temperatures.

When the silicone oil temperature was higher than 130 °C, the solar cooker was closed to solar radiation and left cooling down. During the cooling phase, the average ambient temperature was 17.35 °C and the silicone oil required 0.31 hours to take its temperature from 125 to 100 °C (Table 6.6).

6.7.4 Test with Silicone Oil and Erythritol

Four tests were carry out in the months of July and September 2018 to study the behavior of the solar box cooker coupled with the PCM-based thermal storage unit. The thermal storage system, including 2.5 kg of erythritol, was filled with 1.5 kg of silicone oil. The results of the experimental tests are summarized in Table 6.5 and 6.6 (tests 14 to 17), which refer to the heating phase and the cooling phase, respectively.

Figure 6.17 shows the results obtained on September 25$^{\text{th}}$, when DNI_{av} was 946.62 W/m^2 and $T_{\text{amb,av}}$ was 19.33 °C. From Figure 6.17, it is possible to note that the PCM temperatures measured by the two opposite thermocouples are almost the

Table 6.5: Summary of the heating tests with silicone oil and silicone oil + erythritol.

Quantity	Test 9	Test 10	Test 11	Test 12	Test 13	Test 14	Test 15	Test 16	Test 17
Date	11/06/2018	27/09/2018	11/06/2019	12/06/2019	17/06/2019	24/07/2018	11/09/2018	12/09/2018	25/09/2018
m_f (kg)	1.5	1.5	1.5	1.5	1.5	1.5	1.5	1.5	1.5
m_PCM (kg)	-	-	-	-	-	2.5	2.5	2.5	2.5
T_1 (°C)	55	55	55	55	55	55	55	55	55
T_2 (°C)	125	125	125	125	125	125	125	125	125
DNI_av (W/m^2)	767.22	882.77	720.04	601.80	751.80	834.99	855.53	867.96	946.62
$T_\mathrm{amb,av}$ (°C)	31.38	17.35	30.35	28.15	28.83	28.62	26.70	28.14	19.33
Δt_h (h)	1.11	1.58	1.27	1.01	0.95	1.94	2.30	3.35	2.52
t_s (h m^2/kg)	0.50	0.72	0.57	0.46	0.43	0.88	1.04	1.52	1.14
t_ch (h m^2/kg)	0.43	0.71	0.46	0.31	0.36	0.82	0.99	1.47	1.20
η_av	0.08	0.05	0.08	0.11	0.10	0.04	0.04	0.02	0.03
F_2	0.06	0.04	0.06	0.13	0.08	0.03	0.03	0.02	0.02

Table 6.6: Summary of the cooling tests with silicone oil and silicone oil + erythritol.

Quantity	Test 9	Test 10	Test 11	Test 12	Test 13	Test 14	Test 15	Test 16	Test 17
Date	11/06/2018	27/09/2018	11/06/2019	12/06/2019	17/06/2019	24/07/2018	11/09/2018	12/09/2018	25/09/2018
m_{f} (kg)	1.5	1.5	1.5	1.5	1.5	1.5	1.5	1.5	1.5
m_{PCM} (kg)	-	-	-	-	-	2.5	2.5	2.5	2.5
T_2 (°C)	125	125	125	125	125	125	125	125	125
T_3 (°C)	100	100	100	100	100	100	100	100	100
$T_{\mathrm{amb,av}}$ (°C)	29.24	17.35	29.69	29.02	28.46	29.77	26.46	27.57	19.87
Δt_{c} (h)	0.45	0.31	0.50	0.48	0.46	1.88	2.19	2.03	1.67

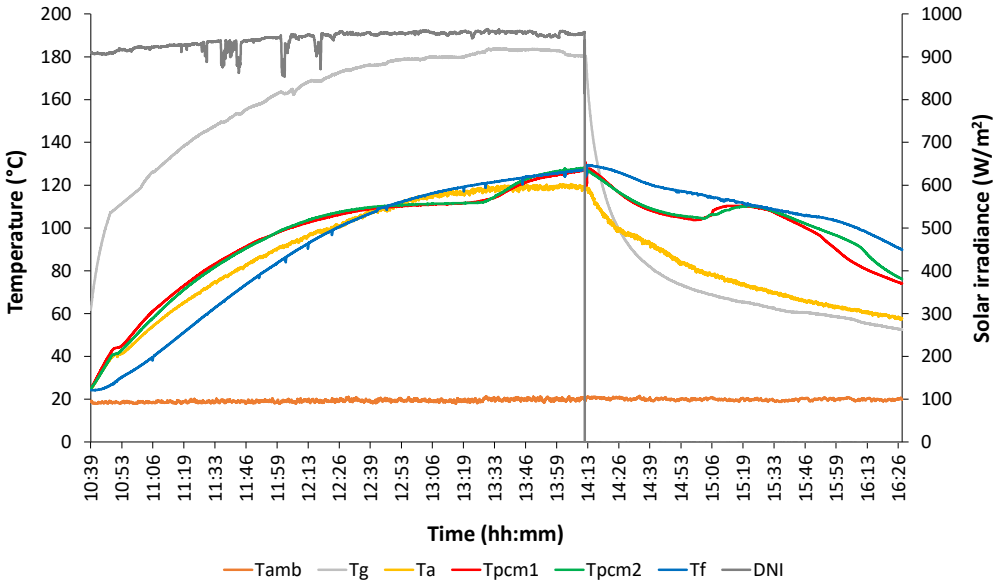

Figure 6.17: Test with silicone oil and erythritol (25/09/2018, Test 17).

same. During the heating phase, the PCM temperature shows a change of slope at around 109 °C, value that identifies the melting point of the erythritol. When the solar cooker was used with the TES, the heating process required about 2.52 hours to take the silicone oil temperature from 55 to 125 °C. In comparison, the silicone oil test carried out on September 27$^{\text{th}}$, 2018 required about 1.58 hours for the heating process in the same temperature range. The increase in the heating time, along with the penalties associated to the cooker average efficiency and the second figure of merit, are due to the presence of the additional mass of PCM.

The cooling phase, instead, required 1.65 hours to decrease the testing fluid temperature from 125 to 100 °C. During this phase, the average ambient temperature was 19.87 °C. Respect to the case without the PCM-based TES ($\Delta t_c = 0.31$ h), the silicone oil cooling time increased by more than 5 times.

In Figure 6.17, it is also possible to see that a supercooling phenomenon takes place in the PCM, i.e. the substance does not solidify immediately below the freezing temperature but its crystallization occurs only after a lower temperature (around 105 °C) is reached. This effect is well-known in literature [218] and, in the TES under study, could be due to heterogeneous nucleation at the surface of the vessel containing the PCM. Even though supercooling leads to lower crystallization temperatures and, therefore, to a non-optimal thermal storage performance [218], in Figure 6.17 it is possible to see that the erythritol supercooling curve rises and stabilizes at the solidification temperature (109 °C) immediately upon crystallization. Thus, the penalty associated to the phenomenon is minimal.

6.7.5 Test with Silicone Oil and Silicone Oil + Xylitol

Among the tests carried out with silicone oil in June 2019 already presented in section 6.7.3 in Table 6.5 and 6.6, Tests 11 to 13 have been re-elaborated and the results obtained are presented in this new section (Tests 18 to 20 in Table 6.7 and Table 6.8). In this case, the temperature range considered for the silicone oil within

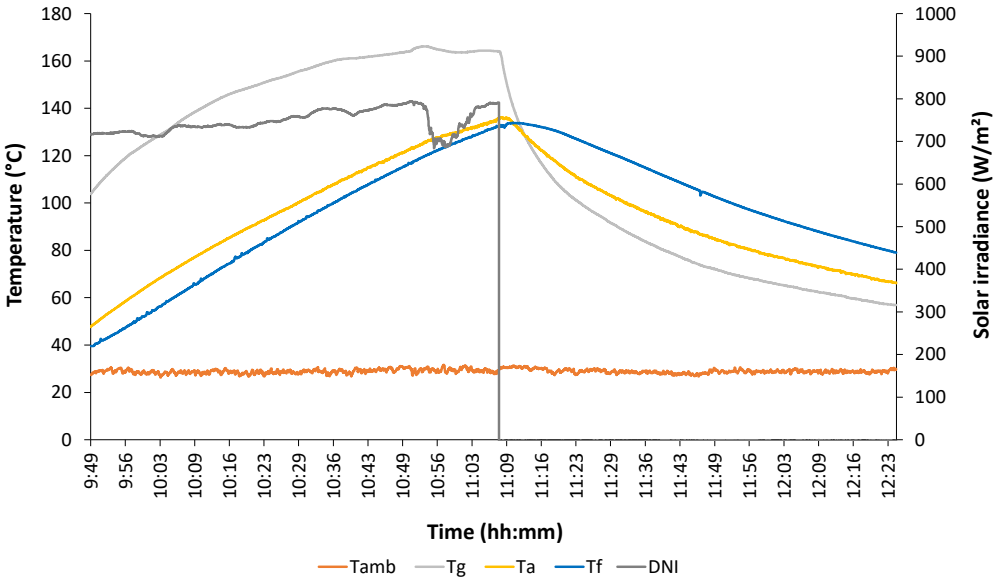

Figure 6.18: Results of a silicone oil test (17/06/2019, Test 20).

which all the parameters in Table 6.7 and 6.8 were calculated was from 55 to 110 °C for the heating phase and from 110 to 80 °C for the cooling phase. The purpose of this second development was to have results in the appropriate temperature range in order to be able to compare these results with those obtained from the tests carried out by placing the TES containing xylitol inside the cooking chamber of the device.

To be noted that only the last three reported tests involved the manual mechanical triggering of xylitol nucleation.

Figure 6.18 shows as example the temperatures trend and the direct normal irradiance detected on June 17$^{\text{th}}$, 2019 (Test 20). Taking as a reference for the heating phase the time required by the silicone oil to take its temperature from 55 to 110 °C (0.71 hours), the corresponding average environmental parameters were found to be 28.57 °C for $T_{\text{amb,av}}$ and 749.41 W/m^2 for DNI_{av}.

Once silicone oil overtook a temperature of 130 °C, the absence of irradiation was emulated by shading the cooker. During the cooling phase, the mean ambient temperature $T_{\text{amb,av}}$ was equal to 28.64 °C and silicone oil required around 0.69 hours to take its temperature from 110 to 80 °C. As can be verified from Table 6.7 and 6.8, the performance parameters used to characterize the cooker assume repeatable values.

Tests with silicone oil and xylitol (without triggering)

Four outdoor tests with 1.5 kg of silicone oil and 2.5 kg of PCM were performed in June 2019 and May 2021 to evaluate the thermal behavior of the solar box cooker integrated with the xylitol-based TES. The results are depicted in Table 6.7 for the heating phase and in Table 6.8 for the cooling phase (Tests 21–24) together with the ones with silicone oil only.

An example of test carried out with the xylitol-based TES is shown in Figure 6.19 (Test 23). In the heating phase, which required 2.13 hours to take the silicone oil temperature from 55 to 110 °C, the mean environmental parameters were $DNI_{\text{av}} = 726.24\,\text{W/m}^2$ and $T_{\text{amb,av}} = 26.09\,°\text{C}$. As evident in Figure 6.19, the phase transition

Table 6.7: Summary of the tests carried out with silicone oil and silicone oil + xylitol during the heating phase.

Quantity	Test 18	Test 19	Test 20	Test 21	Test 22	Test 23	Test 24	Test 25	Test 26	Test 27
Date	11/06/2019	12/06/2019	17/06/2019	05/06/2019	06/06/2019	07/06/2019	10/05/2021	18/05/2021	20/05/2021	31/05/2021
m_{f} (kg)	1.5	1.5	1.5	1.5	1.5	1.5	1.5	1.5	1.5	1.5
m_{PCM} (kg)	-	-	-	2.5	2.5	2.5	2.5	2.5	2.5	2.5
T_1 (°C)	55	55	55	55	55	55	55	55	55	55
T_2 (°C)	110	110	110	110	110	110	110	110	110	110
DNI_{av} (W/m^2)	718.69	588.64	749.41	794.45	719.75	726.24	915.76	923.10	946.13	928.17
$T_{\mathrm{amb,av}}$ (°C)	30.91	28.17	28.57	28.23	26.97	26.09	24.12	24.08	19.91	21.06
Δt_{h} (h)	0.83	0.73	0.71	1.68	2.83	2.13	2.28	1.99	2.26	2.36
t_{s} (h m^2/kg)	0.38	0.33	0.32	0.76	1.28	0.96	1.04	0.91	1.02	1.07
t_{ch} (h m^2/kg)	0.30	0.22	0.27	0.67	1.03	0.78	1.05	0.93	1.08	1.10
η_{av}	0.09	0.13	0.10	0.04	0.03	0.04	0.03	0.03	0.03	0.02
F_2	0.15	0.27	0.17	0.07	0.05	0.06	0.04	0.05	0.04	0.04

Table 6.8: Summary of the tests carried out with silicone oil and silicone oil + xylitol during the cooling phase.

Quantity	Test 18	Test 19	Test 20	Test 21	Test 22	Test 23	Test 24	Test 25	Test 26	Test 27
Date	11/06/2019	12/06/2019	17/06/2019	05/06/2019	06/06/2019	07/06/2019	10/05/2021	18/05/2021	20/05/2021	31/05/2021
m_{f} (kg)	1.5	1.5	1.5	1.5	1.5	1.5	1.5	1.5	1.5	1.5
m_{PCM} (kg)	-	-	-	2.5	2.5	2.5	2.5	2.5	2.5	2.5
T_2 (°C)	110	110	110	110	110	110	110	110	110	110
T_3 (°C)	80	80	80	80	80	80	80	80	80	80
$T_{\mathrm{amb,av}}$ (°C)	30.36	29.87	28.64	28.08	26.26	26.64	26.41	25.35	19.96	21.44
Δt_{c} (h)	0.78	0.78	0.69	1.64	2.11	2.00	1.70	3.79	3.23	3.02
Triggering by mixing	-	-	-	-	-	-	-	yes	yes	yes

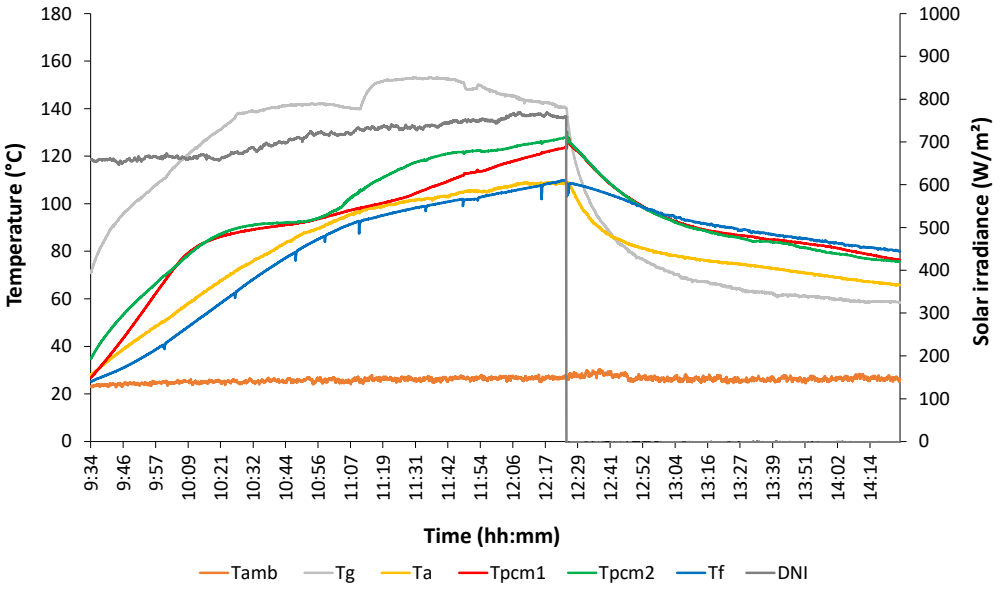

Figure 6.19: Results of a silicone oil + xylitol test without triggering (07/06/2019, Test 23).

of xylitol started at about 92 °C, value that corresponds to the melting point of the substance. Due to the presence of the additional mass of xylitol, the heating phase, if compared to Test 20 (which has comparable mean environmental parameters), lasted about 200% longer.

The cooling phase, instead, required 2 hours to decrease the test fluid temperature from 110 to 80 °C. During this phase, the mean ambient temperature was 26.64 °C. With respect to the same case evaluated without the xylitol-based TES (Test 20, $\Delta t_c = 0.69$ h), the silicone oil cooling time increased by about 190%, allowing a longer thermal stabilization of the test fluid.

Figure 6.19, however, does not show an evident phase transition for xylitol in the cooling phase, in agreement with the discussion of Figure 6.10 about the DSC analysis. This phenomenon was observed in all four tests performed with oil + xylitol; the phase change of the PCM occurred only in the heating phase and always around 92 °C. This behavior is probably caused by the fact that xylitol presents crystallization and supercooling issues. Numerous authors have therefore proposed different techniques to promote the nucleation and crystallization behavior of xylitol, such as seeding/shearing, bubbling or mechanical agitation [92, 98, 219].

Tests with silicone oil and xylitol (with triggering)

In addition to the tests carried out without any triggering of crystallization for xylitol, in May 2021 other three investigations were performed with the same methodology (heating + cooling phase), but during the cooling phase the device installed in the TES was manually activated by an operator in order to promote nucleation and, thus, phase change of the PCM. These tests are also reported in Table 6.7 for the heating phase and in Table 6.8 for the cooling phase (Tests 25–27).

As can be seen in Figure 6.20, which shows the test carried out on May 20$^{\text{th}}$, 2021 (Test 26; $DNI_{\text{av}} = 946.13\,\text{W/m}^2$; $T_{\text{amb,av}} = 19.91\,°\text{C}$), no evident difference can be

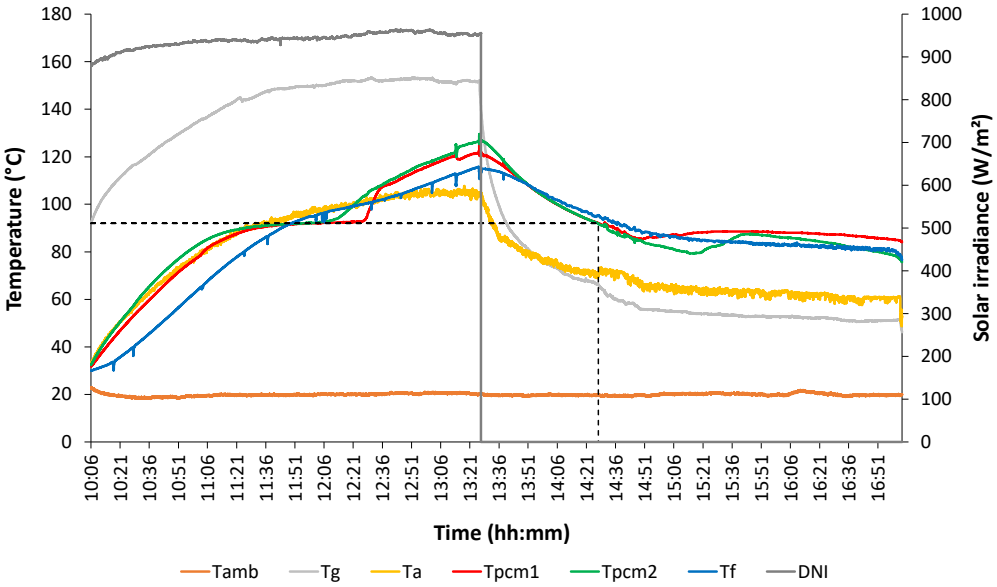

Figure 6.20: Results of a silicone oil + xylitol test with triggering by mixing (20/05/2021, Test 26).

found during the heating stage for the phase change process, that continues to occur at around 92 °C. In the cooling phase, instead, an operator manually triggered for about 5 minutes the PCM by means of the dedicated device when a temperature lower than the melting point was detected. Looking again at Figure 6.20, it is possible to note that the manual activation did not result in an immediate response of the substance, which took around 15-20 minutes to start the phase change process and to increase its temperature. Figure 6.20 also depicts that the activation process is not uniform in the PCM, but it was faster in a portion of the substance ($T_{\mathrm{PCM},1}$) and slower in another ($T_{\mathrm{PCM},2}$). This effect is likely due to non-uniformity of the commercial-grade xylitol, but it may also depend on an imperfect utilization of the activation device.

Besides a possible non-uniformity in the activation process, from Figure 6.20 it is clear that the manual triggering of xylitol allowed to stabilize the thermal capacity of the solar cooker system and, in particular, of the load (silicone oil). This should allow to extend the cooling time interval and, thus, improve the thermal performance of the solar cooker when solar radiation is absent or intermittent. This aspect will be discussed in detail in the following section.

6.8 Summary and Comparison

In order to be able to evaluate the pros and cons of a solar box cooker coupled with a PCM-based TES, a specific methodology was adopted. In particular, a clear distinction between heating and cooling phases of the tests involving silicone oil with and without PCM was necessary.

In detail, it was necessary to compare the heating ($\Delta t_{\mathrm{h,oil}}$ and $\Delta t_{\mathrm{h,oil+PCM}}$) and cooling times ($\Delta t_{\mathrm{c,oil}}$ and $\Delta t_{\mathrm{c,oil+PCM}}$) computed for the two sets. In this way, it was possible to evaluate the increment in time in the heating phase required by the test fluid coupled with PCM with respect to the test fluid only (an unavoidable detrimental

Table 6.9: Average, best and worst heating times of the tests with silicone oil and with silicone oil + erythritol provided in Table 6.5. The best case refers to the silicone oil longest heating time and silicone oil + erythritol shortest heating time; the opposite for the worst case. Deviations are calculated as the percentage difference between the heating times of the two test sets.

Quantity	Average	Best	Worst
$\Delta t_{\mathrm{h,oil}}$ (h)	1.18 (Tests 9–13)	1.58 (Test 10)	0.95 (Test 13)
$\Delta t_{\mathrm{h,oil+PCM}}$ (h)	2.53 (Tests 14–17)	1.94 (Test 14)	3.35 (Test 16)
Deviation (%)	114.41	22.78	252.63

effect due to the presence of more mass in the system), and, more importantly, the increment in time observed in the cooling phase (which is the desired beneficial effect due to the introduction of a TES in a solar box cooker).

As a premise, it should be noted that direct comparisons between the heating and the cooling times for a test are difficult to make. This is due to two reasons:

- during the heating phase, solar radiation provides thermal energy to the system, and this causes the PCM phase transition, while during the cooling phase the PCM is left cooling down naturally;
- the temperature ranges chosen for evaluation are different (70 °C for the heating phase and 25 °C for the cooling phase for erythritol, 55 °C for the heating phase and 30 °C for the cooling phase for xylitol).

It is however useful to run this comparison to quantify the useful effects (slowdown of the system cooling) is superior to the detrimental effect (slowdown of the system heating).

6.8.1 Erythritol as PCM

Heating Phase

Starting from the heating phase, Table 6.5 shows that when the erythritol-based TES is used (Tests from 14 to 17), the heating phase is longer and the calculated experimental parameters are generally worse. Clearly this is due to the PCM additional mass loaded and to its latent heat of fusion.

Table 6.9 provides the average heating times of the experimental tests carried out with silicone oil ($\Delta t_{\mathrm{h,oil}}$, average of the Δt_{h} for the Tests 9–13), and with silicone oil and PCM ($\Delta t_{\mathrm{h,oil+PCM}}$, average of the Δt_{h} for the Tests 14–17). The same table reports the corresponding average deviation, calculated as the percentage difference between the average silicone oil + PCM heating time (2.53 hours) and the average silicone oil heating time (1.18 hours). Hence, the average time increment in the heating phase of the solar cooker equipped with PCM with respect to when it is loaded only with silicone oil is equal to 114.41%.

Cooling Phase

In the same fashion of Table 6.5, Table 6.6 reports the data recorded during the cooling phases of the outdoor tests. In this case, the cooling time Δt_{c} is only influenced

Table 6.10: Average, best and worst cooling times of the tests with silicone oil and with silicone oil + erythritol provided in Table 6.6. The best case refers to the silicone oil shortest cooling time and silicone oil + erythritol longest cooling time; the opposite for the worst case. Deviations are calculated as the percentage difference between the cooling times of the two test sets.

Quantity	Average	Best	Worst
$\Delta t_{\mathrm{c,oil}}$ (h)	0.43 (Tests 9–13)	0.31 (Test 10)	0.50 (Test 11)
$\Delta t_{\mathrm{c,oil+PCM}}$ (h)	1.94 (Tests 14–17)	2.19 (Test 15)	1.67 (Test 17)
Deviation (%)	351.16	606.45	234.00

by the ambient temperature. The advantage derived by the use of the PCM-based TES is evident, resulting in a significant extension of the cooker thermal stability.

Table 6.10 provides the average cooling times of the tests carried out with silicone oil only ($\Delta t_{\mathrm{c,oil}}$, obtained averaging the Δt_{c} for the Tests 9–13), and with silicone oil and PCM ($\Delta t_{\mathrm{c,oil+PCM}}$, average of the Δt_{c} for the Tests 14–17). Additionally, Table 6.10 reports the average deviation calculated as the percentage difference between the two test sets: an increase of around 351.16% was found. It is evident that a substantial enhancement of the cooker thermal stability in absence of solar radiation was therefore obtained, even in the worst case considered.

6.8.2 Xylitol as PCM

As above, a distinction between heating and cooling phases for the tests with a xylitol-based TES was operated. For each test set, the heating times ($\Delta t_{\mathrm{h,oil}}$ and $\Delta t_{\mathrm{h,oil+PCM}}$) and cooling times ($\Delta t_{\mathrm{c,oil}}$, $\Delta t_{\mathrm{c,oil+PCM}}$ and $\Delta t_{\mathrm{c,oil+PCM,trig}}$) were determined. In the cooling phase results a further distinction between the tests performed with and without triggering is applied.

Heating Phase

Analyzing the heating phase, Table 6.7 shows that the additional mass of PCM implies an increasing heating time, and a general deterioration of the performance parameters. It is also possible to note that Δt_{h} varies with ambient conditions and may depend on how often the operator acts on the orientation of the solar cooker.

A detailed analysis of the heating times is provided in Table 6.11. It reports the mean heating time of the experimental tests performed for silicone oil only ($\Delta t_{\mathrm{h,oil}}$, mean value of the Δt_{h} for the Tests 18–20) and for silicone oil and PCM ($\Delta t_{\mathrm{h,oil+PCM}}$, mean value of the Δt_{h} for the Tests 21–27). The corresponding deviation is calculated as the percentage difference between the mean silicone oil + PCM heating time (2.22 hours) and the mean silicone oil heating time (0.76 hours).

As for the case of erythritol, the solar cooker equipped with the xylitol-based TES shows an increase in heating time, this time by 193% on average with respect to the performance obtained with the system without PCM.

Cooling Phase

The cooling times recorded during the outdoor tests are reported in Table 6.8. In this case, the cooling time Δt_{c} is influenced by the ambient temperature and the manual triggering. As expected, the use of the xylitol-based TES allows for a pronounced

Table 6.11: Heating time evaluation of the tests with silicone oil and with silicone oil + xylitol.

Quantity	Average	Best	Worst
$\Delta t_{\mathrm{h,oil}}$ (h)	0.76 (Tests 18–20)	0.83 (Test 18)	0.71 (Test 20)
$\Delta t_{\mathrm{h,oil+PCM}}$ (h)	2.22 (Tests 21–27)	1.68 (Test 21)	2.83 (Test 22)
Deviation (%)	193	102	299

Table 6.12: Cooling time evaluation of the tests with silicone oil and with silicone oil + xylitol (with and without triggering).

Quantity	Average	Best	Worst
$\Delta t_{\mathrm{c,oil}}$ (h)	0.75 (Tests 18–20)	0.69 (Test 20)	0.78 (Test 19)
$\Delta t_{\mathrm{c,oil+PCM}}$ (h)	1.86 (Tests 21–24)	2.11 (Test 22)	1.64 (Test 21)
$\Delta t_{\mathrm{c,oil+PCM,trig}}$ (h)	3.35 (Tests 25–27)	3.79 (Test 25)	3.02 (Test 27)
Deviation w/o triggering (%)	148	206	110
Deviation with triggering (%)	346	449	287
Deviation between trig. and w/o trig. (%)	80	80	84

extension of the test fluid thermal stabilization, extension that is even more dramatic when the triggering procedure is performed.

As for Table 6.11, Table 6.12 reports the mean cooling times of the tests carried out with silicone oil only ($\Delta t_{\mathrm{c,oil}}$, mean value of the Δt_{c} for the Tests 18–20), with silicone oil and PCM without triggering ($\Delta t_{\mathrm{c,oil+PCM}}$, mean value of the Δt_{c} for the Tests 21–24), and for silicone oil and PCM with triggering ($\Delta t_{\mathrm{c,oil+PCM,trig}}$, mean value of the Δt_{c} for the Tests 25–27).

The table shows that, when xylitol is not triggered, the mean deviation is equal to 148%. The "best" condition, which is obtained for Test 20 (silicone oil only, 0.69 hours) and Test 22 (silicone oil and PCM, 2.11 hours), results in a maximum deviation equal to 206%. The "worst" case, instead, takes into account the longest cooling time for silicone oil (Test 19, 0.78 hours) and the shortest cooling time for silicone oil and PCM (Test 21, 1.64 hours), resulting in a minimum deviation of 110%.

Even if the xylitol-based TES without triggering is able to improve the thermal stabilization of the load, by comparing Table 6.11 and Table 6.12 it becomes apparent that the heating time is not well counterbalanced by the increase of the cooling time. The direct conclusion from this is that using xylitol as PCM without triggering is sub-optimal as the two times are comparable, i.e. it is not useful extending the heating time if the cooling time is extended by a similar amount.

This is when the triggering of xylitol by mixing comes into play. In fact, again in Table 6.12, it is possible to note that the deviations when xylitol is manually triggered are much better. In the average case, for instance, the cooling time deviation between the system with a triggered TES and the system without TES is 346%. In other words, the nucleation activation of xylitol extends the cooling time period by 80% with respect to the case without activation.

Manual triggering gives a large boost to the TES performance, prolonging the cooling times by large factors. In this way it is possible to exploit the full potential of xylitol thermodynamic properties, i.e. its high latent heat of solidification. With the mixing technique, even in the worst-case scenario, the use of the xylitol-triggered TES improves greatly the thermal stabilization of the cooking load, and considering that the lowest temperature necessary for cooking many kinds of food is around 75 °C [214, 220],

the extension of the heating time provided by this system in the range 90–80 °C makes a xylitol-based test a very good candidate for use in simple and low-cost solar cookers that reach stagnation temperatures of about 100 °C (e.g., the solar cookers proposed by Kesarwani et al. [221] and Adewole et al. [222], and Saravanan and Janarathanan [223]).

Chapter 7

Mathematical Model of an SBC

In this chapter, a mathematical model of a solar box cooker is described in detail and validated with the results obtained from the outdoor experimental campaign carried out with a prototype of a box cooker. The model takes into account thermal and optical losses in order to calculate the temperatures or heat fluxes on all the components of the device. The model is presented in detail and its implementation in a specific calculation environment is described. The application of the model to a specific solar box cooker prototype is also described. The prototype in question was implemented and tested at Università Politecnica delle Marche and previously described in this thesis work in Chapter 6.

7.1 Selection Criteria of a Solar Box Cooker for the Development of a Mathematical Model

Among the prototypes implemented and tested during the research work presented, this particular box cooker was selected for the development of the mathematical model since it was the most characterized one during the experimental campaign. In fact, different types of tests were carried out with different fluids, and the effect on the entire system of the insertion of a phase change material inside its cooking chamber was also studied. The results obtained from the related outdoor experimental campaign are extensively reported and discussed in Chapter 6.

It is evident, therefore, that the performance of a solar box cooker can be easily obtained through tests, but this experimental approach is not completely satisfactory if optimization is to be achieved in the design of the device and in the fluid masses and thus in the optimum loads to be used. Indeed, an experimental approach makes it possible to know the amount of heat that can be transferred to the fluid under particular working (constant orientation of the cooker as a function of the sun's rotation) and environmental conditions (external conditions, variability of the solar radiation itself). However, this kind of approach does not allow the prediction of the temperatures of the different parts of the device, nor the heat losses due to the different heat exchange mechanisms or the effect of a variation of a single environmental condition, such as ambient temperature or the presence of wind.

Moreover, although rich of experimental works on solar devices, literature on this topic is poor in terms of the mathematical modeling of the problem.

7.2 Elements of Heat Transmissions

In this section, the main notions of heat transmission are reported, retracing the three possible types of transmission. Heat transfer is energy that moves from one system to another as a result of a temperature difference between the two systems. Heat can be transferred in three different ways: by conduction, by convection and by radiation. Each mode of heat transfer requires the existence of a temperature difference and occurs from one region of high temperature to another of lower temperature.

7.2.1 Heat Transmission by Conduction

Thermal conduction is the transfer of energy that occurs as a result of the interaction between particles of a substance with higher energy and adjacent particles with lower energy. It occurs in liquids and gases, but it is more markedly characteristic of solids. The amount of heat that travels by conduction between two regions of a body depends on the geometry and the characteristics of the body, as well as on the temperature difference between the two regions. The thermal power transmitted by conduction through a layer of constant thickness x is directly proportional to the temperature difference ΔT across the layer and the area A of the surface normal to the direction of heat transmission and is inversely proportional to the thickness of the layer:

$$\dot{Q}_{\text{cond}} = \frac{\lambda \Delta T A}{x} \tag{7.1}$$

where λ is the thermal conductivity of the material expressed in (W/m K). The higher the value, the more the material is a good conductor of heat. Conversely, the lower the value of λ, the more the material is a good thermal insulator. The thermal conductivity values of all the different materials are known and tabulated.

7.2.2 Heat Transmission by Convection

Thermal convection is the transfer of energy between two systems at different temperatures, at least one of which being a fluid. Of particular interest is the case of a solid surface and an adjacent moving liquid or gas. Thermal convection involves the combined effects of conduction and mass transport.

It is important to point out that:

- the heat transmitted by convection increases with the velocity of the fluid;
- in the absence of mass transport, the heat transfer between a solid surface and the adjacent fluid occurs only by conduction;
- the presence of mass transport increases the amount of heat transferred between the solid surface and the fluid.

$$\dot{Q}_{\text{conv}} = h_{\text{c}} A (T_{\text{s}} - T_{\infty}) \tag{7.2}$$

Where h_{c} is the convective heat transfer coefficient in $W/(m^2K)$, A the surface area across which convective heat transfer takes place, T_{s} the surface temperature and

T_∞ the temperature of the fluid at a sufficiently large distance from the surface (at the interface surface the temperature of the fluid and that of the solid are equal).

The convective heat transfer coefficient h_c depends on many variables:

- the thermophysical properties of the fluid (density, ρ; specific heat c_p; thermal conductivity λ; dynamic viscosity μ);
- the geometry of the solid-liquid interface, L_c;
- the speed of the fluid, u_∞.

Therefore: $h_\mathrm{c} = f(L_\mathrm{c}, u_\infty, \rho, c_\mathrm{p}, \lambda, \mu)$.

By adimensionalizing, the number of variables that influence the convective heat transfer coefficient are reduced. Therefore, the Nusselt number can be empirically calculated as a function of the Reynolds and Prandtl numbers: $Nu = f(Re, Pr)$.

- The Nusselt number represents the increase in thermal power transmitted by convection through a layer of fluid compared to that transmitted by conduction through the same layer. The unitary value of the Nusselt number ($Nu = 1$) is characteristic of heat transfer by pure conduction through the fluid layer. As the Nusselt number increases ($Nu > 1$), the phenomenon of convection becomes more and more significant:

$$Nu = \frac{h_\mathrm{c} L_\mathrm{c}}{\lambda} \tag{7.3}$$

- The Reynolds number represents the ratio between inertial and viscous forces. For high Reynolds numbers, the inertial forces prevail over the viscous ones so as not to impede the rapid and random fluctuations of the fluid. The motion is, therefore, turbulent. Conversely, for small values of the Reynolds number, the viscous forces prevail over the inertia ones, keeping the fluid fairly steady. The motion in this second case is laminar. The Reynolds number at which the flow becomes turbulent is called the critical Reynolds number. Its numerical value varies with the geometry of the system:

$$Re = \frac{u_\infty \rho L_\mathrm{c}}{\mu} \tag{7.4}$$

- The Prandtl number can be seen as a property of the fluid and provides the relationship between momentum (kinetic viscosity) diffusivity at the molecular level and thermal power by conduction (thermal diffusivity):

$$Pr = \frac{\mu c_\mathrm{p}}{\lambda} \tag{7.5}$$

In the case of natural convection, the velocity field u_∞ becomes the buoyancy force ($g\beta\Delta T$). The buoyancy force is caused by the difference in density between the fluid in contact with the surface and the undisturbed fluid. Therefore, in the case of natural convection, the Reynolds number is replaced by the Grashof number (the ratio between the buoyancy force and the viscous force acting on the fluid):

$$Gr = \frac{(g\beta\Delta T) L_\mathrm{c}^3}{\nu^2} \tag{7.6}$$

Where:

- g is the gravity acceleration;
- β is the coefficient of thermal expansion of the fluid;
- ν is the kinematic viscosity.

The relation $h_c = f(L_c, u_\infty, \rho, c_p, \lambda, \mu)$ can therefore be written in the adimensional form: $Nu = f(Gr, Pr)$.

By applying the inverse formula of equation 7.3, it is therefore possible to obtain the heat transfer convective coefficient. The simple empirical relations to determine the Nusselt number in the case of natural convection can be reduced to the formula:

$$Nu = C(GrPr)^n = CRa^n \tag{7.7}$$

where Ra is the Rayleigh number obtained as the product of the Grashof by the Prandtl number and it is equal to:

$$Ra = GrPr = \frac{(g\beta\Delta T)L_c^3}{\nu^2}\frac{\mu c_p}{\lambda} = \frac{g\beta\Delta T L_c^3 c_p \rho^2}{\lambda\mu} \tag{7.8}$$

The values of the constants C and n depend on the geometry of the surface and on the flow regime, which is characterized by the value of the Rayleigh number. In fact, by calculating Ra, it is possible to predict whether there will be a transition from the laminar to the turbulent regime. The transition to turbulent flow begins for $Ra > 10^9$. The value of n is usually 1/4 for laminar flows and 1/3 for turbulent flows. The value of the constant C is normally less than 1. Some simple relations for calculating the Nusselt number for various geometries are already known. In this thesis, these relationships will be reported as a function of the cases reported in the following which consider the geometry, the respective characteristic length L_c and the ranges of variation of the Rayleigh number within which the relationship is applicable.

7.2.3 Heat Transmission by Radiation

The radiation is the energy emitted by a substance in the form of electromagnetic waves as a result of changes in the electronic configurations of atoms or molecules. The transmission of heat by radiation does not require the presence of an interposed medium, unlike conduction and convection, it occurs at the speed of light and does not undergo attenuation in a vacuum.

In studies on the transmission of heat by radiation, thermal radiation, i.e. the radiation emitted by bodies due to their temperature, is of interest. All bodies at temperatures above absolute zero emit thermal radiation, the maximum amount of which referred to the surface of unit area at the absolute temperature T_s is given by the Stefan-Boltzmann law:

$$\dot{Q}_{rad} = \sigma T_s^4 \tag{7.9}$$

where σ is the Stefan-Boltzmann constant, which is equal to $5.67 \times 10^{-8}\,\mathrm{W/m^2K^4}$. A black body is an ideal surface that emits the maximum power by radiation. The radiation emitted by any real surface, or gray body, is less than that emitted by a black body at the same temperature and can be calculated as:

$$\dot{Q}_{rad} = \epsilon\sigma T_s^4 \tag{7.10}$$

where ϵ is the emissivity of the surface (of the material). This value is included in the interval $0 \leq \epsilon \leq 1$ and measures how closely the behavior of a surface approximates that of a black body (which has $\epsilon = 1$).

The determination of the net thermal power exchanged by radiation between two surfaces is a complicated matter, since it depends on the properties of the surfaces, their relative orientation and the characteristics of the medium between them. Through a demonstration it was shown that the net thermal power exchanged from surface A_1 to surface A_2 is equal to:

$$\dot{Q}_{\mathrm{r},1-2} = \frac{\sigma(T_1^4 - T_2^4)}{\frac{(1-\epsilon_1)}{A_1\epsilon_1} + \frac{1}{A_1 F_{1-2}} + \frac{(1-\epsilon_2)}{A_2\epsilon_2}} \tag{7.11}$$

where F_{1-2} is the view factor indicating the fraction of radiation leaving surface A_1 and reaching surface A_2. This factor therefore depends on the geometric orientation of the two surfaces.

There are simplified forms of equation 7.11 that are suitable for the case studies treated in this thesis.

For a small convex surface A_1 completely enclosed by a very large concave surface A_2, when $A_1 << A_2$, the view factor becomes $F_{12} = 1$, thus equation 7.11 becomes:

$$\dot{Q}_{\mathrm{r},1-2} = A_1\epsilon_1\sigma(T_1^4 - T_2^4) \tag{7.12}$$

7.3 Thermal Analysis

In this section, a detailed overview of the heat transfer mechanisms participating in an SBC is presented.

7.3.1 Energy Balance of The System

The thermal performance of a solar box cooker can be evaluated through an energy balance between the heat absorbed and the heat released by the various components of the system.

A number of simplifying assumptions were adopted to build the mathematical model. In particular, it was assumed that:

- the solar cooker is constantly well oriented towards the sun, i.e. at any time during the test the sun's rays are perpendicular to the glass;
- the physical, thermal and optical properties of the elements of the solar cooker do not depend on temperature;
- each element of the solar cooker has a homogeneous temperature;
- there is no leak of air from the pot nor from the cooking chamber.

In order to better describe the portable solar box cooker system, seven different components were considered: the lid of the pot, the pot, the air inside the pot, the fluid, the cover glass, the cooking chamber and the air inside the cooking chamber. Figure 7.1 shows a section of the portable solar cooker with all the heat exchanges considered, while Figure 7.2 shows the thermal resistance model.

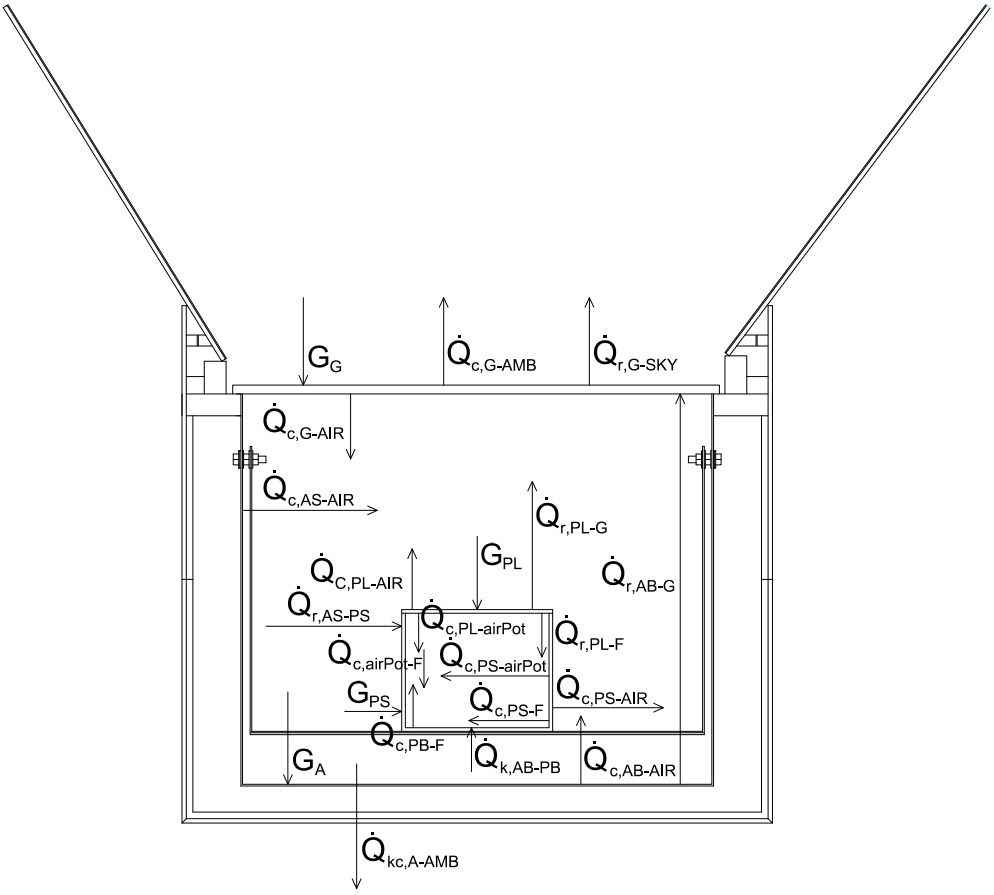

Figure 7.1: Energy balance for an SBC cross-section. The definition of the symbols is provided in Table 7.1.

When the beam radiation hits the glass cover (G_{G}), a fraction of the solar energy heats the glass itself and a part passes through it and enters the cooking chamber. Here it reaches the lid, the side surface of the pot and the base of the absorber.

The lid of the pot is heated by the solar radiation (G_{PL}) and gives off its heat by convection to the air inside the cooking chamber ($\dot{Q}_{\mathrm{c,PL-AIR}}$), by radiation to the glass ($\dot{Q}_{\mathrm{r,PL-G}}$), by convection to the air between lid and fluid inside the pot ($\dot{Q}_{\mathrm{c,PL-airPot}}$), and by radiation to the fluid in the pot ($\dot{Q}_{\mathrm{r,PL-F}}$). Figure 7.3 shows in detail the lid of the pot with the corresponding incoming and outgoing heat flows considered for the development of the final model.

In addition to solar radiation (G_{PS}), the pot is also heated by radiation from the side surface of the absorber ($\dot{Q}_{\mathrm{r,PS-AS}}$) and by conduction from the absorber baseplate ($\dot{Q}_{\mathrm{k,AB-PB}}$). The heat absorbed by the pot partly serves as useful energy for the fluid ($\dot{Q}_{\mathrm{c,PS-F}}$, $\dot{Q}_{\mathrm{c,PB-F}}$), which will increases its temperature, and partly is dispersed by convection into the air inside the pot ($\dot{Q}_{\mathrm{c,PS-airPot}}$) and the air inside the cooking chamber ($\dot{Q}_{\mathrm{c,PS-AIR}}$). Figure 7.4 shows in detail the pot with the corresponding incoming and outgoing heat flows considered for the development of the final model.

The fluid inside the pot is therefore heated by conduction from the bottom of the

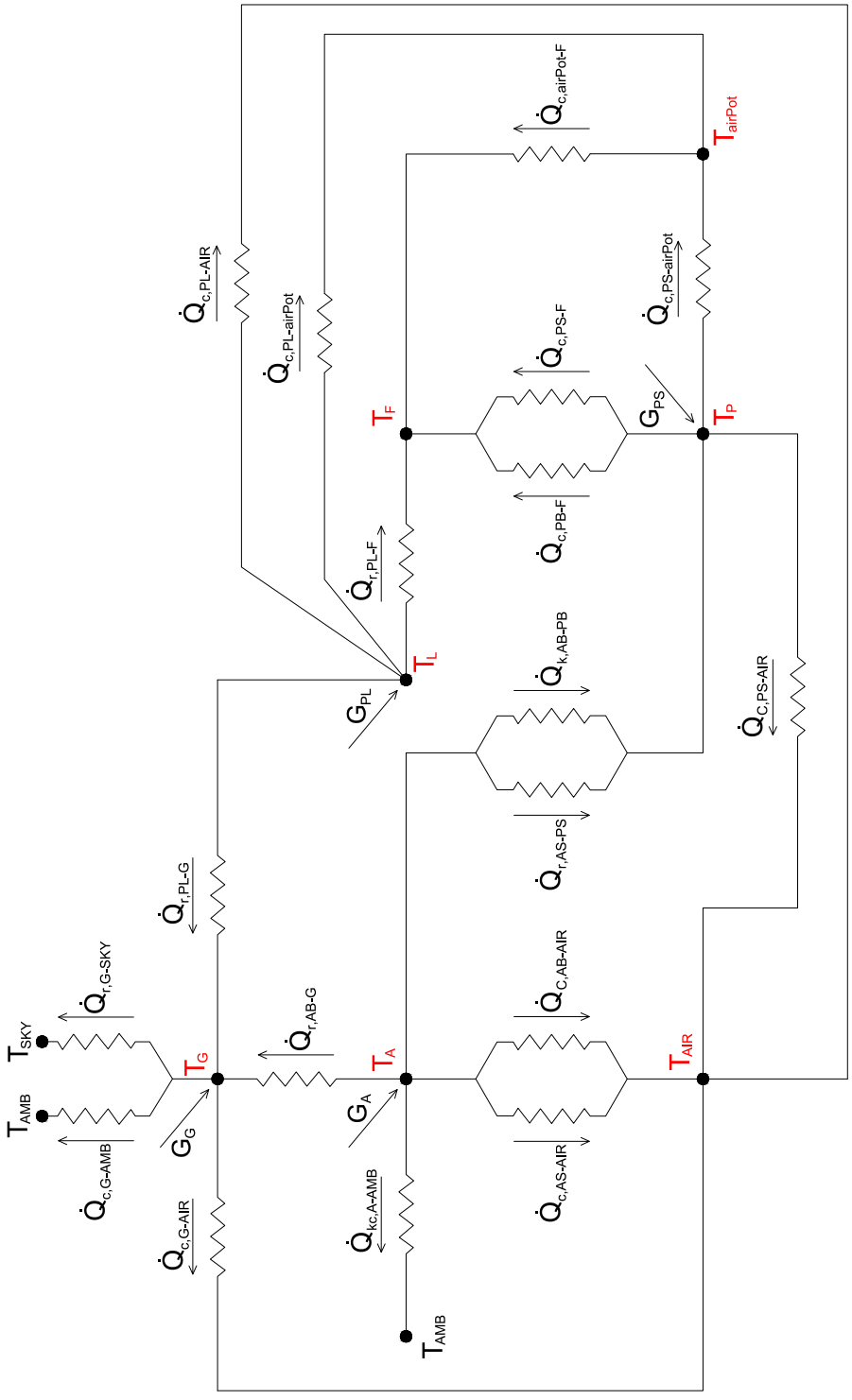

Figure 7.2: Thermal resistance model of the solar box cooker system.

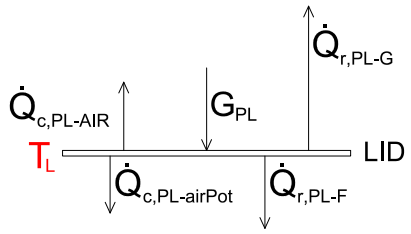

Figure 7.3: Scheme diagram of the lid of the pot with incoming and outgoing heat flows.

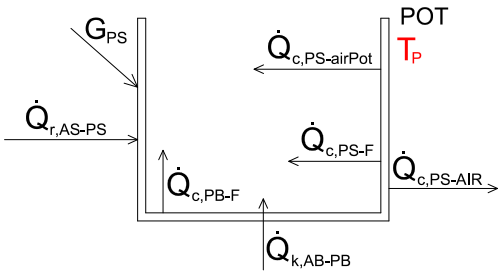

Figure 7.4: Scheme diagram of the pot with incoming and outgoing heat flows.

pot ($\dot{Q}_{\mathrm{c,PB-F}}$), from the side surface of the pot ($\dot{Q}_{\mathrm{c,PS-F}}$), and from the air inside the pot ($\dot{Q}_{\mathrm{c,airPot-F}}$). It is also heated by radiation from the lid of the pot ($\dot{Q}_{\mathrm{r,PL-F}}$). Figure 7.5 shows in detail the fluid in the pot with the corresponding incoming and outgoing heat flows considered for the development of the final model.

In addition to solar radiation (G_{G}), the glass is also heated by convection from the air inside the cooking chamber ($\dot{Q}_{\mathrm{c,G-AIR}}$), by radiation from the lid of the pot ($\dot{Q}_{\mathrm{r,PL-G}}$) and from the pot-free portion of the absorber base ($\dot{Q}_{\mathrm{r,AB-G}}$). In turn, the glass disperses heat by convection and radiation to the outside environment ($\dot{Q}_{\mathrm{c,G-AMB}}$ and $\dot{Q}_{\mathrm{r,G-SKY}}$). Figure 7.6 shows in detail the glass cover with the corresponding incoming and outgoing heat flows considered for the development of the final model.

The cooking chamber of the solar cooker is heated only by solar radiation (G_{A}), whereas it gives off its heat by conduction to the bottom of the pot ($\dot{Q}_{\mathrm{k,AB-PB}}$), by convection to the air inside the cooking chamber ($\dot{Q}_{\mathrm{c,AS-AIR}}$ and $\dot{Q}_{\mathrm{c,AB-AIR}}$), and by radiation to the side surface of the pot ($\dot{Q}_{\mathrm{r,AS-PS}}$) and the glass ($\dot{Q}_{\mathrm{r,AB-G}}$). It also releases its heat to the outside environment through the insulation layer ($\dot{Q}_{\mathrm{kc,A-AMB}}$).

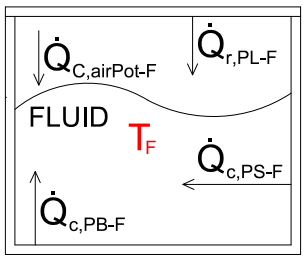

Figure 7.5: Scheme diagram of the fluid with incoming and outgoing heat flows.

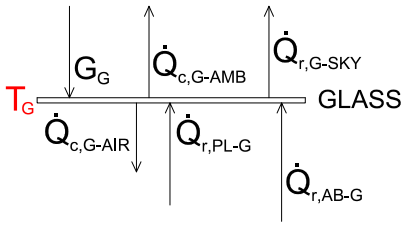

Figure 7.6: Scheme diagram of the glass cover with incoming and outgoing heat flows.

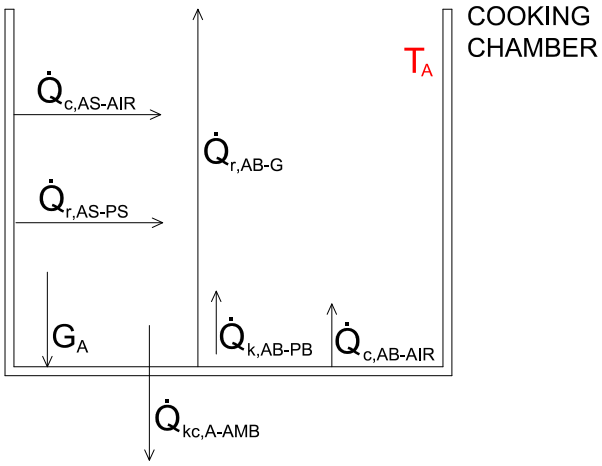

Figure 7.7: Scheme diagram of the absorber plate/cooking chamber with incoming and outgoing heat flows.

Figure 7.7 shows in detail the absorber plate with the corresponding incoming and outgoing heat flows considered for the development of the final model.

The air inside the cooking chamber is heated by convection from the base and side surfaces of the absorber ($\dot{Q}_{\mathrm{c,AS-AIR}}$ and $\dot{Q}_{\mathrm{c,AB-AIR}}$), from the glass ($\dot{Q}_{\mathrm{c,G-AIR}}$), from the lid of the pot ($\dot{Q}_{\mathrm{c,PL-AIR}}$) and from the side surface of the pot ($\dot{Q}_{\mathrm{c,PS-AIR}}$). Figure 7.8 shows in detail the air inside the cooking chamber with the corresponding incoming and outgoing heat flows considered for the development of the final model.

The air inside the pot is heated by convection from the lid ($\dot{Q}_{\mathrm{c,PL-airPot}}$) and the side surface of the pot that remains empty in terms of the fluid level ($\dot{Q}_{\mathrm{c,PS-airPot}}$), while it gives off heat by convection to the fluid below ($\dot{Q}_{\mathrm{c,airPot-F}}$). Figure 7.9 shows in detail the air inside the pot with the corresponding incoming and outgoing heat flows considered for the development of the final model.

The system of energy-balance equations is determined by applying the first principle of thermodynamics at each element of the system:

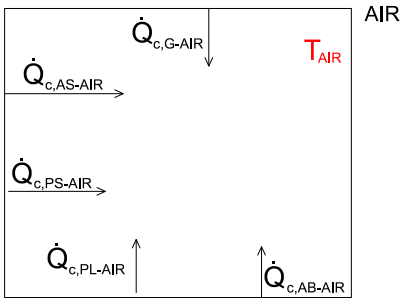

Figure 7.8: Scheme diagram of the air inside the cooking chamber with incoming and outgoing heat flows.

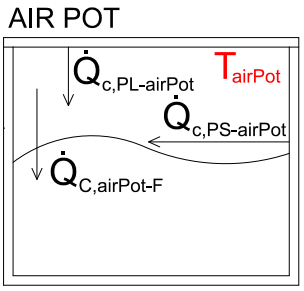

Figure 7.9: Scheme diagram of the air inside the pot with incoming and outgoing heat flows.

$$
\begin{cases}
m_{\mathrm{L}} c_{\mathrm{p,L}} \dfrac{dT_{\mathrm{L}}}{dt} = G_{\mathrm{PL}} - \dot{Q}_{\mathrm{c,PL-AIR}} - \dot{Q}_{\mathrm{c,PL-airPot}} - \dot{Q}_{\mathrm{r,PL-G}} - \dot{Q}_{\mathrm{r,PL-F}} \\
m_{\mathrm{P}} c_{\mathrm{p,P}} \dfrac{dT_{\mathrm{P}}}{dt} = G_{\mathrm{PS}} + \dot{Q}_{\mathrm{k,AB-PB}} - \dot{Q}_{\mathrm{c,PS-F}} - \dot{Q}_{\mathrm{c,PS-airPot}} - \dot{Q}_{\mathrm{c,PB-F}} \\
\qquad\qquad - \dot{Q}_{\mathrm{c,PS-AIR}} + \dot{Q}_{\mathrm{r,AS-PS}} \\
m_{\mathrm{F}} c_{\mathrm{p,F}} \dfrac{dT_{\mathrm{F}}}{dt} = \dot{Q}_{\mathrm{c,PB-F}} + \dot{Q}_{\mathrm{c,PS-F}} + \dot{Q}_{\mathrm{c,airPot-F}} + \dot{Q}_{\mathrm{r,PL-F}} \\
m_{\mathrm{G}} c_{\mathrm{p,G}} \dfrac{dT_{\mathrm{G}}}{dt} = G_{\mathrm{G}} - \dot{Q}_{\mathrm{c,G-AMB}} - \dot{Q}_{\mathrm{c,G-AIR}} + \dot{Q}_{\mathrm{r,AB-G}} + \dot{Q}_{\mathrm{r,PL-G}} \\
\qquad\qquad - \dot{Q}_{\mathrm{r,G-SKY}} \\
m_{\mathrm{A}} c_{\mathrm{p,A}} \dfrac{dT_{\mathrm{A}}}{dt} = G_{\mathrm{A}} - \dot{Q}_{\mathrm{kc,A-AMB}} - \dot{Q}_{\mathrm{k,AB-PB}} - \dot{Q}_{\mathrm{c,AS-AIR}} \\
\qquad\qquad - \dot{Q}_{\mathrm{c,AB-AIR}} - \dot{Q}_{\mathrm{r,AS-PS}} - \dot{Q}_{\mathrm{r,AB-G}} \\
m_{\mathrm{AIR}} c_{\mathrm{p,AIR}} \dfrac{dT_{\mathrm{AIR}}}{dt} = \dot{Q}_{\mathrm{c,AS-AIR}} + \dot{Q}_{\mathrm{c,G-AIR}} + \dot{Q}_{\mathrm{c,PL-AIR}} + \dot{Q}_{\mathrm{c,PS-AIR}} \\
\qquad\qquad + \dot{Q}_{\mathrm{c,AB-AIR}} \\
m_{\mathrm{AirPot}} c_{\mathrm{p,AirPot}} \dfrac{dT_{\mathrm{AirPot}}}{dt} = \dot{Q}_{\mathrm{c,PL-airPot}} + \dot{Q}_{\mathrm{c,PS-airPot}} - \dot{Q}_{\mathrm{c,airPot-F}}
\end{cases}
$$

where the subscripts have the following meaning:

- the first letter indicates the type of heat transfer mode: k for conduction, c for

Table 7.1: Heat flux involved in the energy balance of the SBC system.

Heat flux	Description
G_{PL}	Global solar radiation transmitted by the glass and absorbed by the lid of the pot
G_{PS}	Global solar radiation transmitted by the glass and absorbed by the pot
G_{G}	Global solar radiation absorbed by the glass
G_{A}	Global solar radiation transmitted by the glass and absorbed by the absorber
$\dot{Q}_{\mathrm{c,PL-AIR}}$	Convection heat flow from the lid to the air inside the cooking chamber
$\dot{Q}_{\mathrm{c,PL-airPot}}$	Convection heat flow from the lid to the air inside the pot
$\dot{Q}_{\mathrm{r,PL-G}}$	Radiation heat flow from the lid to the glass
$\dot{Q}_{\mathrm{r,PL-F}}$	Radiation heat flow from the lid to the fluid
$\dot{Q}_{\mathrm{k,AB-PB}}$	Conduction heat flow from: bottom of the absorber plate to the bottom of the pot
$\dot{Q}_{\mathrm{c,PS-F}}$	Convection heat flow from the pot's side to the fluid
$\dot{Q}_{\mathrm{c,PS-airPot}}$	Convection heat flow from the pot's side to the air inside the pot
$\dot{Q}_{\mathrm{c,PB-F}}$	Convection heat flow from the bottom of the pot to the fluid
$\dot{Q}_{\mathrm{c,PS-AIR}}$	Convection heat flow from the pot's side to the air inside the cooking chamber
$\dot{Q}_{\mathrm{r,AS-PS}}$	Radiation heat flow from the side absorber to the pot's side
$\dot{Q}_{\mathrm{c,airPot-F}}$	Convection heat flow from the air inside the pot to the fluid
$\dot{Q}_{\mathrm{c,G-AMB}}$	Convection heat flow from the glass to the external ambient temperature
$\dot{Q}_{\mathrm{c,G-AIR}}$	Convection heat flow form the glass to the air inside the cooking chamber
$\dot{Q}_{\mathrm{r,AB-G}}$	Radiation heat flow from the bottom of the absorber plate to the glass
$\dot{Q}_{\mathrm{r,G-SKY}}$	Radiation heat flow from the glass to the sky
$\dot{Q}_{\mathrm{kc,A-AMB}}$	Heat flow from the absorber to the external ambient
$\dot{Q}_{\mathrm{c,AS-AIR}}$	Convection heat flow from the absorber side to the air inside the cooking chamber
$\dot{Q}_{\mathrm{c,AB-AIR}}$	Convection heat flow: bottom of the absorber to the air inside the cooking chamber

convection, r for radiation, and kc is for the equivalent resistance;

- the letters before the dash indicate the element of the system that is losing heat (in accordance with the sign and the verse of the vectors in Fig. 7.1);
- the letters after the dash indicate the element of the system that is acquiring heat (in accordance with the sign and the verse of the vectors in Fig. 7.1).

The description of all terms in the system is provided in Table 7.1.
The following is a breakdown of all the terms of Table 7.1.

G_{PL} — Direct and reflected solar radiation transmitted by the glass and absorbed by the lid of the pot

This term can be written as:

$$G_{\mathrm{PL}} = (G_{\mathrm{bm}} + A_{\mathrm{pl}} G_{\mathrm{bn}}) \tau_{\mathrm{g}} \alpha_{\mathrm{l}} \tag{7.13}$$

where:

- G_{bn} is the direct solar irradiance, i.e. DNI;
- G_{bm} is the solar radiation reflected by the mirrors.

Regarding the latter, the contribution from each mirror of the concentrating system had to be considered. In particular, the inclination with respect to the glass, the areas and the view factors with the lid of the 4 square mirrors as well as those of the 4 wedge-shaped mirrors were taken into account.

Considering that the solar cooker is constantly optimally positioned with respect to the sun, it was assumed that all solar radiation incident on the mirrors reached the glass surface. The view factors represent the fraction of reflected solar radiation leaving the reflective surfaces of the square and wedge mirrors and intercepting the element being considered. If the element considered is the glass, as a consequence of the assumption above, the view factor is equal to 1 for every mirror.

The solar radiation collected in the lid of the pot is:

$$G_{\mathrm{PL}} = (DNI \cdot P_m(Flid_{\mathrm{mq}} 4A_{\mathrm{mq}} \cos\phi_{\mathrm{mq}} + Flid_{\mathrm{mc}} 4A_{\mathrm{mc}} \cos\phi_{\mathrm{mc}}) + A_{\mathrm{pl}} DNI)\tau_{\mathrm{g}}\alpha_{\mathrm{l}} \quad (7.14)$$

where:

- P_m is the reflectance of mirrors;
- $Flid_{\mathrm{mq}}$ and $Flid_{\mathrm{mc}}$ are the view factors of the square and wedge-shaped mirrors with the lid;
- A_{mq} and A_{mc} are the areas of the square and wedge-shaped mirrors;
- ϕ_{mq} and ϕ_{mc} are the inclinations of square and wedge-shaped mirrors with respect to the horizontal;
- A_{pl} is the area of the lid of the pot;
- τ_{g} is the transmittance of glass;
- α_{l} is the absorbance of the lid of the pot.

G_{PS} — Direct and reflected solar radiation transmitted by the glass and absorbed by the pot

This term can be written as:

$$G_{\mathrm{PS}} = (G_{\mathrm{bm_p}} + A_{\mathrm{ps}} G_{\mathrm{bn_p}})\tau_{\mathrm{g}}\alpha_{\mathrm{p}} \quad (7.15)$$

where:

- $G_{\mathrm{bn_p}}$ is the direct solar irradiance, i.e. DNI;
- $G_{\mathrm{bm_p}}$ is the solar radiation reflected by the mirrors and then transmitted by the glass and absorbed by one half of pot.

For the first term, i.e. $G_{\mathrm{bn_p}}$, only the amount of direct solar radiation incident on one half of the lateral surface of the pot was considered: being the solar cooker always correctly oriented with respect to the sun's rays, only the front face of the pot was affected by direct rays. The other half of the surface of the pot remained unlit inside the cooking chamber.

Regarding the latter, as for the G_{bm} term in equation 7.13, the contribution from each mirror of the concentrating system had to be considered. In particular, the inclination with respect to the glass, the areas and the view factors with the lid of the 4 square mirrors as well as those of the 4 wedge-shaped mirrors were taken into account.

Thus, the solar radiation collected in the pot was:

$$G_{\mathrm{PS}} = (DNI \cdot P_m(Fp_{\mathrm{mq}} 4A_{\mathrm{mq}} \cos\phi_{\mathrm{mq}} + Fp_{\mathrm{mc}} 4A_{\mathrm{mc}} \cos\phi_{\mathrm{mc}}) + 0.5A_{\mathrm{ps}} DNI)\tau_{\mathrm{g}}\alpha_{\mathrm{p}} \quad (7.16)$$

where:

- Fp_{mq} and Fp_{mc} are the view factors of the square and wedge-shaped mirrors with the pot;
- A_{ps} is the area of the pot's side;
- α_{p} is the absorbance of the pot.

G_{G} — Direct and reflected solar radiation reflected from the mirrors and absorbed by the glass

$$G_{\mathrm{G}} = (G_{\mathrm{g_rif}} + A_{\mathrm{g}} G_{\mathrm{g_d}})\alpha_{\mathrm{g}} \quad (7.17)$$

where:

- $G_{\mathrm{g_d}}$ is the direct solar irradiance, i.e. DNI;
- $G_{\mathrm{g_rif}}$ is the solar radiation reflected by the mirrors to the glass.

Regarding the latter, also in this case, as for the previous solar radiation reflected terms G_{bm} and $G_{\mathrm{bm_p}}$, the contribution from each mirror of the concentrating system has to be considered.

Thus, the solar radiation collected in the glass is:

$$G_{\mathrm{G}} = (DNI \cdot P_m(Fg_{\mathrm{mq}} 4A_{\mathrm{mq}} \cos\phi_{\mathrm{mq}} + Fg_{\mathrm{mc}} 4A_{\mathrm{mc}} \cos\phi_{\mathrm{mc}}) + A_{\mathrm{g}} DNI)\alpha_{\mathrm{g}} \quad (7.18)$$

where:

- Fg_{mq} and Fg_{mc} are the view factors of the square and wedge-shaped mirrors with the glass;
- A_{g} is the area of the glass;
- α_{g} is the absorbance of the glass.

G_{A} — Direct and reflected solar radiation transmitted from the glass and absorbed by the absorber

$$G_{\mathrm{A}} = (G_{\mathrm{a_rif}} + (A_{\mathrm{ab}} - A_{\mathrm{pb}})G_{\mathrm{a_d}})\tau_{\mathrm{g}}\alpha_{\mathrm{a}} \quad (7.19)$$

where:

- $G_{\mathrm{a_d}}$ is the direct solar irradiance, i.e. DNI;
- $G_{\mathrm{a_rif}}$ is the solar radiation reflected by the mirrors to the absorber.

In this case, the final area involved in the absorption of direct solar radiation is given by the difference between the base surface of the absorber plate and the surface of the base of the pot.

Regarding the latter, also in this case, as for the previous solar radiation reflected terms G_{bm}, $G_{\mathrm{bm_p}}$ and $G_{\mathrm{g_rif}}$, the contribution from each mirror of the concentrating system has to be considered.

Thus, the solar radiation collected in the absorber is:

$$G_{\mathrm{A}} = (DNI \cdot P_m(Fa_{\mathrm{mq}} 4A_{\mathrm{mq}} \cos\phi_{\mathrm{mq}} + Fa_{\mathrm{mc}} 4A_{\mathrm{mc}} \cos\phi_{\mathrm{mc}}) + (A_{\mathrm{ab}} - A_{\mathrm{pb}})DNI)\tau_{\mathrm{g}}\alpha_{\mathrm{a}} \tag{7.20}$$

where:

- Fa_{mq} and Fa_{mc} are the view factors of the square and wedge-shaped mirrors with the absorber;
- A_{ab} and A_{pb} are the areas of the bottom of the absorber plate and of the bottom of the pot, respectively;
- α_{a} is the absorbance of the absorber plate.

$\dot{Q}_{\mathrm{c,PL-AIR}}$ — Convection heat flow from the lid of the pot to the air inside the cooking chamber

This term can be written as:

$$\dot{Q}_{\mathrm{c,PL-AIR}} = h_{\mathrm{c,PL-AIR}} A_{\mathrm{pl}} (T_{\mathrm{l}} - T_{\mathrm{air}}) \tag{7.21}$$

where T_{l} and T_{air} are the lid and the air temperatures, respectively, and A_{pl} is the area of the lid of the pot. The convective heat transfer coefficient of the air, $h_{\mathrm{c,PL-AIR}}$ was calculated using equation 7.3.

In this case, for this particular geometry, it was possible to use a known relationship by [224] to calculate the Nusselt number: the horizontal plate, i.e. the lid, has a higher temperature than the air inside the cooking chamber above it. This is the case of an upper surface of a hot plate.

As previously shown in section 7.2.2, the formula to calculate the Nusselt number, depends in turn on the Rayleigh number. In this case, with this particular geometry the check to be made is:

$$Nu = \begin{cases} 0.54 Ra^{1/4} & \text{if } 10^4 \leq Ra \leq 10^7 \\ 0.15 Ra^{1/3} & \text{if } 10^7 \leq Ra \leq 10^{11} \end{cases}$$

where Ra is the Rayleigh number, calculated using equation 7.8. It was then necessary to consider the coefficient of thermal expansion β, the specific heat c_{p}, the density ρ, the thermal conductivity λ and the dynamic viscosity μ of the air. As for the temperature delta, the difference between the lid temperature and the temperature of the air inside the cooking chamber was taken into account. The characteristic length relates to the ratio of the area of the lid to its perimeter.

In this case of laminar motion conditions the convective heat transfer coefficient is:

$$h_{\mathrm{c,PL-AIR}} = 0.54 Ra^{1/4} \frac{\lambda_{\mathrm{air}}}{L_{\mathrm{c,PL-AIR}}} \tag{7.22}$$

$\dot{Q}_{\mathrm{c,PL-airPot}}$ — **Convection heat flow from the lid of the pot to the air inside the pot**

This term can be written as:

$$\dot{Q}_{\mathrm{c,PL-airPot}} = h_{\mathrm{c,PL-airPot}} A_{\mathrm{pl}} (T_{\mathrm{l}} - T_{\mathrm{airPot}}) \tag{7.23}$$

where T_{airPot} is the temperature of the air inside the pot. The convective heat transfer coefficient of the air $h_{\mathrm{c,PL-airPot}}$ is calculated using equation 7.3.

The horizontal plate, i.e. the lid, has a higher temperature than the air inside the pot. In this case the Nusselt number is given by [224]:

$$(10^5 \leq Ra \leq 10^{11}) \qquad\qquad Nu = 0.27 Ra^{1/4} \tag{7.24}$$

Again, the Rayleigh number (equation 7.8) was calculated considering the thermophysical properties of the air. The temperature delta, on the other hand, was given by the difference between the temperature of the lid and the temperature of the air inside the pot.

Thus, the convective heat flux from the lid of the pot to the air inside the pot is:

$$\dot{Q}_{\mathrm{c,PL-airPot}} = 0.27 Ra^{1/4}_{\mathrm{PL-airPot}} \frac{\lambda_{\mathrm{air}}}{L_{\mathrm{c,PL-airPot}}} A_{\mathrm{pl}} (T_{\mathrm{l}} - T_{\mathrm{airPot}}) \tag{7.25}$$

$\dot{Q}_{\mathrm{r,PL-G}}$ — **Radiation heat flow from the lid of the pot to the glass**

This term can be written as:

$$\dot{Q}_{\mathrm{r,PL-G}} = A_{\mathrm{pl}} \epsilon_{\mathrm{l}} \sigma (T_{\mathrm{l}}^4 - T_{\mathrm{g}}^4) \tag{7.26}$$

where T_{g} is the glass temperature and ϵ_{l} is the emissivity of the lid.

The heat transfer by radiation between two surfaces A_1 and A_2 (the lid and the cover) could be calculated using expression 7.11, which, in this case, could be approximated with 7.12.

$\dot{Q}_{\mathrm{r,PL-F}}$ — **Radiation heat flow from the lid of the pot to the fluid**

This term can be written as:

$$\dot{Q}_{\mathrm{r,PL-F}} = A_{\mathrm{pl}} \epsilon_{\mathrm{l}} \sigma (T_{\mathrm{l}}^4 - T_{\mathrm{f}}^4) \tag{7.27}$$

where T_{f} is the fluid temperature.

It can be seen from the equation that, as with the previous radiant heat flow term $\dot{Q}_{\mathrm{r,PL-G}}$, this quantity could also be calculated using the simplified equation 7.12.

$\dot{Q}_{\mathrm{k,AB-PB}}$ — **Conduction heat flow from the bottom of the absorber plate to the bottom of the pot**

This term can be written as:

$$\dot{Q}_{\mathrm{k,AB-PB}} = \frac{\lambda_{\mathrm{p}} (T_{\mathrm{a}} - T_{\mathrm{p}}) A_{\mathrm{pb}}}{X_{\mathrm{p}}} \tag{7.28}$$

where T_{a} and T_{p} are the temperatures of the absorber plate and the pot, respectively. A_{pb} and X_{p} are the area of the bottom pot and the thickness of the pot, respectively. λ_{p} is the thermal conductivity of the pot.

$\dot{Q}_{\mathrm{c,PS-F}}$ — **Convection heat flow from the pot's side to the fluid**

This term can be written as:

$$\dot{Q}_{\mathrm{c,PS-F}} = h_{\mathrm{c,PS-F}} A_{\mathrm{ps}} (T_{\mathrm{p}} - T_{\mathrm{f}}) \tag{7.29}$$

where T_{p} and T_{f} are the temperatures of the pot and the fluid, respectively, and A_{ps} is the are of the pot's side. The geometry of the pot is that of a vertical cylinder, therefore the case could be treated as a vertical plate when the following condition is met:

$$D_{\mathrm{p}} \geq \frac{35 L_{\mathrm{p}}}{Gr^{1/4}} \tag{7.30}$$

where:

- D_{p} is the pot diameter;
- L_{p} is the pot height;
- Gr is the Grashof number.

The Grashof number could be calculated using equation 7.6 by including in the formula the thermophysical properties of the fluid, specifically the coefficient of thermal expansion β and the kinematic viscosity ν. As far as the temperature delta is concerned, the difference between pot temperature and fluid temperature was considered.

Once the previous condition 7.30 is met, it is possible to relate the cylinder (i.e. the pot) to the case of a vertical plate. The Nusselt number could then be calculated using the equation:

$$Nu = \left(0.825 + \frac{0.387 Ra^{1/6}}{\left(1 + (\frac{0.492}{Pr})^{9/16}\right)^{8/27}} \right)^2 \tag{7.31}$$

where Ra and Pr are the Rayleigh and the Prandtl numbers and could be computed using equations 7.8 and 7.5, respectively. For their determination, the thermophysical properties of the fluid in the pot, i.e. the coefficient of thermal expansion β, the specific heat c_{p}, the density ρ, the thermal coefficient λ and kinematic viscosity ν were used. As far as the temperature delta is concerned, the difference between pot temperature and fluid temperature was considered. For the determination of the Prandtl number, the dynamic viscosity μ, the specific heat c_{p} and the thermal conductivity λ of the fluid were taken into consideration.

Thus, the convective heat transfer coefficient is:

$$h_{\mathrm{c,PS-F}} = \frac{\lambda_{\mathrm{f}}}{L_{\mathrm{c,PS-F}} Nu_{\mathrm{PS-F}}} \tag{7.32}$$

$\dot{Q}_{\mathrm{c,PS-airPot}}$ — **Convection heat flow from the pot's side to the air inside the pot**

This term can be written as:

$$\dot{Q}_{\mathrm{c,PS-airPot}} = h_{\mathrm{c,PS-airPot}} A_{\mathrm{ps}} (T_{\mathrm{p}} - T_{\mathrm{airPot}}) \tag{7.33}$$

where T_{airPot} is the temperature of the air inside the pot. T_{p} and A_{ps} are the pot temperature and the pot's side area as defined for the previous term.

As in the previous case ($\dot{Q}_{\mathrm{c,PS-F}}$), the cylinder (i.e. the pot) could be treated as a vertical plate. It was therefore possible to calculate the Nusselt number using equation 7.31 as done before. In this case, the only difference with respect to the previous case was that for the calculation of the Rayleigh and the Prandtl numbers, the thermophysical properties to be considered were no longer the ones of the fluid but those of the air. As far as the temperature delta is concerned, the difference between pot temperature and temperature of the air inside the pot was considered.

$\dot{Q}_{\mathrm{c,PB-F}}$ — Convection heat flow from the bottom of the pot to the fluid

This term can be written as:

$$\dot{Q}_{\mathrm{c,PB-F}} = h_{\mathrm{c,PB-F}} A_{\mathrm{pb}} (T_{\mathrm{p}} - T_{\mathrm{f}}) \tag{7.34}$$

where T_{f} and A_{pb} are the fluid temperature and the area of the bottom of the pot.

In this case, the horizontal plate, i.e. the bottom of the pot, has a higher temperature than that of the fluid inside the pot, which is the case of an upper surface of a hot plate. With this particular geometry, the check to be made is therefore the same as for the case of heat transfer by convection between the air inside the pot and the lid ($\dot{Q}_{\mathrm{c,PL-airPot}}$).

Surely the case is again of laminar motion conditions so the convective heat transfer coefficient is:

$$h_{\mathrm{c,PB-F}} = 0.54 Ra^{1/4} \frac{\lambda_{\mathrm{f}}}{L_{\mathrm{c,PB-F}}} \tag{7.35}$$

where Ra is the Rayleigh number. The formula for its calculation is equation 7.8. In this case it was necessary to consider the coefficient of thermal expansion β, the specific heat c_{p}, the density ρ, the thermal conductivity λ and the dynamic viscosity μ of the fluid. As for the temperature delta, the difference between the pot temperature and fluid temperature was taken into consideration.

$\dot{Q}_{\mathrm{c,PS-AIR}}$ — Convection heat flow from the pot's side to the air inside the cooking chamber

This term can be written as:

$$\dot{Q}_{\mathrm{c,PS-AIR}} = h_{\mathrm{c,PS-AIR}} A_{\mathrm{ps}} (T_{\mathrm{p}} - T_{\mathrm{air}}) \tag{7.36}$$

where T_{air} and A_{ps} are the temperature of the air inside the cooking chamber and the area of the pot's side, respectively. The geometry of the pot, as said before, is a vertical cylinder, therefore the problem could be treated as a vertical plate when the condition 7.30 is verified met. For the calculation of the Grashof number using equation 7.6, it was important to consider the thermophysical properties of the air.

It was then possible to calculate the Nusselt number using equation 7.31 where, for the determination of the Rayleigh and the Prandtl numbers, the thermophysical properties of the air were used. With regards to the temperature delta, the difference between pot temperature and temperature of the air inside the cooking chamber was considered.

$\dot{Q}_{\mathrm{r,AS-PS}}$ — **Radiation heat flow from the side absorber to the pot's side**

This term can be written as:

$$\dot{Q}_{\mathrm{r,AS-PS}} = A_{\mathrm{ps}}\epsilon_{\mathrm{p}}\sigma(T_{\mathrm{a}}^4 - T_{\mathrm{p}}^4) \tag{7.37}$$

where T_{a} and T_{p} are the absorber and the pot temperatures, respectively. ϵ_{p} is the emissivity of the pot while σ is the Stefan-Boltzmann constant.

$\dot{Q}_{\mathrm{c,airPot-F}}$ — **Convection heat flow from the air inside the pot to the fluid**

This term can be written as:

$$\dot{Q}_{\mathrm{c,airPot-F}} = h_{\mathrm{c,airPot-F}}A_{\mathrm{pb}}(T_{\mathrm{airPot}} - T_{\mathrm{f}}) \tag{7.38}$$

where T_{airPot} and T_{f} are the air inside the pot and the fluid temperatures. A_{pb} is the area of the bottom of the pot.

As for the quantity $\dot{Q}_{\mathrm{c,PL-airPot}}$ also in this case, thhe air inside the pot had a higher temperature than that of the fluid. Therefore, to determine the Nusselt and Rayleigh numbers necessary for the calculation of the convective heat transfer coefficient $h_{\mathrm{c,airPot-F}}$ the same known relation could be used [224].

Thus, the convective heat flux from the air inside the pot to the fluid is:

$$\dot{Q}_{\mathrm{c,airPot-F}} = 0.27Ra_{\mathrm{airPot-F}}^{1/4}\frac{\lambda_{\mathrm{air}}}{L_{\mathrm{c,airPot-F}}}A_{\mathrm{pb}}(T_{\mathrm{airPot}} - T_{\mathrm{f}}) \tag{7.39}$$

$\dot{Q}_{\mathrm{c,G-AMB}}$ — **Convection heat flow from the glass to the external ambient temperature**

This term can be written as:

$$\dot{Q}_{\mathrm{c,G-AMB}} = h_{\mathrm{c,G-AMB}}A_{\mathrm{g}}(T_{\mathrm{g}} - T_{\mathrm{amb}}) \tag{7.40}$$

where T_{g} and T_{amb} are the glass and the ambient temperatures. A_{g} is the glass cover area. The convective heat transfer coefficient was calculated from the following relationship [225]:

$$h_{\mathrm{c,G-AMB}} = 5.7 + 3.8U \tag{7.41}$$

with U equal to the wind speed.

$\dot{Q}_{\mathrm{c,G-AIR}}$ — **Convection heat flow from the glass to the air inside the cooking chamber**

This term can be written as:

$$\dot{Q}_{\mathrm{c,G-AIR}} = h_{\mathrm{c,G-AIR}}A_{\mathrm{g}}(T_{\mathrm{g}} - T_{\mathrm{air}}) \tag{7.42}$$

This is the case of a lower surface of a hot plate, with ($10^5 \leq Ra \leq 10^{11}$). The glass is at a higher temperature than the air inside the cooking chamber. With equation 7.25 it was possible to calculate the Nusselt and the Rayleigh numbers for the air.

Thus, the convective heat flux from the glass cover to the air inside the cooking chamber is:

$$\dot{Q}_{\mathrm{c,G-AIR}} = 0.27Ra_{\mathrm{G-AIR}}^{1/4}\frac{\lambda_{\mathrm{air}}}{L_{\mathrm{c,G-AIR}}}A_{\mathrm{g}}(T_{\mathrm{g}} - T_{\mathrm{air}}) \tag{7.43}$$

$\dot{Q}_{\mathrm{r,AB-G}}$ — Radiation heat flow from the bottom of the absorber plate to the glass

This term can be written as:

$$\dot{Q}_{\mathrm{r,AB-G}} = (A_{\mathrm{ab}} - A_{\mathrm{pb}})\epsilon_{\mathrm{a}}\sigma(T_{\mathrm{a}}^4 - T_{\mathrm{g}}^4) \tag{7.44}$$

where T_{a} and T_{g} are the absorber plate and the glass temperatures. A_{ab} and A_{pb} are the bottom of the absorber plate and the bottom of the pot areas. ϵ_{a} and σ are the emissivity of the absorber plate and the Stefan-Boltzmann constant.

In this case, the final area involved in the radiative heat exchange was not the total surface of the absorber plate. In fact, the base area of the pot, which did not exchange directly with the glass, was removed.

$\dot{Q}_{\mathrm{r,G-SKY}}$ — Radiation heat flow from the glass to the sky

This term can be written as:

$$\dot{Q}_{\mathrm{r,G-SKY}} = A_{\mathrm{g}}\epsilon_{\mathrm{g}}\sigma(T_{\mathrm{g}}^4 - T_{\mathrm{sky}}^4) \tag{7.45}$$

where T_{sky} is the sky temperature while A_{g} is the glass cover area. ϵ_{g} is the emissivity of the glass. It could be calculated according to the relationship [225]:

$$T_{\mathrm{sky}} = 0.0552T_{\mathrm{amb}}^{1.5} \tag{7.46}$$

where T_{amb} is the ambient temperature.

$\dot{Q}_{\mathrm{kc,A-AMB}}$ — Heat flow from the absorber to the external ambient

This term can be written as:

$$\dot{Q}_{\mathrm{kc,A-AMB}} = (A_{\mathrm{ab}} + A_{\mathrm{as}})R_{\mathrm{eq}}(T_{\mathrm{a}} - T_{\mathrm{amb}}) \tag{7.47}$$

where A_{ab} and A_{as} are the areas of the bottom of the absorber and the absorber side. T_{a} and T_{amb} are the absorber and the ambient temperatures. R_{eq} is the equivalent resistance and is equal to:

$$R_{\mathrm{eq}} = \frac{1}{(\frac{X_{\mathrm{i}}}{\lambda_{\mathrm{i}}}) + (\frac{1}{h_{\mathrm{c,i-amb}}})(\frac{A_{\mathrm{i}}}{A_{\mathrm{ab}}+A_{\mathrm{as}}})} \tag{7.48}$$

where:

- X_{i} is the thickness of the insulation;
- λ_{i} is the thermal conductivity of the insulation;
- $h_{\mathrm{c,i-amb}}$ is the thermal convection coefficient between the insulation layer and the external temperature (refer to equation 7.41);
- A_{i}, A_{ab} and A_{as} are the insulation, the bottom of the absorber and the absorber side areas.

$\dot{Q}_{\mathrm{c,AS-AIR}}$ — **Convection heat flow from the absorber side to the air inside the cooking chamber**

This term can be written as:

$$\dot{Q}_{\mathrm{c,AS-AIR}} = h_{\mathrm{c,AS-AIR}} A_{\mathrm{as}} (T_{\mathrm{a}} - T_{\mathrm{air}}) \tag{7.49}$$

where T_{a} and T_{air} are respectively the absorber temperature and the temperature of the air inside the cooking chamber.

The side surface of the absorber is a vertical plate, so in this case it is possible to use equation 7.31 to compute the Nusselt number. Whereas for the determination of the Rayleigh and the Prandtl numbers needed for the calculation of the Nusselt number, the thermophysical properties of the air were used.

$\dot{Q}_{\mathrm{c,AB-AIR}}$ — **Convection heat flow from the bottom of the absorber to the air inside the cooking chamber**

This term can be written as:

$$\dot{Q}_{\mathrm{c,AB-AIR}} = h_{\mathrm{c,AB-AIR}} (A_{\mathrm{ab}} - A_{\mathrm{pb}}) (T_{\mathrm{a}} - T_{\mathrm{air}}) \tag{7.50}$$

where A_{ab} and A_{pb} are the bottom of the absorber and the bottom of the pot areas.

In this case, the horizontal plate, i.e. the bottom of the absorber plate, has a higher temperature than that of the bottom of the pot. This is the condition of an upper surface of a hot plate.

With no doubt the case is again that of laminar motion conditions ($10^4 \leq Ra \leq 10^7$) so the convective heat transfer coefficient is:

$$h_{\mathrm{c,AB-AIR}} = 0.54 Ra_{\mathrm{AB-AIR}}^{1/4} \frac{\lambda_{\mathrm{air}}}{L_{\mathrm{c,AB-AIR}}} \tag{7.51}$$

The formula for the calculation of the Rayleigh number was equation 7.8. It is then necessary to consider the coefficient of thermal expansion β, the specific heat c_{p}, the density ρ, the thermal conductivity λ and the dynamic viscosity μ of the air. As for the temperature delta, the difference between the temperature of the absorber and the temperature of the air inside the cooking chamber was considered.

The surface area subject to convection is not the entire base of the absorber: the bottom of the pot, which exchanges heat by conduction with the absorber, must be removed. Therefore, since the surface has an irregular shape, the characteristic length $L_{\mathrm{c,AB-AIR}}$ is calculated as the ratio between the difference of the area of the absorber base and that of the bottom of the pot and the average of the perimeters: $L_{\mathrm{c,AB-AIR}} = 2(A_{\mathrm{ab}} - A_{\mathrm{pb}})/(p_{\mathrm{ab}} - p_{\mathrm{pb}})$.

7.4 Model Implementation

The system of equations representing the behavior of the portable solar box cooker is a system of seven coupled nonlinear differential equations of fourth order. The unknowns are the temperatures of the seven elements composing the solar box cooker.

The mathematical model was developed entirely in MATLAB [196].

The convective heat transfer coefficients h_c, which depend on the temperature difference of the two bodies participating in the heat exchange process (and hence

change as the temperatures evolve), were also calculated at each step based on the considerations reported above.

7.4.1 Input Parameters and Input Variables

In this section, the information which constituted an input for the mathematical model is listed.

To begin with, two different types of input values must be distinguished: input parameters and input variables. The former represent the geometrical, optical and thermal characteristics of the various elements composing the chosen solar box cooker prototype. These parameters do not change with temperature nor over time. All numerical values for the input parameters are detailed in Appendix C. The latter instead represent physical quantities that do change during an experimental test. Such parameters are ambient temperature and DNI.

The mathematical model developed gives the flexibility to set constant values for the input variables or to consider the actual values measured during a test when comparing the output of the model with experimental data. This is an important feature for the evaluation of the model's fidelity and thus for its validation.

7.4.2 Resolutive Methods

The system of differential equations is solved numerically through time using the 4^{th} order Runge-Kutta method, in particular making use of the function *ode*45 which is already available in MATLAB [226].

Figure 7.10 depicts the n-th integration step and the process to calculate the next step parameters, and also lists the initial conditions.

Each solution is calculated in a time interval between t_{start} and t_{end}, which represents the duration of the experimental test with which the results were compared.

As an initial condition, the temperature for all the elements of the system is set equal to the fluid temperature at the beginning of the test considered.

7.4.3 Model Output

The output of the model are the temperature evolutions in time of all the elements of the solar box cooker during the selected time interval given the considered initial conditions and external factors.

Of particular interest is, of course, the fluid temperature, which was used to evaluate the adherence to reality of the model.

7.5 Results

In this section, a comparison between the output of the model and the quantities measured on the actual solar cooker prototype modelled is presented. In particular, a test with water and a test with silicone oil were taken as examples.

7.5.1 Test with Water

On the 1^{st} of June 2018 the solar box cooker was loaded with 2 kg of water. Given the mild ambient temperature of around 27 °C and a particularly favorable solar radiation, the water was brought to boiling in about 1.5 hours.

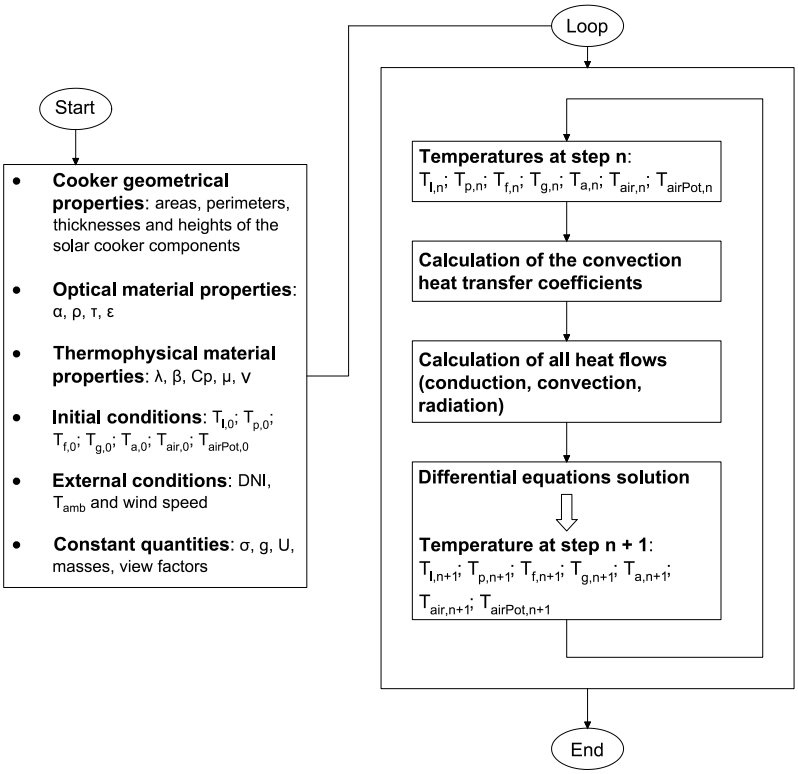

Figure 7.10: Integration loop scheme.

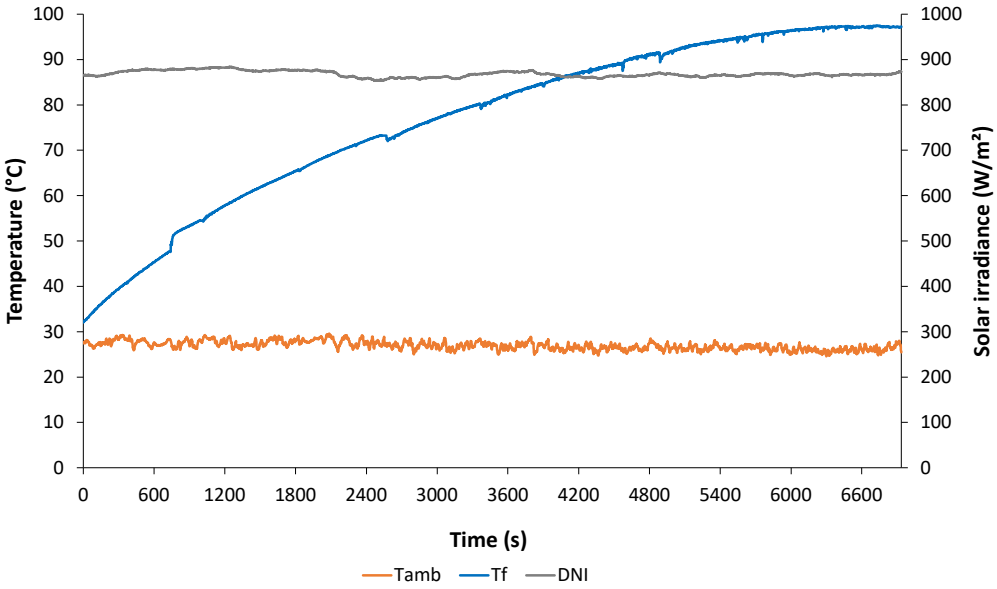

Figure 7.11: Test with water carried out on 01/06/2018.

Table 7.2: Model outputs for the test with water of 01/06/2018 sampled every 20 minutes.

Date	Time (hh:mm:ss)	Tl (°C)	Tp (°C)	Tf (°C)	Tg (°C)	Ta (°C)	Tair (°C)	TairPot (°C)
01/06/2018	11:49:40	32.01	32.01	32.01	32.01	32.01	32.01	32.01
01/06/2018	12:09:40	156.65	60.63	55.78	38.99	60.67	66.17	76.51
01/06/2018	12:29:40	168.63	76.21	73.05	45.39	76.26	79.86	91.93
01/06/2018	12:49:40	175.19	85.89	83.80	48.31	85.92	87.81	101.34
01/06/2018	13:09:40	178.84	92.02	90.76	50.26	92.00	92.61	107.24
01/06/2018	13:29:40	181.67	95.97	95.36	51.72	95.96	95.65	111.18

Figure 7.11 reports the trends of water and ambient temperatures, and direct normal solar irradiance for the mentioned test. The average solar irradiance was 868 $\mathrm{W/m^2}$.

The model was set up to simulate this test. As explained above, the DNI and T_{amb} measured during the test were taken as input for the model.

Table 7.2 reports a subset of the temperatures for the various solar cooker components calculated by the model. Figure 7.12 shows the comparison between the fluid temperature measured during the test and the one calculated via the model. As it can be seen, the temperature measured and the numerical results are in very good agreement, showing a maximum relative error of 3% throughout most of the test.

In particular, the temperature trends between the experimental and numerical data are matching, which demonstrates that the model simulated the solar box cooker performance with a high degree of precision.

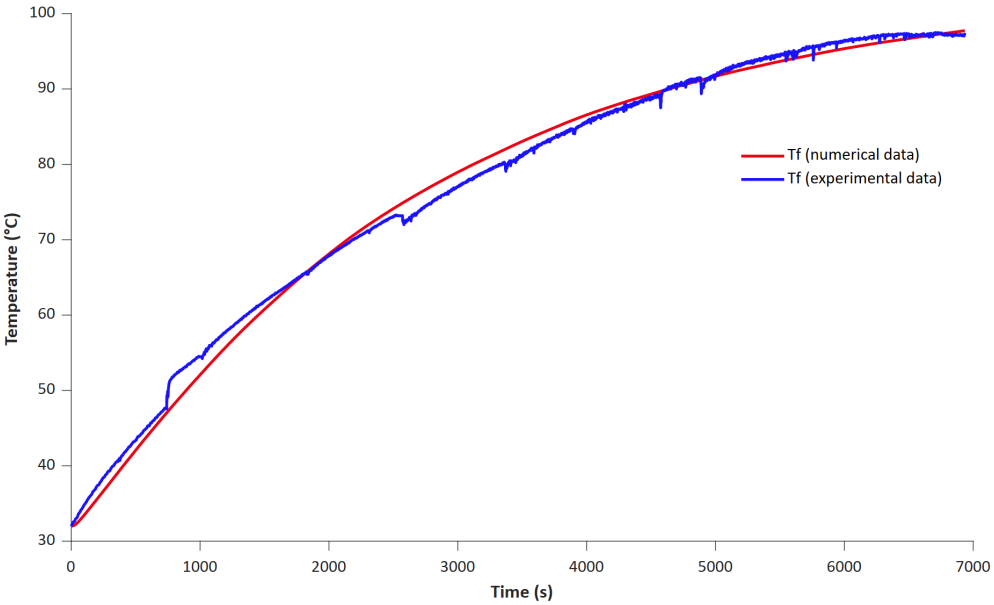

Figure 7.12: Comparison between experimental water temperature (test of 01/06/2018) and numerical results.

7.5.2 Test with Silicone Oil

On the 10th of July 2018 a test with silicone oil was conducted. The fluid mass in this case was 1.5 kg and its temperature was brought from 50 °C to more than 175 °C by the solar box cooker in about 4 hours.

Figure 7.13 reports the trends of the silicone oil and ambient temperatures, and direct normal solar irradiance for the mentioned test. The average solar irradiance was 830 W/m^2, while the average ambient temperature was 30 °C.

Table 7.3 reports a subset of the temperatures for the various solar cooker components calculated by the model. Figure 7.14 shows the comparison between the silicone oil temperature measured during the test and the one obtained as output from the model. It can be seen that also in this case the measured temperature and the numerical results are in good agreement. The maximum relative error throughout most of the test amounted to 8%.

As for the previous test, a good match can be observed between the temperature trends of the two curves, i.e. the numerical results follow the experimental silicone oil heat up-phase with good agreement. There is, however, a seemingly bigger thermal inertia at the beginning of the numerical simulation, which caused the temperature curve produced by the model to be shifted in time, thus provoking the larger aforementioned deviation.

The reason for this delta is to be found in the initial conditions of the test.

While the solar box cooker was being positioned and exposed to the sun, the test bench set up and the test fluid loaded inside the cooking chamber, the temperature of its various components was already starting to increase because of the high performance of the device. Therefore, in this short time interval, a significant temperature difference between the fluid and the solar box cooker was already appreciable.

This in practice invalidates the initial conditions chosen for the model and causes

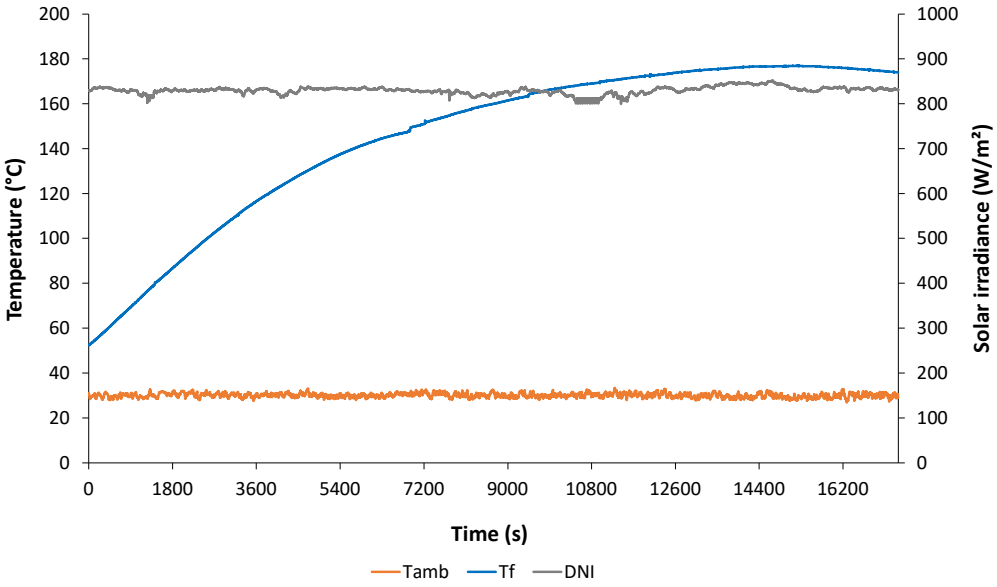

Figure 7.13: Test with silicone oil carried out on 10/07/2018.

the divergence observed between the experimental data and the numerical results. Trying to adapt the initial conditions to obtain better results is not very effective, as there is not enough information regarding the initial temperatures required by the model and this unfortunately is true also for the other tests.

When the experimental campaigns were performed, the purpose of the tests was to thermally characterize the solar box cooker and there was no intention yet of building a mathematical model of it and hence also no farsightedness in taking care of the initial conditions of each test, which, however, are of great importance when test data is used to validate a model.

Nevertheless, these results can still be considered good because, apart from the issue with the initial conditions, the model is able to represent the real behavior of the fluid temperature, whether it is water or silicone oil, and therefore it simulates the performance of the solar box cooker with a high level of precision.

7.6 Future Developments

As presented above, the mathematical model developed for the simulation of the behavior of the selected solar box cooker produces results which are in line with experimental data and follows with good agreement the trends observed during the real tests.

Of course there is room for improvement, for instance in the modelling of heat exchanges with the external environment and thus the evaluation of thermal losses. Another aspect to keep in mind for the future is a better control over the starting configuration of an experimental test, such as to avoid unnecessary difficulties in the selection of initial conditions when it comes to the mathematical model validation.

A big improvement for the model will be the introduction of a TES in the system equipped with a phase change material: this would allow the simulation of the additional material mass to be heated up together with the test fluid, the phase change of the

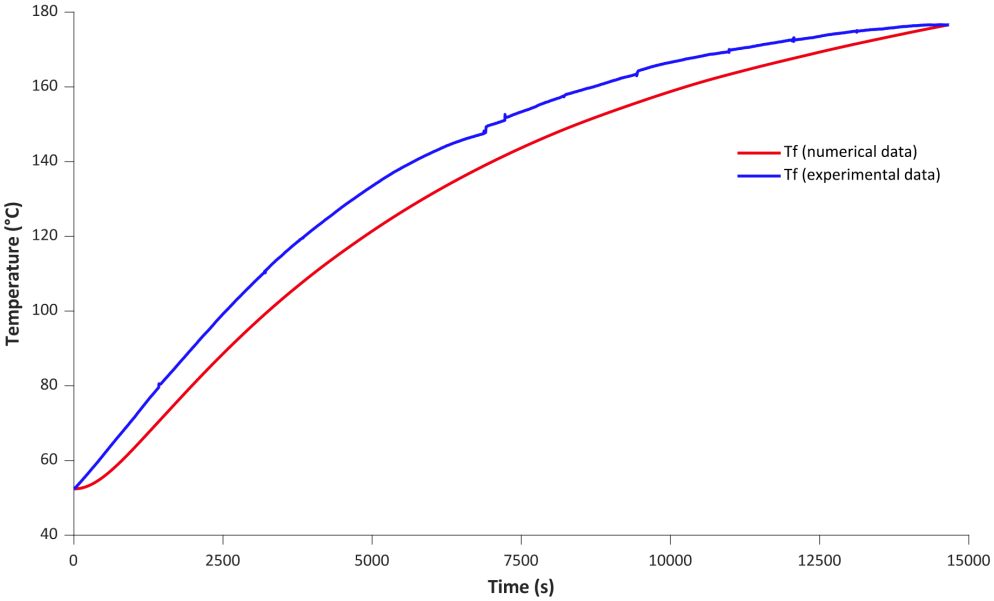

Figure 7.14: Comparison between experimental silicone oil temperature (test of 10/07/2018) and numerical results.

Table 7.3: Model outputs for the test with silicone oil of 10/07/2018 sampled every 20 minutes.

Date	Time (hh:mm:ss)	Tl (°C)	Tp (°C)	Tf (°C)	Tg (°C)	Ta (°C)	Tair (°C)	TairPot (°C)
10/07/2018	10:20:14	52.42	52.42	52.42	52.42	52.42	52.42	52.42
10/07/2018	10:40:14	180.05	133.30	66.60	60.32	133.34	123.41	123.53
10/07/2018	11:00:14	194.16	146.21	87.00	69.71	146.24	135.94	138.93
10/07/2018	11:20:14	199.62	150.36	104.69	72.09	150.31	139.85	147.49
10/07/2018	11:40:14	203.94	153.26	119.24	73.76	153.25	142.65	154.90
10/07/2018	12:00:14	207.60	155.30	131.37	74.42	155.26	144.57	160.38
10/07/2018	12:20:14	210.18	157.04	141.44	75.92	157.00	146.32	164.53
10/07/2018	12:40:14	211.69	157.29	149.78	75.90	157.29	146.65	167.06
10/07/2018	13:00:14	214.38	158.82	156.66	76.50	158.82	148.10	170.04
10/07/2018	13:20:14	214.43	158.31	162.55	76.79	158.28	147.76	170.97
10/07/2018	13:40:14	216.72	159.48	167.42	77.00	159.46	148.84	173.06
10/07/2018	14:00:14	219.30	161.17	171.83	77.59	161.16	150.40	175.40
10/07/2018	14:20:14	221.70	162.85	175.80	78.27	162.82	151.94	177.58
10/07/2018	14:40:14	221.65	162.38	179.23	78.24	162.36	151.61	177.65
10/07/2018	15:00:14	222.65	163.03	181.90	78.75	163.00	152.23	178.65

PCM and also, something that was not done yet, simulate the cooling phase of the system when the solar radiation is missing. This is of course of particular interest in the scope of compensating for the intermittent nature of this source of energy, because the larger the energy accumulated in the PCM, the longer the cooling period, which in turn allows for cooking or keeping the food warm also when the solar radiation is absent.

Chapter 8

Conclusions

The main objective of this thesis was to investigate the thermal performance of different types of solar cookers with the aim of understanding whether these devices can be considered a viable alternative to traditional cooking. The analyzed devices, belonging to the category of solar thermal systems, showed and shared among them many problems, but also many advantages that will be discussed and listed in this concluding chapter.

Indeed, the experimental campaigns carried out to experimentally characterize the devices have shown limitations by confirming that some categories of solar cookers are more performing than others, but also proved that all prototypes are able to make water reach boiling point in a relatively short time.

The experimental campaign carried out for the thermal and optical characterization of the Kimono and Newton, i.e. the two solar panel devices, confirmed the common judgment about this type of device. The prototypes proved to be very easy to make given the few manufacturing steps required, simple in their use and easily transportable. Having used mainly recycled materials, their final cost remained low. Of all the devices tested, they turned out to be the least performing, as expected from the beginning. The Kimono especially, being an open device with no thermally insulated and closed cooking chamber, is the prototype that suffered the most from the external conditions. In fact, among all the prototypes, it was the most affected by either the variability of solar radiation or wind intensity, leading to record a rapid drop in temperatures if at least one of the two listed conditions occurred. However, the devices were still able to not only bring water to a boil, but to reach temperatures in excess of 110 °C when tested with silicone oil and glycerin, but with extremely longer times than the other cookers tested.

Tests conducted to characterize the concentrating solar cooker have shown that, although it falls under the open devices category not being provided with an enclosed and insulated cooking chamber, the prototype is capable of cooking food in a healthy and fast manner. A key role is played by the Fresnel lens, which is able to concentrate a large amount of direct solar radiation onto the reflective surface and then onto the cooking surface. The prototype was found to perform very well in that it was able to bring 3 kg of water to a boil in about 30 minutes and heat 3 kg of silicone oil to 170 °C in less than an hour, confirming that if used to cook food it would certainly be able to and in a suitable time.

Experimental characterization performed on the high-efficiency solar box cooker proved that the prototype is capable of cooking food quickly and at high temperatures.

Excellent results were obtained in terms of the time required for the device to heat the test fluid to a chosen temperature, both by testing the prototype with water and by using peanut oil. In fact, the achieved temperature of 220 °C makes it possible to say that the cooker is able to cook food easily, in a short time, and sustainably. An unavoidable drawback of cooking at high temperatures is that a high level of solar concentration is required. This implies that only direct radiation can be used for this purpose, and this condition puts a limitation on the range of use of these devices, namely the need to have days with a clear sky, that is, free of clouds. In addition, solar cooking during the evening hours is very difficult to achieve, especially in the winter season during which the availability of solar radiation is limited to a few central hours of the day. This is a key aspect that has been evaluated in the planning of all experimental campaigns of the solar cookers under investigation.

These limitations can be overcome by considering the use of a thermal storage system. Its effect on the whole system when used together with a solar prototype was evaluated through the experimental campaign with the medium-efficiency solar box cooker. Starting from the solutions proposed and found in the literature, the thermal energy storage (TES) system was built. The latter consisted of two cylindrical steel pots connected to each other with, inside the cavity formed between them, the chosen phase change material. Considering the various properties that a phase change material should have in order to be considered suitable for the realization of the TES, considering the maximum temperature reached by the medium-efficiency box cooker, and considering that the selected material could come into contact with food, two sugar alcohols were selected as PCMs to be tested within the TES. The results obtained showed that not only did the inclusion of PCM-based TES help stabilize the entire system, but that cooking could continue even when radiation was intermittent or even absent. In fact, during the tests, the absence of solar radiation was simulated by darkening the device. The results showed that the heating times of the fluid contained in the TES during the heating phase increased compared to the times recorded when the device was tested with the normal pot. This effect was to be expected because of the additional mass of PCM to be heated along with that of the fluid. As for the cooling times calculated during the cooling phase, these were more than 350% longer than when calculated without the TES solution. The solar box cooker combined with the TES system was therefore able to maintain a given temperature for a much longer period of time allowing the operator to continue cooking.

From the various analyses carried out, regardless of the type of cooker, it has been found that having the receiver painted black allows the water to be brought to a boil or the tested fluid to reach high temperatures in relatively less time than when considering a standard pot. The geometry of the cooker and particularly the amount of mirrors the device is equipped with is another key aspect that affects the final thermal and optical performance. The choice of the storage system in terms of geometry, type of phase change material, and mass of the latter are also all aspects that play a primary role.

For this reason, the development of the mathematical model of the medium-efficiency solar box cooker is intended to be a starting point for being able to optimize the geometry of the prototype, the materials used in its construction, and the fluid masses to be tested. To date, the model has been validated with experimental tests carried out with water and with silicone oil obtaining results that deviate by an average of about 5% between real and numerical trends. The incorporation in the model of the latent contribution due to the insertion of a TES inside the cooking chamber with the aim of studying its effect on the whole system is something that is currently being studied. This would allow to evaluate numerically first and experimentally later

alternative solutions to sugars as phase change materials.

With this thesis, therefore, it has been confirmed that solar cookers can indeed be considered a viable alternative to traditional types of cooking. They are clean systems, easily implemented and usable by all, and the energy they require is abundant in nature, nonpolluting, accessible by all, and free. It has also been shown that the major disadvantage these devices have, namely the variability of the primary energy source, can be easily solved by using a thermal storage system based on phase change materials.

Appendix A

Standard International Procedures

A.1 Introduction

The growing need for alternative fuels for cooking purposes caused a boost in the research and development of solar cookers.

It is of crucial importance to use common coefficients and parameters in order to measure and catalogue the performance of such devices in order to ease the experiments results communication among the different researchers around the world and ultimately spread knowledge.

The goal of this appendix is therefore to present solar cooker test standards which analyse the behaviour and performance of the device and calculate its efficiency.

In order to achieve this, four test standards already existing in literature were taken as reference: these describe the parameters, environment and solar cooker conditions necessary to obtain standardized results.

The test procedures are:

- Procedure proposed by Khalifa et al. [172];
- Experimental test proposed by Mullick [19];
- Standard procedure by Funk [7];
- COR procedure [173].

A.2 Procedure Proposed by Khalifa et al.

The procedures to evaluate the performance of solar cookers consist in the determination of the following parameters:

- Cooking time for the different food products
- Required time to heat up a known quantity of fluid to the boiling point

Or

- Maximum measured temperature during a test without load.

The second and third methods are the best approaches considering that the first one implies uncertainties related to fluctuations in the ingredients and to personal taste of the observer in judging the cooking level of food. It is safe therefore to state that the first method is too subjective for the purpose of this thesis.

Khalifa et al. [172] used the second method to evaluate the solar cooker performance through the computation of the total thermal efficiency η_{av}, the specific boiling time t_s and the characteristic boiling time t_c.

The first and first parameter is t_s, expressed in $\text{h} \cdot \text{m}^2/\text{kg}$, which represents the required time to boil 1 kg of water using a solar cooker with $1\,\text{m}^2$ of aperture area; t_c, $\text{h} \cdot \text{m}^2/\text{kg}$, is used as a comparing parameter between different solar cookers with various levels of solar radiation.

The mathematical expressions to calculate t_s, t_c and η_{av} are provided in [172] and are:

$$t_s = \frac{\Delta t_h A_a}{m_f} \tag{A.1}$$

$$t_{\text{ch}} = t_s \frac{DNI_{\text{av}}}{DNI_{\text{ref}}} \tag{A.2}$$

$$\eta_{\text{av}} = \frac{m_f c_f \Delta T_f}{DNI_{\text{av}} A_a \Delta t_h} \tag{A.3}$$

where m_f and c_f are the mass (kg) and specific heat (J/kg K) of the fluid, Δt_h is the required time to reach the maximum temperature of the fluid, DNI_{av} the average direct normal solar irradiance (W/m^2) during the time interval Δt_h. DNI_{ref} represents the reference direct normal solar irradiance equal to $900\,\text{W/m}^2$. ΔT_f is the temperature difference between the final and initial fluid temperature during the time interval Δt_h, while A_a is the aperture area (m^2) of the solar cooker.

A.3 Experimental Test Proposed by Mullick

A.3.1 F_1 and F_2 Figures of Merit Determination

Mullick [19] proposed a standard test procedure for box solar cookers where the figures of merit F_1 and F_2 are determined respectively via the stagnation test (without load) and via heating up a known quantity of fluid.

The first figure of merit F_1 ($^\circ\text{C}/(\text{W/m}^2)$) is defined as:

$$F_1 = \frac{T_{\text{a,max}} - T_{\text{amb}}}{DNI} \tag{A.4}$$

where $T_{\text{a,max}}$ is the maximum temperature reachable by the absorber plate, while T_{amb} and DNI are the corresponding ambient temperature and normal solar irradiance measured when the stagnation temperature is reached.

The second figure of merit F_2 implies the measurement of the temperature increase over time of a known quantity of fluid contained in a pot, as described in the following:

$$F_2 = \frac{F_1 m_f\, c_f}{A_a \Delta t_h} \ln \left[\frac{1 - \frac{1}{F_1}(T_1 - T_{\text{amb,av}})/DNI_{\text{av}}}{1 - \frac{1}{F_1}(T_2 - T_{\text{amb,av}})/DNI_{\text{av}}} \right] \tag{A.5}$$

where Δt_h represents the time interval (s) required for the fluid to increase its temperature from T_1 (initial fluid temperature) to T_2 (final fluid temperature). DNI_{av} and $T_{\text{amb,av}}$ are the average solar irradiance (W/m^2) and the ambient temperature (°C) respectively in the considered time interval Δt_h. m_f, c_f and A_a are respectively, as mentioned above, the fluid mass (kg), specific heat (J/kg K) and the solar cooker aperture area (m^2).

A.4 Standard Procedure by Funk

Given the need to find a common format for the researchers to share their results and considering also the need for a single performance measure in order to ease the solar cooker selection by the consumers, the committee at the Third International Conference on Solar Cookers, convened in Coimbatore on the 9$^{\text{th}}$ of January 1997, agreed that the best parameter to represent the thermal performance is the effective cooking power expressed in W.

On this regard, Funk [7] analysed via experiments the thermal performance of a box solar cooker, studying the effects of all variables impacting the cooker and noticing that the best performance can be achieved with the maximum load in the pot.

A.4.1 Environmental Variables (Uncontrollable)

Hereafter are reported the uncontrolled weather variables and the optimal conditions for running tests as recommended by the committee [7].

Wind

Conduct solar cooker tests when wind is less than 1.0 m/s at the elevation of the cooker being tested. If the wind is over 2.5 m/s for more than 10 minutes, discard the test data.

Reason: heat loss is strongly influenced by wind velocity. Wind velocities less than 1.0 m/s help to maintain a heat loss coefficient close to the natural convection loss coefficient, yielding results that are more consistent and repeatable.

If wind shelter is required, it must be designed so as to not interfere with incoming total radiation.

Ambient Temperature

Conduct solar cooker tests when ambient temperatures are between 20 and 35 °C.

Reason: ambient extremes experienced in one location may be difficult to replicate at another location. Cooking power is influenced by temperature difference. A range of 15 °C keeps variability moderate, yet permits testing in most locations for at least half the year. Unavoidable exceptions need to be noted.

Pot Contents Temperature

Record data for water temperatures between 40 and 90 °C.

Reason (low end): pot contents must be above ambient for there to be heat losses.

Reason (high end): boiling temperature varies with elevation, and latent heat of vaporization severely depresses apparent cooking power as water nears boiling. Avoiding the upper limit reduces the probability of having anomalies in the data.

Insolation

Available solar energy is to be measured in the plane perpendicular to direct beam radiation (the maximum reading) using a radiation pyranometer. Variation in measured insolation greater than $100\,\mathrm{W/m^2}$ during a 10-minutes interval, or readings below $450\,\mathrm{W/m^2}$ or above $1100\,\mathrm{W/m^2}$ during the test render the test invalid.

Reason: maintaining moderate fluctuations in isolation levels reduces the variability caused by thermal inertia effects. Taking readings within 65% of the standard insolation level (which is $700\,\mathrm{W/m^2}$) reduces errors introduced by adjusting cooking power for available insolation. It is expected that most locations will meet these criteria. If not, exceptions need to be specially noted.

Solar Altitude and Azimuth

The committee strongly recommends that tests be conducted between 10:00 and 14:00 solar time.

Reason: solar zenith angle is somewhat constant at midday, and the difference between insolation measured in the plane of the cooker aperture and the plane perpendicular to direct beam radiation will vary least. Exceptions necessitated by solar variability (presence of clouds at midday during monsoon season) or ambient temperature (midday is too hot) must be specially noted.

A.4.2 Controlled (Cooker) Variables

Loading

Cookers are to have $7\,\mathrm{kg\,water/m^2}$ intercept area distributed evenly between the pots supplied with the cooker. Intercept area is defined as the sum of the reflector and aperture areas projected onto the plane perpendicular to direct beam radiation. The beam radiation zenith angle may be averaged over the test period. Tracking may compensate for the beam azimuth angle. These two strategies should result in a constant intercept area, facilitating load calculations.

Reasons: water closely resembles food in density and specific heat, but is more consistent. Intercepted radiation is the best measure of available energy. Thermal performance is sensitive to loading rate. This particular value is close to the various loading rates cited in previous publications.

Tracking

Azimuth angle tracking frequency must be appropriate to the cooker's acceptance angle. Box-type cookers typically require adjustment every 15 to 30 minutes or when shadows appear on the absorber plate. Parabolic-type units may require more frequent adjustment to keep the solar image focused on the pot or absorber. With box-type cookers, zenith angle tracking may be unnecessary during a 2-hours test conducted at midday. Testing should be representative of anticipated consumer habits.

Temperature Sensing

Thermocouples are recommended for their low cost, accuracy and rapid response. Use pot(s) supplied with the cooker. If unavailable, use inexpensive aluminium pots most likely to be employed by the consumer. Thermocouple junctions should be immersed in the fluid in the pot(s) and secured 10 mm above the pot bottom, at the

centre. Thermocouple leads are to come through the pot lid (or wall above the fluid line) inside a thermally nonconductive sleeve that will protect the thermocouple wire from bending and from temperature extremes. Secure the sleeve with silicone caulk to reduce vapor loss.

Reasons: proper thermocouple placement can minimize errors that might be caused by thermal stratification and sensor intrusion into the pot. The thermal storage capacity of inexpensive aluminium cooking pots is insignificant compared to the thermal storage capacity of the fluid contained by them.

A.4.3 Test Protocol

Hereafter are reported the steps to follow for the elaboration of the data collected during the test in order to obtain the final graph. This graph will be fundamental to explain in an efficient way the performance of the solar cooker under test.

Recording

The average fluid temperature (°C) of all the pots in one cooker is to be recorded every 10 minutes, to one tenth of a degree if possible. The solar insolation (W/m^2) and ambient temperature are recorded at least as frequently. Record and report the frequency of attended (manual) tracking, if any. Report azimuth angle(s) during the test. Report the rest site latitude and the date(s) of testing.

Reason: ten minutes is a long enough time that the minor fluctuations in heat loss due to ambient temperature and wind variability are expected to be negligible. Ten minutes is a short enough time that the heat gain variability due to gradual sun angle changes may be considered constant during the interval.

Calculating Cooking Power

The change in fluid temperature for each 10-minutes interval is to be multiplied by the mass and specific heat capacity of the fluid contained in the pots. Dividing this product by the 600 s contained in a 10-minutes interval yields the cooking power in Watts. The solar cooker cooking power was proposed by Funk [7] as:

$$P = \frac{m\, c\, \Delta T}{\Delta t} \tag{A.6}$$

where, for each 10-minutes time interval, ΔT is the fluid temperature difference and Δt is equal to 600 s.

The average fluid temperature, average ambient temperature and average solar irradiance, together with the initial and final fluid temperature of each interval have to be determined, too.

Standardizing Cooking Power

Funk [7] presented an additional term called standard (or adjusted) cooking power, which corrects the cooking power for each interval by multiplying it by 700 W/m^2 and dividing by the average insolation recorded during the corresponding interval:

$$P_s = P\, \frac{G_{ref}}{G_{av}} \tag{A.7}$$

where G_{av} is the average solar irradiance for each time interval and G_{ref} is a reference solar irradiance equal to $700\,\text{W/m}^2$.

It is worth to point out, however, that the ASAE S580.1 Standard [7, 186] procedure for the calculation of the standardized power was recently shown not to be physically consistent by Ruivo et al. [227].

Temperature Difference

Ambient temperature for each interval is to be subtracted from the average pot contents temperature for each corresponding interval.

$$T_d = T_f - T_{\text{amb}} \tag{A.8}$$

Reason: heat loss increases with the difference in temperature between the solar cooker interior and the cooker's surroundings; pot contents temperature correlates to cooker interior temperature.

Plotting

The standardized cooking power (W) is to be plotted against the temperature difference (°C) for each time interval.

Regression

A linear regression of the plotted points is to be used to find the relationship between cooking power and temperature difference in terms of intercept, a (W) and slope b (W/°C):

$$P_s = a + b \cdot T_d \tag{A.9}$$

At least 30 observations are required. The coefficient of determination (R^2) or proportion of variation in cooking power that can be attributed to the relationship found by regression should be better than 75% or specially noted.

Reason: statistical measures of goodness of fit for the regression line require a fairly large sample, and systematic errors are less likely to be repeated on different days. Excessive experimental error may invalidate the test.

Single Measure of Performance

The value for standardized cooking power, P_s (W), is to be computed for a temperature difference T_d of 50 °C using equation A.9.

Reason: one single number in common units familiar to most consumers best facilitates the comparison of different devices. A temperature difference of 50 °C strikes a balance between overemphasis on the start-up cooking power (where concentrating ovens are strongest) and stagnation temperature (where box cookers tend to be superior) and is just below that critical temperature when cooking begins to occur, the temperature when a solar cooker succeeds or fails.

Note: for product labelling and sales literature it is a strongly recommended that this number be calculated from a regression found by an independent laboratory using a statistically adequate number of trials. While this value, like the fuel economy rating of an automobile, is not a guarantee of performance, it provides consumers with a useful tool for comparison and selection.

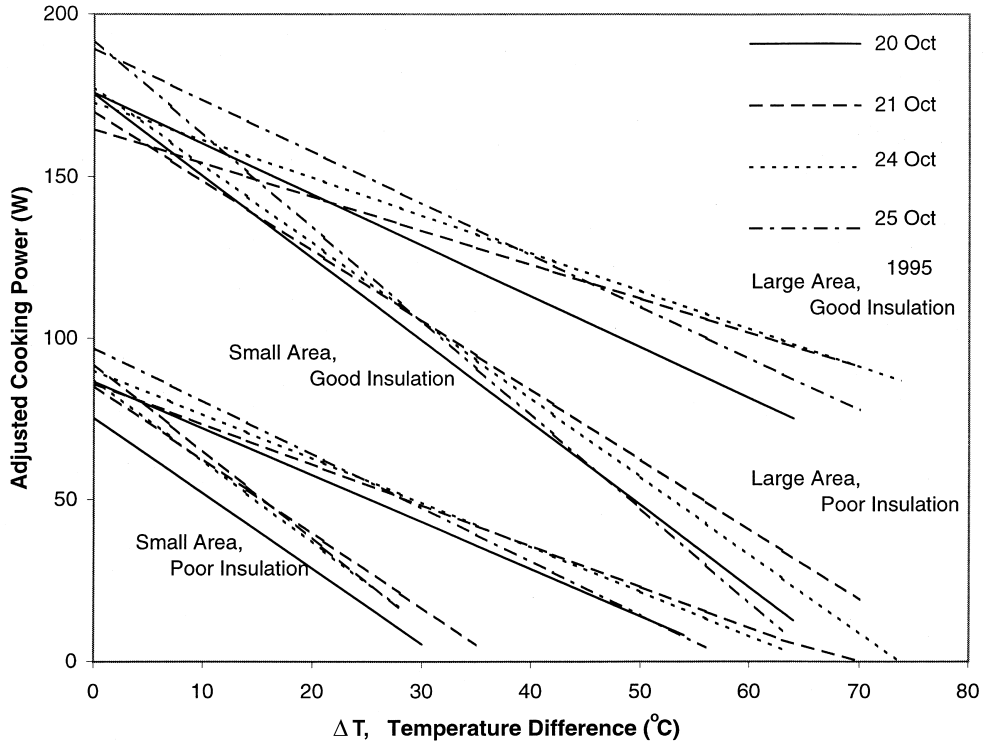

Figure A.1: A comparison of cooking power curves for four cookers with two levels of intercept area and heat loss. International standard was applied to data recorded over 4 days in 1995 [7].

Reporting

Plot the relationship between standardized cooking power and temperature difference, and present the equation. State the cooking power (standardized) at a temperature difference of 50 °C.

A.5 COR Procedure

This standard [173] proposes a parameter to represent the performance of different types of solar cookers named cooker opto-thermal ratio (COR). It is based on the thermal efficiency equation of solar collectors proposed by Hottel-Whillier-Bliss (HWB) and can be experimentally determined with a test procedure. The test protocol has been formulated carefully in order to make it common for all cooker types. To determine its utility two types of solar cooker were initially compared: the box-type (BC) and the parabolic-type (CC). The mean value of COR for the parabolic- and the box-type solar cookers were 0.155 and 0.136 respectively.

This procedure was selected as the best to calculate performance and efficiency of solar cooker, given that it allowed a simpler and immediate results collection and in particular it is based on the solar cooker energy balance and on the efficiency curve.

A.5.1 Premise

The utility of a certain solar cooker is evaluated through its performance in terms of thermal efficiency and objective parameters. The thermal performance parameter (TPP) and the respective test procedure are available to facilitate the evaluation and grading of the different types of solar cookers. However, they allow for the classification of just one type of solar cooker, i.e. a given TPP cannot be used to compare the performance of different solar cookers. Hence, there is the need for a common TPP and a corresponding test procedure which can be used to compare different types of solar cookers.

The test procedure designed to determine the thermal efficiency should be simple and should require less time. Among the available parameters which can be used to compare the performance of different solar cookers there are the figures of merit (F_1 and F_2), the overall efficiency (η_{av}), the cooking power (P), the heat loss factor ($F'U_l$) and the optical efficiency factor ($F'\eta_0$).

While the figures of merit (F_1 and F_2) can be used only for the box-type solar cooker, the heat loss factor and the optical efficiency factor ($F'U_l$ and $F'\eta_0$) were suggested for the parabolic-type solar cooker only. Each of these parameters has a different procedure for its determination.

From the Hottel-Whillier-Bliss (HWB) equation for solar collectors (equation 5.1) it is observed that optical efficiency factor ($F'\eta_0$) and heat loss factor ($F'U_l$) are the parameters which play a crucial role in determining the thermal performance.

The optical efficiency factor identifies the upper limit of performance and is basically dependent on the optical property of the glass cover of the cooking box, absorber, cooking pot and reflectance of reflector mirrors.

The heat loss factor, on the other hand, depends on design parameters and operational conditions such that it increases with the temperature of the pot fluid and wind velocity. Moreover, it is also influenced by the vapour loss.

The COR parameter was also used to derive the maximum achievable fluid temperature (T_{fx}), i.e. the highest reachable temperature obtainable by a standard fluid contained in the pot for a given location.

A.5.2 Basic Notions for Comparing Thermal Performance of Different Solar Cookers

The COR parameter is defined as the ratio between the optical efficiency factor ($F'\eta_0$) multiplied by the concentration factor (C) and the heat loss factor ($F'U_l$). A high product $\eta_0 C$ and a low U_l are necessary to optimize the performance.

The COR procedure seems to be similar to the F_1 figure of merit one proposed by Funk, but the following has to be noted:

- In the first place, COR was derived analytically from the HWB equation for concentration collectors, thus it is a function of the concentration factor (C). Therefore the thermal performance of any solar cooker can be described with COR. It has to be noted also that for box-type solar cookers C is about 1, while for the parabolic-type it is more than 1.

- Secondly, it is appropriate to have a thermal performance parameter (TPP) which describes the global cooker efficiency, i.e. it should describe the performance of the used devices.

- Thirdly, the proposed test procedure is based on the temperature measurement of the load (standard fluid) in order to make it simple and compliant with the primary objective of the procedure.

To determine this thermal parameter there is the need to split the test duration in intervals of 5 minutes each. In every interval the thermal efficiency η has to be calculated with equation A.3, where Δt is equal to 300 s.

Plotting the thermal efficiency η against the term $(T_f - T_{\text{amb}})/DNI$ it is possible to obtain the thermal efficiency linear fitting. By comparing this curve with the HWB equation (5.1), it is possible to note that the intercept q and slope m of the thermal efficiency equation give the parameters $F'\eta_0$ and $F'U_l/C$, respectively, where F' is the heat exchange efficiency factor, η_0 the optical efficiency and U_l the heat loss factor.

In detail, the linear regression equation $y = mx + q$ is composed of:

$$m = -\frac{F'U_l}{C} \tag{A.10}$$

$$q = F'\eta_0 \tag{A.11}$$

So, the regression coefficients can be used to determine the cooker opto-thermal ratio, COR:

$$COR = \frac{F'\eta_0 C}{F'U_l} \tag{A.12}$$

The COR parameter appears to be similar to the first figure of merit F_1 ([19]), however it differs from the other parameters in two aspects:

- It is derived analitically from the HWB equation for concentrating collectors (CCs), therefore, unlike other parameters, can be used to denote the performance of any cooker design;
- It indicates the performance of the devices used to increase solar radiation.

Another paramter obtained from experimental results is the fluid maximum reachable temperature (T_{fx}), which can be higher than the water boiling point. Under steady-state conditions, η in the HWB equation is equal to 0. Substituting T_f with T_{fx} and rearranging the resultant equation, the expression to calculate this temperature will be:

$$T_{\text{fx}} = T_{\text{amb,av}} + \frac{F'\eta_0 DNI}{\frac{F'U_l}{C}} \tag{A.13}$$

Appendix B

Test Bench

This appendix reports the test benches description for both the outdoor experimental campaign and for the PCM characterisation.

B.1 Outdoor Experimental Campaign

The test bench is a system designed for the characterization of a solar cooker. The test bench allows the determination of performance parameters in different time intervals for each test day. The system used in the outdoor experimental campaigns is shown in Figure B.1 and consists of the following five elements:

- T and K-thermocouples, needed to measure temperatures inside and outside the solar cooker prototypes;
- Pyrheliometer, needed to detect the direct normal solar irradiance (DNI or G_{bn});
- Pyranometer, needed to detect the global horizontal solar irradiance (G);
- Data Logger, used to acquire the sensors signals;
- Laptop, used to acquire, visualize and elaborate measurements and results.

Hereafter is reported a detailed description of all used instruments to understand their operating principle.

B.1.1 Thermocouples

A thermocouple is a temperature transducer which works exploiting the thermoelectric effect. They are widely used because they are cheap, easy to be substituted, standardized and able to measure a wide range of temperatures. Their biggest limit is accuracy: in fact, systematic errors less than one degree Celsius are difficult to obtain. Moreover, thermocouples are non-linear devices. A group of thermocouples in series is named thermopile.

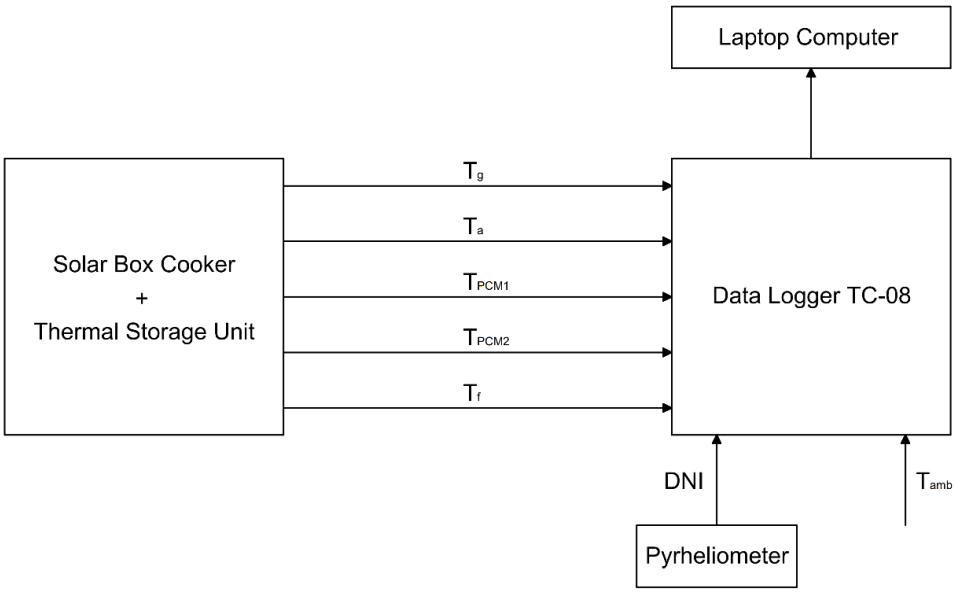

Figure B.1: Test bench scheme.

Operating principle

In 1821, Thomas Johann Seebeck, an Estonian physicist, discovered that in a circuit made with two conductors of different nature, if subject to a temperature gradient, a potential difference is generated. This phenomenon, called Seebeck effect, is exploited by thermocouples.

This effect cannot be originated in a circuit constituted by a single homogeneous conductor, therefore a thermocouple consists in a couple of different electrical conductors joint together in one point. This junction is conventionally called hot joint or hot junction and is the point where the temperature to be measured is detected. The other part of the circuit, constituted by the free ends of the two conductors, is conventionally called cold joint or cold junction.

When there is a temperature difference between the area where the hot junction is and the one where the cold junction is, it is possible to detect an electrical potential between the free ends of the thermocouple, which correspond to the cold junction. The value of such electrical potential is a function of the temperature difference and follows a non-linear law.

In practice, the thermocouple is inserted into a protection sheath which is positioned inside the device whose temperature is wished to be known. Externally, the two conductors are connected to a terminal which is also contained within a protection head. From this terminal, two additional electrical metal conductors, equal to the ones of the thermocouple, prolong the electrical link to the terminal of an indicating instrument or temperature recorder, in our case an acquisition system, as it is possible to notice in Figure B.2.

In this way, the cold junction is physically subjected to the same temperature of the terminal. This temperature is measured via a thermistor and used within the instrument to electrically correct the signal coming from the thermocouple. Using

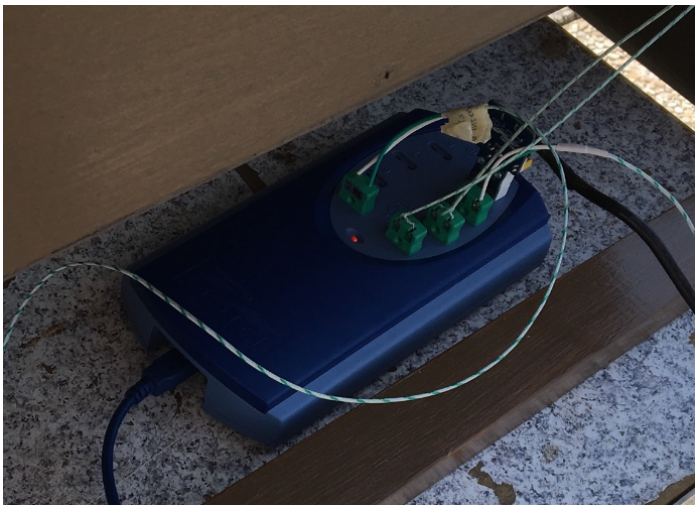

Figure B.2: Thermocouples linked to the acquisition system.

this method, whatsoever temperature is present at the terminal, it is like the cold junction is at the temperature of 0 °C. This process is called ambient temperature compensation and ensures the maximum measurement precision.

The measurement device indicates directly on its scale or on its display the temperature in °C (and not in mV) given that it has internal systems to keep into account the non-linearity of the input signal.

Thermocouples Reliability

The thermocouples reliability problem is a complex one, strictly linked to the intended usage, measurement conditions more or less hard, and the required uncertainty on the measurement.

The first cause of loss of reliability in thermocouples lies in the presence of inhomogeneities in the cables, due to chemical or physical factors like: volatilization of a component or contamination due to the presence of corrosive agents, mechanical stresses such as bending or stretching, mutation of the crystalline structure of the material due to different heat treatments suffered by different portions of wire.

This is the reason why it is good practice to use new wires, free of the above-mentioned anomalies which can happen during the use.

Used Thermocouples: Type K and Type T

There is a wide variety of thermocouples on the market which differ from each other according to the two electrical conductors that compose the junction and the application field (industrial, scientific, medical, etc.).

The thermocouples used during the experimental campaign to measure the various necessary temperatures to perform the analyses are of type K, to measure the temperatures of the solar cooker, both close to the glass and inside the absorber, and of type T, to measure the temperature of the fluid used during tests with load.

Thermocouples of type K (Figure B.3 on the left) are of common use, inexpensive and available in many different configurations. Their measurement range goes from

−200 °C to 1260 °C. The sensibility is around 41 μV/°C. Type K thermocouples are composed of Chromel (Ni-Cr) (+) and Alumel (Ni-Al) (-), and are typically used in place of noble metals thermocouples at high temperatures: in fact they can be used till 1260 °C with an uncertainty of ±2.2 °C in inert or oxidizing atmospheres [225]. They have however reproducibility and stability problems: recently it was proposed to substitute them with type N thermocouples (yet to be standardized).

Thermocouples of type T (Figure B.3 on the right) on the other hand are composed of copper (Cu) (+) and constantan (Cu-Ni) (-). This kind of thermocouples is suited for measurements at temperatures below 0 °C with an upper limit of 350 °C. They can be used in an oxidizing or reducing atmosphere or with an inert gas and do not suffer corrosion in humid atmospheres.

Thermocouples must be chosen carefully considering the environment in which they are going to be positioned and the average temperature values that are going to be measured.

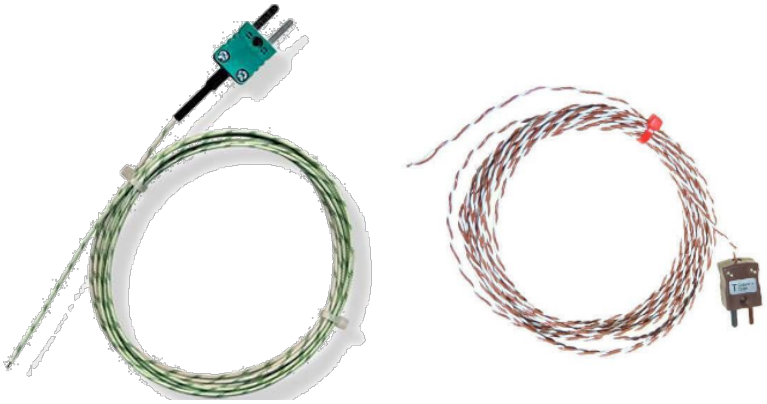

Figure B.3: Type K (left) and type T (right) thermocouples.

B.1.2 Pyrheliometer

The pyrheliometer is an instrument used to measure the direct solar radiation, i.e. the radiation which reaches the ground at a determined angle excluding all reflexions. It is generally constituted by a long cylinder at which extremity, perpendicularly, the sensor is placed.

The sensor is in general a black body that absorbs, heating up, all received solar radiation. By measuring the sensor temperature, it is possible to determine the absorbed energy and consequently the radiation intensity that caused it.

Premise

The atmospheric radiation measurement is typically divided into two separate spectral regions: the solar region (short wave) and terrestrial region (long waves). Solar radiation is a term used to describe the visible and near-visible radiation from the sun. The different regions are described by their wave length within the broadband range of 0.20 - 0.40 μm.

Terrestrial radiation is a term used to describe the infrared radiation emitted by the atmosphere. About 99% of the solar radiation on Earth's surface is contained

Figure B.4: Pyrheliometer.

Table B.1: Specifications of the Normal Incidence Pyrheliometer

Quantity	Value
Sensitivity	Approximately 8 μV/W/m^2
Impedance	Approximately 200 Ω
Temperature Dependence	$\pm$1% over ambient temperature range -20 to 40 °C
Linearity	$\pm$0.5% from 0 to 1400 W/m^2
Response time	1 second

within the region 0.3 - 3.0 nm, while the majority of the infrared radiation is contained within the region 4.0 - 50 nm. Short wave radiation is measured with pyranometers and pyrheliometers, while long wave radiation is measured with pyrgeometers.

Pyrheliometer Structure

The Normal Incidence Pyrheliometer (NIP) [228], shown in Figure B.4 and Figure B.5, integrates a wired thermopile at the cylinder base, the entrance aperture for the solar radiation has a length ratio comprised between 1 and 10, which subtends an angle of 5° 43' 30".

Inside the brass cylinder is blackened. It is filled with dry air at atmospheric pressure and sealed at the extremities. At one end of the cylinder is positioned a detector to point directly towards the sun, while the alignment is obtained mounting the NIP on a solar tracker [229].

Table B.1 reports the specifications of the pyreliometer used in the experimental campaign.

Figure B.5: Pyrheliometer main body.

Installation and Maintenance

The NIP measures the short-wave direct radiation beam pointing directly towards the sun. Eppley Laboratory Inc. produces two kinds of solar tracker used to reach the alignment:

- The Tracker ST model is a single-axis with a motor watch;
- The Tracker SMT model is a double-axis computer-controlled with an automatic tracker.

It is of importance that the pyrheliometer is checked every day of utilization, making use of the dedicated pointer for a proper sun tracking. The glass must be properly cleaned with a soft cloth, paying attention to not scratch the surface. This instrument is equipped with a calibration constant (sensibility) that, divided by the detected signal, gives the radiation in W/m^2.

B.1.3 Pyranometer

The pyranometer is an instrument used to measure the solar irradiance on a planar surface and is designed to measure the solar radiation flux density W/m^2 from the hemisphere above within a wavelength range $0.3\,\mu$m to $3\,\mu$m.

The pyranometer used in the experimental campaign is a thermopile pyranometer.

Thermopile Pyranometers

A thermopile pyranometer is a sensor based on thermopiles designed to measure solar radiation flux density with a 180° field of view. Spectral sensitivity ranges from 300 to 2800 nm.

These sensors measure the difference of potential generated in the thermopile due to the temperature difference between a black sector, exposed to the sun, and a white sector, not exposed to the sun. This voltage is in turn proportional to irradiation.

Figure B.6: SR30-M2-D1 pyranometer [230].

Construction

In order to attain the proper directional and spectral characteristics, a thermopile pyranometer is constructed with the following main components:

- A thermopile sensor with a black coating;
- A glass dome;
- A second inner glass dome;
- A heater and ventilator;
- A tilt sensor.

In the outdoor experimental campaign of the Newton and Kimono solar cookers, the global horizontal solar irradiance was measured using a pyranometer SR30-M2-D1, shown in Figure B.6, with linearity $\pm 3.0\%$ from 0 to 4000 $\mathrm{W/m^2}$ placed horizontally near the testing area. For additional information regarding the specification and the operating principle, please refer to [230].

B.1.4 Laptop and Acquisition System

The signals provided by the T- and K-thermocouples together with the one of the pyrheliometer are acquired and elaborated by a Pico Technology TC-08 thermocouple data logger [8] that has 8 input channels. The logger can measure and record temperatures ranging from $-270\,^{\circ}\mathrm{C}$ to $1820\,^{\circ}\mathrm{C}$ quickly and accurately using different types of thermocouples: B, E, J, K, N, R, S, T. Through the TC-08 single-channel USB terminal block PP624 (Figure B.7) connected to one of the 8 channels of the data logger, the pyreliometer sensor is registered. In fact, the terminal block has a series of

Figure B.7: PP624 connector used for the pyreliometer signal [8].

Table B.2: Specifications of the TC-08 data logger [8].

Quantity	Value
Number of channels	8
Conversion time	100 ms per thermocouple channel + 100 ms for CJC
Temperature accuracy	Sum of ±0.2% of reading and ±0.5 °C
Voltage accuracy	Sum of ±0.2% of reading and ±10 μV
Overvoltage protection (V)	±30
Maximum common-mode voltage (V)	±7.5
Input impedance (MΩ)	2
Input range (mV)	±70
Resolution (bit)	20
Operating temperature range (°C)	0 to 50
Input connectors	Miniature thermocouple
PC connection	USB 2.0
Dimension (mm)	201 x 104 x 34

screw terminals that allow sensors with voltage or current outputs to be connected to the data logger without the need for soldering. The four possible input ranges are ±50 mV, ±500 mV, ±5 V and 4–20 mA.

The logger is provided with built-in cold junction compensation (CJC) and draws power from the USB port, so no external power supply is necessary. All the specification of the TC-08 are collected in Table B.2.

During the experimental tests, the channels were always occupied by the same sensor. The first channel was reserved for the pyrheliometer and the value of the direct solar irradiance was registered both in mV and converted in W/m^2. The remaining 7 channel were used to connect the thermocouples: one thermocouple was used to measure ambient temperature, while the other thermocouples were located in different points of the cooker. All the temperature signals were registered in °C. The temperatures of the various cooker elements changed according to the type of prototype and experimental campaign being carried out. Hereafter is reported, as an example, the complete list of the quantities detected during the tests using the portable solar box cooker equipped with TES based on PCM:

- Channel 1: direct normal irradiance (DNI);
- Channel 2: ambient temperature, T_{amb} (T-type thermocouple);
- Channel 3: outer glass temperature, T_{go} (K-type thermocouple);

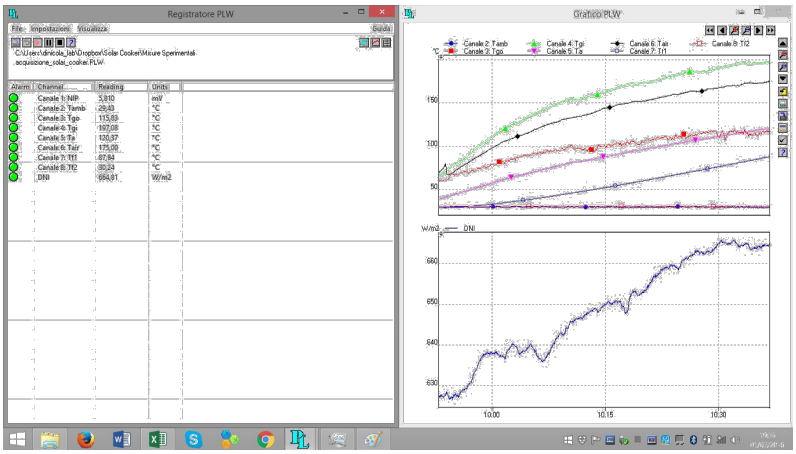

Figure B.8: Display example of the acquisition software during the tests (PicoLog software).

- Channel 4: inner glass temperature, T_{gi} (K-type thermocouple);
- Channel 5: absorber plate temperature, T_{a} (T-type thermocouple);
- Channel 6: phase change material temperature, T_{pcm1} (K-type thermocouple);
- Channel 7: phase change material temperature, T_{pcm2} (K-type thermocouple);
- Channel 8: fluid temperature, T_{f} (T-type thermocouples);

Through the PicoLog data acquisition program it was possible to visualize the temperature and solar radiation trends and their evolution during the tests in real-time on the laptop. Figure B.8 shows a screen of the acquisition software during a test. From Figure B.8 it is evident that during each test it was possible to follow the various trends of the detected quantities in order to check anomalies in the measurement. This software can analyze and display data over long or short time periods. Data can be viewed both during and after data collection in spreadsheet or graphical format, and can be easily exported to other applications.

B.2 PCM Characterisation

To determine the thermophysical parameters and properties of the materials chosen as PCM, two different analyses were conducted: the differential scanning calorimetry and the thermogravimetric analysis (TGA). The first analysis is carried out with an instrument called Differential Scanning Calorimeter (DSC), the latter with a thermogravimetric analyzer.

Hereafter is reported a detailed description of all the two instruments to understand their operating principle. Figure B.9 and Figure B.10 show the two instruments used to perform the differential scanning calorimetry and the thermogravimetric analysis during the experimental campaign at WiB.

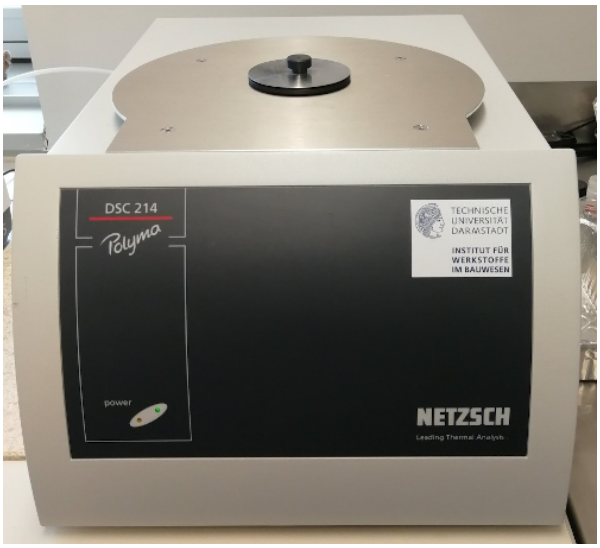

Figure B.9: The NETZSCH DSC 214 POLYMA at WiB.

Figure B.10: The TGA NETZSCH STA 449 F5 JUPITER at WiB.

B.2.1 Differential Scanning Calorimeter

The DSC is a device which measures the difference between the heat fluxes to heat (or cool) a sample of material and a reference. The heating or the cooling processes are driven by the instrument and are conducted in a controlled way. The DSC makes sure that, at any point in time during the test, the sample and the reference are at the same temperature.

The test is prepared starting from two crucibles, one meant for the material to be tested and one for the reference. A small quantity of material (a few mg) is loaded in the first crucible, while the other one is left empty and will serve as reference. The weight of the crucibles and of the substance are important parameters for the analysis, thus all items are to be weighted carefully before the test. The crucibles are then placed inside the instrument's furnace, a temperature-controlled oven, which can afterwards be closed ermetically.

The DSC allows for setting the heating behavior, typically a linearly increasing temperature. It is also possible to set different slopes at different points of the test, for instance to increase resolution in the temperature range around an expected phase change of the material.

As the test starts, the samples are immersed in an inert atmosphere realized by the instrument through a continuous flow of a purging gas, typically argon or nitrogen.

The instrument's furnace will heat up, exchanging heat with the two crucibles. Their temperatures are constantly monitored. Given that the DSC control loop keeps the sample and the reference crucible at the same temperature, any variation in the heat flux between the two must be due to the thermal properties of material under test.

The temperatures of the two crucibles during the test are elaborated by a software which processes the data and produces the output for further elaboration by the operator.

Of particular interest is the detection of phase transitions in the tested material. When a substance changes its phase, it either requires heat (for instance when going from the solid to the liquid phase), or it releases heat (when returning to the solid phase). Given that during the test the temperatures of the crucible containing the material and the reference one are kept at the same value, a marked drop or spike in heat flow corresponding to the transition temperature is detected by the instrument: in fact, when the material is changing phase it requires more or less heat from the furnace to keep the same temperature.

B.2.2 Thermogravimetric Analysis

The thermogravimetric analysis is a thermal characterization method which consists in precisely measuring the mass variation of a material samples over time as temperature increases in a controlled way. A small quantity of the substance, prepared in an aluminum crucible, is placed in a temperature-controlled furnace and immersed in a controlled atmosphere, which can be inert (for instance composed of nitrogen), oxidant or reductant. As temperature changes, the material undergoes a degradation which depends on its thermophysical properties, the atmosphere which it is subject to and of course temperature.

A thermogravimetric analyzer is made of a precision scale with sample holders placed inside a furnace. Apart from controlling temperature and temperature variation over time, it is usually possible also to control the pressure inside the testing compartment.

With this analysis it is possible to determine the thermal stability of a material at different temperature ranges and discover its upper endurance limit, after which it starts degrading by loosing mass.

Appendix C

Input parameters: numerical values

This appendix reports the numerical values of all the parameters used as input for the mathematical model.

C.1 Geometrical Properties

Table C.1 shows the geometrical parameters of the solar box cooker under investigation, which were directly measured on the prototype used for the experimental campaign. Along with the information regarding the glass, the absorber plate, the square- and wedge-shaped mirrors and the insulation layers, also the geometric information of the pot and its lid, which is necessary to determine the characteristic lengths in the calculation of convective heat transfer coefficients, were included.

C.2 Optical Properties of The Materials of The Solar Cooker Elements

Table C.2 collects all the optical properties of the materials making up the various solar cooker elements. For most of them, the values were taken from the material data sheets issued by the manufacturer at the time of delivery. The remaining values were taken from scientific literature. It is important to mention that the absorber (the cooking chamber of the prototype) is made of 6/10 mm galvanised sheet metal with a selective black coating, the insulation layer is made of glass wool sheets and flakes, the mirrors are covered with a special aluminum film, the glass is made of a single tempered sheet and the pot and its lid are made of aluminum.

C.3 Thermophysical Properties of The Solar Cooker Elements Materials

Tables C.3 and C.4 respectively contain the thermophysical properties of the materials of the solar cooker elements and the fluids used in the pot during the various tests of the outdoor experimental campaign.

Table C.1: Geometrical properties of the solar cooker elements.

Quantity	Value	Unit	Description	Source of the data
ϕ_{mq}	63.43	°	Square mirror inclination	Prototype
ϕ_{mc}	56.98	°	Wedge-shape mirror inclination	Prototype
X_{p}	0.003	m	Pot thickness	Prototype
X_{i}	0.050	m	Insulation thickness	Prototype
X_{a}	0.0006	m	Absorber plate thickness	Prototype
X_{g}	0.004	m	Glass thickness	Prototype
H_{p}	0.130	m	Pot height	Prototype
H_{a}	0.250	m	Cooking chamber height	Prototype
H_{f}	0.0705	m	Fluid column height	Prototype
H_{airPot}	0.0595	m	Air column height inside the pot	Prototype
p_{pb}	0.5969	m	Base pot perimeter	Prototype
p_{pl}	0.5969	m	Pot lid perimeter	Prototype
p_{g}	1.60	m	Glass perimeter	Prototype
p_{ab}	1.60	m	Absorber bottom perimeter	Prototype
A_{mq}	0.16	m^2	Square mirror area	Prototype
A_{mc}	0.1047	m^2	Wedge-shape mirror area	Prototype
A_{g}	0.16	m^2	Glass area	Prototype
A_{ab}	0.16	m^2	Absorber bottom area	Prototype
A_{as}	0.40	m^2	Absorber side area	Prototype
A_{pl}	0.02835	m^2	Pot lid area	Prototype
A_{pb}	0.0284	m^2	Pot bottom area	Prototype
A_{ps}	0.0776	m^2	Pot side area	Prototype
A_{i}	0.75	m^2	Insulation area	Prototype

C.4 Constant Quantities

Tables C.5 contains the constant quantities, both the physical constants and the prototype parameters.

Table C.2: Optical properties of the materials of the solar cooker elements.

Quantity	Value	Unit	Description	Source of data
Mirrors				
P_m	0.94	-	Reflectance of mirrors	[231]
Glass				
α_{g}	0.02	-	Glass absorbance	[232]
P_g	0.08	-	Glass reflectance	[232]
τ_{g}	0.90	-	Glass transmittance	[232]
ϵ_{g}	0.90	-	Glass emissivity	[232]
Lid pot				
α_{l}	0.90	-	Pot lid absorbance	[233]
ϵ_{l}	0.35	-	Pot lid emissivity	[233]
Pot				
α_{p}	0.90	-	Pot absorbance	[233]
ϵ_{p}	0.35	-	Pot emissivity	[233]
Absorber plate/Cooking chamber				
α_{a}	0.90	-	Absorber absorbance	[233]
ϵ_{a}	0.30	-	Absorber emissivity (black cover)	[233]
Air inside the cooking chamber				
α_{air}	0.90	-	Air absorbance	[224]
ϵ_{air}	0.35	-	Air emissivity	[224]
Insulation layer				
ϵ_{i}	0.05	-	Insulation emissivity	-

Table C.3: Thermophysical properties of the materials of the solar cooker elements.

Quantity	Value	Unit	Description	Source of data
λ_{p}	204	W/mK	Thermal conductivity of the pot (aluminum)	[224]
λ_{p}	15	W/mK	Thermal conductivity of the pot (steel)	[224]
λ_{i}	0.037	W/mK	Thermal conductivity of the insulation (glass wool)	-
λ_{a}	15	W/mK	Thermal conductivity of the absorber (steel)	[224]
$c_{\mathrm{p,p}}$	896	J/kgK	Specific heat of the pot (aluminum)	[224]
$c_{\mathrm{p,p}}$	502	J/kgK	Specific heat of the pot (steel)	[224]
$c_{\mathrm{p,i}}$	1030	J/kgK	Specific heat of the insulation (glass wool)	-
$c_{\mathrm{p,g}}$	800	J/kgK	Specific heat of the glass	-
$c_{\mathrm{p,a}}$	502	J/kgK	Specific heat of the absorber (steel)	[224]
ρ_{p}	2700	kg/m^3	Density of the pot at 20 °C (aluminum)	[224]
ρ_{p}	7500	kg/m^3	Density of the pot at 20 °C (steel)	[224]
ρ_{i}	15	kg/m^3	Density of the insulation (glass wool)	-
ρ_{g}	2500	kg/m^3	Density of the glass	-

Table C.4: Thermophysical properties of the fluids using during the experimental campaign.

Quantity	Value	Unit	Description	Source of data
Water				
ρ_{water}	1000	kg/m^3	Density of water	[224]
$c_{\text{p,water}}$	4187	J/kgK	Specific heat of water	[224]
λ_{water}	0.037	W/mK	Thermal conductivity of water at 20 °C	[224]
$\beta_s water$	0.21e-3	1/K	Coefficient of thermal expansion of water	[224]
μ_{water}	0.001	Pa · s	Dynamic viscosity of water	[224]
Silicone oil				
ρ_{oil}	965	kg/m^3	Density of silicone oil	[234]
$c_{\text{p,oil}}$	1498	J/kgK	Specific heat of silicone oil at 25 °C	[234]
λ_{oil}	0.16	W/mK	Thermal conductivity of silicone oil at 20 °C	[234]
β_{oil}	9.45e-4	1/K	Coefficient of thermal expansion of silicone oil	[234]
μ_{oil}	96500	Pa · s	Dynamic viscosity of silicone oil	[234]
Air				
ρ_{air}	1225	kg/m^3	Density of air	[224]
$c_{\text{p,air}}$	1005	J/kgK	Specific heat of air	[224]
λ_{air}	0.025	W/mK	Thermal conductivity of air	[224]
β_{air}	3.66e-3	1/K	Coefficient of thermal expansion of air	[224]
μ_{air}	1.81e-5	Pa · s	Dynamic viscosity of air	[224]
ν_{air}	1.478e-5	m^2/s	Kinematic viscosity of air	[224]

Table C.5: Constant quantities

Quantity	Value	Unit	Description	Source of data
σ	5.67e-8	(W/m^{2}K^4)	Stefan-Boltzmann constant	[224]
g	9.807	(m/s^2)	Gravity acceleration	[224]
U	0.5	(m/s)	Wind speed	-
m_{l}	0.2.	(kg)	Lid mass	Prototype
m_{p}	0.848	(kg)	Pot mass	Prototype
m_{g}	1.60	(kg)	Glass mass	Prototype
m_{a}	0.907	(kg)	Cooking chamber mass	Prototype
m_{air}	0.04	(kg)	Air inside the cooking chamber mass	Prototype
m_{airPot}	0.002	(kg)	Air inside the pot mass	Prototype
m_{i}	0.563	(kg)	Insulation layer mass	Prototype
$Flid_{\text{mq}}$	0.125	(-)	View factor square mirrors - lid	Prototype
$Flid_{\text{mc}}$	0.1	(-)	View factor wedge-shaped mirrors - lid	Prototype
Fp_{mq}	0.125	(-)	View factor square mirrors - pot	Prototype
Fp_{mc}	0	(-)	View factor wedge-shaped mirrors - pot	Prototype
Fg_{mq}	1	(-)	View factor square mirrors - glass	Prototype
Fg_{mc}	1	(-)	View factor wedge-shaped mirrors - glass	Prototype
Fa_{mq}	0.3	(-)	View factor square mirrors - absorber	Prototype
Fa_{mc}	0.3	(-)	View factor wedge-shaped mirrors - absorber	Prototype

Appendix D

Nomenclature

D.1 Latin Symbols

A	Area (m^2)
C	Concentration ratio
COR	Cooker opto-thermal ratio (°C/(W/m^2))
c	Specific heat (J/(kg K))
CR	Cooling rate (°C/min)
D	Diameter (m)
DNI	Direct normal irradiance (W/m^2)
E	Equation of time (min), energy (J)
$F^{'}$	Heat exchange efficiency factor
F_1	First figure of merit (°C/(W/m^2))
F_2	Second figure of merit
G	Global horizontal solar irradiance (W/m^2)
G_{bn}	Direct normal solar irradiance (W/m^2)
G_{n}	Global normal solar irradiance (W/m^2)
h_{air}	Convective heat transfer coefficient (W/(m^2 K))
HR	Heating rate (°C/min)
I	Local intensity in the medium (W/m^2)
L_{m}	Length (m)
m	Mass (kg)

Nu	Nusselt number
P	Power (W), cooking power (W)
Pr	Prandtl number
Q	Heat flux (W)
R^2	Coefficient of determination
Ra	Rayleigh number
Re	Reynolds number
r	Radius (m)
T	Temperature (°C)
$T_{\max}$	Maximum thermal stable temperature (°C)
t	Time (s), time constant (s), boiling time (s), thickness (m)
U_{L}	Overall loss coefficient ($\mathrm{W/(m^2\,K)}$)
v	Velocity (m/s)
W	Aperture (m)
X	Input quantity
x	Abscissa, input observation
Y	Output quantity
y	Ordinate
z	Height

D.2 Greek Symbols

α	Absorptance, altitude angle (°)
β	Coefficient of thermal expansion
Δ	Delta difference
ϵ	Emissivity
ΔH	Latent heat (J/g)
η	Thermal efficiency
η_0	Optical efficiency
θ	Inclination angle (°)

λ	Thermal conductivity ($\mathrm{W/(m\,K)}$)
μ	Dynamic viscosity ($\mathrm{Pa\,s}$)
ν	Kinematic viscosity ($\mathrm{m^2/s}$)
ρ	Reflectance, density ($\mathrm{kg/m^3}$)
σ	Stefan-Boltzmann constant ($\mathrm{W/(m^2\,K^4)}$)
τ	Transmittance

D.3 Subscripts

a	Absorber, absorption, aperture
air	Air
airPot	Air inside the pot
amb	Ambient
av	Average
c	Cover, collector, convective, characteristic, crystallization
dod	Dodecagon
deg	Degradation
d	Diffuse
e	Effective, environment
eff	Effective
f	Fluid
g	Glass
i	Inner, inlet, ineffective
k	Conductive
l	Lid
max	Maximum
m	Mean, mirror, melting
n	Normal
p	Pot
o	Outer, outlet

r	Receiver, radiative, reflection, refraction
ref	Reference
s	Solar, stabilized, specific, standard
std	Standard
tot	Total
x	Stagnation
u	Utilizable

D.4 Acronyms

CC	Concentrating cooker
DIISM	Department of Industrial Engineering and Mathematical Sciences
DNI	Direct Normal Irradiance (W/m^2)
DSC	Differential Scanning Calorimeter
ENEA	Italian National Agency for New Technologies, Energy and Sustainable Economic Development
FAO	Food and Agriculture Association
FTIR	Fourier Transform Infrared
GHG	Greenhouse Gases
HSM	Heat Storage Material
HWB	Hottel-Whillier-Bliss
LHTES	Latent Heat Thermal Energy Storage
NFPA	National Fire Protection Association
NIP	Normal Incidence Pyrheliometer
NSC	Newton Solar Cooker
PCM	Phase Change Material
SA	Sugar alcohol
SBC	Solar Box Cooker
SDG	Sustainable Development Goals
SHTES	Sensible heat thermal energy storage
TES	Thermal Energy Storage

TGA	Thermogravimetric Analysis
UNGA	United Nations General Assembly
UNIVPM	Marche Polytechnic University
WiB	Institut für Werkstoffe im Bauwesen
WHO	World Health Organization

Bibliography

[1] Gianluca Coccia, Giovanni Di Nicola, Mariano Pierantozzi, Sebastiano Tomassetti, and Alessia Aquilanti. "Design, manufacturing, and test of a high concentration ratio solar box cooker with multiple reflectors". In: *Sol. Energy* 155 (2017), pp. 781–792 (cit. on pp. ix, 34–36, 105).

[2] Gianluca Coccia, Alessia Aquilanti, Sebastiano Tomassetti, Akiko Ishibashi, and Giovanni Di Nicola. "Design, manufacture and test of a low-cost solar cooker with high-performance light-concentrating lens". In: *Sol. Energy* 224 (2021), pp. 1028–1039 (cit. on pp. ix, 54, 55).

[3] Alessia Aquilanti, Sebastiano Tomassetti, Matteo Muccioli, and Giovanni Di Nicola. "Design and experimental characterization of a solar cooker with a prismatic cooking chamber and adjustable panel reflectors". In: *Renewable Energy* (2022) (cit. on pp. x, 69, 70, 91).

[4] Alessia Aquilanti, Sebastiano Tomassetti, Gianluca Coccia, Matteo Muccioli, and Giovanni Di Nicola. "Experimental characterization and performance comparison of four prototypes of panel solar cooker for low to high sun elevations". In: *Journal of Cleaner Production* (2023), p. 136158 (cit. on pp. x, 87, 94).

[5] Gianluca Coccia, Alessia Aquilanti, Sebastiano Tomassetti, Gabriele Comodi, and Giovanni Di Nicola. "Design, realization, and tests of a portable solar box cooker coupled with an erythritol-based PCM thermal energy storage". In: *Solar Energy* 201 (2020), pp. 530–540 (cit. on pp. xi, 17, 108).

[6] Gianluca Coccia, Alessia Aquilanti, Sebastiano Tomassetti, Pio Francesco Muciaccia, and Giovanni Di Nicola. "Experimental Analysis of Nucleation Triggering in a Thermal Energy Storage Based on Xylitol Used in a Portable Solar Box Cooker". In: *Energies* 14.18 (2021), p. 5981 (cit. on pp. xi, 17, 108).

[7] Paul A Funk. "Evaluating the international standard procedure for testing solar cookers and reporting performance". In: *Sol. Energy* 68.1 (2000), pp. 1–7 (cit. on pp. xii, 41, 43, 44, 48, 57, 77, 92, 167, 169, 171–173).

[8] Pico Technology. *Pico Technology TC-08 thermocouple data logger*. Accessed 20 February 2023. URL: `https://www.picotech.com/data-logger/tc-08/thermocouple-data-logger` (cit. on pp. xii, xiv, 183, 184).

[9] A Miliozzi, E Veca, S Sau, R Grena, M Celino, M Falconieri, and F Rondino. "Individuazione e caratterizzazione di miscele di materiali a cambiamento di fase e nanoparticelle da impiegare come sistemi alternativi di accumulo termico". In: *Report Ricerca di Sistema Elettrico, Accordo di Programma Ministero dello Sviluppo Economico–ENEA* (2013) (cit. on pp. xii, 14, 16).

[10] A Eisentraut and A Brown. “Heating without global warming: market developments and policy considerations for renewable heat”. In: *Paris: International Energy Agency* (2014) (cit. on p. 1).

[11] WC Turkenburg. “Renewable energy technologies”. In: *World Energy Assessment: Energy and the Challenge of Sustainability* (2000), pp. 219–272 (cit. on p. 1).

[12] Dolf Gielen, Francisco Boshell, Deger Saygin, Morgan D Bazilian, Nicholas Wagner, and Ricardo Gorini. “The role of renewable energy in the global energy transformation”. In: *Energy strategy reviews* 24 (2019), pp. 38–50 (cit. on p. 2).

[13] Rajendra K Pachauri, Myles R Allen, Vicente R Barros, John Broome, Wolfgang Cramer, Renate Christ, John A Church, Leon Clarke, Qin Dahe, Purnamita Dasgupta, et al. *Climate change 2014: synthesis report. Contribution of Working Groups I, II and III to the fifth assessment report of the Intergovernmental Panel on Climate Change*. Ipcc, 2014 (cit. on p. 2).

[14] E Cuce and PM Cuce. “A comprehensive review on solar cookers”. In: *Appl. Energy* 102 (2013), pp. 1399–1421 (cit. on pp. 2, 5, 6, 9).

[15] NM Nahar. “Performance and testing of a hot box storage solar cooker”. In: *Energy Convers. Manage.* 44.8 (2003), pp. 1323–1331 (cit. on pp. 2, 7, 14).

[16] F Yettou, B Azoui, A Malek, A Gama, and NL Panwar. “Solar cooker realizations in actual use: An overview”. In: *Renewable and Sustainable Energy Reviews* 37 (2014), pp. 288–306 (cit. on pp. 2, 6).

[17] RM Muthusivagami, R Velraj, and R Sethumadhavan. “Solar cookers with and without thermal storage – A review”. In: *Renewable and Sustainable Energy Reviews* 14.2 (2010), pp. 691–701 (cit. on pp. 2, 6, 8).

[18] Beth Halacy and Daniel Stephen Halacy. *Cooking with the Sun*. Morning Sun Press, 1992 (cit. on p. 3).

[19] SC Mullick, TC Kandpal, and AK Saxena. “Thermal test procedure for box-type solar cookers”. In: *Sol. Energy* 39.4 (1987), pp. 353–360 (cit. on pp. 3, 42, 57, 93, 118, 167, 168, 175).

[20] Mohamad Aramesh, Mehdi Ghalebani, Alibakhsh Kasaeian, Hosein Zamani, Giulio Lorenzini, Omid Mahian, and Somchai Wongwises. “A review of recent advances in solar cooking technology”. In: *Renew. Energy* 140 (2019), pp. 419–435 (cit. on p. 4).

[21] Suhail Zaki Farooqui. “A review of vacuum tube based solar cookers with the experimental determination of energy and exergy efficiencies of a single vacuum tube based prototype”. In: *Renewable and Sustainable Energy Reviews* 31 (2014), pp. 439–445 (cit. on p. 4).

[22] N Nallusamy, S Sampath, and RJRE Velraj. “Experimental investigation on a combined sensible and latent heat storage system integrated with constant/-varying (solar) heat sources”. In: *Renewable energy* 32.7 (2007), pp. 1206–1227 (cit. on p. 5).

[23] Abdulla H Algifri and Hussain A Al-Towaie. “Efficient orientation impacts of box-type solar cooker on the cooker performance”. In: *Solar Energy* 70.2 (2001), pp. 165–170 (cit. on p. 5).

[24] H Kurt, E Deniz, and Z Recebli. “An investigation into the effects of box geometries on the thermal performance of solar cookers”. In: *International Journal of Green Energy* 5.6 (2008), pp. 508–519 (cit. on p. 5).

[25] BS Negi and Ishan Purohit. “Experimental investigation of a box type solar cooker employing a non-tracking concentrator”. In: *Energy Conversion and Management* 46.4 (2005), pp. 577–604 (cit. on p. 5).

[26] OV Ekechukwu and NT Ugwuoke. “Design and measured performance of a plane reflector augmented box-type solar-energy cooker”. In: *Renewable Energy* 28.12 (2003), pp. 1935–1952 (cit. on p. 5).

[27] SS Nandwani. “Solar cookers – Cheap technology with high ecological benefits”. In: *Ecological Economics* 17.2 (1996), pp. 73–81 (cit. on p. 6).

[28] NV Patel and SK Philip. “Performance evaluation of three solar concentrating cookers”. In: *Renewable Energy* 20.3 (2000), pp. 347–355 (cit. on p. 6).

[29] ML Ghai and TD Bansal. “Design of reflector type direct solar cooker”. In: *Journal of Scientific & Industrial Research* 12 (1953), pp. 165–175 (cit. on p. 6).

[30] GOG Lof, DA Fester, and JA Duffie. “Energy balances on a parabolic cylinder solar collector”. In: (1962) (cit. on p. 6).

[31] Ashok Kundapur and CV Sudhir. “Proposal for new world standard for testing solar cookers”. In: *Journal of engineering science and technology* 4.3 (2009), pp. 272–281 (cit. on p. 6).

[32] CZM Kimambo. “Development and performance testing of solar cookers”. In: *Journal of energy in Southern Africa* 18.3 (2007), pp. 41–51 (cit. on p. 6).

[33] Hilde M Toonen. “Adapting to an innovation: Solar cooking in the urban households of Ouagadougou (Burkina Faso)”. In: *Physics and chemistry of the earth, Parts A/B/C* 34.1-2 (2009), pp. 65–71 (cit. on p. 6).

[34] Alberto Regattieri, Francesco Piana, Marco Bortolini, Mauro Gamberi, and Emilio Ferrari. “Innovative portable solar cooker using the packaging waste of humanitarian supplies”. In: *Renewable and Sustainable Energy Reviews* 57 (2016), pp. 319–326 (cit. on p. 6).

[35] Ramalingam Senthil and Marimuthu Cheralathan. “Effect of the phase change material in a solar receiver on thermal performance of parabolic dish collector”. In: *Thermal Science* 21.6 Part B (2017), pp. 2803–2812 (cit. on p. 7).

[36] Lameck Nkhonjera, Tunde Bello-Ochende, Geoffrey John, and Cecil K Kingondu. “A review of thermal energy storage designs, heat storage materials and cooking performance of solar cookers with heat storage”. In: *Renewable and Sustainable Energy Reviews* 75 (2017), pp. 157–167 (cit. on p. 7).

[37] Maxime Mussard, Alexandre Gueno, and Ole Jørgen Nydal. “Experimental study of solar cooking using heat storage in comparison with direct heating”. In: *Solar Energy* 98 (2013), pp. 375–383 (cit. on p. 7).

[38] SD Sharma, Takeshi Iwata, Hiroaki Kitano, and Kazunobu Sagara. “Thermal performance of a solar cooker based on an evacuated tube solar collector with a PCM storage unit”. In: *Solar Energy* 78.3 (2005), pp. 416–426 (cit. on pp. 7, 105).

[39] Avinash Chaudhary, Amit Kumar, and Avadhesh Yadav. “Experimental investigation of a solar cooker based on parabolic dish collector with phase change thermal storage unit in Indian climatic conditions”. In: *Journal of Renewable and Sustainable Energy* 5.2 (2013), p. 023107 (cit. on pp. 7, 17, 104).

[40] A Mawire, M McPherson, and RRJ Van den Heetkamp. “Discharging simulations of a thermal energy storage (TES) system for an indirect solar cooker”. In: *Solar energy materials and solar cells* 94.6 (2010), pp. 1100–1106 (cit. on p. 7).

[41] Ashmore Mawire. “Experimental de-stratification and heat loss in a storage tank containing different thermal oils”. In: *Journal of the Brazilian Society of Mechanical Sciences and Engineering* 39.6 (2017), pp. 2279–2288 (cit. on p. 7).

[42] MRI Ramadan, S Aboul-Enein, and AA El-Sebaii. “A model of an improved low cost-indoor-solar-cooker in Tanta”. In: *Solar & Wind Technology* 5.4 (1988), pp. 387–393 (cit. on pp. 7, 103).

[43] K Schwarzer and MEV Da Silva. “Solar cooking system with or without heat storage for families and institutions”. In: *Solar Energy* 75.1 (2003), pp. 35–41 (cit. on pp. 7, 14).

[44] Hassan Nazir, Mariah Batool, Francisco J Bolivar Osorio, Marllory Isaza-Ruiz, Xinhai Xu, K Vignarooban, Patrick Phelan, Arunachala M Kannan, et al. “Recent developments in phase change materials for energy storage applications: A review”. In: *International Journal of Heat and Mass Transfer* 129 (2019), pp. 491–523 (cit. on p. 9).

[45] A Sharma, CR Chen, VVS Murty, and A Shukla. “Solar cooker with latent heat storage systems: A review”. In: *Renewable and Sustainable Energy Reviews* 13.6 (2009), pp. 1599–1605 (cit. on p. 9).

[46] Ashok Kundapur. *A Treatise on Solar Cookers*. Ed. by International Alternate Energy Trust. First. International Alternate Energy Trust, 2018. ISBN: 978-93-5279-162-0 (cit. on p. 9).

[47] Francis Agyenim, Neil Hewitt, Philip Eames, and Mervyn Smyth. “A review of materials, heat transfer and phase change problem formulation for latent heat thermal energy storage systems (LHTESS)”. In: *Renewable and sustainable energy reviews* 14.2 (2010), pp. 615–628 (cit. on p. 11).

[48] A Abhat. “Low temperature latent heat thermal energy storage: heat storage materials”. In: *Solar energy* 30.4 (1983), pp. 313–332 (cit. on p. 11).

[49] Luisa F Cabeza, Albert Castell, C de Barreneche, A De Gracia, and AI Fernández. “Materials used as PCM in thermal energy storage in buildings: A review”. In: *Renewable and Sustainable Energy Reviews* 15.3 (2011), pp. 1675–1695 (cit. on pp. 11, 14).

[50] Ming Liu, Yanping Sun, and Frank Bruno. “A review of numerical modelling of high-temperature phase change material composites for solar thermal energy storage”. In: *Journal of Energy Storage* 29 (2020), p. 101378 (cit. on p. 12).

[51] Yvan Dutil, Daniel R Rousse, Nizar Ben Salah, Stéphane Lassue, and Laurent Zalewski. “A review on phase-change materials: Mathematical modeling and simulations”. In: *Renewable and sustainable Energy reviews* 15.1 (2011), pp. 112–130 (cit. on p. 12).

[52] Murat M Kenisarin. “Thermophysical properties of some organic phase change materials for latent heat storage. A review”. In: *Solar Energy* 107 (2014), pp. 553–575 (cit. on pp. 12, 13).

[53] Aran Solé, Laia Miró, Camila Barreneche, Ingrid Martorell, and Luisa F Cabeza. "Review of the T-history method to determine thermophysical properties of phase change materials (PCM)". In: *Renewable and Sustainable Energy Reviews* 26 (2013), pp. 425–436 (cit. on p. 12).

[54] Eva Günther, Stefan Hiebler, Harald Mehling, and Robert Redlich. "Enthalpy of phase change materials as a function of temperature: required accuracy and suitable measurement methods". In: *International Journal of Thermophysics* 30.4 (2009), pp. 1257–1269 (cit. on p. 12).

[55] Weiguang Su, Liying Gao, Li Wang, and Hui Zhi. "Calibration of differential scanning calorimeter (DSC) for thermal properties analysis of phase change material". In: *Journal of Thermal Analysis and Calorimetry* 143.4 (2021), pp. 2995–3002 (cit. on p. 12).

[56] Heinrich Badenhorst and Luisa F Cabeza. "Critical analysis of the T-history method: A fundamental approach". In: *Thermochimica Acta* 650 (2017), pp. 95–105 (cit. on p. 12).

[57] Lovelyn Theresa, R Velraj, et al. "Thermophysical characterization and comparison of PCMs using DSC and T-History experimental setup". In: *Materials Research Express* 6.12 (2019), p. 125527 (cit. on p. 12).

[58] A Hasan, SJ McCormack, MJ Huang, and B Norton. "Characterization of phase change materials for thermal control of photovoltaics using Differential Scanning Calorimetry and Temperature History Method". In: *Energy Conversion and Management* 81 (2014), pp. 322–329 (cit. on p. 12).

[59] Christoph Rathgeber, Laia Miró, Luisa F Cabeza, and Stefan Hiebler. "Measurement of enthalpy curves of phase change materials via DSC and T-History: When are both methods needed to estimate the behaviour of the bulk material in applications?" In: *Thermochimica Acta* 596 (2014), pp. 79–88 (cit. on p. 12).

[60] D Gaona, E Urresta, J Marínez, and G Guerrón. "Medium-temperature phase-change materials thermal characterization by the T-History method and differential scanning calorimetry". In: *Experimental Heat Transfer* 30.5 (2017), pp. 463–474 (cit. on p. 12).

[61] Xue-Feng Shao, Sheng Yang, Chao Wang, Yong-Jian Yang, Wu-Jun Wang, Yi Zeng, and Li-Wu Fan. "Screening of sugar alcohols and their binary eutectic mixtures as phase change materials for low-to-medium temperature thermal energy storage.(II): Isothermal melting and crystallization behaviors". In: *Energy* 180 (2019), pp. 572–583 (cit. on pp. 12, 18).

[62] Gerard Ferrer, Aran Solé, Camila Barreneche, Ingrid Martorell, and Luisa F Cabeza. "Review on the methodology used in thermal stability characterization of phase change materials". In: *Renewable and Sustainable Energy Reviews* 50 (2015), pp. 665–685 (cit. on pp. 12, 13).

[63] Manish K Rathod and Jyotirmay Banerjee. "Thermal stability of phase change materials used in latent heat energy storage systems: A review". In: *Renewable and sustainable energy reviews* 18 (2013), pp. 246–258 (cit. on p. 12).

[64] Xue-Feng Shao, Sheng Yang, Chao Wang, Wu-Jun Wang, Yi Zeng, and Li-Wu Fan. "Screening of sugar alcohols and their binary eutectic mixtures as phase change materials for low-to-medium temperature thermal energy storage.(III): Thermal endurance". In: *Energy* 209 (2020), p. 118483 (cit. on p. 12).

[65] Shazim Ali Memon. “Phase change materials integrated in building walls: A state of the art review”. In: *Renewable and sustainable energy reviews* 31 (2014), pp. 870–906 (cit. on p. 13).

[66] Christoph Rathgeber, Stefan Hiebler, Rocío Bayón, Luisa F Cabeza, Gabriel Zsembinszki, Gerald Englmair, Mark Dannemand, Gonzalo Diarce, Oliver Fellmann, Rebecca Ravotti, et al. “Experimental Devices to Investigate the Long-Term Stability of Phase Change Materials under Application Conditions”. In: *Applied Sciences* 10.22 (2020), p. 7968 (cit. on p. 13).

[67] E Oró, A De Gracia, Albert Castell, Mohammed M Farid, and Luisa F Cabeza. “Review on phase change materials (PCMs) for cold thermal energy storage applications”. In: *Applied Energy* 99 (2012), pp. 513–533 (cit. on p. 14).

[68] Jaume Gasia, Marc Martin, Aran Solé, Camila Barreneche, and Luisa F Cabeza. “Phase change material selection for thermal processes working under partial load operating conditions in the temperature range between 120 and 200 °C”. In: *Applied Sciences* 7.7 (2017), p. 722 (cit. on pp. 14, 29).

[69] José Miguel Maldonado, Margalida Fullana-Puig, Marc Martín, Aran Solé, Ángel G Fernández, Alvaro De Gracia, and Luisa F Cabeza. “Phase change material selection for thermal energy storage at high temperature range between 210 °C and 270 °C”. In: *Energies* 11.4 (2018), p. 861 (cit. on p. 14).

[70] Binjian Nie, Anabel Palacios, Boyang Zou, Jiaxu Liu, Tongtong Zhang, and Yunren Li. “Review on phase change materials for cold thermal energy storage applications”. In: *Renewable and Sustainable Energy Reviews* 134 (2020), p. 110340 (cit. on p. 14).

[71] Kinga Pielichowska and Krzysztof Pielichowski. “Phase change materials for thermal energy storage”. In: *Progress in materials science* 65 (2014), pp. 67–123 (cit. on p. 14).

[72] Guruprasad Alva, Lingkun Liu, Xiang Huang, and Guiyin Fang. “Thermal energy storage materials and systems for solar energy applications”. In: *Renewable and Sustainable Energy Reviews* 68 (2017), pp. 693–706 (cit. on p. 14).

[73] Amar M Khudhair and Mohammed M Farid. “A review on energy conservation in building applications with thermal storage by latent heat using phase change materials”. In: *Energy conversion and management* 45.2 (2004), pp. 263–275 (cit. on p. 14).

[74] Luisa F Cabeza, Ana Inés Fernández, Camila Barreneche, and Svetlana Ushak. “PCM storage”. In: *Handbook of Clean Energy Systems* (2015), pp. 1–23 (cit. on p. 14).

[75] Yantong Li, Natasa Nord, Qiangqiang Xiao, and Tymofii Tereshchenko. “Building heating applications with phase change material: A comprehensive review”. In: *Journal of Energy Storage* 31 (2020), p. 101634 (cit. on p. 14).

[76] Nicholas R Jankowski and F Patrick McCluskey. “A review of phase change materials for vehicle component thermal buffering”. In: *Applied energy* 113 (2014), pp. 1525–1561 (cit. on p. 14).

[77] Joris Jaguemont, Noshin Omar, Peter Van den Bossche, and Joeri Mierlo. “Phase-change materials (PCM) for automotive applications: A review”. In: *Applied thermal engineering* 132 (2018), pp. 308–320 (cit. on p. 14).

[78] HMS Hussein, HH El-Ghetany, and SA Nada. "Experimental investigation of novel indirect solar cooker with indoor PCM thermal storage and cooking unit". In: *Energy Conversion and Management* 49.8 (2008), pp. 2237–2246 (cit. on pp. 17, 103).

[79] AA El-Sebaii, S Al-Amir, FM Al-Marzouki, AS Faidah, AA Al-Ghamdi, and S Al-Heniti. "Fast thermal cycling of acetanilide and magnesium chloride hexahydrate for indoor solar cooking". In: *Energy Conversion and Management* 50.12 (2009), pp. 3104–3111 (cit. on pp. 17, 103).

[80] Nidal H Abu-Hamdeh and Khaled A Alnefaie. "Assessment of thermal performance of PCM in latent heat storage system for different applications". In: *Solar Energy* 177 (2019), pp. 317–323 (cit. on pp. 17, 104).

[81] Angad Keith, Nick John Brown, and John L Zhou. "The feasibility of a collapsible parabolic solar cooker incorporating phase change materials". In: *Renewable Energy Focus* 30 (2019), pp. 58–70 (cit. on pp. 17, 104).

[82] Atul G Bhave and Chirag K Kale. "Development of a thermal storage type solar cooker for high temperature cooking using solar salt". In: *Solar Energy Materials and Solar Cells* 208 (2020), p. 110394 (cit. on pp. 17, 105).

[83] Gianluca Coccia, Giovanni Di Nicola, Sebastiano Tomassetti, Mariano Pierantozzi, Manila Chieruzzi, and Luigi Torre. "Experimental validation of a high-temperature solar box cooker with a solar-salt-based thermal storage unit". In: *Solar Energy* 170 (2018), pp. 1016–1025 (cit. on pp. 17, 105).

[84] Sunil Geddam, G Kumaravel Dinesh, and Thirugnanasambandam Sivasankar. "Determination of thermal performance of a box type solar cooker". In: *Solar Energy* 113 (2015), pp. 324–331 (cit. on p. 17).

[85] Antonio Lecuona, José-Ignacio Nogueira, Rubén Ventas, Mathieu Legrand, et al. "Solar cooker of the portable parabolic type incorporating heat storage based on PCM". In: *Applied energy* 111 (2013), pp. 1136–1146 (cit. on pp. 17, 105).

[86] G Kumaresan, VS Vigneswaran, S Esakkimuthu, and R Velraj. "Performance assessment of a solar domestic cooking unit integrated with thermal energy storage system". In: *Journal of energy storage* 6 (2016), pp. 70–79 (cit. on p. 17).

[87] John M DeMan, John W Finley, W Jeffrey Hurst, and Chang Yong Lee. *Principles of food chemistry*. Vol. 478. Springer, 1999 (cit. on p. 18).

[88] Hubert Schiweck, Albert Bär, Roland Vogel, Eugen Schwarz, and Markwart Kunz. "Sugar alcohols". In: *Ullmann's Encyclopedia of Industrial Chemistry* (2000) (cit. on p. 18).

[89] Huaichen Zhang, Marie Duquesne, Alexandre Godin, Sophia Niedermaier, Elena Palomo del Barrio, Silvia V Nedea, and Camilo CM Rindt. "Experimental and in silico characterization of xylitol as seasonal heat storage material". In: *Fluid Phase Equilibria* 436 (2017), pp. 55–68 (cit. on pp. 18, 23).

[90] Kota Nakano, Yasuaki Masuda, and Hirofumi Daiguji. "Crystallization and melting behavior of erythritol in and around two-dimensional hexagonal mesoporous silica". In: *The Journal of Physical Chemistry C* 119.9 (2015), pp. 4769–4777 (cit. on pp. 18, 26).

[91] Xue-Feng Shao, Chao Wang, Yong-Jian Yang, Biao Feng, Zi-Qin Zhu, Wu-Jun Wang, Yi Zeng, and Li-Wu Fan. "Screening of sugar alcohols and their binary eutectic mixtures as phase change materials for low-to-medium temperature latent heat storage.(I): Non-isothermal melting and crystallization behaviors". In: *Energy* 160 (2018), pp. 1078–1090 (cit. on pp. 18, 22–26).

[92] Ari Seppälä, Arttu Meriläinen, Lisa Wikström, and Pertti Kauranen. "The effect of additives on the speed of the crystallization front of xylitol with various degrees of supercooling". In: *Experimental thermal and fluid science* 34.5 (2010), pp. 523–527 (cit. on pp. 18, 22, 23, 128).

[93] Aran Solé, Hannah Neumann, Sophia Niedermaier, Ingrid Martorell, Peter Schossig, and Luisa F Cabeza. "Stability of sugar alcohols as PCM for thermal energy storage". In: *Solar energy materials and solar cells* 126 (2014), pp. 125–134 (cit. on p. 18).

[94] G Diarce, I Gandarias, A Campos-Celador, A García-Romero, and UJ Griesser. "Eutectic mixtures of sugar alcohols for thermal energy storage in the 50–90 C temperature range". In: *Solar Energy Materials and Solar Cells* 134 (2015), pp. 215–226 (cit. on pp. 18, 22, 23).

[95] Elena Palomo Del Barrio, Régis Cadoret, Julien Daranlot, and Fouzia Achchaq. "New sugar alcohols mixtures for long-term thermal energy storage applications at temperatures between 70 C and 100 C". In: *Solar Energy Materials and Solar Cells* 155 (2016), pp. 454–468 (cit. on pp. 18, 23).

[96] National Fire Protection Association et al. *NFPA 704, Standard System for the Identification of the Hazards of Materials for Emergency Response*. National Fire Protection Association, 2017 (cit. on pp. 18, 19).

[97] Sebastiano Tomassetti, Alessia Aquilanti, Pio Francesco Muciaccia, Gianluca Coccia, Christoph Mankel, Eduardus AB Koenders, and Giovanni Di Nicola. "A review on thermophysical properties and thermal stability of sugar alcohols as phase change materials". In: *Journal of Energy Storage* 55 (2022), p. 105456 (cit. on pp. 20, 26).

[98] Mónica Delgado, Miguel Navarro, Ana Lázaro, Séverine AE Boyer, and Edith Peuvrel-Disdier. "Triggering and acceleration of xylitol crystallization by seeding and shearing: Rheo-optical and rheological investigation". In: *Solar Energy Materials and Solar Cells* 220 (2021), p. 110840 (cit. on pp. 23, 29, 128).

[99] Salla Puupponen, Valtteri Mikkola, Tapio Ala-Nissila, and Ari Seppälä. "Novel microstructured polyol–polystyrene composites for seasonal heat storage". In: *Applied energy* 172 (2016), pp. 96–106 (cit. on pp. 23, 24).

[100] Guido Barone, Giuseppe Della Gatta, Daniela Ferro, and Vincenzo Piacente. "Enthalpies and entropies of sublimation, vaporization and fusion of nine polyhydric alcohols". In: *Journal of the Chemical Society, Faraday Transactions* 86.1 (1990), pp. 75–79 (cit. on p. 23).

[101] Chengbin Huang, Zhenxuan Chen, Yue Gui, Chenyang Shi, Geoff GZ Zhang, and Lian Yu. "Crystal nucleation rates in glass-forming molecular liquids: D-sorbitol, D-arabitol, D-xylitol, and glycerol". In: *The Journal of chemical physics* 149.5 (2018), p. 054503 (cit. on p. 23).

[102] Vincenza Brancato, Andrea Frazzica, Alessio Sapienza, and Angelo Freni. “Identification and characterization of promising phase change materials for solar cooling applications”. In: *Solar Energy Materials and Solar Cells* 160 (2017), pp. 225–232 (cit. on pp. 22, 23).

[103] Riku A Talja and Yrjö H Roos. “Phase and state transition effects on dielectric, mechanical, and thermal properties of polyols”. In: *Thermochimica Acta* 380.2 (2001), pp. 109–121 (cit. on p. 23).

[104] L Carpentier, S Desprez, and M Descamps. “Crystallization and glass properties of pentitols”. In: *Journal of thermal analysis and calorimetry* 73.2 (2003), pp. 577–586 (cit. on p. 23).

[105] Akihide Kaizawa, Nobuhiro Maruoka, Atsushi Kawai, Hiroomi Kamano, Tetsuji Jozuka, Takeshi Senda, and Tomohiro Akiyama. “Thermophysical and heat transfer properties of phase change material candidate for waste heat transportation system”. In: *Heat and mass transfer* 44.7 (2008), pp. 763–769 (cit. on pp. 23, 29).

[106] Hao Zhou, Laiquan Lv, Yize Zhang, Mengting Ji, and Kefa Cen. “Preparation and characterization of a shape-stable xylitol/expanded graphite composite phase change material for thermal energy storage”. In: *Solar Energy Materials and Solar Cells* 230 (2021), p. 111244 (cit. on pp. 23, 29).

[107] E Palomo del Barrio, A Godin, M Duquesne, J Daranlot, J Jolly, W Alshaer, T Kouadio, and A Sommier. “Characterization of different sugar alcohols as phase change materials for thermal energy storage applications”. In: *Solar Energy Materials and Solar Cells* 159 (2017), pp. 560–569 (cit. on p. 23).

[108] Rui Jia, Keyan Sun, Rongchun Li, Youyou Zhang, Wenxia Wang, Heng Yin, Dawei Fang, Quan Shi, and Zhicheng Tan. “Heat capacities of some sugar alcohols as phase change materials for thermal energy storage applications”. In: *The Journal of Chemical Thermodynamics* 115 (2017), pp. 233–248 (cit. on p. 23).

[109] Stephan Höhlein, Andreas König-Haagen, and Dieter Brüggemann. “Thermophysical characterization of MgCl2 · 6H2O, xylitol and erythritol as phase change materials (PCM) for latent heat thermal energy storage (LHTES)”. In: *Materials* 10.4 (2017), p. 444 (cit. on pp. 22, 23).

[110] V Saikrishnan, A Karthikeyan, and B Selvaraj. “Experimental study on thermal performance of xylitol in a latent heat storage combined with sensible heat storage”. In: *AIP Conference Proceedings*. Vol. 2161. 1. AIP Publishing LLC. 2019, p. 020038 (cit. on p. 23).

[111] Bo Tong, Zhi-Cheng Tan, Quan Shi, Yan-Sheng Li, Dan-Ting Yue, and Shao-Xu Wang. “Thermodynamic investigation of several natural polyols (I): Heat capacities and thermodynamic properties of xylitol”. In: *Thermochimica acta* 457.1-2 (2007), pp. 20–26 (cit. on pp. 23, 29).

[112] V Saikrishnan, A Karthikeyan, A Laksmisankar, and N Beemkumar. “Thermophysical Characteristic Analysis Of Edible Erythritol And Xylitol For Their Use As Phase Change Materials”. In: *Int. J. Sci. Tech* 8.11 (2019), pp. 644–649 (cit. on pp. 23, 29).

[113] Hermínio P Diogo, Susana S Pinto, and Joaquim J Moura Ramos. “Slow molecular mobility in the crystalline and amorphous solid states of pentitols: a study by thermally stimulated depolarisation currents and by differential scanning calorimetry”. In: *Carbohydrate research* 342.7 (2007), pp. 961–969 (cit. on pp. 22, 23, 26).

[114] HK Cammenga and ID Steppuhn. “Polymorphic status of sorbitol: solution calorimetry versus DSC”. In: *Thermochimica acta* 229 (1993), pp. 253–256 (cit. on p. 23).

[115] Á Gombás, P Szabó-Révész, G Regdon, and I Erős. “Study of thermal behaviour of sugar alcohols”. In: *Journal of thermal analysis and calorimetry* 73.2 (2003), pp. 615–621 (cit. on p. 23).

[116] Dmitrii N Bolmatenkov, Mikhail I Yagofarov, Andrey A Sokolov, Marat A Ziganshin, and Boris N Solomonov. “The heat capacities and fusion thermochemistry of sugar alcohols between 298.15 K and Tm: The study of D-sorbitol, D-mannitol and myo-inositol”. In: *Journal of Molecular Liquids* 330 (2021), p. 115545 (cit. on p. 23).

[117] B Tong, Z Tan, Q Shi, Y Li, and S Wang. “Thermodynamic investigation of several natural polyols (II) Heat capacities and thermodynamic properties of sorbitol”. In: *Journal of thermal analysis and calorimetry* 91.2 (2008), pp. 463–469 (cit. on pp. 23, 29).

[118] Amale Nezzal, Luc Aerts, Marleen Verspaille, Geert Henderickx, and Andreas Redl. “Polymorphism of sorbitol”. In: *Journal of Crystal Growth* 311.15 (2009), pp. 3863–3870 (cit. on p. 23).

[119] Balamurugan Jeganathan and Vijayalakshmi Prakya. “Design and Optimization of Novel Sugar Alcohol Based Extended Release Tablets Prepared by Melt Dispersion Technique”. In: *Iranian Journal of Pharmaceutical Sciences* 8.2 (2012), pp. 83–98 (cit. on p. 23).

[120] K Bitchikh, AH Meniai, and W Louaer. “Measurement and prediction of binary and ternary liquid-solid equilibria of pharmaceutical and food systems”. In: *Energy Procedia* 18 (2012), pp. 1152–1164 (cit. on p. 23).

[121] Haishan Che, Qianqiao Chen, Qin Zhong, and Si He. “The effects of nanoparticles on morphology and thermal properties of erythritol/polyvinyl alcohol phase change composite fibers”. In: *e-Polymers* 18.4 (2018), pp. 321–329 (cit. on p. 24).

[122] Bin Yang, Ning Wang, Yawei Song, and Jiemei Liu. “Study on the improvement of supercooling and thermal properties of erythritol-based phase change energy storage materials”. In: *Renewable Energy* 175 (2021), pp. 80–97 (cit. on p. 24).

[123] Mayilvelnathan Vivekananthan and Valan Arasu Amirtham. “Characterisation and thermophysical properties of graphene nanoparticles dispersed erythritol PCM for medium temperature thermal energy storage applications”. In: *Thermochimica Acta* 676 (2019), pp. 94–103 (cit. on p. 24).

[124] Heyao Zhang, Jinxing Cheng, Qingbo Wang, Dongbo Xiong, Jinliang Song, Zhongfeng Tang, and Xiangdong Liu. “The graphite foam/erythritol composites with ultrahigh thermal conductivity for medium temperature applications”. In: *Solar Energy Materials and Solar Cells* 230 (2021), p. 111135 (cit. on pp. 24, 29).

[125] Ju-Lan Zeng, Lei Zhou, Yue-Fei Zhang, Sai-Ling Sun, Yu-Hang Chen, Li Shu, Lin-Ping Yu, Ling Zhu, Liu-Bin Song, and Zhong Cao. "Effects of some nucleating agents on the supercooling of erythritol to be applied as phase change material". In: *Journal of Thermal Analysis and Calorimetry* 129.3 (2017), pp. 1291–1299 (cit. on p. 24).

[126] Yi Wang, Shuang Li, Ting Zhang, Deyi Zhang, and Hui Ji. "Supercooling suppression and thermal behavior improvement of erythritol as phase change material for thermal energy storage". In: *Solar Energy Materials and Solar Cells* 171 (2017), pp. 60–71 (cit. on p. 24).

[127] Ni Tan, Ting Xie, Yang Feng, Ping Hu, Qi Li, Liu-Mo Jiang, Wen-Bo Zeng, and Ju-Lan Zeng. "Preparation and characterization of erythritol/sepiolite/exfoliated graphite nanoplatelets form-stable phase change material with high thermal conductivity and suppressed supercooling". In: *Solar Energy Materials and Solar Cells* 217 (2020), p. 110726 (cit. on pp. 24, 29).

[128] Yu-Hang Chen, Liu-Mo Jiang, Yu Fang, Li Shu, Yu-Xiang Zhang, Ting Xie, Kun-Yu Li, Ni Tan, Ling Zhu, Zhong Cao, et al. "Preparation and thermal energy storage properties of erythritol/polyaniline form-stable phase change material". In: *Solar Energy Materials and Solar Cells* 200 (2019), p. 109989 (cit. on pp. 24, 29).

[129] Mengdi Yuan, Chao Xu, Tieying Wang, Tianying Zhang, Xinyu Pan, and Feng Ye. "Supercooling suppression and crystallization behaviour of erythritol/expanded graphite as form-stable phase change material". In: *Chemical Engineering Journal* 413 (2021), p. 127394 (cit. on p. 24).

[130] Shengyou Bao, Qiuping Wei, Jun Cao, Haichao Li, Li Ma, Junjie An, Cheng-Te Lin, Jingting Luo, and Kechao Zhou. "Hydrophilic modification of carbon nanotube to prepare a novel porous copper network-carbon nanotube/erythritol composite phase change material". In: *Composite Interfaces* 28.2 (2021), pp. 175–189 (cit. on p. 24).

[131] AB Shobo and A Mawire. "Experimental comparison of the thermal performances of acetanilide, meso-erythritol and an In-Sn alloy in similar spherical capsules". In: *Applied Thermal Engineering* 124 (2017), pp. 871–882 (cit. on p. 24).

[132] Ahmet Sari, Ramazan Eroglu, Alper Bicer, and Ali Karaipekli. "Synthesis and thermal energy storage properties of erythritol tetrastearate and erythritol tetrapalmitate". In: *Chemical engineering & technology* 34.1 (2011), pp. 87–92 (cit. on p. 24).

[133] Yi Wang, Zhengfei Zhang, Ting Zhang, Ziyi Qin, Deyi Zhang, and Hui Ji. "Preparation and Characterization of Erythritol/Graphene Oxide Shape-Stable Composites with Improved Thermal-Physical Property". In: *ChemistrySelect* 4.4 (2019), pp. 1149–1157 (cit. on pp. 24, 29).

[134] Aran Solé, Hannah Neumann, Sophia Niedermaier, Luisa F Cabeza, and Elena Palomo. "Thermal stability test of sugar alcohols as phase change materials for medium temperature energy storage application". In: *Energy Procedia* 48 (2014), pp. 436–439 (cit. on pp. 25, 26).

[135] Ahmet Sari. "Thermal energy storage properties of mannitol–fatty acid esters as novel organic solid–liquid phase change materials". In: *Energy conversion and management* 64 (2012), pp. 68–78 (cit. on p. 25).

[136] Srikanth Salyan, B Praveen, Harjit Singh, S Suresh, and A Sarath Reddy. "Liquid Metal Gallium in Metal Inserts for Solar Thermal Energy Storage: A Novel Heat Transfer Enhancement Technique". In: *Solar Energy Materials and Solar Cells* 208 (2020), p. 110365 (cit. on pp. 25, 28, 29).

[137] Vignesh Pethurajan, Suresh Sivan, Alan Johny Konatt, and A Sarath Reddy. "Facile approach to improve solar thermal energy storage efficiency using encapsulated sugar alcohol based phase change material". In: *Solar Energy Materials and Solar Cells* 185 (2018), pp. 524–535 (cit. on pp. 25, 28, 29).

[138] Lijuan He, Songping Mo, Pengcheng Lin, Lisi Jia, Ying Chen, and Zhengdong Cheng. "Synthesis and properties of nanoencapsulated D-mannitol for medium temperature thermal energy storage". In: *Solar Energy Materials and Solar Cells* 209 (2020), p. 110473 (cit. on pp. 25, 29).

[139] Xusheng Zhang, Zheng Du, Yudong Zhu, Chuan Li, Xianfeng Hu, Tingbin Yang, Bin-Bin Yu, Rui Gu, Yulong Ding, and Zhubing He. "A novel volumetric absorber integrated with low-cost D-Mannitol and acetylene-black nanoparticles for solar-thermal-electricity generation". In: *Solar Energy Materials and Solar Cells* 207 (2020), p. 110366 (cit. on pp. 25, 29).

[140] R Bayón and E Rojas. "Characterization of organic PCMs for medium temperature storage". In: *Materials and Technologies for Energy Efficiency, Brown Walker Press, Boca Ratón, Florida (US)* (2015), pp. 157–161 (cit. on p. 25).

[141] Huan Liu, Zhiqiang Qian, Qianwei Wang, Dezhen Wu, and Xiaodong Wang. "Development of Renewable Biomass-Derived Carbonaceous Aerogel/Mannitol Phase-Change Composites for High Thermal-Energy-Release Efficiency and Shape Stabilization". In: *ACS Applied Energy Materials* 4.2 (2021), pp. 1714–1730 (cit. on pp. 25, 29).

[142] DK Singh, S Suresh, and H Singh. "Graphene nanoplatelets enhanced myo-inositol for solar thermal energy storage". In: *Thermal Science and Engineering Progress* 2 (2017), pp. 1–7 (cit. on p. 25).

[143] Rafael Turra Alarcon, Caroline Gaglieri, Flávio Junior Caires, Aroldo Geraldo Magdalena, Ricardo António Esteves de Castro, and Gilbert Bannach. "Thermoanalytical study of sweetener myo-inositol: α and β polymorphs". In: *Food chemistry* 237 (2017), pp. 1149–1154 (cit. on pp. 25, 29).

[144] Songping Mo, Yuanhong Li, Shaofei Shan, Lisi Jia, and Ying Chen. "Synthesis and Properties of Inositol Nanocapsules". In: *Materials* 14.19 (2021), p. 5481 (cit. on p. 25).

[145] Ahmet Sarı, Alper Biçer, Özgür Lafçı, and Mustafa Ceylan. "Galactitol hexa stearate and galactitol hexa palmitate as novel solid–liquid phase change materials for thermal energy storage". In: *Solar energy* 85.9 (2011), pp. 2061–2071 (cit. on pp. 26, 29).

[146] Noé Beaupere, U Soupremanien, and Laurent Zalewski. "Nucleation triggering methods in supercooled phase change materials (PCM), a review". In: *Thermochimica Acta* 670 (2018), pp. 184–201 (cit. on p. 26).

[147] ISO11358–1. *Plastics–Thermogravimetry (TG) of Polymers–Part 1: General Principles*. 2014 (cit. on p. 27).

[148] Srikanth Salyan and S Suresh. "Liquid metal gallium laden organic phase change material for energy storage: an experimental study". In: *International Journal of Hydrogen Energy* 43.4 (2018), pp. 2469–2483 (cit. on pp. 28, 29).

[149] Geoffrey John, Andreas König-Haagen, Cecil K King'ondu, Dieter Brüggemann, and Lameck Nkhonjera. "Galactitol as phase change material for latent heat storage of solar cookers: Investigating thermal behavior in bulk cycling". In: *Solar Energy* 119 (2015), pp. 415–421 (cit. on pp. 28, 29).

[150] Srikanth Salyan and S Suresh. "Study of thermo-physical properties and cycling stability of D-Mannitol-copper oxide nanocomposites as phase change materials". In: *Journal of Energy Storage* 15 (2018), pp. 245–255 (cit. on pp. 28, 29).

[151] Srikanth Salyan and S Suresh. "Multi-walled carbon nanotube laden with D-Mannitol as phase change material: characterization and experimental investigation". In: *Advanced Powder Technology* 29.12 (2018), pp. 3183–3191 (cit. on pp. 28, 29).

[152] Ahmad Mojiri, Nikola Grbac, Brendan Bourke, and Gary Rosengarten. "D-mannitol for medium temperature thermal energy storage". In: *Solar Energy Materials and Solar Cells* 176 (2018), pp. 150–156 (cit. on pp. 28, 29).

[153] Yifei Wang, Liang Wang, Ningning Xie, Xipeng Lin, and Haisheng Chen. "Experimental study on the melting and solidification behavior of erythritol in a vertical shell-and-tube latent heat thermal storage unit". In: *International Journal of Heat and Mass Transfer* 99 (2016), pp. 770–781 (cit. on p. 29).

[154] Ju-Lan Zeng, Yu-Hang Chen, Li Shu, Lin-Ping Yu, Ling Zhu, Liu-Bin Song, Zhong Cao, and Li-Xian Sun. "Preparation and thermal properties of exfoliated graphite/erythritol/mannitol eutectic composite as form-stable phase change material for thermal energy storage". In: *Solar Energy Materials and Solar Cells* 178 (2018), pp. 84–90 (cit. on p. 29).

[155] B Tong, ZC Tan, JN Zhang, and SX Wang. "Thermodynamic investigation of several natural polyols". In: *Journal of thermal analysis and calorimetry* 95.2 (2009), pp. 469–475 (cit. on p. 29).

[156] Liu-Mo Jiang, Yu-Hang Chen, Li Shu, Yu-Xiang Zhang, Ting Xie, Ni Tan, Yu Fang, Shao-Fen Wang, Ling Zhang, and Ju-Lan Zeng. "Preparation and characterization of erythritol/polyaniline form-stable phase change materials containing silver nanowires". In: *International Journal of Energy Research* 43.14 (2019), pp. 8385–8397 (cit. on p. 29).

[157] Bo Tong, Rui-Bin Liu, Chang-Gong Meng, Feng-Yun Yu, Shou-Hua Ji, and Zhi-Cheng Tan. "Heat capacities and nonisothermal thermal decomposition reaction kinetics of D-mannitol". In: *Journal of Chemical & Engineering Data* 55.1 (2010), pp. 119–124 (cit. on p. 29).

[158] Miguel Angel Gallegos Lazcano and Weidong Yu. "Thermal performance and flammability of phase change material for medium and elevated temperatures for textile application". In: *Journal of Thermal Analysis and Calorimetry* 117.1 (2014), pp. 9–17 (cit. on p. 29).

[159] Govindaraj Kumaresan, Ramalingom Velraj, and S Iniyan. "Thermal analysis of D-mannitol for use as phase change material for latent heat storage". In: *Journal of applied sciences* 11.16 (2011), pp. 3044–3048 (cit. on p. 29).

[160] Abhijit Paul, Li Shi, and Christopher W Bielawski. "A eutectic mixture of galactitol and mannitol as a phase change material for latent heat storage". In: *Energy Conversion and Management* 103 (2015), pp. 139–146 (cit. on p. 29).

[161] Rocío Bayón and Esther Rojas. “Feasibility study of D-mannitol as phase change material for thermal storage”. In: *AIMS Energy* 5.3 (2017), pp. 404–424 (cit. on p. 29).

[162] S Mahavar, N Sengar, P Rajawat, M Verma, and P Dashora. “Design development and performance studies of a novel single family solar cooker”. In: *Renew. Energy* 47 (2012), pp. 67–76 (cit. on pp. 31, 65).

[163] Mulu Bayray Kahsay, John Paintin, Anwar Mustefa, Asfafaw Haileselassie, Meseret Tesfay, and Biniam Gebray. “Theoretical and experimental comparison of box solar cookers with and without internal reflector”. In: *Energy Procedia* 57 (2014), pp. 1613–1622 (cit. on p. 31).

[164] Naveen Kumar, Sagar Agravat, Tilak Chavda, and HN Mistry. “Design and development of efficient multipurpose domestic solar cookers/dryers”. In: *Renewable Energy* 33.10 (2008), pp. 2207–2211 (cit. on p. 31).

[165] N Kumar, T Chavda, and HN Mistry. “A truncated pyramid non-tracking type multipurpose domestic solar cooker/hot water system”. In: *Applied Energy* 87.2 (2010), pp. 471–477 (cit. on p. 32).

[166] Manpreet Singh and VP Sethi. “On the design, modelling and analysis of multi-shelf inclined solar cooker-cum-dryer”. In: *Solar Energy* 162 (2018), pp. 620–636 (cit. on p. 32).

[167] Abhishek Saxena and Nitin Agarwal. “Performance characteristics of a new hybrid solar cooker with air duct”. In: *Solar Energy* 159 (2018), pp. 628–637 (cit. on p. 32).

[168] Atul A Sagade, SK Samdarshi, PJ Lahkar, and Narayani A Sagade. “Experimental determination of the thermal performance of a solar box cooker with a modified cooking pot”. In: *Renew. Energy* 150 (2020), pp. 1001–1009 (cit. on pp. 32, 66, 75).

[169] G Crovatto. *Costruzione di un Forno ad Alta Efficienza*. 2011. URL: `http://digilander.libero.it/giannicrovatto/f-effic.htm` (cit. on p. 32).

[170] OO Fasina and Z Colley. “Viscosity and specific heat of vegetable oils as a function of temperature: 35 °C to 180 °C”. In: *International Journal of Food Properties* 11.4 (2008), pp. 738–746 (cit. on p. 40).

[171] G Coccia, G Di Nicola, and A Hidalgo. *Parabolic Trough Collector Prototypes for Low-Temperature Process Heat*. Springer, 2016 (cit. on p. 41).

[172] AMA Khalifa, MMA Taha, and M Akyurt. “Solar cookers for outdoors and indoors”. In: *Energy* 10.7 (1985), pp. 819–829 (cit. on pp. 42, 57, 93, 118, 167, 168).

[173] PJ Lahkar, RK Bhamu, and SK Samdarshi. “Enabling inter-cooker thermal performance comparison based on cooker opto-thermal ratio (COR)”. In: *Appl. Energy* 99 (2012), pp. 491–495 (cit. on pp. 42, 43, 48, 57, 77, 92, 93, 167, 173).

[174] SC Mullick, TC Kandpal, and S Kumar. “Testing of box-type solar cooker: second figure of merit F2 and its variation with load and number of pots”. In: *Solar Energy* 57.5 (1996), pp. 409–13 (cit. on pp. 44, 120).

[175] D Buddhi, SD Sharma, and RL Sawhney. “Performance test of a box-type solar cooker: effect of load on the second figure of merit”. In: *International Journal of Energy Research* 23.9 (1999), pp. 827–830 (cit. on p. 44).

[176] AA El-Sebaii and A Ibrahim. “Experimental testing of a box-type solar cooker using the standard procedure of cooking power”. In: *Renew. Energy* 30.12 (2005), pp. 1861–1871 (cit. on pp. 44, 57).

[177] VP Sethi, DS Pal, and K Sumathy. “Performance evaluation and solar radiation capture of optimally inclined box type solar cooker with parallelepiped cooking vessel design”. In: *Energy Conversion and Management* 81 (2014), pp. 231–241 (cit. on p. 47).

[178] Ndiaga Mbodji and Ali Hajji. “Performance testing of a parabolic solar concentrator for solar cooking”. In: *Journal of Solar Energy Engineering* 138.4 (2016) (cit. on p. 51).

[179] Yunsheng Zhao, Hongfei Zheng, Boyang Sun, Chenji Li, and Yin Wu. “Development and performance studies of a novel portable solar cooker using a curved Fresnel lens concentrator”. In: *Solar Energy* 174 (2018), pp. 263–272 (cit. on p. 51).

[180] Muhammad Noman, Ahmad Wasim, Muzaffar Ali, Mirza Jahanzaib, Salman Hussain, Hafiz Muhammad Khurram Ali, and Hafiz Muhammad Ali. “An investigation of a solar cooker with parabolic trough concentrator”. In: *Case Studies in Thermal Engineering* 14 (2019), p. 100436 (cit. on p. 51).

[181] SM Masum Ahmed, Md Rahmatullah Al-Amin, Shakil Ahammed, Foysal Ahmed, Ahmed Mortuza Saleque, and Md Abdur Rahman. “Design, construction and testing of parabolic solar cooker for rural households and refugee camp”. In: *Solar Energy* 205 (2020), pp. 230–240 (cit. on p. 52).

[182] Atul A Sagade, Xabier Apaolaza-Pagoaga, Celestino Rodrigues Ruivo, and Antonio Carrillo-Andrés. “Concentrating solar cookers in urban areas: Establishing usefulness through realistic intermediate temperature rating and grading”. In: *Solar Energy* 241 (2022), pp. 157–166 (cit. on p. 52).

[183] Heliac. *Heliac*. 2020. URL: `https://www.heliac.dk/` (cit. on p. 52).

[184] H Huseyin Ozturk. “Energy and exergy efficiencies of a solar box-cooker”. In: *Int. J. Exergy* 1.2 (2004), pp. 202–214 (cit. on p. 65).

[185] Seth M Ebersviller and James J Jetter. “Evaluation of performance of household solar cookers”. In: *Sol. Energy* 208 (2020), pp. 166–172 (cit. on pp. 66, 75, 94).

[186] ASAE. *Standard 580.1, Testing and Reporting Solar Cooker Performance*. American Society of Agricultural Engineers, Michigan, USA, 2013 (cit. on pp. 66, 75, 94, 172).

[187] Atul A Sagade, SK Samdarshi, and PS Panja. “Experimental determination of effective concentration ratio for solar box cookers using thermal tests”. In: *Sol. Energy* 159 (2018), pp. 984–991 (cit. on p. 66).

[188] Atul A Sagade, SK Samdarshi, and Partha S Panja. “Enabling rating of intermediate temperature solar cookers using different working fluids as test loads and its validation through a design change”. In: *Sol. Energy* 171 (2018), pp. 354–365 (cit. on pp. 66, 75).

[189] Amanuel Weldu, Li Zhao, Shuai Deng, Nigussie Mulugeta, Ying Zhang, Xianhua Nie, and Weicong Xu. “Performance evaluation on solar box cooker with reflector tracking at optimal angle under Bahir Dar climate”. In: *Sol. Energy* 180 (2019), pp. 664–677 (cit. on p. 66).

[190] Celestino Rodrigues Ruivo, Antonio Carrillo-Andrés, and Xabier Apaolaza-Pagoaga. “Experimental determination of the standardised power of a solar funnel cooker for low sun elevations”. In: *Renew. Energy* 170 (2021), pp. 364–374 (cit. on pp. 66, 76, 89–91).

[191] Xabier Apaolaza-Pagoaga, Antonio Carrillo-Andrés, and Celestino Rodrigues Ruivo. “Experimental thermal performance evaluation of different configurations of Copenhagen solar cooker”. In: *Renew. Energy* 184 (2022), pp. 604–618 (cit. on pp. 66, 76, 91).

[192] Celestino Rodrigues Ruivo, Xabier Apaolaza-Pagoaga, Giovanni Di Nicola, and Antonio Carrillo-Andrés. “On the use of experimental measured data to derive the linear regression usually adopted for determining the performance parameters of a solar cooker”. In: *Renew. Energy* 181 (2022), pp. 105–115 (cit. on p. 66).

[193] Celestino Rodrigues Ruivo, Xabier Apaolaza-Pagoaga, Gianluca Coccia, and Antonio Carrillo-Andrés. “Proposal of a non-linear curve for reporting the performance of solar cookers”. In: *Renew. Energy* (2022) (cit. on p. 66).

[194] Xabier Apaolaza-Pagoaga, Antonio Carrillo-Andrés, and Celestino Rodrigues Ruivo. “Experimental characterization of the thermal performance of the Haines 2 solar cooker”. In: *Energy* 257 (2022), p. 124730 (cit. on pp. 66, 76, 91).

[195] NewtonSolarOven. *Solar cooking Wiki*. Accessed 20 May 2022. URL: `https://solarcooking.fandom.com/wiki/Newton_Solar_Oven` (cit. on p. 67).

[196] MathWorks. *MATLAB, Available online*. Accessed 2 June 2022. URL: `https://www.mathworks.com/products/matlab.html` (cit. on pp. 71, 154).

[197] MathWorks. *Constrained Particle Swarm Optimization*. Accessed 2 June 2022. URL: `https://www.mathworks.com/matlabcentral/fileexchange/25986-constrained-particle-swarm-optimization` (cit. on p. 71).

[198] Marche Region. *Civil Protection Service*. Accessed 2 June 2022. URL: `http://84.38.48.145/sol/info.sol?lang=en` (cit. on pp. 75, 94).

[199] PA Funk. “Testing and reporting solar cooker performance”. In: *ASAE Standards* (2003), pp. 825–826 (cit. on pp. 75, 94).

[200] Celestino Rodrigues Ruivo, Xabier Apaolaza-Pagoaga, Antonio Carrillo-Andrés, and Gianluca Coccia. “Influence of the aperture area on the performance of a solar funnel cooker operating at high sun elevations using glycerine as load”. In: *Sustainable Energy Technol. Assess.* 53 (2022), p. 102600 (cit. on pp. 75, 76, 90, 91).

[201] SA Kalogirou. *Solar Energy Engineering: Processes and Systems*. Second edition. Processes and Systems Series. Elsevier Science, 2013 (cit. on pp. 76, 91).

[202] KimonoSolarCooker. *Solar cooking Wiki*. Accessed 9 February 2021. URL: `https://solarcooking.fandom.com/wiki/Kimono_Solar_Cooker` (cit. on p. 87).

[203] Celestino Solar Funnel Cooker. *Solar cooking Wiki*. Accessed 2 December 2022. URL: `https://solarcooking.fandom.com/wiki/Celestino_Solar_Funnel_Cooker` (cit. on p. 89).

[204] Bernhard Müller. *Instructions and Analysis of Solar Funnel Cookers*. Accessed 31 November 2022. URL: https://static.wikia.nocookie.net/solarcooking/images/2/27/Instructions_and_Analysis_of_Solar_Funnel_Cookers_-_M%C3%BCller_2017.pdf/revision/latest?cb=20170112044408 (cit. on p. 89).

[205] Dual-SettingPanelCooker. *Solar cooking Wiki*. Accessed 9 February 2021. URL: https://solarcooking.fandom.com/wiki/Dual-Setting_Panel_Cooker (cit. on p. 89).

[206] Cookit. *Solar cooking Wiki*. Accessed 15 September 2022. URL: https://solarcooking.fandom.com/wiki/CooKit (cit. on p. 89).

[207] Teong H. Tan. *The Modified CooKit*. Accessed 9 October 2022. URL: https://static.wikia.nocookie.net/solarcooking/images/b/b5/The_Modified_CooKit_11Nov2011.pdf/revision/latest?cb=20111120144211 (cit. on p. 89).

[208] Jean Meeus. "Astronomical algorithms". In: *Richmond* (1991) (cit. on p. 89).

[209] Xabier Apaolaza-Pagoaga, Antonio Carrillo-Andrés, and Celestino Rodrigues Ruivo. "New approach for analysing the effect of minor and major solar cooker design changes: Influence of height trivet on the power of a funnel cooker". In: *Renewable Energy* 179 (2021), pp. 2071–2085 (cit. on p. 90).

[210] Xabier Apaolaza-Pagoaga, Atul A Sagade, Celestino Rodrigues Ruivo, and Antonio Carrillo-Andrés. "Performance of solar funnel cookers using intermediate temperature test load under low sun elevation". In: *Sol. Energy* 225 (2021), pp. 978–1000 (cit. on p. 90).

[211] D Buddhi, SD Sharma, and Atul Sharma. "Thermal performance evaluation of a latent heat storage unit for late evening cooking in a solar cooker having three reflectors". In: *Energy Conversion and Management* 44.6 (2003), pp. 809–817 (cit. on p. 104).

[212] SD Sharma, D Buddhi, RL Sawhney, and A Sharma. "Design, development and performance evaluation of a latent heat storage unit for evening cooking in a solar cooker". In: *Energy Conversion and Management* 41.14 (2000), pp. 1497–1508 (cit. on p. 104).

[213] Shyam S Nandwani, Josef Steinhart, HM Henning, M Rommel, and V Wittwer. "Experimental study of multipurpose solar hot box at Freiburg, Germany". In: *Renewable Energy* 12.1 (1997), pp. 1–20 (cit. on p. 104).

[214] R Domanski, AA El-Sebaii, and M Jaworski. "Cooking during off-sunshine hours using PCMs as storage media". In: *Energy* 20.7 (1995), pp. 607–616 (cit. on pp. 104, 132).

[215] D Buddhi and LK Sahoo. "Solar cooker with latent heat storage: design and experimental testing". In: *Energy Conversion and Management* 38.5 (1997), pp. 493–498 (cit. on p. 104).

[216] Chee Woh Foong, Ole Jørgen Nydal, and Jørgen Løvseth. "Investigation of a small scale double-reflector solar concentrating system with high temperature heat storage". In: *Applied Thermal Engineering* 31.10 (2011), pp. 1807–1815 (cit. on p. 105).

[217] Gianni Crovatto. *Costruzione di un forno a media efficienza*. Accessed 21 February 2023. URL: https://digilander.libero.it/giannicrovatto/f-m-eff.htm (cit. on pp. 106, 107).

[218] A Safari, R Saidur, FA Sulaiman, Yan Xu, and Joe Dong. "A review on supercooling of Phase Change Materials in thermal energy storage systems". In: *Renewable and Sustainable Energy Reviews* 70 (2017), pp. 905–919 (cit. on p. 124).

[219] Marie Duquesne, Elena Palomo Del Barrio, and Alexandre Godin. "Nucleation triggering of highly undercooled Xylitol using an air lift reactor for seasonal thermal energy storage". In: *Applied Sciences* 9.2 (2019), p. 267 (cit. on p. 128).

[220] AMA Khalifa, MMA Taha, and M Akyurt. "Design, simulation, and testing of a new concentrating type solar cooker". In: *Solar Energy* 38.2 (1987), pp. 79–88 (cit. on p. 132).

[221] Sonali Kesarwani, Ajeet Kumar Rai, and Vivek Sachann. "An experimental study on box-type solar cooker". In: *Int J Adv Res Eng Technol* 6.7 (2015), pp. 1–6 (cit. on p. 133).

[222] BZ Adewole, OT Popoola, and AA Asere. "Thermal performance of a reflector based solar box cooker implemented in Ile-Ife, Nigeria". In: (2015) (cit. on p. 133).

[223] K Saravanan and B Janarathanan. "Comparative study of single and double exposure Box-type solar cooker". In: *International Journal of Scientific & Engineering Research* 5.5 (2014), pp. 620–624 (cit. on p. 133).

[224] YA Çengel and AJ Ghajar. *Heat and Mass Transfer: Fundamentals & Applications*. McGraw-Hill, 2011 (cit. on pp. 148, 149, 152, 191, 192).

[225] JA Duffie and WA Beckman. *Solar Engineering of Thermal Processes*. Fourth edition. Wiley, 2013 (cit. on pp. 152, 153, 180).

[226] MathWorks. *ode45*. Accessed 20 February 2023. URL: `https://de.mathworks.com/help/matlab/ref/ode45.html` (cit. on p. 155).

[227] Celestino Rodrigues Ruivo, Gianluca Coccia, Giovanni Di Nicola, Antonio Carrillo-Andrés, and Xabier Apaolaza-Pagoaga. "Standardised power of solar cookers with a linear performance curve following the Hottel-Whillier-Bliss formulation". In: *Renew. Energy* (2022) (cit. on p. 172).

[228] *ISO 9060:2018, Solar energy - Specification and classification of instruments for measuring hemispherical solar and direct solar radiation*. 2018 (cit. on p. 181).

[229] Eppley Laboratory, Inc. *ST-1 Normal Incedence Pyrheliometer*. 12 Sheffield Avenue, PO Box 419, Newport, RI (cit. on p. 181).

[230] Hukseflux. Accessed 28 February 2023. URL: `https://www.hukseflux.com/uploads/product-documents/SR30-M2-D1_manual_v2203.pdf` (cit. on p. 183).

[231] Alanod. Accessed 28 February 2023. URL: `https://alanod.com/_Resources/Persistent/b/a/4/4/ba440e1e595951e1fd28de8b3d11b6888b0835b0/Alanod-Solar_Reflexion_EN.pdf` (cit. on p. 191).

[232] AGC. Accessed 28 February 2023. URL: `https://www.agc-yourglass.com/it-IT/marchi/planibel-clear` (cit. on p. 191).

[233] SOLEC – Solar Energy Corporation (cit. on p. 191).

[234] Bluestar Silicones. Accessed 28 February 2023. URL: `https://www.silitech.ch/wp-content/uploads/2021/03/32.pdf` (cit. on p. 192).

List of publications

Papers on International Journals

1. Gianluca Coccia, Giovanni Di Nicola, Mariano Pierantozzi, Sebastiano Tomassetti, and Alessia Aquilanti. "Design, manufacturing, and test of a high concentration ratio solar box cooker with multiple reflectors." In: *Solar Energy* 155 (2017): 781-792. http://dx.doi.org/10.1016/j.solener.2017.07.020

2. Gianluca Coccia, Alessia Aquilanti, Sebastiano Tomassetti, Gabriele Comodi, and Giovanni Di Nicola. "Design, realization, and tests of a portable solar box cooker coupled with an erythritol-based PCM thermal energy storage." In: *Solar Energy* 201 (2020): 530-540. https://doi.org/10.1016/j.solener.2020.03.031

3. Gianluca Coccia, Alessia Aquilanti, Sebastiano Tomassetti, Akiko Ishibashi, and Giovanni Di Nicola. "Design, manufacture and test of a low-cost solar cooker with high-performance light-concentrating lens." In: *Solar Energy* 224 (2021): 1028-1039. https://doi.org/10.1016/j.solener.2021.06.025

4. Gianluca Coccia, Alessia Aquilanti, Sebastiano Tomassetti, Pio Francesco Muciaccia, and Giovanni Di Nicola. "Experimental Analysis of Nucleation Triggering in a Thermal Energy Storage Based on Xylitol Used in a Portable Solar Box Cooker." In: *Energies* 14.18 (2021): 5981. https://doi.org/10.3390/en14185981

5. Sebastiano Tomassetti, Alessia Aquilanti, Pio Francesco Muciaccia, Gianluca Coccia, Christoph Mankel, Eduardus A.B. Koenders, and Giovanni Di Nicola. "A review on thermophysical properties and thermal stability of sugar alcohols as phase change materials." In: *Journal of Energy Storage* 55 (2022): 105456. https://doi.org/10.1016/j.est.2022.105456

6. Alessia Aquilanti, Sebastiano Tomassetti, Matteo Muccioli, and Giovanni Di Nicola. "Design and experimental characterization of a solar cooker with a prismatic cooking chamber and adjustable panel reflectors." In: *Renewable Energy* 202 (2023): 405-418. https://doi.org/10.1016/j.renene.2022.11.083

7. Alessia Aquilanti, Sebastiano Tomassetti, Gianluca Coccia, Matteo Muccioli, and Giovanni Di Nicola. "Experimental characterization and performance comparison of four prototypes of panel solar cooker for low to high sun elevations." In: *Journal of Cleaner Production* 390 (2023): 136158. https://doi.org/10.1016/j.jclepro.2023.136158

Conference proceedings

1. Giovanni Di Nicola, Alessia Aquilanti, Sebastiano Tomassetti, and Pio Francesco Muciaccia. "Thermophysical properties and thermal stability of different sugar alcohols as phase change materials: a comprehensive review." 13th IIR Phase Change Materials and Slurries for Refrigeration and Air Conditioning Conference, Italy, 1st- 3rd Sept., 2021

2. Giovanni Di Nicola, Alessia Aquilanti, Pio Francesco Muciaccia, Matteo Muccioli, and Sebastiano Tomassetti. "Design and experimental characterization of a simple solar box cooker with adjustable mirrors and its possible development as a solar dryer." XXVI Convegno Associazione Italiana Proprietà Termofisiche (AIPT), Modena (Italy), 23 September 2022